IDENTIFICATION OF SOFT TISSUE MECHANICAL MATERIAL MODEL AND CORRESPONDING PARAMETERS FROM IN VIVO EXPERIMENTAL DATA BY USING INVERSE FINITE ELEMENT METHOD

A THESIS SUBMITTED TO
THE GRADUATE SCHOOL OF NATURAL AND APPLIED SCIENCES
OF
MIDDLE EAST TECHNICAL UNIVERSITY

BY

KEREM ÜSÜ

IN PARTIAL FULFILLMENT OF THE REQUIREMENTS
FOR
THE DEGREE OF MASTER OF SCIENCE
IN
MECHANICAL ENGINEERING

SEPTEMBER 2008

IDENTIFICATION OF SOFT TISSUE MECHANICAL MATERIAL MODEL AND CORRESPONDING PARAMETERS FROM IN VIVO EXPERIMENTAL DATA BY USING INVERSE FINITE ELEMENT METHOD

submitted by **KEREM ÜSÜ** in partial fulfillment of the requirements for the degree of **Master of Science in Mechanical Engineering Department, Middle East Technical University** by,

Prof. Dr. Canan Özgen
Dean, Graduate School of **Natural and Applied Sciences** _____

Prof. Dr. S. Kemal İder
Head of Department, **Mechanical Engineering** _____

Assist. Prof. Dr. Ergin Tönük
Supervisor, **Mechanical Engineering Dept., METU** _____

Examining Committee Members

Assist. Prof. Dr. Cüneyt Sert _____
Mechanical Engineering Dept., METU

Assist. Prof. Dr. Ergin Tönük _____
Mechanical Engineering Dept., METU

Assist. Prof. Dr. Buğra Koku _____
Mechanical Engineering Dept., METU

Assist. Prof. Dr. Yiğit Yazıcıoğlu _____
Mechanical Engineering Dept., METU

Assist. Prof. Dr. Serdar Arıtan _____
SSST, Hacettepe Unv.

Date: 05.09.2008

I hereby declare that all information in this document has been obtained and presented in accordance with academic rules and ethical conduct. I also declare that, as required by these rules and conduct, I have fully cited and referenced all material and results that are not original to this work.

Name, Last name: Kerem ÜSÜ

Signature :

ABSTRACT

IDENTIFICATION OF SOFT TISSUE MECHANICAL MATERIAL MODEL AND CORRESPONDING PARAMETERS FROM IN VIVO EXPERIMENTAL DATA BY USING INVERSE FINITE ELEMENT METHOD

Üsü, Kerem

M.S., Department of Mechanical Engineering

Supervisor : Assist. Prof. Dr. Ergin Tönük

September 2008, 299 pages

The purpose of this thesis is to search for the best material model for soft biological tissues in general. Different sections of human body exhibit different responses like stress relaxation, creep, hysteresis and preconditioning to external loading conditions. These body sections can be assumed as viscoelastic, poroelastic or pseudoelastic. After making the choice of the material model from one of these for the current study, the finite element model and the material code to be used with this model have been created. The material code has also been tried on a simple finite element model before implementing to the real model to prove the fact that it is working properly. Then, the constants in the code which simulates the in vivo experimental data that was obtained by indenting the elliptic indenter tip into the forearm, medial part as close as possible, have been derived by inverse finite element method. Consequently, the characteristic behaviors of the soft tissue could be simulated. Despite the big size of the finite element model and very long submission

times (up to one day for preconditioning simulation), relaxation and creep behaviors could be simulated with the maximum normalized sum of square errors of 0.74 % and 0.43 %, respectively. The number of square errors for the hysteresis and preconditioning behaviors appeared as 2.56 % and 3.89 % which are also acceptable values. These values prove that these material models are well suited for the simulation of the behavior of soft biological tissues. By using different experimental data obtained from other sections of human body, simulation of the behavior of different soft tissues can be achieved by using these material models.

Keywords: Soft Tissue, Viscoelastic, Inverse Finite Elements.

ÖZ

YUMUŞAK DOKU MEKANİK MALZEME MODELİ VE MODEL PARAMETRELERİNİN CANLI DOKUDA VE YERİNDE DENEYLERDEN ELDE EDİLEN VERİLERLE EVRİK SONLU ELEMANLAR YÖNTEMİ KULLANILARAK KESTİRİLMESİ

Üsü, Kerem

Yüksek Lisans, Makina Mühendisliği Bölümü

Tez Yöneticisi : Yrd. Doç. Dr. Ergin Tönük

Eylül 2008, 299 sayfa

Bu tezin amacı genel olarak yumuşak biyolojik dokular için en iyi malzeme modelini araştırmaktır. İnsan vücudunun farklı bölgeleri dış yükleme durumlarına gerilim gevşemesi, sünme, histeris ve alışma gibi farklı tepkiler verirler. Bu bölgeler viskoelastik, poroelastik veya psödoelastik olarak kabul edilebilirler. Bu çalışmada, yumuşak doku malzemesi olarak bunlardan birinin seçimi yapıldıktam sonra, sonlu elemanlar modeli ve bu modelle beraber kullanılacak malzeme kodu meydana getirilmiştir. Malzeme kodunun uygun şekilde çalıştığı, gerçek modelden önce daha basit bir sonlu elemanlar modelinde denenerek ispatlanmıştır. Daha sonra, malzeme kodunun içerisindeki ön kolun orta kısmına eliptik uç ile yapılan basma deneyleri sonucu alınan deneysel veriyi mümkün olduğu kadar yakın kestiren katsayılar evrik sonlu elemanlar yöntemi kullanılarak elde edilmiştir. Sonuç olarak yumuşak dokunun karakteristik özellikleri kestirilebilmiştir. Sonlu elemanlar modelinin büyüklüğüne ve hesaplama sürelerinin uzunluğuna rağmen (alışma etkisinin

hesaplanmasında bir güne kadar), gevşeme ve sünme davranışları sırasıyla % 0.74 ve % 0.43 normalize edilmiş hata kareleri toplamı değerleriyle kestirilebilmiştir. Histeris ve alışma etkilerinin kestiriminde ise bu hata oranları kabul edilebilir olan % 2.56 ve % 3.89 olarak ortaya çıkmıştır. Bu değerler, kullanılan malzeme modellerinin yumuşak biyolojik doku davranışının kestirimine uygun olduğunu göstermektedir. İnsan vücudunun farklı yerlerinden alınan yumuşak doku deney sonuçları kullanılarak farklı yumuşak dokuların davranışlarının kestirimi de bu malzeme modelleri kullanılarak yapılabilir.

Anahtar Kelimeler: Yumuşak Doku, Viskoelastik, Evrik Sonlu Elemanlar.

TABLE OF CONTENTS

LIST OF TABLES

TABLES

LIST OF FIGURES

FIGURES

CHAPTER 1

INTRODUCTION

Human beings are consistently in touch with their surrounding environment in all their life times. Sometimes they smell or listen to notice, or sometimes they touch. Even in a day, people have plenty of physical contacts with the materials around them unconsciously. For example they sit on a chair and do not stand for hours, or sleep on top of the same arm all the night.

The outer surface of human body is mainly composed of soft tissues. So, most of the mechanical interactions with the surrounding environment is by these soft tissues. For example, short after one sits on his hip, it takes the shape of the place where he sat. When that person moves, the shape of his hip changes again and tries to adapt to its new position. When a person takes a long walk, the soles of his feet can be bruised due to harmonic force applied to them by the floor as a result of his weight. People who have paralysis have to lie on a bed for long hours. Because, it is impossible for them to move their body. In that case, the interaction between their tissues and the bed causes some bruises (which are called bed bruises). People who have prosthesis or orthesis are generally complainant about their bruises which happens due to interaction between their soft tissues and prosthesis or orthesis.

For being able to identify these mechanical interactions between human body and the surrounding environment accurately, firstly the structure of the soft tissues must be known. How they react against different loadings must be known in detail and accurately. The determination of this is done by soft tissue experiments. There are three types of experiments:

In *ex vivo* experiments, polymer like materials which have similar characteristics with soft tissues are used instead of real soft tissues. So, this experiment type is the one which gives the least meaningful results. But using materials with known geometries makes this experiment type easier to be applied. In *in vitro* experiments, real but dead soft tissues which are cut out of a cadaver are used. The facts that the soft tissue is not in its original surrounding and it is not alive cause some characteristics to change. The results obtained by in vitro experiments are better than the ones obtained by ex vivo experiments, but not as satisfactory as in vivo experiments. Because, *in vivo* experiments are performed on a living human body when the soft tissue is alive. Consequently, this type of experiments gives the most accurate information about the mechanical behavior of the soft tissue. One disadvantage of this experiment type is the difficulty in performing due to complex geometry of soft tissues and the complex interaction of soft tissue with its surrounding. The experimental data used in this study was obtained by in vivo experiments applied on the forearm, medial part.

The mechanical behavior of soft biological tissues can be simulated by using models and by developing mathematical equations. The aim of this approach is to get complete idea of the behavior of the biological materials under mechanical constraints. Then, this knowledge can be used to predict their behavior under those constraints.

For the simulation of the mechanical behaviors of soft biological tissues, one needs to use the finite element theory. Finite element theory has frequently been used for the simulation of many material behaviors so far. By the usage of the material library within the context of finite element software, one can create the model and simulate its behavior in many conditions. For the common materials it is relatively easier to model the behavior, because these materials are available in the material library of the finite element software. However, biological tissues exhibit complex mechanical behaviors not easily accounted for in classic elastomeric constitutive models. For example, because of their oriented fibrous structures, they often exhibit pronounced mechanical anisotropy, nonlinear stress-strain relationships, large deformations and

strains, viscoelasticity, poroelasticity and strong mechanical coupling. In addition, biological soft tissues are comprised of a dense network of collagen and elastic fibers which can undergo large rotations and exhibit nonlinear stress-strain behavior that can induce complex behaviors at the macro scale not easily accounted for in classic material models (Sun et al., 2003).

Despite a considerable number of investigations, it is difficult to find a satisfactory constitutive model for the nonlinear viscoelastic behavior of soft tissues. This can be explained by the following reasons:

- Some models in the nonlinear theory of viscoelasticity were proposed by employing a mathematical apparatus, which is too general to be applied to real materials. These constitutive models include several unknown functions which are extremely difficult to be determined with the necessary level of accuracy by using the standard experiments.

- The constitutive equations should be sufficiently simple in order to allow explicit solutions to be obtained at least for the simplest mechanical problems, such as uniaxial tension, or simple shear of a specimen. Unfortunately, this requirement rejects a number of models for the nonlinear viscoelastic behavior, since they do not even allow explicit inversion of the stress strain relationship.

- While simulating the mechanical behavior of soft tissues, they were assumed to be in their natural state. But, some special conditions affect them and cause them behave different than natural state. For instance, cutting a vessel (physical phenomenon) has an influence on the blood pressure and therefore the function of other organs. On the contrary, the development of tumorous lesions (physiological phenomenon) modifies locally the tissue mechanical properties (Delingette, 1998).

- Consequently, for more complicated materials like soft biological tissues, one needs to create a special material law which should be able to mimic the stress-strain-time relations first because, the constitutive equations (see Chapter 2) of soft tissues are not like common materials as explained above. The development of these special constitutive equations (see Appendices A, B and C) and related material codes (see Appendices I, K and M) constituted the main part of this study.

Then, these constitutive equations were used for the simulation of tissues. The constants in these material codes were identified by using inverse finite element method (see Appendix G).

Testing methods that include comprehensive testing protocols which allow large variations in stress and strain states are required for accurate material parameter estimation when attempting to determine material constants for complex nonlinear constitutive models.

If one examines the history of soft tissue simulation studies, he would not be able to find any model which can simulate all the characteristic behaviors of soft tissues. So far, many scientists have worked on soft tissue simulation. Some of them could only simulate the relaxation behavior and some others could simulate the creep response by using the relaxation data. Some tried to fit soft tissue responses to mathematical series and some tried to decrease the number of constants in these formulations. These studies in the literature will be presented in detail in the following chapters. In Chapter 2, some basic information about the constitutive equations will be given. In Chapters 3, 4, 5 and 6 soft tissue modeling studies which have been performed so far by using pseudoelasticity, viscoelasticity, hyperelasticity and poroelasticity will be presented, respectively. Chapter 7 examines some alternative material formulations not used for soft tissue modeling before. In Chapter 8, material and finite element models will be discussed deeply and the results will be presented in Chapter 9. Finally, conclusion remarks will be discussed in Chapter 10.

This study aims to simulate all the characteristic behaviors of soft biological tissues with only one constitutive equation with minimum possible change of material constant.

CHAPTER 2

CONSTITUTIVE EQUATIONS

Constitutive equations describe the stress-strain (or stress-strain-time history) relationship of a material under a general, three-dimensional stress field. Constitutive equations must be known before any structural analysis can be performed. In order to predict the mechanical response of biological soft tissues one has to know the material law (*i.e.* the constitutive equation) of the soft tissues. Yet, for all the biological materials, with the possible exception of the aorta, there is no single constitutive equation. This is partly due to the difficulties in testing and measuring biological tissues, and partly due to the difficulty in reducing the experimental data to a mathematical expression (Tong et al., 1976).

It is not surprised that there are a great many constitutive equations describing an almost infinite variety of materials. What should be surprising, therefore, is the fact that three simple, idealized stress-strain relationships, namely, the nonviscous fluid, the Newtonian viscous fluid and the Hookean elastic solid, give a good description of the mechanical properties of many materials. They are the simplest laws that can be devised to relate the stress and strain, or strain rate. Within certain limits of strain and strain rate, air, water and many engineering structural materials can be described by these idealized equations. Most biological materials, however, cannot be described so simply (Fung, 1993).

Since a constitutive equation describes a physical property of a material, it must be independent of any particular set of coordinates of reference with respect to which the components of various physical quantities (like stress and strain) are resolved. Therefore, tensors are used to express constitutive equations.

In the development of deformable body biomechanics, the most crucial step is the identification of the constitutive equations of the tissues involved. If the constitutive equations are known, then biomechanics problems can be formulated as mathematical problems and solutions can be definite. Without constitutive equations, biomechanics will remain qualitative in character. After the form of the constitutive equation is determined, the next step is to systematically collect data on the material constants of various tissues. Until a complete set of data on material constants is obtained, the power of biomechanics to predict the function of a soft tissue will be limited (Fung, 1984).

CHAPTER 3

PSEUDO-ELASTIC MODELING

The mechanical properties of most of the soft biological tissues are qualitatively similar. As an example, arteries are inelastic materials. They do not meet the definition of an elastic body. Elastic materials have a single-valued relationship between stress and strain (which also means that they have a single-valued relationship between force and displacement), but arteries show hysteresis when they are subjected to cycling loading and unloading. As shown in Figure 1, they are represented by different force-displacement curves in loading and unloading. The existence of the loop shows that the tissue is inelastic. Since the loop is repeatable one can treat the loading and unloading curves separately and borrow the method of the theory of elasticity to describe the mechanical properties (Fung, 1984).

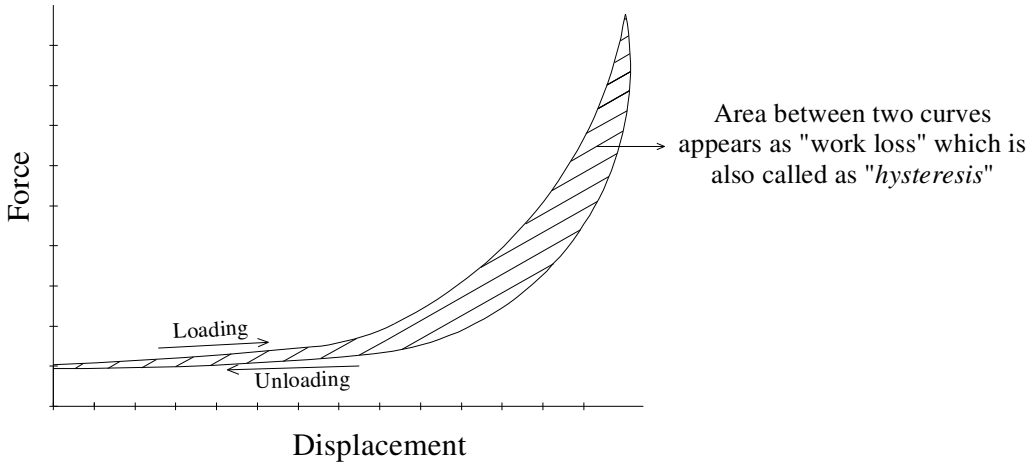

Figure 1 - Basic Force-Displacement Curve for Inelastic Materials
(adopted from *Introduction to Biomechanics Lecture Notes,* Tönük, E., 2006)

They show stress relaxation when held at a constant strain. They show creep when held at a constant stress. Those kinds of behaviors are shown in Figure 2a and 2b, respectively. They are anisotropic. Their stress-strain relationships are nonlinear. After all these factors, the problem of how to describe the mechanical properties of inelastic materials in a simple and accurate mathematical form becomes quite acute. A popular approach to nonlinear elasticity uses the incremental law: a linearized relationship between the incremental stresses and strains obtained by subjecting a material to a small perturbation about a condition of equilibrium. This approach was applied to the arteries in the 1950s but the elastic constants so determined are meaningful only if the initial state from which the perturbations are applied is known, and are applicable only to that state. It turns out that these incremental moduli are strongly dependent on the initial state of stress. A full documentation of this dependence is very difficult to do experimentally and has not been accomplished so far. The difficulty is not due to any lack of technology of recording or patience of the experimenter, but due to the viscoelastic character of the material (Fung, 1980).

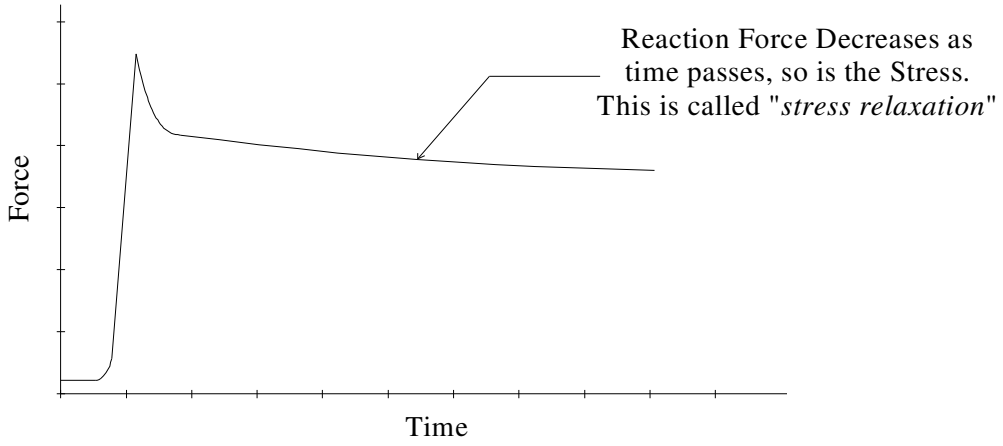

Figure 2a - Force-Relaxation Curve for Viscoelastic Materials <u>at Constant Displacement</u>
(adopted from *Introduction to Biomechanics Lecture Notes,* Tönük, E., 2006)

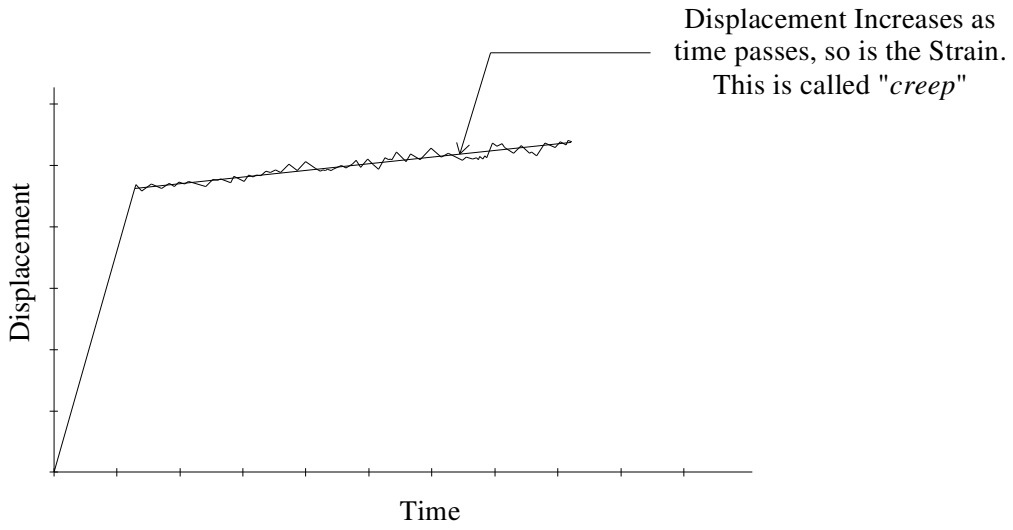

Figure 2b - Creep Curve for Viscoelastic Materials at Constant Load
(adopted from *Introduction to Biomechanics Lecture Notes,* Tönük, E., 2006)

All experimenters agree that to test a biological soft tissue in any specified procedure of loading and unloading it is necessary to perform the loading cycle a number of times before the stress-strain relationship becomes repeatable (Fung, 1970, Bischoff et al, 1999, 2006, 2004, Abramowitch et al, 2004, Fulin et al, 2007). This process is called *preconditioning (Mullin's effect).* A testing protocol such as loading and unloading at a constant rate or sinusoidal stretching and shortening must be selected.

Focusing attention to preconditioned arteries subjected to cycling loading and unloading at constant strain rates, one can see that, by definition, the stress-strain relationship is well defined, repeatable, and predictable. For the *loading branch* and the *unloading branch* separately, the stress strain relationship is unique. Since stress and strain are uniquely related in each branch of a specific cyclic process, the material can be treated as one elastic material in loading (increasing strain), and another elastic material in unloading (decreasing strain). Thus the method of the theory of elasticity can be borrowed to handle an inelastic material and two different

equations for these two branches can be used. Because of the fact that inelastic materials are being dealt with, it is called pseudo-elasticity.

Pseudo-elasticity is, therefore, not an intrinsic property of the material. It is a convenient description of the stress-strain relationship in specific cyclic loading. The usefulness of the concept of pseudo-elasticity is greatly enhanced because of the fact that it is rather insensitive to strain rate. The stress-strain relationships of some tissues have been tested in a range of strain rate covering a million-fold difference between the slowest and the fastest cycling, and the stresses at the same strain are usually found to differ by less than a factor of two (Fung et al, 1967, 1975, 1984, 1993, 1994).

The stiffness of soft biological tissues increases rapidly as tensile stresses increase because of the composite nature of the materials. These tissues are composed of collagen networks, elastin networks, smooth muscles, and ground substances. The fibers of collagen, elastin, and smooth muscles are curved: they gradually take up more and more stresses as they become straightened and stretched. Collagen fibers, when straight, have Young's modulus which is two or three orders of magnitude higher than that of the elastin. Smooth muscle has very large hysteresis in cyclic deformation. The network configuration of these fibers, as embedded in the ground substance, changes with the strain. Speculations abound, but the details are not known very clearly (Fung, 1980, Dehoff, 1978, Henry et al, 2005).

3.1. Pseudo-Strain Energy Function

Biological specimens must be tested in a manner as close as to *in vivo* conditions as possible. By saying in vivo conditions one means that, the specimens must be as close as to physiological conditions. So, choosing the most appropriate method for testing becomes quite important. The shape and size of the specimens are limited by nature. Also the type of loading that can be imposed is often restricted due to the lack

of the accuracy of the testing apparatus. As a result of these factors, one has to be satisfied with certain approximations.

By considering the body of the specimen tested two-dimensional, the circumferential and longitudinal coordinates are denoted by θ and z as shown in Figure 3. Then, the stretch ratios in these directions are denoted by λ_θ and λ_z, the Green's strains (referred to undeformed state) by $E_{\theta\theta}$ and E_{zz}, the Cauchy stresses (referred to deformed state) by $\sigma_{\theta\theta}$ and σ_{zz}, and the Kirchoff stresses (referred to undeformed state) by $S_{\theta\theta}$ and S_{zz} (Malvern, 1969).

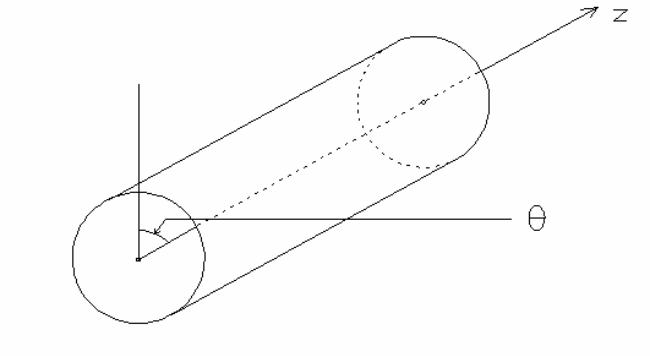

Figure 3 - Representative Coordinate Directions of the Specimen
(adopted from *Introduction to the Mechanics of a Continuous Medium, Malvern,* 1969)

Considering a periodic loading and unloading at a constant rate of stretching, Kirchoff stresses can be written in terms of Green's strains as;

$$S_{ij} = \frac{\partial(\rho_0 W)}{\partial E_{ij}} \qquad \text{.....(1)}$$

where; ρ_0 denotes the density of the material in the unstressed state and W denotes the strain energy per unit mass. In this formulation, the term $\rho_0 W$ is called *pseudo-strain energy function.*

Pseudo-strain energy functions, however, do not have the thermodynamic meaning of the strain energy function, because they depend not only on preconditioning, but also on whether the process is loading or unloading. Nevertheless, the assumption of the existence of a strain energy function for either loading or unloading does simplify the mathematical problem of data reduction. The best strain energy function is the one which involves only a minimum number of material constants. Biological specimens vary a great deal, not only from animal to animal and specimen to specimen, but also for the same specimen as the strain history changes. An empirical expression that involves many material constants is likely to experience difficulty in determining these constants. In the selection of a proper form for the strain energy function, the common fact is; many biological materials are very flexible for quite a large range of deformation (with stretch ratios up to the order of 1.5 or 2.0), and then they become very stiff (Tong et al., 1976).

There are many pseudo-strain energy functions in the literature used for different soft tissues some of which are mentioned below.

3.1.1. Pseudo-Strain Energy Function for Arteries and Veins

For arteries there are two forms of pseudo-strain energy function used much widely. These are the polynomials used by Patel, Vaishnav and their associates (1972), and exponential functions used by Fung et al. (1979).

The polynomial form is;

$$\rho_0 W = A E_{\theta\theta}^{\ 2} + B E_{\theta\theta} E_{zz} + C E_{zz}^{\ 2} + D E_{\theta\theta}^{\ 3} + E E_{\theta\theta}^{\ 2} E_{zz} + F E_{\theta\theta} E_{zz}^{\ 2} + G E_{zz}^{\ 3}$$

……(2)

where; A, B, C, D, E, F and G are material constants (Fung, 1973). The exponential form is;

$$\rho_0 W = \frac{C}{2} \exp[a_1 E_{\theta\theta}^{\ 2} + a_2 E_{zz}^{\ 2} + 2 a_4 E_{\theta\theta} E_{zz}] \text{……..……(3)}$$

where; C, a_1, a_2 and a_4 are material constants (Fung et al., 1979). It is shown by experiments that both of the pseudo-strain energy function forms can fit experimental data quite well in the range of physiological stresses and strains. The correlation coefficients are usually better for equation (3) than for equation (2) (Vaishnav, 1972).

3.1.2. Pseudo-Strain Energy Function for Skin

The skin is also an inelastic material, but after preconditioning the stress-strain loop becomes unique in cyclic loading and unloading, and it is insensitive to strain rate. Keeping these properties in mind, one can use equation (1) for skin, too.

For the skin in a state of generalized plane stress, the pseudo-strain energy function proposed by Tong et al (1976) is the following;

$$\rho_0 W = f(\alpha, E) + C \exp[F(a, E)] \text{…….....(4)}$$

where;

$$f(\alpha, E) = \alpha_1 E_{11}^{\ 2} + \alpha_2 E_{22}^{\ 2} + 2\alpha_4 E_{11} E_{22} + \alpha_3 (E_{12} + E_{21})^2 \text{.....(5)}$$

$$F(a, E) = a_1 E_{11}^{\ 2} + a_2 E_{22}^{\ 2} + 2 a_4 E_{11} E_{22} + a_3 (E_{12} + E_{21})^2 \text{.....(6)}$$

E_{11} and E_{22} are Green's strains in the longitudinal direction X_1, and transverse direction X_2, respectively; E_{12} and E_{21} are shear strains in these directions; $C, \alpha_1, \alpha_2, \alpha_3, \alpha_4, a_1, a_2, a_3$ and a_4 are material constants (Tong et al., 1976).

Tong and Fung also examined the function $F(a,E)$ in the following form (Tong et al., 1976);

$$F(a,E) = a_1 {E_{11}}^2 + a_2 {E_{22}}^2 + 2a_4 E_{11} E_{22} + a_3 (E_{12} + E_{21})^2 + \gamma_1 {E_{11}}^3 + \gamma_2 {E_{22}}^3 + \gamma_4 {E_{11}}^2 E_{22} + \gamma_5 E_{11} {E_{22}}^2 \quad \text{.....(7)}$$

where; $\gamma_1, \gamma_2, \gamma_4, \gamma_5$ are also constants to include the higher order terms in the equation. This improves the fitting between the theoretical expression and the experimental data.

After further examination, Tong was able to obtain a good fit with the experimental data of the skin by expressing W as an exponential function of a polynomial of the second and third degree, omitting the first degree terms.

Let the orthogonal coordinates x_1, x_2 be chosen in the plane of the skin, with x_1 pointing the longitudinal (head to tail) direction, and x_3 be perpendicular to x_1, x_2. Then the normal stress S_{33} and the shear stresses $S_{31} = S_{13}$, $S_{32} = S_{23}$ all vanish due to generalized plane stress case. Hence, if equation (1) applied, the pseudo-strain energy function $\rho_0 W$ will not contain $E_{33}, E_{31}, E_{13}, E_{32}, E_{23}$ because $S_{33} = 0$ implies $\partial(\rho_0 W) / \partial E_{33} = 0$. Therefore, pseudo-strain energy function is only a function of E_{11}, E_{12}^2, E_{22} for two-dimensional specimens in a state of plane stress.
It is shown by Fung (1965) that;

$$E_{11} = \frac{1}{2}(\lambda_1^2 - 1)$$

$$E_{22} = \frac{1}{2}(\lambda_2^2 - 1) \qquad \text{……(8)}$$

$$E_{12} = \frac{1}{2}\left(\frac{\partial x_k}{\partial a_1}\frac{\partial x_k}{\partial a_2}\right)$$

where; E_{11}, E_{22} and E_{12} are Green's strains; $\lambda_1 = \partial x_1 / \partial a_1$ and $\lambda_2 = \partial x_2 / \partial a_2$ are the stretch ratios in the directions of x_1 and x_2, respectively; a_1 and a_2 are the location of a particle in the undeformed state; x_1 and x_2 are the location of the same particle in the deformed state. The pseudo-strain energy function for the skin (for the two-dimensional case by assuming the skin as orthotropic material) can be written shortly as;

$$\begin{aligned} W = {} & \frac{1}{2}(\alpha_1 E_{11}^2 + \alpha_2 E_{22}^2 + \alpha_3 E_{12}^2 + 2\alpha_4 E_{11} E_{22}) \\ & + \frac{1}{2} c \exp(a_1 E_{11}^2 + a_2 E_{22}^2 + a_3 E_{12}^2 + 2a_4 E_{11} E_{22} \\ & + \gamma_1 E_{11}^3 + \gamma_2 E_{22}^3 + \gamma_4 E_{11}^2 E_{22} + \gamma_5 E_{11} E_{22}^2) \end{aligned} \qquad \text{……(9)}$$

where; α's, a's, γ's and c are constants. Then stress-strain relationships can be obtained by equation (1) as;

$$S_{11} = \frac{\partial W}{\partial E_{11}} = \alpha_1 E_{11} + \alpha_4 E_{22} + c A_1 X$$

$$S_{22} = \frac{\partial W}{\partial E_{22}} = \alpha_4 E_{11} + \alpha_2 E_{22} + c A_2 X \qquad \text{……..(10)}$$

$$S_{12} = \frac{\partial W}{\partial E_{12}} = \alpha_3 E_{12} + c a_3 E_{12} X$$

where;

$$A_1 = a_1 E_{11} + a_4 E_{22} + \frac{3}{2}\gamma_1 E_{11}^2 + \gamma_4 E_{11} E_{22} + \frac{1}{2}\gamma_5 E_{22}^2 \quad \text{.....(11)}$$

$$A_2 = a_4 E_{11} + a_2 E_{22} + \frac{3}{2}\gamma_2 E_{22}^2 + \frac{1}{2}\gamma_4 E_{11}^2 + \gamma_5 E_{11} E_{22} \quad \text{.....(12)}$$

$$X = \exp[a_1 E_{11}^2 + a_2 E_{22}^2 + a_3 E_{12}^2 + 2a_4 E_{11} E_{22} + \gamma_1 E_{11}^3 + \gamma_2 E_{22}^3 + \gamma_4 E_{11}^2 E_{22} + \gamma_5 E_{11} E_{22}^2] \quad \text{.....(13)}$$

Since only tensile testing data are available, only those constants associated with tensile strains can be determined. That means, the shear strain E_{12} is zero in all the experiments and consequently α_3 and a_3 cannot be determined. Remaining elastic coefficients to be determined $(\alpha_1, \alpha_2, \alpha_4, c, a_1, a_2, a_4, \gamma_1, \gamma_2, \gamma_4, \gamma_5)$ are defined by equation (10) as;

$$\frac{\partial S_{11}}{\partial E_{11}} = \alpha_1 + c[a_1 + 3\gamma_1 E_{11} + \gamma_4 E_{22} + 2A_1^2] X \quad \text{.....(14)}$$

$$\frac{\partial S_{22}}{\partial E_{22}} = \alpha_2 + c[a_2 + 3\gamma_2 E_{22} + \gamma_5 E_{11} + 2A_2^2] X \quad \text{.....(15)}$$

$$\frac{\partial S_{11}}{\partial E_{22}} = \frac{\partial S_{22}}{\partial E_{11}} = \alpha_4 + c[a_4 + \gamma_4 E_{11} + \gamma_5 E_{22} + 2A_1 A_2] X \quad \text{.....(16)}$$

There are two situations explained below;

i) All the γ' s are set to zero. In this case there are seven constants to be determined, namely: $\alpha_1, \alpha_2, \alpha_4, c, a_1, a_2, a_4$. Using subscripts A, B, etc. to denote experimental data points A, B, etc. one chooses the following seven pieces of experimental information;

$S_{11} = (S_{11})_A$ at A.....(17)

$S_{22} = (S_{22})_A$ at A.....(18)

$$\frac{\partial S_{11}}{\partial E_{11}} = \left(\frac{\partial S_{11}}{\partial E_{11}}\right)_A \qquad \text{at A} \ldots\ldots(19)$$

$$\frac{\partial S_{22}/\partial E_{22} - \alpha_2}{S_2 - \alpha_4 e_1 - \alpha_2 e_2} = \left(\frac{\partial S_{22}/\partial E_{22} - \alpha_2}{S_2 - \alpha_4 e_1 - \alpha_2 e_2}\right)_C \qquad \text{at C} \ldots\ldots(20)$$

$$S_{11} = (S_{11})_B \qquad \text{at B} \ldots\ldots(21)$$

$$S_{22} = (S_{22})_B \qquad \text{at B} \ldots\ldots(22)$$

$$S_{22} = (S_{22})_D \qquad \text{at D} \ldots\ldots(23)$$

From equations (14) – (23) one can find;

$$a_1 = 0.5\,[X_1 - (E_{11} + a_4 E_{22}/a_1)^{-1}]\,[E_{11} + a_4 E_{22}/a_1]_A^{-1} \qquad \text{at A} \ldots\ldots(24)$$

$$a_2 = 0.5\,[X_2 - (E_{22} + a_4 E_{11}/a_2)^{-1}]\,[E_{22} + a_4 E_{11}/a_2]_C^{-1} \qquad \text{at C} \ldots\ldots(25)$$

$$a_4 = a_1\left[\left(X_3 E_{11} - \frac{a_2}{a_1} E_{22}\right)\Big/\left(E_{11} - X_3 E_{22}\right)\right]_A \ldots\ldots(26)$$

$$c = [(S_{11} - \alpha_1 E_{11} - \alpha_4 E_{22})/(a_1 E_{11} + a_4 E_{22})X\,]_A \ldots\ldots(27)$$

$$\alpha_2 = [S_D (E_{11})_B - S_B (E_{11})_D\,]/\,[(E_{22})_D (E_{11})_B - (E_{22})_B (E_{11})_D] \ldots\ldots(28)$$

$$\alpha_4 = [(S_B - \alpha_2 E_{22})/E_{11}\,]_B \ldots\ldots(29)$$

$$\alpha_1 = [(S_A - \alpha_4 E_{22})/E_{11}\,]_B \ldots\ldots(30)$$

where;

$$X_1 = \left[\left(\frac{\partial S_{11}}{\partial E_{11}} - \alpha_1\right)\Big/\left(S_{11} - \alpha_1 E_{11} - \alpha_4 E_{22}\right)\right]_A \qquad \text{at A} \ldots\ldots(31)$$

$$X_2 = \left[\left(\frac{\partial S_{22}}{\partial E_{22}} - \alpha_2\right)\Big/\left(S_{22} - \alpha_4 E_{11} - \alpha_2 E_{22}\right)\right]_C \qquad \text{at C} \ldots\ldots(32)$$

$$X_3 = [(S_{22} - \alpha_4 E_{11} - \alpha_2 E_{22})/(S_{11} - \alpha_1 E_{11} - \alpha_4 E_{22})]_A \qquad \text{at A} \ldots\ldots(33)$$

$$X = \exp\left(a_1 E_{11}^2 + a_2 E_{22}^2 + 2a_4 E_{11}E_{22}\right) \ldots\ldots(34)$$

$$S_A = [S_{11} - c(a_1 E_{11} + a_2 E_{22})X\,]_B \ldots\ldots(35)$$

$$S_B = \left[S_{22} - c\left(a_4 E_{11} + a_2 E_{22}\right) X \right]_B \quad \text{.....(36)}$$

$$S_D = \left[S_{22} - c\left(a_4 E_{11} + a_2 E_{22}\right) X \right]_D \quad \text{.....(37)}$$

From the equations, an iteration scheme can be set up to determine the constants $\alpha_1, \alpha_2, \alpha_4, c, a_1, a_2, a_4$. Starting with an initial guess of α's and $a's$, one may evaluate the updated $a's$ from equations (24) – (26) and (31) – (33). The iteration process is continued with fixed α's until a set of convergent $a's$ are obtained. Then equations (27) – (30) and (34) – (37) is used to evaluate the updated *c' s* and α's. If α's converged, the iteration stops; otherwise, the updated α's and the current $a's$ are used to start the iteration again from equations (25) – (26) and (31) – (33).

If the stresses (or strains) at points A and C are much higher than those at points B and D, an excellent guess of α's can be obtained by evaluating equations (28) – (39) and (35) – (37) with $a's$, set to zero.

ii) γ_1 *and* γ_2 *are set to zero and* γ_4 *is set to equal* γ_5. In this case, there are eight constants to be determined, namely: $\alpha_1, \alpha_2, \alpha_4, c, a_1, a_2, a_4, \gamma_4 (=\gamma_5)$. Then in addition to conditions (19) – (23), one requires;

$$\frac{\partial S_{22}}{\partial E_{11}} = \left(\frac{\partial S_{22}}{\partial E_{11}} \right)_A \qquad \text{at A} \quad \text{.....(38)}$$

The special case where the experimental data $\left(E_{22}\right)_A = \left(E_{22}\right)_B = 0$ will be considered. Then, all the equations for iteration are the same as those of equations (24) – (37), except that equations (25), (26) and (34) are replaced by;

$$\frac{\gamma_4}{a_1} = 2\left[E_{11}\left(\frac{\partial S_{22}/\partial E_{11} - \alpha_4}{S_{11} - \alpha_1 E_{11}} \right) - \left(1 + 2a_1 E_{11}^2\right) X_3 \right]_A \quad \text{.....(39)}$$

$$\frac{a_4}{a_1} = \left(X_3 - \frac{1}{2}\frac{\gamma_4}{a_1} E_{11} \right)_A \quad \text{.....(40)}$$

$$a_2 = 0.5\{ X_2 - [1 + (\gamma_4 E_{11}/a_2)]\,[E_{22} + a_4 E_{11}/a_2 + \gamma_4 \left(E_{11}E_{22} + \frac{1}{2}E_{11}^2 \right) \Big/ a_2]^{-1} \}$$

$$*(E_{22} + a_4 E_{11}/a_2 + \gamma_4 \left(E_{11}E_{22} + \frac{1}{2}E_{11}^2 \right) \Big/ a_2 \}^{-1} \qquad \text{at C} \quad \text{.....(41)}$$

$$X = \exp\{a_1 E_{11}^2 + a_2 E_{22}^2 + E_{11}E_{22}[2a_4 + \gamma_4 (E_{11} + E_{22})]\} \quad \text{.....(42)}$$

and equation (37) is replaced by;

$$S_D = \left[S_{22} - c\left(a_4 E_{11} + a_2 E_{22} + \frac{1}{2}\gamma_4 E_{11}^2 + \gamma_4 E_{11}E_{22} \right) X \right]_D \quad \text{.....(43)}$$

The iteration procedure is similar to that of case *i.* It should be noted that, since $(E_{22})_A = (E_{22})_B = 0$, no initial guess of a_1 or a_4 is necessary. Once the initial guess of α's is made, a_1 can be evaluated from equation (24), γ_4 is then evaluated from equation (39), a_4 is evaluated from equation (40), and then a_2 is determined from equation (41) by iteration.

It is found that the fit between these mathematical formulas and the experimental data is good. However, if one uses the constants in one experiment with a specific protocol and preconditioning to compute the stress-strain relationship in other experiments on the same specimen, but with a different protocol, the success is uniform. The agreement between the mathematical formula and the experimental data is still reasonable when $\lambda_y = 1.23$, but in the case of $\lambda_y = 1.41$ there is no correlation at all (Tong et al., 1976).

3.1.3. Pseudo-Strain Energy Function for Lung Parenchyma

The Lung parenchyma is a big organ with a complex structure. Its shape looks like a foam rubber which means that it is a very soft tissue. Pseudo-strain energy function for the lung parenchyma is deduced by Hoppin et al. (1975) as;

$$\rho_0 W = \sum_{i=1}^{4} a_i \,(\lambda_1^{2i} + \lambda_2^{2i} + \lambda_3^{2i}) + \sum_{i=1}^{2} b_i \,(\lambda_1^{2i}\lambda_2^{2i} + \lambda_2^{2i}\lambda_3^{2i} + \lambda_1^{2i}\lambda_3^{2i}) + c_1 \lambda_1^2 \lambda_2^2 \lambda_3^2$$

$$+ \sum_{i=2}^{3} c_i \,(\lambda_1^{2i}\lambda_2^2 + \lambda_2^{2i}\lambda_3^2 + \lambda_3^{2i}\lambda_1^2 + \lambda_1^2\lambda_2^{2i} + \lambda_2^2\lambda_3^{2i} + \lambda_3^2\lambda_1^{2i}) \quad \text{.....(44)}$$

where; a_i, b_i and c_i are material constants. This equation was obtained by applying triaxial loading on a lung tissue specimen of cubic geometry. So, stretch ratios in three directions are included in the equation. Also slabs of lung tissue were tested which was bathed in saline and subjected to cyclic biaxial loading at constant rate of stretching and strain. The experimental results were quite extensive. When equation (45) is applied to experimental data, the fitting is excellent;

$$\rho_0 W = C \exp[a_1 E_{11}^2 + a_2 E_{22}^2 + 2a_4 E_{11} E_{22}] \; + \; \text{symmetric terms by permutation}$$

.....(45)

in which the last line means the sum of all terms obtained by cyclic permutation of the subscripts 1. 2 of E by 2, 3 and 3, 1.

A major difference between equation (44) and (45) is that isotropy is assumed in the former but not in the latter. For fitting latter experimental data, the anisotropic expression leads to higher correlation coefficients (Fung, 1980).

3.1.4. Pseudo-Strain Energy Function for Mesentery and Muscles

For the mesentery and muscles (in the passive state), Fung has shown that the following equation provides an excellent fit of the experimental data of uni-axial tension tests, except for a small region very near the state of zero stress (Fung, 1973, 1967);

$$\frac{dT}{dE} = \alpha T + \beta \quad \text{.....(46)}$$

where; T is the stress per unit original area; E is the strain relative to an initially undeformed state; and α , β are constants determined experimentally. Integration of equation (46) yields a stress T as an exponential function of strain, E.

3.1.5. Pseudo-Strain Energy Function for Lower Extremity Residual Limb Tissues

The bulk soft tissue was approximated as a single, homogeneous, isotropic (in the undeformed configuration), nonlinear elastic, incompressible material represented by the James-Green-Simpson strain energy density function (Mooney, 1940), as follows;

$$W = 2C_1(I-3) + 2C_2(I-3)^2 + C_3(I-3)^3 \quad \text{.....(47)}$$

where; W is the strain energy density (energy-per-unit undeformed volume); I is the invariant of Green-Lagrange strain tensor ($I_1 = I_2 = I$; the first and second strain invariants are equivalent for an incompressible material under axisymmetric loading conditions); C_i are the nonlinear elastic material coefficients to be determined (Tönük et al., 2003).

Equation (47) was used to simulate the nonlinear force displacement behavior of residual limb soft tissues, as measured during cyclic rate-controlled indentation. This model, one of the simplest phenomenological nonlinear elastic formulations available in the literature, was capable of simulating experimentally observed nonlinear compressive force displacement behavior of the residual limb bulk soft tissue of individuals with transtibial amputations.

The individual soft tissue constituents (e.g., skin, fat, muscle) at the test location are modeled as a single, homogeneous, isotropic, nonlinear elastic material. The behavior of the individual constituents and their interaction with each other are not modeled. Other potential source of error for this model is the axisymmetric approximation of the indenter and residual limb geometry. Also, the frictionless contact assumption between the indenter tip and soft tissue during computer simulations can cause some errors.

James-Green-Simpson equation is an elastic formulation. The time-dependent phenomena, such as creep and relaxation, as well as hysteresis during cyclic loading, have been observed for residual limb tissues. These behaviors cannot be simulated with the present elastic model. The compressive behavior of lower extremity soft tissues is nonlinear and viscoelastic. So, with the addition of viscoelastic material properties, a wide range of loading spectra can perhaps be simulated.

Another of the disadvantages of this formulation is the fact that the material parameters do not have any physiological meaning. They are only constants for fitting the equation to the experimental data.

3.1.6. Generalized Pseudo-Strain Energy Function

There are many more forms of strain energy functions proposed for various tissues. Undoubtedly all forms proposed for rubber-like materials could and should be examined for biological applications, but it is known that the most popular ones do

not fit experimental data on the soft tissues like arteries, skin, lung parenchyma which were presented in this thesis.

Fung proposed a generalized constitutive equation for the biological materials in the form of a strain energy function which can be written in tensor notation as follows (Fung, 1973);

$$W = \frac{1}{2}\alpha_{ijkl} E_{ij} E_{kl} + \beta_0 \beta_{mnpq} E_{mn} E_{pq} \exp(v_{ij} E_{ij} + \frac{1}{2}\gamma_{ijkl} E_{ij} E_{kl} + ...) \quad \text{.....(48)}$$

Where; α_{ijkl}, β_{mnpq}, v_{ij}, γ_{ijkl}, and β_0 are constants to be determined experimentally. In practice, the second term is used to express the behavior of the material at a high stress level, and the first term is used to remedy the situation at a lower stress level.

3.2. The Effect of Strain Rate

Strain energy functions are generally used to define perfectly elastic materials. Since soft biological tissues are treated as one elastic material in loading and another elastic material in unloading, one can borrow this method to describe these loading and unloading branches separately. But pseudo-elasticity has no generality; it can be defined only for a specific cyclic loading at a specific frequency after preconditioning. In practice, it is rather insensitive to strain rate and, therefore, has a certain degree of generality. Experiments show that it is a general feature of most biological soft tissues (such as muscle, the artery, the mesentery, the skin, the ureter) that the stress-strain relationship is rather insensitive to strain rate.

Having a modest variation over a wide range of strain rates does not mean, of course, that the strain-rate effect is unimportant. There are occasions in which the characteristic strain-rate effect is certain limited ranges of frequencies can serve to identify the conditions of health in a tissue. Often theoretical and experimental results cannot be identified without taking the dynamic material characteristics into

account. But any theory of viscoelasticity of living tissues must account for the fact that the pseudo-elasticity of these tissues does not vary very much over a very wide range of strain rates (Fung, 1980).

All the experiments and mathematical expressions of pseudo-elasticity presented above are limited to stresses and strains in physiological range (for example physiological range of circumferential stretch ratio for arteries lies in the range of 1.4 to 1.8 (Fung, 1980)). They cannot be applied when the stress closes to the breaking point. Furthermore, virtually no data are available for soft tissues loaded in compression, because these tissues are very soft in the neighborhood of zero stress, and therefore buckle under small compressive stress.

As a conclusion main advantages and disadvantages of modeling thye soft tissue material behavior with the pseudo-elastic constitutive equation can be summarized as follows:

Advantages:

- Soft biological tissues are not elastic materials. It is hard to model the full behavior. Assuming loading and unloading branches as two different materials, there is seen a single-valued relationship between stress and strain which allows using the theory of elasticity.
- Convenient for modeling almost all biological soft tissues, because the method of theory of elasticity can be borrowed for these inelastic materials.
- The usefulness of the concept of pseudo-elasticity is greatly enhanced because of the fact that it is rather insensitive to strain rate.
- The assumption of the existence of a strain energy function for either loading or unloading does simplify the mathematical problem of data reduction.
- Bu virtue of the strain-rate insensitivity, pseudo-elasticity acquires a certain measure of independence.

Disadvantages:

- It is necessary to perform the loading cycle a number of times before the stress-strain relationship is repeatable which is called as preconditioning.
- Pseudo-strain energy functions do not have the thermodynamic meaning of the strain energy function.
- Pseudo-elasticity has no generality; it can be defined only for a specific cyclic loading at a specific frequency after preconditioning.
- If one uses the constants in one experiment with a specific protocol and preconditioning to compute the stress-strain relationship in other experiments on the same specimen, but with a different protocol, the success is uniform.
- Elasticity allows modeling by considering the loading and unloading branches separately, but the soft tissue is not elastic at all.
- The agreement between mathematical formulas and the experimental data is reasonable until a specific stretch ratio (about 1.2 – 1.3).

CHAPTER 4

VISCOELASTIC MODELING

As mentioned in Chapter 3, soft biological tissues are not elastic. Viscoelasticity describes materials that exhibit both viscous and elastic characteristics. . Newtonian viscous fluids, like honey, resist shear flow and strain linearly with time when a stress is applied. Elastic materials strain instantaneously when stressed and just as quickly return to their original state once the stress is removed. Viscoelastic materials have elements of both of these properties and exhibit time dependent strain. Many viscoelastic materials exhibit rubber like behavior. They show hysteresis in the stress-strain curve with the area of the loop being equal to mechanical energy lost during the cycle as presented in Figure 1.

Unlike purely elastic materials, a viscoelastic substance has an elastic component and a viscous component. The viscosity of a viscoelastic substance makes it strain rate dependent with time. Purely elastic materials do not dissipate mechanical energy (into heat) when a load is applied, then removed. However, a viscoelastic substance dissipates energy when a load is applied, then removed (Fung, 1994).

4.1. Constitutive Models of Linear Viscoelasticity

A mathematical model of viscoelasticity of a tissue must cover all features of hysteresis, relaxation, and creep. One of the most popular models of linear viscoelasticity is the Maxwell model of a spring in series with a dashpot (Figure 4a). The other is the Voigt model with a spring and dashpot in parallel (Figure 5a). A third is the Kelvin model which is a combination of a spring in parallel with a

Maxwell body (Figure 6a). None of these can represent a soft tissue, because when a material represented by any one of these models is subjected to a cyclic strain, the hysteresis will not be insensitive to strain rate: as frequency increases, the dashpot in the Maxwell body will move less and less at same load so the hysteresis decrease with frequency (Figure 4b). On the other hand, the Voigt body will let the dashpot take up more and more of the load so that the hysteresis increases with frequency (Figure 5b). For the Kelvin body there exist a characteristic frequency at which the hysteresis is a maximum (Figure 6b). None of these has the feature of nearly constant hysteresis as soft tissues do (Schwartz et al., 2005).

4.1.1. Maxwell Model

The Maxwell model can be represented by a purely linear viscous damper (dashpot) and a purely linear elastic spring connected in series, as shown in Figure 4a. The same force F is transmitted from the spring to the dashpot. This force produces a displacement F/μ in the spring and a velocity F/η in the dashpot. Then the velocity of the spring extension becomes $\dot{F}/\mu$. The total velocity $\dot{u}$ is the sum of these two;

$$\dot{u} = \frac{\dot{F}}{\mu} + \frac{F}{\eta} \qquad \text{.....(49)}$$

Obtained by using equation (49), the model can be represented by the following constitutive equation;

$$\frac{d\varepsilon_{total}}{dt} = \frac{d\varepsilon_D}{dt} + \frac{d\varepsilon_S}{dt} = \frac{\sigma}{\eta} + \frac{1}{\mu}\frac{d\sigma}{dt} \qquad \text{.....(50)}$$

where; ε_{total} is the total strain and ε_D and ε_S are strains at the damper and spring, respectively; σ is the stress; μ is the elastic modulus of the material and η is the viscosity of the material.

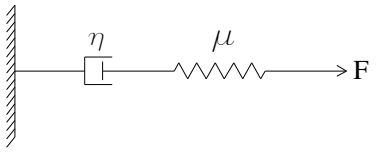

Figure 4a - Maxwell Model

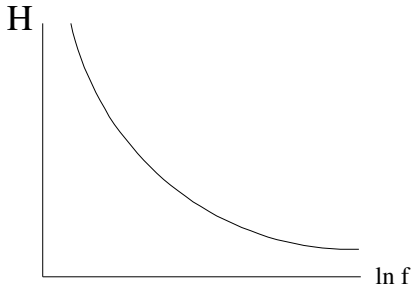

Figure 4b - Hysteresis-Frequency Curve of Maxwell Model

If the material having the Maxwell model is put under a constant strain, the stresses gradually relax to zero. When a material is put under a constant stress, the strain has two components. First, an elastic component occurs instantaneously, corresponding to the spring, and relaxes immediately upon release of the stress. The second is a viscous component that grows with time as long as the stress is applied.

Furthermore, if the force is suddenly applied at the instant of time $t = 0$, the spring will be suddenly deformed to $u(0) = F(0)/\mu$, but the initial dashpot deflection would be zero, because there is no time to deform. Thus, the initial condition for differential equation (49) is;

$$u(0) = \frac{F(0)}{\mu} \qquad \text{.....(51)}$$

The Maxwell model predicts that stress decays exponentially with time. It is important to note limitations of such a model, as it is unable to predict creep in materials based on a simple dashpot and spring connected in series.

4.1.2. Voigt Model

The Voigt model consists of a purely linear viscous damper (dashpot) and a purely linear elastic spring connected in parallel, as shown in Figure 5a. The spring and the dashpot have the same displacement. If the displacement is *u*, the velocity $\dot{u}$, and the spring and the dashpot will produce forces μu and $\eta \dot{u}$, respectively. The total force *F* is therefore;

$$F = \mu u + \eta \dot{u} \quad \text{.....(52)}$$

Obtained by using equation (52), the constitutive equation of the Voigt model is expressed as a linear first-order differential equation;

$$\sigma(t) = \mu \varepsilon(t) + \eta \frac{d\varepsilon(t)}{dt} \quad \text{.....(53)}$$

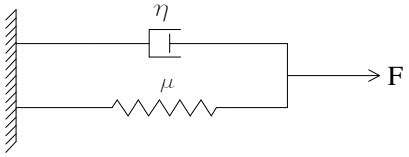

Figure 5a - Voigt Model

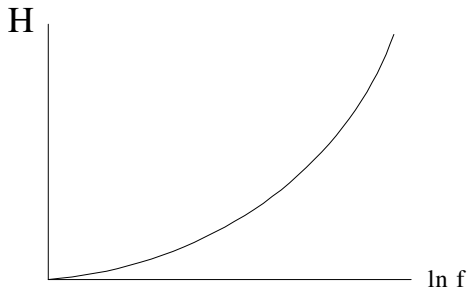

Figure 5b - Hysteresis-Frequency Curve

Upon application of a constant stress to a material having the Voigt model, the material deforms at a decreasing rate, asymptotically approaching the steady-state strain. When the stress is released, the material gradually relaxes to its undeformed initial state. At constant stress, the model is quite realistic as it predicts strain to tend to σ / μ as time continues to infinity. Because of the fact that the dashpot and the spring are connected parallel, no deflection will occur in both of them if the force is applied suddenly. So, the appropriate initial condition is;

$$u(0) = 0 \quad \text{.....(54)}$$

Similar to the Maxwell model, the Voigt model also has limitations. The model is extremely good with modeling creep in materials; but with regards to relaxation the model is much less accurate. Further, it cannot model immediate elastic response which can be done by Kelvin model.

4.1.3. Kelvin Model

The Kelvin model effectively combines the Maxwell model and an elastic spring in parallel, as shown in Figure 6a. A viscous material is modeled as a spring and a dashpot in series both of which are in parallel with a lone spring. This time, let us break down the displacement u_1 (of the lower branch) into u_2 for the dashpot and u_2' for the spring (of the upper branch), where as the total force *F* is the sum of the force F_1 from the spring (of the lower branch) and F_2 from the Maxwell element. Thus;

$$u_1 = u_2 + u_2' \quad \text{.....(55a)}$$

$$F = F_1 + F_2 \quad \text{.....(55b)}$$

$$F_1 = \mu_1 u_1 \quad \text{.....(55c)}$$

$$F_2 = \eta \dot{u}_2 = \mu_2 u_2' \quad \text{.....(55d)}$$

Substituting equations (55c) and (55d) into (55b), we obtain;

$$F = \mu_1 u_1 + \mu_2 u_2^{'} \quad \text{.....(56)}$$

Substituting the term $u_2^{'}$ obtained from equation (55a) into equation (56);

$$F = \mu_1 u_1 + \mu_2 (u_1 - u_2) = (\mu_1 + \mu_2) u_1 - \mu_2 u_2 \quad \text{.....(57)}$$

Hence;

$$F + \frac{\eta}{\mu_2}\dot{F} = (\mu_1 + \mu_2) u_1 - \mu_2 u_2 + \frac{\eta}{\mu_2}(\mu_1 + \mu_2)\dot{u}_1 + \eta \dot{u}_2 \quad \text{.....(58)}$$

Replacing the last term by $\mu_2 u_2^{'}$ and using equation (55a), we obtain;

$$F + \frac{\eta}{\mu_2}\dot{F} = \mu_1 u_1 + \eta\left(1 + \frac{\mu_1}{\mu_2}\right)\dot{u} \quad \text{.....(59)}$$

Equation (59) can also be written as;

$$F + \tau_\varepsilon \dot{F} = E_R (u + \tau_\sigma \dot{u}) \quad \text{.....(60)}$$

where; $\tau_\varepsilon = \frac{\eta}{\mu_2}$ is called *the relaxation time for constant strain*; $\tau_\sigma = \frac{\eta}{\mu_1}\left(1 + \frac{\mu_1}{\mu_2}\right)$ is called *the relaxation time for constant stress* and $E_R = \mu_0$ is called *the relaxed elastic modulus.*

For a sudden applied force $F(0)$ and displacement $u(0)$, the initial condition is;

$$\tau_\varepsilon F(0) = E_R \tau_\sigma u(0) \quad \text{.....(61)}$$

For the Kelvin model, the governing constitutive equation can also be given as;

$$\frac{d\varepsilon}{dt} = \frac{\frac{\mu_2}{\eta}\left(\frac{\eta}{\mu_2}\frac{d\sigma}{dt} + \sigma - \mu_1\varepsilon\right)}{\mu_1 + \mu_2} \quad \text{.....(62)}$$

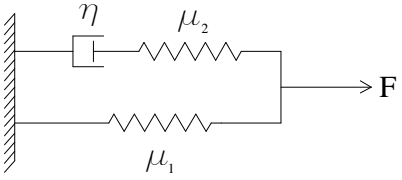

Figure 6a - Kelvin Model

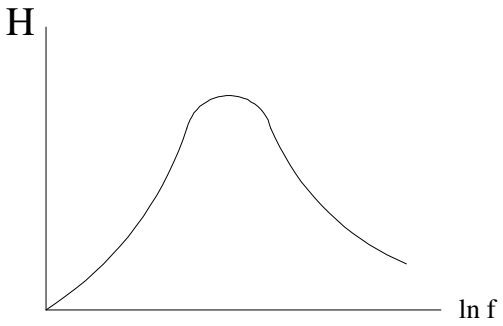

Figure 6b - Hysteresis-Frequency Curve of Kelvin Model

Under a constant stress, the modeled material will instantaneously deform to some strain, which is the elastic portion of the strain, and after that it will continue to deform and asymptotically approach a steady-state strain. This last portion is the viscous part of the strain. Kelvin model is more accurate than the Maxwell and Voigt models in predicting material responses, mathematically it returns inaccurate results for strain under specific loading conditions and is rather difficult to calculate (Malvern, 1969, Tönük, 2006).

4.1.4. Maxwell-Weichert Model

A suitable model for soft tissues is the Maxwell-Weichert model, as shown in Figure 7a. This model has an infinite number of springs and dashpots. In the corresponding hysteresis diagram shown in Figure 7b, there are an infinite number of bell-shaped curves which add up to a continuous curve of nearly constant height over a very wide range of frequencies.

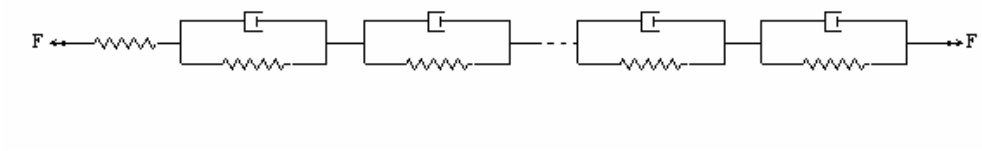

Figure 7a – Infinite Number of Springs and Dashpots
(adopted from *Introduction to the Mechanics of a Continuous Medium, Malvern,* 1969)

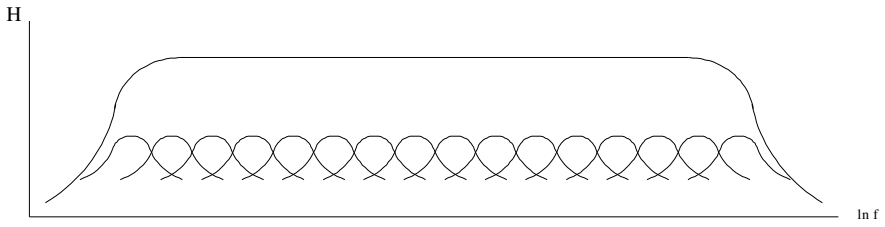

Figure 7b - Hysteresis Diagram of Infinite Number of Springs and Dashpots
(adopted from *Introduction to the Mechanics of a Continuous Medium, Malvern,* 1969)

It takes into account that relaxation does not occur at a single time, but at a distribution of times. Due to molecular segments of different lengths with shorter ones contributing less than longer ones, there is a varying time distribution. The

Maxwell-Weichert model shows this by having as many spring-dashpot Maxwell elements as are necessary to accurately represent the distribution (Malvern, 1969).

4.1.5. Generalized Maxwell-Element

The basic constitutive elements of linear viscoelasticity are an elastic spring called *Hooke-element* (Figure 8a) and a viscous *Newton-element* (Figure 8b). The elastic material constant μ gives the linear relation (Kaliske et al., 1997);

$$\sigma^e = \mu \varepsilon^e \quad \text{.....(63)}$$

between elastic stress σ^e and elastic strain ε^e. The viscous stress σ^v of the Newton-element depends on the strain rate $\dot{\varepsilon}^v$. For the Newton-element these quantities are related linearly by the coefficient of viscosity η;

$$\sigma^v = \eta \dot{\varepsilon}^v \quad \text{.....(64)}$$

analogously to the elastic Hooke-element. The viscosity η can also be expressed in terms of the elastic constant μ;

$$\eta = \tau \mu \quad \text{.....(65)}$$

by introducing the relaxation time τ.

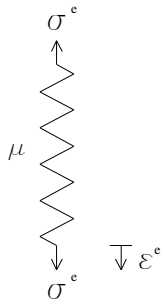

Figure 8a - Hooke-element

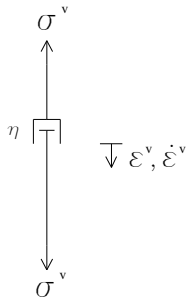

Figure 8b - Newton-element

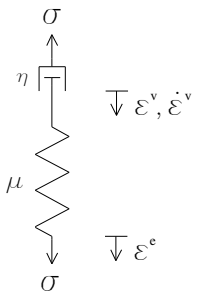

Figure 8c - Maxwell-element

The combination of Hooke-element and Newton-element in series yields the so-called Maxwell-element (Figure 8c) where the total strain ε consists of an additive combination $\varepsilon = \varepsilon^e + \varepsilon^v$ of an elastic ε^e and a viscous ε^v component while the stress;

$$\sigma = \mu \varepsilon^e = \eta \dot{\varepsilon}^v \qquad \text{.....(66)}$$

is the same in both rheological elements. Using the equation $\varepsilon = \varepsilon^e + \varepsilon^v$ and equations (65) and (66), we can obtain;

$$\dot{\varepsilon}^v = \frac{1}{\tau}\left(\varepsilon - \varepsilon^v\right) \qquad \text{.....(67)}$$

At the state of equilibrium, i.e. $\dot{\varepsilon}^v = 0$, the viscous strain of a Maxwell-element converges to the total strain $\varepsilon^v = \varepsilon$ and the elastic strain vanishes $\varepsilon^e = 0$. Alternatively, we get the fundamental differential equation;

$$\dot{\varepsilon} = \frac{1}{\mu}\dot{\sigma} + \frac{1}{\eta}\sigma \qquad \text{.....(68)}$$

If we carry out a relaxation test the Maxwell-element will deform at a constant strain, i.e., $\varepsilon(0) = \varepsilon(t) = const.$. In this case the solution of differential equation (68) yields;

$$\sigma = c \exp\left(-\frac{t}{\tau}\right) \quad \text{.....(69)}$$

By using the initial condition $\sigma(0) = \mu\, \varepsilon(0)$, the constant $c = \mu\varepsilon(0)$ is determined. Thus, we get the solution;

$$\sigma(t) = \mu \exp\left(-\frac{t}{\tau}\right) \varepsilon(0) \quad \text{.....(70)}$$

where, the relaxation function;

$$G(t) = \mu \exp\left(-\frac{t}{\tau}\right) \quad \text{.....(71)}$$

defines the specific viscoelastic characteristics of a material. At an infinite large time the stress is fully relaxed, i.e. $\sigma(\infty) = 0$.

The preceding relaxation test of one Maxwell-element is easily applied to an extended viscoelastic formulation where a finite number of separate, Maxwell-elements are arranged in parallel with an elastic Hooke-element (Figure 9). The stress relaxation for the generalized Maxwell-element is given by;

$$\begin{aligned}\sigma(t) &= \mu_0\, \varepsilon(0) + \sum_{j=1}^{N} \mu_j \exp\left(-\frac{t}{\tau_j}\right) \varepsilon(0) \\ &= G(t)\, \varepsilon(0) \quad \text{.....(72)}\end{aligned}$$

where;

$$G(t) = \mu_0 + \sum_{j=1}^{N} \mu_j \exp\left(-\frac{t}{\tau_j}\right) \quad \text{.....(73)}$$

defines the characteristic relaxation function of *N* Maxwell-elements. The time-independent elastic part of the deformation is represented by the term μ_0 which is constant with respect to time.

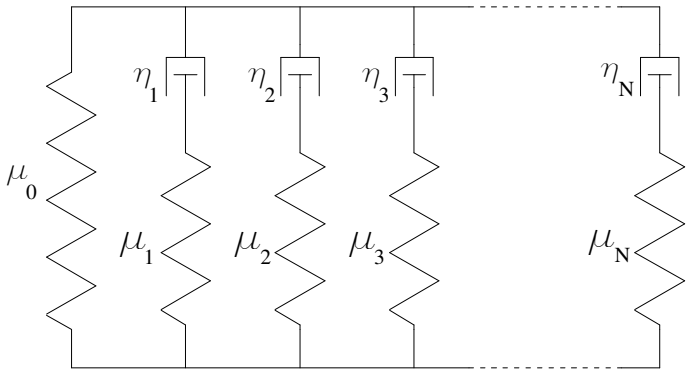

Figure 9 - Generalized Maxwell-element
(adopted from *Biomechanics: Mechanical Properties of Living Tissues,* Fung, 1993)

The generalized Maxwell-model has been derived from basic considerations and the constitutive assumption has been proved to be valid for a large number of materials by experiments.

Some scientists (Tönük et al., 2004) used generalized Maxwell-model with two dampers to simulate the relaxation and creep data of biological soft tissues. They used the following constitutive equation for relaxation;

$$F(t) = F_0\left\{1 - \delta_1\left(1 - e^{(-t/\tau_1)}\right) - \delta_2\left(1 - e^{(-t/\tau_2)}\right)\right\} \quad \text{.....(74)}$$

where; $F(t)$ is the force-relaxation response; t is time ($0 \le t \le 120 s.$; $t = 0$ corresponds to the end of initial loading and beginning of relaxation); F_0 is the reaction force at time $t = 0$; δ_1 and τ_1 are the short-term relaxation magnitude and associated time constant; δ_2 and τ_2 are the long-term relaxation magnitude and associated time constant, respectively. The total tissue relaxation is therefore $F_0(\delta_1 + \delta_2)$.

And the following one was used for creep;

$$d(t) = d_0\left\{1 + \delta_1'\left(1 - e^{(-t/\tau_1')}\right) + \delta_2'\left(1 - e^{(-t/\tau_2')}\right)\right\} \quad (75)$$

where; $d(t)$ is the displacement-creep response; t is time ($0 \le t \le 120 s.$; $t = 0$ corresponds to the end of initial loading and beginning of creep); d_0 is the tissue indentation at time $t = 0$; δ_1' and τ_1' are the short-term creep magnitude and associated time constant; δ_2' and τ_2' are the long-term creep magnitude and associated time constant, respectively. The total tissue creep is therefore $d_0(\delta_1' + \delta_2')$.

4.2. Linear Elastic Tensor-Mass Method

Some scientists used the *linear elastic tensor-mass method* which allows fast (real-time) computation of nonlinear and viscoelastic mechanical forces and deformations for the simulation of biological soft tissues. They showed that most of the tissues are highly nonlinear, and that a viscoelastic constitutive model is most suitable for modeling deformations. The model they presented integrates physical nonlinearity and viscoelasticity into the tensor-mass framework while keeping a linear strain tensor (Schwartz et al., 2005).

4.3. Modeling Elastic and Viscous Behaviors Separately

It is thought by some other scientists (Sanjeevi, 1982) that the stress (σ) generated in a biological material can be represented as a combination of the Hookean stress $E\varepsilon$ (E is a constant and ε is the strain) and the Newtonian hydrodynamic viscous stress $\eta\, d\varepsilon/dt$ (η is a constant and $d\varepsilon/dt$ is the strain rate). Therefore;

$$\sigma = E\varepsilon + \eta\frac{d\varepsilon}{dt} \qquad \text{.....(76)}$$

By proposing this model, it is aimed to take both viscous and elastic components into account using a suitable procedure. Stress-relaxation and creep curves are tried to be predicted.

For this type of modeling different amounts of strains (2%, 5%, 8%, etc.) are applied to the material. Then the stresses developed are allowed to decay for long enough to ensure that there is no further decay of stresses with time (Figure 10). By this figure using least-square technique, the elastic and the viscous components of the stress developed can be found as;

$$\sigma_{elastic} = E_1\,\varepsilon + E_2\,\varepsilon^2 \qquad \text{.....(77)}$$

$$\sigma_{viscous} = \eta_1\frac{d\varepsilon}{dt} + \eta_2\,\varepsilon\,\frac{d\varepsilon}{dt} \qquad \text{.....(78)}$$

By using the experimental data, the complete viscoelastic equation can be found as;

$$\sigma = 55.12\varepsilon - 110.11\varepsilon^2 + 0.42\,\frac{d\varepsilon}{dt} + 29\varepsilon\,\frac{d\varepsilon}{dt} \qquad \text{.....(79)}$$

It can be seen that this equation is closely similar to the stress developed by a Voigt model responding to higher orders of strain levels.

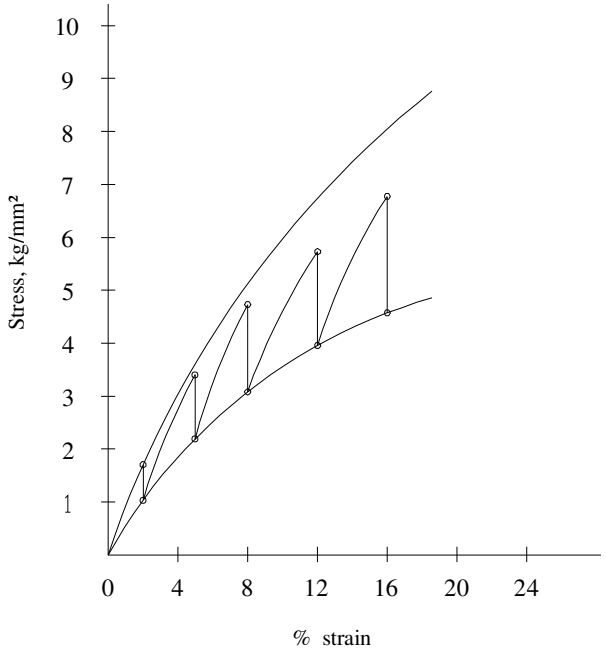

Figure 10 - The Stress Decay at Small Strain Intervals
(adopted from *A Viscoelastic Model for the Mechanical Properties of Biological Materials,* Sanjeevi, 1982)

4.4. Haut and Little Equations

Two approximate constitutive equations which have proved useful for characterizing the nonlinear viscoelastic behavior of polymers are proposed as candidate theories to characterize soft biological tissues (Dehoff, 1978). By using these equations, Haut and Little equations which represent the relaxation behavior of collagen can be derived.

Haut and Little equation is known as;

$$\sigma(t) = \int_0^t G(t-\tau)\,\frac{d\sigma^e}{d\lambda}\,[\lambda(\tau)]\;\frac{d\lambda(\tau)}{d\tau}\,d\tau \qquad \text{.....(80)}$$

where; σ is the nominal stress; σ^e is the elastic stress generated instantly when the tissue is subjected to a uniaxial step extension ratio (λ); t is the present time in minutes; τ is the time history in minutes; $G(t)$ is a normalized relaxation function defined by Fung such that $G(0)=1$. For small strains equation (80) can be rewritten as;

$$\sigma(t)=\int_0^t G(t-\tau)\frac{d\sigma^e}{d\varepsilon}[\varepsilon(\tau)]\ \frac{d\varepsilon(\tau)}{d\tau}d\tau \qquad \text{.....(81)}$$

where; ε is the uniaxial strain.

Experimentally it is not possible to generate a step strain input. Instead of that, constant strain rate tests can be used if the material is insensitive to strain rate at high rates like biological soft tissues. Haut and Little used elastic stress and normalized relaxation function in the forms;

$$\sigma^e = C'\varepsilon^2 \qquad \text{.....(82)}$$

$$G(t) = A'\ln t + B' \qquad \text{.....(83)}$$

where; C' is strain rate constant and; A' and B' are non-dimensional relaxation constants.

For a relaxation strain history given by $\varepsilon(t)=\varepsilon_0 H(t)$, substituting equations (82) and (83) into equation (80) leads to;

$$\sigma(t) = E\varepsilon_0^2[\mu\ \ln t + 1] \qquad \text{.....(84)}$$

where; H is stress relaxation material function; $E = 2B'C'$ and $\mu = A'/B'$. E and μ were experimentally found equal to $23x10^{10}\ dyn/cm^2$ and -0.23, respectively (Dehoff, 1978).

For a constant strain rate test for which $\varepsilon = \beta t$, equation (80) becomes;

$$\sigma(t) = \frac{E}{2}\varepsilon^2\left[1 + \mu\left(\ln\frac{\varepsilon}{\beta} - 3/2\right)\right] \quad \text{.....(85)}$$

where; β is strain rate.

As mentioned before, this equation can be derived from two constitutive equations. The first one was suggested by *Lianis* (1963) which based on the finite linear theory of viscoelasticity. The second constitutive equation is an incompressible elastic fluid theory developed by *Bernstein, Kearsley* and *Zapas* (1963). These theories will not be analyzed in detail. Shortly it can be said that these theories are used to predict the relaxation behavior of polymers. They are capable of handling nonlinear, time dependent and multi-dimensional stress and strain histories for both isotropic and anisotropic materials. Many of the situations of interest in biological tissues can be treated as special cases of these continuum theories (Dehoff, 1978).

4.5. Quasi-Linear Viscoelastic Model

The quasi-linear viscoelastic theory introduced by Fung has been frequently used to model nonlinear time-dependent and history-dependent viscoelastic behavior of many soft tissues. It is common to use five constants to describe the instantaneous elastic response (constants *A* and *B*) and reduced relaxation function (constants *C,* τ_1 and τ_2) on experiments with finite ramp times followed by stress relaxation to equilibrium. However, a limitation is that the theory is based on a step change in strain which is not possible to perform experimentally. By taking into account the ramping phase of the experiment, the approach allows for viscoelastic properties to be determined independent of the strain rate applied. Thus, the results obtained from different laboratories and from different tissues may be compared (Abramowitch, 2004).

In the quasi-linear viscoelastic theory, the reduced relaxation function, with constants *C*, τ_1 and τ_2, describes the time dependent stress relaxation of a tissue normalized by the stress at the time of a step input of strain.

The quasi-linear viscoelastic theory assumes that the relation between stress σ and strain ε for a soft tissue in simple elongation can be expressed as (Sauren et al., 1983, 1984);

$$\sigma(t) = \int_{\tau=0}^{t} G(t-\tau) \frac{\partial \sigma^{(e)}(\varepsilon)}{\partial \varepsilon} \frac{\partial \varepsilon}{\partial \tau} d\tau \quad \text{.....(86)}$$

where; $\sigma(t)$ is the stress at time *t*; $G(t)$ is the reduced relaxation function that represents the time-dependent stress response of the tissue normalized by the stress at the time of the step input of strain; $\sigma^{(e)}(\varepsilon)$ is the instantaneous elastic response, i.e., the maximum stress in response to an instantaneous step input of strain, ε.

with $\sigma(t) = 0$ and $\varepsilon(t) = 0$ for t < 0

$G(0) = 1.$

The dependence of stress on both strain and time is separately described by the nonlinear elastic response $\sigma^{(e)}(\varepsilon)$ and the reduced relaxation function $G(t)$, respectively.

For soft tissues whose stress-strain relationship and hysteresis are not overly sensitive to strain rate, the following expression was proposed by Fung for $G(t)$ based upon a continuous spectrum of relaxation;

$$G(t) = \frac{1 + C\left[E_1(t/\tau_2) - E_1(t/\tau_1)\right]}{1 + C \ln(\tau_2/\tau_1)} \quad \text{.....(87)}$$

where; $E_1(y) = \int_y^\infty e^{-z}/z\, dz$ is the first exponential integral; C is the dimensionless positive constant that determines the degree to which viscous effects are present; τ_1 and τ_2 are time constants that govern the fast and slow viscous phenomena. An exponential approximation has been chosen to describe the instantaneous elastic response;

$$\sigma^{(e)}(\varepsilon) = A\left(e^{B\varepsilon} - 1\right) \qquad \text{.....(88)}$$

where; A and B are material constants.

The stress resulting from a ramp phase with a constant strain rate γ over the times $0 < t < t_0$ can be written by substituting equations (87) and (88) into equation (86);

$$\sigma(\theta) = \frac{A\,B\,\gamma}{1 + C\,\ln(\tau_2/\tau_1)} \int_0^{t_0} \{1 + C\,(E_1[(t-\tau)/\tau_2] - E_1[(t-\tau)/\tau_1])\}\, e^{B\gamma\tau}\, \partial\tau \qquad \text{.....(89)}$$

Similarly, the subsequent stress relaxation from t_0 to $t = \infty$ can be described as;

$$\sigma(\theta) = \frac{A\,B\,\gamma}{1 + C\,\ln(\tau_2/\tau_1)} \int_{t_0}^{\infty} \{1 + C\,(E_1[(t-\tau)/\tau_2] - E_1[(t-\tau)/\tau_1])\}\, e^{B\gamma\tau}\, \partial\tau \qquad \text{.....(90)}$$

where; $\theta = \{t, A, B, C, \tau_1, \tau_2\}$

By a preliminary analysis the initial guesses for the constants were determined. After some iteration, it was found that the algorithm is relatively insensitive to the initial guess; that is, the algorithm consistently converges to a unique solution.

It is necessary to check the variability of these constants if there is any systematic deviation between the model and the experimental data because of experimental noise, and numerical instabilities. Boot-strapping method was used to check the variability of the constants and as the result it was proved that there are relatively small variations in the constants between the model and the experimental data (variation of a constant was found to be smaller than 5 % with respect to its median value). Then the constants may be said to be insensitive to systematic deviations between the model and the experimental data due to experimental noise and numerical instabilities.

While this theory is only an approximation and no approach can guarantee that the obtained constants are true, the fact that the strain history approach is able to estimate reasonable constants based on data with ramp time 1-2 orders of magnitude slower than previous studies is a significant advancement. Thus, issues associated with fast strain rates can be avoided (Abramowitch, 2004).

As mentioned before, it is physically impossible to realize a true step change in strain. It is therefore assumed by some scientists that the stress response to a fast steplike change in strain (Figures 11a, b) can be used as a fair approximation of the response to a true step change. The steplike change in strain in an experiment means straining a sample from $\varepsilon = 0$ to $\varepsilon = \varepsilon_0$ at a high strain rate within a time interval $[0, t_s]$, followed by maintaining $\varepsilon = \varepsilon_0$ during the time interval $[t_s, t_m]$.

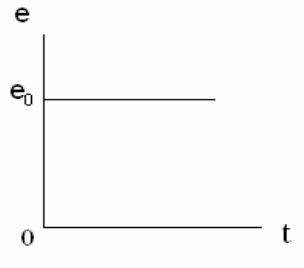

Figure 11a - Step Change in Strain

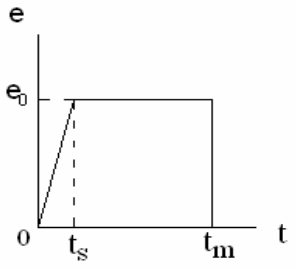

Figure 11b - Steplike Change in Strain

After the studies based on the steplike change in the strain, it was found that it is only possible to separate the elastic and time dependent effects in accordance with $\sigma(t) = \sigma^e(\varepsilon_0)\, G(t)$ when there is a true step change in the strain. The accuracy of the determination of the constants τ_1, τ_2 and C, which describe the time-dependent behavior from a relaxation experiment depends greatly upon the time required to accomplish a sudden change in strain. This is not too unexpected because, during straining within a finite interval $[0, t_s]$, a certain amount of relaxation can occur.

4.6. Modeling Viscoelastic Behavior with Prony Series and Bailey Norton Law

The viscoelastic behavior of soft biological tissues can also be simulated with Prony series and Bailey Norton Law. The constitutive equation using Prony series can be expressed as;

$$\sigma = \int_0^t E_R(t, \varepsilon) \frac{d\varepsilon}{dt} dt \quad \text{.....(91)}$$

where; $E_R(t) = k_0 + \sum_{i=1}^{l} k_i\, e^{-t/\tau_i}$ linear elastic

and $E_R(t, \varepsilon) = k_0\, \varepsilon + \sum_{i=1}^{l} k_i\, e^{-t/\tau_i}$ nonlinear one

while the following equation shows the Bailey-Norton Law;

$$\dot{\varepsilon} = \dot{\varepsilon}_{cr} + \dot{\varepsilon}_{el} \quad \text{.....(92)}$$

where; $\dot{\varepsilon}_{cr} = A\, \sigma_{cr}^n\, t^m$ for creep

and $\sigma_{el} = E\, \varepsilon_{el}$ linear elastic

and $\sigma_{el} = E\, \varepsilon_{el}^2$ nonlinear elastic

Equations (91) and (92) have been used to simulate creep, stress relaxation, constant strain rate loading, and cycling loading. They can simulate the same viscoelastic behavior with different respective model parameter constants such as k_0, k_i, τ_i or A, m, n.

As a conclusion main advantages and disadvantages of modeling soft biological tissues with a viscoelastic constitutive equation can be summarized as follows:

Advantages:

- The real character of soft biological tissues is much closer to the viscoelastic behavior than the pseudo-elastic one, so it can be thought that modeling these tissues by treating them as viscoelastic will give the best result. However, it is not an advantage in fact, due to difficulties.
- The Voigt model is extremely good with modeling creep in materials.
- Kelvin model is more accurate than the Maxwell and Voigt models in predicting material responses.
- The linear elastic tensor-mass method allows fast (real-time) computation of nonlinear and viscoelastic mechanical forces and deformations for the simulation of biological soft tissues.
- Haut and Little equations are capable of handling nonlinear, time dependent and multi-dimensional stress and strain histories for both isotropic and anisotropic materials like soft tissues.
- Quasi-linear viscoelastic theory can be used to model the time-dependent and history-dependent viscoelastic behavior of many soft tissues.
- By taking into account the ramping phase of the experiment, the quasi-linear viscoelastic theory approach allows for viscoelastic properties to be determined independent of the strain rate applied.

Thus, the results obtained from different laboratories and from different tissues may be compared.

- The strain history approach based on the quasi-linear viscoelasticity enables us to fit the entire experiment, i.e., from the beginning of the ramping phase to the end of the stress relaxation.
- The strain history approach of the quasi-linear viscoelastic theory is able to estimate reasonable constants based on data with ramp time 1-2 orders of magnitude slower than previous studies.

Disadvantages:

- It is rather complicated to model the materials which are viscoelastic compared to elastic ones.
- Viscoelastic materials are distinguished from materials which are idealized as being purely elastic. They exhibit properties such as relaxation, creep and frequency-dependent stiffness and dissipative characteristics (Kaliske, 1997).
- When a material represented by any one of the basic viscoelastic models (Maxwell, Voigt, or Kelvin) is subjected to a cyclic strain, the hysteresis will not be insensitive to strain rate.
- The Maxwell model is unable to predict creep in materials based on a simple dashpot and spring connected in series.
- The Voigt model is much less accurate for relaxation.
- Viscoelastic materials show hysteresis in the stress-strain curve with the area of the loop being equal to the energy lost during the loading cycle.
- A limitation of the quasi-linear viscoelastic theory is based on a step change in strain which is not possible to perform experimentally.
- Since it is impossible to apply a step increase in strain, extensions are needed to be applied at relatively high rates.
- It is difficult to apply the quasi-linear viscoelastic theory approach, because it is hard to measure these high strain rates accurately

CHAPTER 5

HYPERELASTIC MODELING

Tissue deformation can be very large due to low tissue stiffness and lack of physical constraints. As a result, deformation modeling of such organs often requires a treatment, which reflects nonlinear behavior. Some scientists (Samani et al., 2004) described an inversion technique to infer the hyperelastic parameters of breast tissues and used these parameters to create nonlinear finite element tissue deformation models.

In order to model breast tissue deformation, a finite deformation formulation of elasticity is used where the geometry change in the tissue is assumed to be significant. Under static conditions, the equilibrium equations governing the tissue are;

$$\sum_{i,j=1}^{3} \frac{\partial \sigma_{ij}}{\partial x_j} + f_i = 0 \qquad \text{.....(93)}$$

where; σ_{ij} represents components of the stress tensor and f_i denotes the body forces. For strain definition, the deformation gradient $F = \partial x / \partial X$ is defined where the variables x and X are deformed and undeformed positions of a point p, respectively. Using $B = F.F^T$, the strain invariants can be defined as;

$$\begin{aligned} I_1 &= tr(B) \\ I_2 &= \frac{1}{2}\left(I_1^2 - tr(B.B)\right) \\ I_3 &= \det(F) \end{aligned} \qquad \text{.....(94)}$$

A constitutive equation for isotropic hyperelastic tissue undergoing finite strains can be obtained based on a selected strain energy function $U(I_1, I_2, I_3)$. By assuming breast tissue as isotropic incompressible material, there can be written a number of strain energy functions. The most broadly used one in modeling rubber can be simplified for tissue modeling as;

$$W = \sum_{i+j=1}^{N} C_{ij} (I_1 - 3)^i (I_2 - 3)^j \quad \text{.....(95)}$$

where; $N = 2$ is the most commonly used in rubber modeling; C_{ij} represent the hyperelastic parameters which characterize the intrinsic nonlinear elastic behavior of the tissue. The strain energy in equation (95) depends on the strain invariants I_1 and I_2 while it is independent of I_3 (because for incompressible materials $I_3 = 1/I_1 I_2$). This implies that the breast tissue is isotropic and incompressible. Based on the strain energy function *W,* the constitutive equation required for tissue deformation modeling can be obtained as follows;

$$\sigma = \frac{2}{\sqrt{I_3}} \left[\left(\frac{\partial W}{\partial I_1} + I_1 \frac{\partial W}{\partial I_2} \right) B - \frac{\partial W}{\partial I_2} B.B + I_3 \frac{\partial W}{\partial I_3} I \right] \text{.....(96)}$$

where; σ is the Cauchy's stress tensor (related to the deformed area) and *I* is the identity matrix. To calculate tissue displacements, equations (93) through (96) must be solved simultaneously. This is done numerically using the finite element method.

Tissue hyperelastic parameter calculation from force-displacement data which can be obtained from tissue indentation experiment is called an inverse problem. The aim here is to find a set of hyperelastic parameters such that the difference between the measured and calculated force-displacement data is a minimum. The force $F_c(C_{ij})$ is a function of the hyperelastic parameters C_{ij} and can be calculated using a nonlinear finite element model. The finite element represents a nonlinear function

relating the forces $F_c\left(C_{ij}\right)$ resulting from the tissue indentation simulation to the unknown hyperelastic parameters C_{ij}. This problem can be classified as a constrained nonlinear least squares problem as follows;

$$R\left(C_{ij}\right) = F_e - F_c\left(C_{ij}\right) \qquad \text{minimize} \qquad f\left(C_{ij}\right) \text{.....(97)}$$

$$f\left(C_{ij}\right) = \frac{1}{2} R^T\left(C_{ij}\right).R\left(C_{ij}\right) \qquad \text{subject to} \qquad L_l \le L\left(C_{ij}\right) \le L_u \text{ .....(98)}$$

where; F_e is the experimental force data; $L\left(C_{ij}\right)$ is a linear operator and L_l and L_u are lower and upper bounds of L, respectively. If a polynomial strain energy function (equation (95)) is used, given that $E = 6\left(C_{10} + C_{01}\right)$ for incompressible materials having infinitesimal strains, the following constraints can be used;

$$E_l \le 6\left(C_{10} + C_{01}\right) \le E_u \text{ .....(99)}$$

where; E_l and E_u are the lower and upper bound estimates of the tissue Young' s modulus.

In this study, to measure the hyperelastic parameters of breast tissues, a measurement system was developed that indents an unconstrained block of the tissue while measuring the resulting forces. Breast tissue specimens obtained from women who underwent breast reduction surgery were obtained and transported to the measurement laboratory within two hours after the surgery.

To calculate the hyperelastic parameters of the tissue specimens, the force-displacement experimental data obtained from the indentation test were inverted using an inversion technique. Unloading portion of the experiment was ignored in calculating the hyperelastic parameters. Using the loading portion as a representative of the force data $\left(F_e\right)$, the inversion technique was used to calculate the hyperelastic parameters of the tissue specimens.

The calculated hyperelastic parameters were found to be acceptable to calculate similar stress distributions as experiments. Fitting between the experimental results and calculated ones is passable. Although the focus of this research is the hyperelastic properties of the breast tissue, the proposed technique can be applied for other biological soft tissues as the prostate or liver.

CHAPTER 6

POROELASTIC MODELING

Poroelasticity is a method of modeling fluid flow within elastic porous materials, where the flow of the fluid and the deformation of the solid matrix are coupled. This has application to many fields in science and engineering such as soil consolidation, filtration and biological soft tissue modeling including cartilage, skin, myocardium and arterial walls (Berry et al., 1999).

The theory of poroelastic materials is a model for fluid infiltrated porous solids. The basic ideas underlying the theory of porous elastic materials are that the pore fluid pressure contributes to the total stress in the porous matrix medium and that the pore fluid pressure alone can strain the porous matrix medium. There is fluid movement in a porous medium due to differences in pore fluid pressure created by different pore volume strains associated with the mechanical loading of the porous medium (Cowin, 2004).

Bone is the main constituent of the skeletal system and differs from the connective tissues in rigidity and hardness. In the case of bone tissue the deformation of the porous medium has a significant effect on the movement of pore fluid, but the low pore fluid pressure has only a small effect on the deformation of the whole bone (Cowin, 2004).

Poroelastic constitutive equations are generally used for hard materials or for soft biological materials but in *in vitro* conditions. Consequently, the poroelasticity approach has not been used much for in vivo soft biological tissue modeling due to difficulties in determining the model parameters.

CHAPTER 7

ALTERNATIVE MATERIAL FORMULATIONS

Biological materials are complex microstructurally and complex in their mechanical behaviors. To describe them with a single robust model is a formidable challenge (Oza et al., 2006). The goal of this study is to find the most appropriate material law to simulate hysterisis, preconditioning (Mullin's effect) creep and relaxation behaviors of soft biological tissues with a reasonable size equation and with the same coefficients or if not possible with minimum possible change in coefficients. Therefore it worths examining other material formulations as well which have similar mechanical response to that of soft tissues.

7.1. Thermoplastic Elastomers

Thermoplastic elastomers are polymer materials that combine mechanical properties of vulcanized rubber (large deformations with elongations to break up to $\lambda = 10$ and higher) with high-speed processability and recyclability (Drozdov et al., 2006). Uni-axial tensile tests with constant strain rates at moderate finite deformations, creep and relaxation tests were applied at room temperature. A constitutive model is developed for the viscoelastic response of thermoplastic elastomers by treating them as incompressible heterogeneous transient network of strands.

Here is a summary of testing protocol and modeling:

Tensile relaxation tests were carried out at the elongation ratios $\lambda = 1.2$, 1.4 and 1.6. In each relaxation test, a specimen was stretched with a constant cross-head speed of

50 mm/min up to a given elongation ratio λ that was preserved constant during the relaxation time (the relaxation time $t_r = 20$ min was used in all experiments).

$$\bar{\sigma}(t) = 1 - \kappa \int_0^{\infty} \left[1 - \exp\left(-\Gamma(\upsilon) t\right)\right] p(\upsilon) d\upsilon \quad \text{.....(100)}$$

where; $\bar{\sigma}(t) = \sigma(t) / \sigma_0$ is the dimensionless tensile stress with *t* as the time and σ_0 as the stress at the beginning of the relaxation process; κ is a constant; $\Gamma(\upsilon) = \exp(-\upsilon)$ with υ as the dimensionless activation energy; and $p(\upsilon)$ is another function calculated by the following formula;

$$p(\upsilon) = \begin{cases} p_0 \exp\left[-\dfrac{(\upsilon - V)^2}{2\Sigma^2} \right] & for \quad \upsilon \geq 0 \\ 0 & for \quad \upsilon < 0 \end{cases} \quad \text{.....(101)}$$

where; V and Σ are constants to be adjusted; and p_0 is determined by the normalization condition, $\int_0^{\infty} p(\upsilon) d\upsilon = 1$.

Tensile creep tests were performed at the engineering tensile stresses σ = 3.3 and 4.2 MPa. In each creep test, a specimen was stretched with a constant cross-head speed of 50 mm/min up to a given longitudinal stress σ that was preserved constant during the test (the creep time $t_c = 20$ min was chosen).

$$\frac{dr}{dt}(t) = \frac{1 - A(t)}{\Lambda_p(t)} \frac{d\lambda}{dt}(t) \quad \text{.....(102)}$$

where; $r(t) = \lambda(t) / \Lambda_p(t)$ with $\lambda(t)$ as elongation ratio and $\Lambda_p(t)$ as another function to be calculated.

As seen in the formulations, there are functions in functions in almost all the equations. This property makes the estimation of constants rather difficult. Also, there are many thermodynamic coefficients to be known. For example, the dimensionless activation energy, υ is calculated by the formula $\upsilon = \omega / (k_B T_0)$, where; k_B is Boltzmann' s constant; T_0 is the reference temperature and ω is the activation energy. To calculate the activation energy, one also needs two more constants called *frequency factor* and *rate coefficient*. But these constants are not known for the soft tissues, so these constants have to be estimated first.

Another disadvantage of this formulation is the fact that it is based on the tensile tests. Creep and relaxation behaviors are simulated by using tensile experimental data. Since our study is based on compression tests which differ from tensile tests done on the soft tissues, these method is seen to be inappropriate for our formulation.

7.2. Isothermal Nonlinear Viscoelastic Response in Polymers

This model is based on the concept of transient networks, and treats a polymer as a system of nonlinear elastic springs, which break and emerge due to micro-Brownian motion of chains. The breakage and reformation rates for those springs are assumed to depend on some strain energy density (Drozdov, 1998). All those springs are assumed to be parallel to each other for simplicity. So, the stress would be the sum of all the stresses on individual springs.

The viscoelastic behavior is described by an integral constitutive equation, where the relaxation functions satisfy partial differential equations with coefficients depending on the strain history. Adjustable parameters of the model are found by fitting experimental data for a number of polymers in tension at strains up to 400 percent.

This formulation was mainly performed to estimate the effect of strain on relaxation time. It has been proved that increasing strain causes relaxation time to decrease but this feature is out of our scope. Also, stress-extension rate curves are simulated

which is not our goal in this study, either. Together with these factors, the fact that the tensile experiments are applied on the specimen makes this formulation inappropriate for our study.

7.3. Rabotnov's Equation for Materials with Memory

There are some models for nonlinear time-dependent materials (called as materials with memory) that can also be used for relaxation and creep simulations. Development of these formulations can be summarized as follows:

The material (polyoximethylene) was tested at creep conditions with three levels of stress and at relaxation conditions with three levels of strain (Suvorora et al., 2003). Nonlinear equation was constructed by assuming that all the nonlinearity may be gathered on the left hand side of the following equation;

$$\varphi(\varepsilon) = \sigma(t) + \int_0^t K(t-\tau)\sigma(\tau)d\tau \quad \text{.....(103)}$$

where; $\varphi(\varepsilon)$ may be interpreted as the instantaneous stress-strain curve (curve of instantaneous deformation).

Experiments on creep were carried out at three levels of stress σ^* = 74. 70 and 66 MPa. The material was first loaded with a constant stress rate of $\dot{\sigma}$ = 0.8 MPa/s up to σ^* and the stress was then kept at this value. For this procedure, the final aspect of equation (103) appears as;

$$\varphi(\varepsilon) = \sigma^* + \frac{k\sigma^*}{(1-\alpha)(2-\alpha)}\left[t^{1-\alpha} - (1+\alpha)(t-t^*)^{1-\alpha}\left(1-\frac{t^*}{t}\right)\right] \quad \text{.....(104)}$$

where; t^* is the beginning time of creep; k and α are constants to be estimated. Testing data (the time at which the desired strain is reached) from three different stress levels are substituted into this equation and unknown constants are estimated.

Experiments on relaxation, ε^* = constant, were performed for three values of ε^*: 3, 6, 9 %. To reach these values of ε^*, the specimens were loaded with constant loading rate (corresponding times t^* = 1.25, 2.5 and 3.75 minutes). On reaching ε^*, these values were kept constant for the rest of the test. Considering the relaxation behavior of the material at long times, $t \geq t^*$, equation (103) can finally be written as;

$$\sigma = \varphi(\varepsilon)\left[1 - \beta \int_0^t \exists_\alpha(-\beta, t-\tau)\, d\tau\right] \qquad \text{.....(105)}$$

where;

$\beta = k\ \Gamma(1-\alpha)$ with Γ as the gamma-function;

$$\exists_\alpha(-\beta, t) = \sum_{n=0}^{\infty} \frac{(-\beta)^n\, t^{n(1-\alpha)-\alpha}}{\Gamma[(1-\alpha)(n+1)]} \qquad \text{.....(106)}$$

Calculation of equation (105) can be performed either with the help of the tables of the $\exists_\alpha$ integral functions, or with one of the symbolic computation softwares.

By this method one can use the same constitutive equation with the same set of parameters to model various types of loadings. But there are two different equations for two different cases, creep and relaxation. There is no interrelation between them. Since our aim is to simulate creep and relaxation behaviors with one material formulation, this method does not seem to be appropriate for our study.

7.4. Polymers under Quasi-Static and Dynamic Loading

Polymers are known to exhibit time-dependent mechanical behavior and also display highly nonlinear response during loading and unloading like biological soft tissues. Further, unlike metals, significant relaxation and creep phenomena may be observed even at room temperature. The mechanisms of inelastic deformation of polymers, which are explained by considering the molecular structure of the material, are different from that of metals. For example, the molecular chain flexibility and entanglement is believed to be related to inelastic deformation of polymers. This will result in a different response in tension and compression. Therefore, some of the constitutive modeling of polymeric materials are based on characteristics of micro-structure of polymeric materials. One of the drawbacks of this method is that the developed models are complex and it is very complicated and time consuming to determine material parameters in such models (Khan et al., 2001).

Here is a summary of modeling a commercial polymer, polytetrafluoroethylene, at room temperature under various complex loading and unloading conditions.

In relaxation tests, the strain controlled constant strain rate loadings were interrupted by several relaxation segments both during the loading and the unloading periods. The engineering strains, or displacements, were held constant for several hours at different strain levels. The constant strain rate loading with the strain rate of 0.01/s was interrupted by relaxation segments by holding engineering strain, or displacement, constant for six hours at engineering strain levels of 0.0832 and 0.1832 both during loading and unloading. During these holding periods, it is observed that there is a significant amount of relaxation. There is clear evidence that the stress decreased during the relaxation segments during the loading, while the stress increased during the holding segment during the unloading (Khan et al., 2001).

In creep tests, the stress controlled constant stress rate loadings were interrupted by several creep segments. The engineering stresses, or loads, were held constant for several hours at different stress levels. The load controlled constant engineering

stress rate loading with the rate of 89 N/s was interrupted by several constant engineering stress segments. The controlled stress was held constant for six hours at engineering stress levels of 9.65 MPa, 14.82 MPa and 17.58 MPa during loading. During several 6-hour hold periods at constant stress, significant amounts of creep were observed, i.e. the strain increased by a fair amount during each constant engineering stress segments (Khan et al., 2001).

The viscoelastic deformation is represented by a Kelvin model (fig. 6a). It means that the stress is decomposed into rate dependent equilibrium stress (σ_e) in the spring μ_1 and the rate dependent overstress (σ_v) components in the spring μ_2 and the dashpot η, i.e. $\sigma = \sigma_e + \sigma_v$. The strain in the Maxwell element and in the elastic spring parallel to the element, are the same, denoted by ε_{ve}.

So, the governing equation of this model can directly be written as;

$$\sigma + \frac{\eta}{\mu_2}\dot{\sigma} = \mu_1 \varepsilon_{ve} + \frac{\eta}{\mu_2}(\mu_1 + \mu_2)\dot{\varepsilon}_{ve} \quad \text{.....(107)}$$

where; $\dot{\sigma}$ and $\dot{\varepsilon}_{ve}$ are the stress and viscoelastic strain rates, respectively.

The viscosity (η) is not constant and has been found to be a decreasing function of strain rate in polymers. It was assumed to be a function of both strain and stress in order to accurately represent observed behavior of polymers, given as;

$$\eta = \varepsilon_{ve}^{r} \frac{\eta_0}{\left(1 + \left(a\,\dot{\varepsilon}_{ve}\right)^2\right)^b} \quad \text{.....(108)}$$

where; *r, a, b and* η_0 are material constants. It can be seen from this equation that the viscosity increases with increasing strain. It should also be noted that the increasing strain rate causes viscosity to decrease.

Solution of equation (107) for relaxation by assuming $\varepsilon_{ve} = \varepsilon_0 = const.$ ($\dot{\varepsilon}_{ve} = 0$) yields;

$$\sigma = (\sigma_0 - \mu_1 \varepsilon_0) e^{-\frac{\mu_2 t}{\varepsilon_0^r \eta_0}} + \mu_1 \varepsilon_0 \quad \text{.....(109)}$$

where; σ_0 is the stress at the beginning of the relaxation process; t is relaxation time; ε_0 is the viscoelastic strain from which the relaxation started. When time tends to infinity, stress is tending to the equilibrium stress which is $\mu_1 \varepsilon_0$.

Solution of equation (107) for creep by assuming $\sigma = \sigma_0 = const.$ (i.e. $\dot{\sigma} = 0$) yields;

$$\varepsilon_{ve} = \frac{\varepsilon_{ve}^n \eta_0}{\left(1 + (a \varepsilon_{ve})^2\right)^b} \left(\frac{\mu_1 + \mu_2}{\mu_1 \mu_2} \dot{\varepsilon}_{ve} \right) - \frac{\sigma_0}{\mu_1} \quad \text{.....(110)}$$

Modeling of relaxation and creep were done by a three-element Kelvin material. Experimental data could not be simulated well by this model, because it is believed that there is not enough parameter in this model to follow the material response accurately. A spring dashpot model with more elements is expected to be developed.

CHAPTER 8

SOFT TISSUE MECHANICAL FINITE ELEMENT MODELS

So far, almost all material models, either specifically developed for soft tissues or may be used to model the soft tissues as well available in the literature were analyzed. After each chapter, advantages and disadvantages of the models and methods presented were summarized. As a result, what can be seen is the fact that the most meaningful and successful models are the ones which rely on the theory of quasi-linear viscoelasticity (QLV). Because, as mentioned before;

- The real character of soft biological tissues is much closer to the viscoelastic behavior; they show relaxation, creep, preconditioning and hysteresis behaviors which are typical characteristics of viscoelastic materials.
- Viscoelasticity can be used under both isotropic and anisotropic conditions.
- By taking into account the ramping phase of the experiment, the quasi-linear viscoelastic theory approach allows for viscoelastic properties to be determined independent of the strain rate applied. Thus, the results obtained from different laboratories and from different tissues may be compared.
- For the time dependent and history dependent analysis of soft biological tissues, the best responses in the literature are the ones obtained by using the theory of QLV.

By taking the QLV as a basis, three different material models for the simulation of mechanical behavior of soft biological tissues may be constituted, which are;

1. QLV modeling by assuming soft tissue as an isotropic material.
2. Enhanced QLV modeling by assuming soft tissue as an isotropic material.

3. Enhanced QLV modeling by assuming soft tissue as an anisotropic material.

With the increasing number of these methods, modeling becomes more complicated, but the same amount accurate. Third one gives more accurate results than second one, because it assumes the soft tissue as an anisotropic material, and soft tissues are anisotropic in real life because of the structure of its constitutive elements (collagen fibers, muscles, skin, etc.). However, second one gives more accurate results than first one, because it also takes strain into account. The first one is only able to simulate the stress relaxation and the creep behaviors and only depends on time.

8.1. QLV Modeling by Assuming Soft Tissue as an Isotropic Material

As mentioned in Section 4.5, the QLV theory has been frequently used to model nonlinear time-dependent and history-dependent viscoelastic behavior of many soft tissues. According to this theory, the stress history equation can be written as;

$$\sigma(t)=\int_0^t G(t-\tau)\frac{\partial\sigma^e[\varepsilon(\tau)]}{\partial\tau}d\tau \qquad (112)$$

where; $\sigma(t)$ is the 2^{nd} Piola-Kirchoff stress depending on the time *t;* $G(-)$ is the reduced relaxation function (see Appendix D) and $\sigma^e(-)$ is the elastic stress function. The reduced relaxation function and the elastic stress function are;

$$G(t)=\frac{1+C\left[E_1(t/\tau_2)-E_1(t/\tau_1)\right]}{1+C\,\ln(\tau_2/\tau_1)} \qquad (113)$$

$$\sigma^e[\varepsilon(\tau)]=A\left(e^{B\varepsilon}-1\right) \qquad (114)$$

where; *C,* τ_1 and τ_2 are material parameters related to the level of viscous damping and the strain rates over which hysteresis is nearly constant, respectively; $E_1(-)$ is

the first exponential integral function; A and B are material parameters for instantaneous stress response (for the full derivation of the constitutive equations see Appendix A).

8.1.1. Finite Element Modeling

This work was aimed to identify the soft tissue material properties using in vivo indentation data by inverse finite element method. This simulation was done by using the finite element software MSC.Marc.Mentat 2005r2. The material library of this software does not contain such special and advanced material models therefore proposed material model was implemented by a user subroutine. Consequently, writing the correct subroutine constitutes the most important and time consuming part of this simulation (see Appendix I for the code of the subroutine). The user subroutine template *hypela.f* (see Appendix H) supplied with the software has been used as a basis and modified as given in Appendix I. This subroutine was written and compiled during simulation with the software Digital Fortran 6.0. The parameters in this subroutine were given casually (similar to the ones in the literature) and the subroutine has been checked with a simple three dimensional finite element model whether it works correctly (see Appendix J). The values of these parameters will be estimated by using the in vivo indenter data during this study.

After the verification of the user subroutine, the finite element model was created by using the software MSC.Patran 2004. While creating the model, there are some rules must be obeyed.

1. The model should have the capability of being indented up to 50 % of its thickness to be able to simulate experimental conditions.
2. The displacements and principal strains on the nodes far from the deformation area must be at most the 3-4 % of the maximum values for this model. The displacements and strains smaller than that percentage are

accepted to be zero during the simulation processes therefore the material may safely be truncated after this point.

3. The tissue under the indenter tip must have a fine mesh to simulate contact with indenter tip as well as to be able to model high stress and strain gradients that may exist here.
4. The number of elements should be large enough to model the actual deformation accurately yet, should be limited to have reasonable run time.

The axes of the ellipsoid indenter tip are (x-y-z) 8-2-2 milimeters. These are constant and not changed during the model creation processes.

A. Modeling of tissue with MSC.Patran has firstly started with the following dimensions (x-y-z):

Tissue size (mm) : 20-8-20
Fine mesh region (mm) : 10-2.5-2.5

This geometric model has been created with MSC.Patran and imported into MSC.Mentat to define other properties. The boundary conditions have been defined as fixed displacement along three mutually perpendicular coordinates at the bone contact and symmetry planes in x and z directions (i. e. fixed displacement along the normal of the symmetry planes) since this is a quarter model of the tissue (Figure 12).

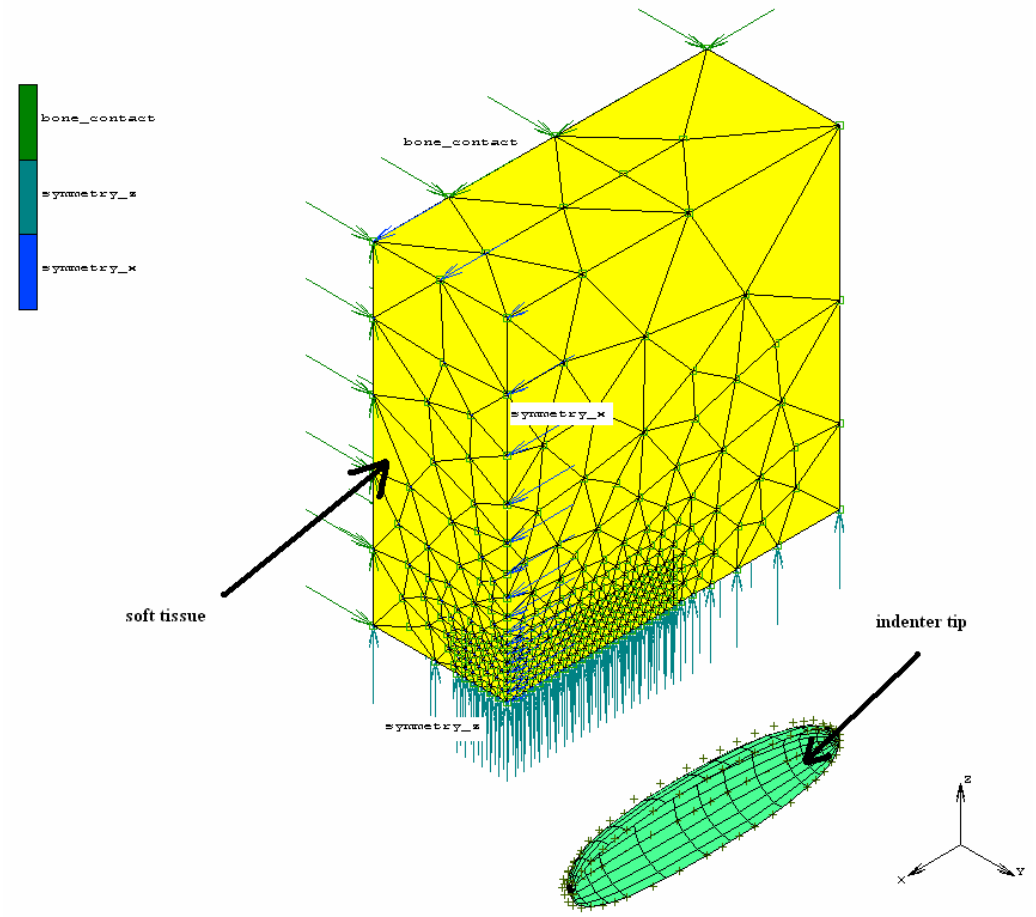

Figure 12 – Boundary Conditions of Model A

Material properties have been chosen as hypoelastic for all materials to be able to use the subroutine written on hypela.

For the initial evaluation of the model proposed, the contact bodies; the surface of the indenter tip has been chosen as rigid that has a velocity (and also an approach velocity) of 1mm/s in –y direction. The foremost elements of the tissue (in fine mesh zone) have been chosen as deformable body and contact situation has been set to *touching*. Total loadcase time has been set to 4 seconds in 80 equal time steps (increments). So, the rigid indenter tip will indent to the tissue 4 milimeters in total.

Large displacement and large strain-total Lagrange analysis options have been chosen and the model has been submitted with the user subroutine.

When the program was finished sucessfully, the postprocessor has been opened and the model has been investigated. The main problem seen in this submission was the unexpected deformation of the elements in the fine mesh zone behind the indenter tip. This can be seen in Figure 13. Some of the elements in this zone could not deform any more after the 59th increment. These elements are seen in light color behind the indenter tip in Figure 13. In this figure, the colors represent the magnitude of deformation. In ideal case, there should be a progressive increase of the deformation as seen in Figure 14. Figure 13 shows the elements behind the indenter tip that could not be deformed after 59th increment of the analysis.

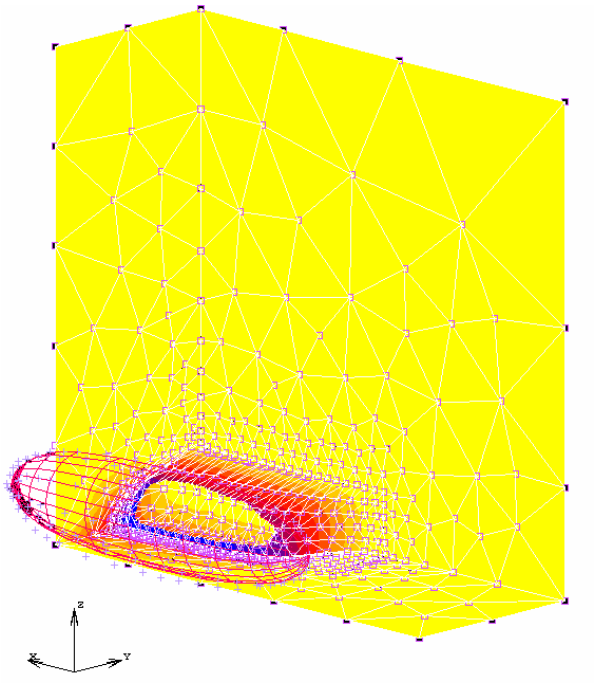

Figure 13 - Unexpected Deformation in the Fine Mesh Zone of Model A

To rectify this situation, number of deformable contact elements has been increased in the direction of the rigid body motion. More elements have been chosen as deformable and the model has been submitted again.

When analyzed, this unexpected deformation observed in the previous model seemed to disappear. As seen in Figure 14, there is no light colored element behind the indenter tip which represents the unexpected deformation.

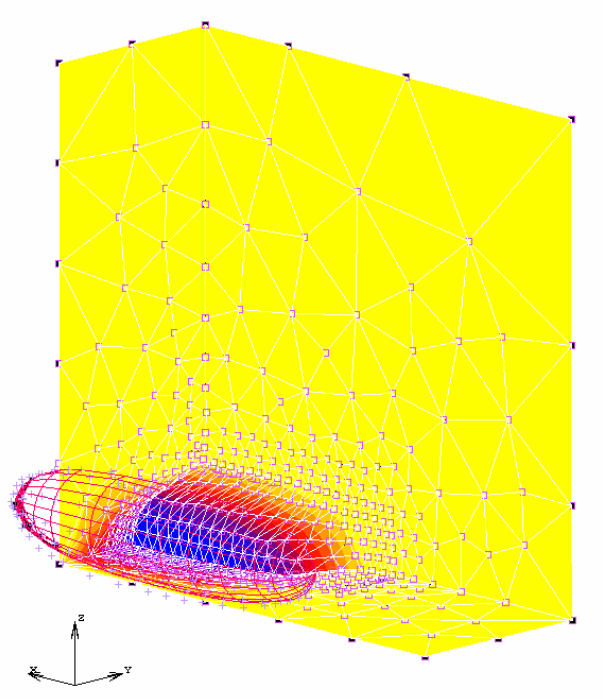

Figure 14 – Rectifying the Unexpected Deformation in the Fine Mesh Zone of Model A

As seen in Figure 14, there is a sudden deformation change along the z axes. The reason of this situation is the length of fine mesh zone in the z direction. To rectify this situation the fine mesh zone has been remodeled slightly larger in z direction

(Figure 15). It could not be enlarged very much not to increase the number of elements in the model that causes it to work very slowly.

B. To decrease the sudden increase in the deformation along the z axis, the model has been modified with the following dimensions (x-y-z):

Tissue size (mm) : 20-8-20
Fine mesh region (mm) : 10-2.5-3

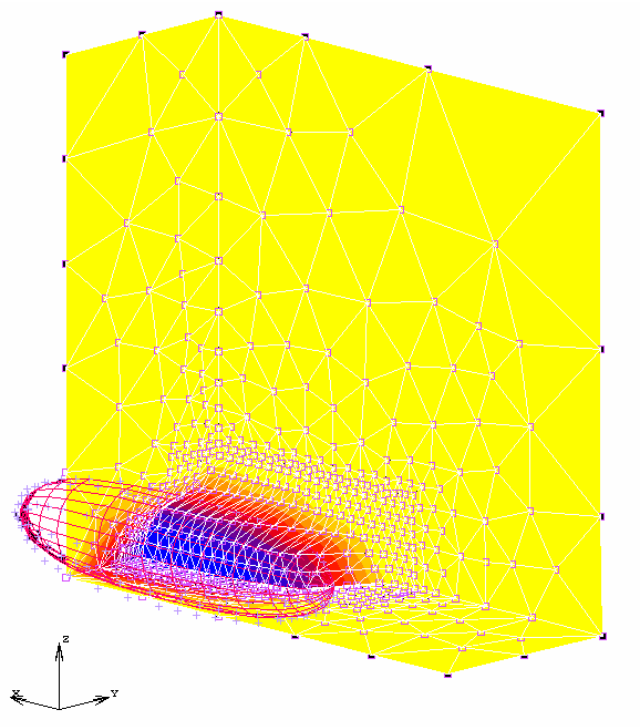

Figure 15 – Increased Fine Mesh Length of Model B in z Direction

By examining Figure 15, one can see that the fine mesh zone is larger in z direction, and so, the deformation increase in that direction is more progressive. This is the most appropriate form of the fine mesh zone. Making it larger causes the model to

run rather slowly. Surely, the best way is creating that area as large as possible and using the elements as small as possible to obtain more accurate results. But under technological constraints, one has to find the optimum model for simulation processes.

As mentioned before, the displacements and principal strains on the nodes far from the deformation area must be at most the 3-4 % of the total values. The displacements and strains smaller than that percentage are accepted to be zero during the simulation processes. In this model, two key nodes (marked in Figure 16) have been analyzed whether they have displacements and strains under desired limits. The results are given in Table 1.

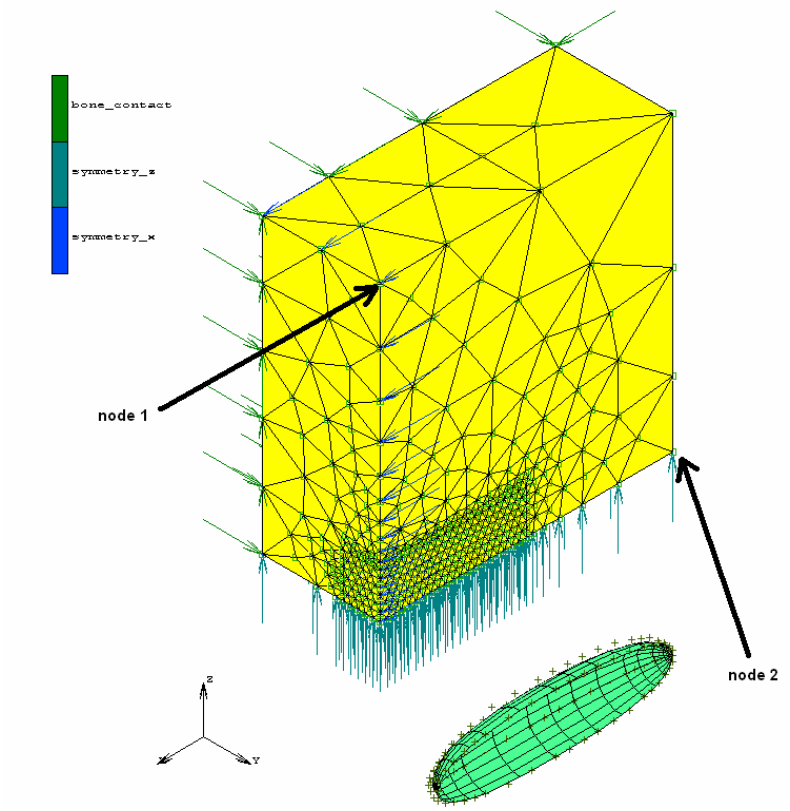

Figure 16 – Nodes to be Analyzed

Table 1 – Displacement and Principal Strain Values at the Given Nodes for Model B

$Node Number$	***1***	***2***
$Max. Displacement\,(mm)$	6.653E-2	3.089E-1
$\left(\frac{Max. Displacement}{Max. Displacement\ in\ the Model}\right) x100$	1.663 %	7.723%
$Max. Principal\ Strain$	8.324E-3	4.595E-2
$\left(\frac{Max. Principal\ Strain}{Max. Principal\ Strain\ in\ the\ Model}\right) x100$	0.855 %	4.722 %

As seen in Table 1, the values of principal strains and displacements are under the limits at node 1. But the values of displacements and principal strains could not stay under the limits of 3-4 % at node 2. For example the displacement at the node 2 is 7.723 % of the maximum value in the model. These values are not acceptable and so, the model must be enlarged in x and z directions. The enlargement in the x direction should be more, because the values at the node 2 on the x-axis are deviating from the limits more than the values at the node 1 on the z-axis. As a result, one more model has been created by multiplying the lengths of z-axis with 2 and x-axis with 2.5.

C. To decrease the values of displacements and strains at the nodes mentioned before, the new model has been created with the following dimensions (x-y-z) (Figure 17);

Tissue size (mm) : 50-8-40
Fine mesh region (mm) : 10-2.5-3

As seen in Figure 17, this tissue is larger than the previous ones. Now, the displacements and principal strains can be checked whether they pass the limits. The results are presented in Table 2.

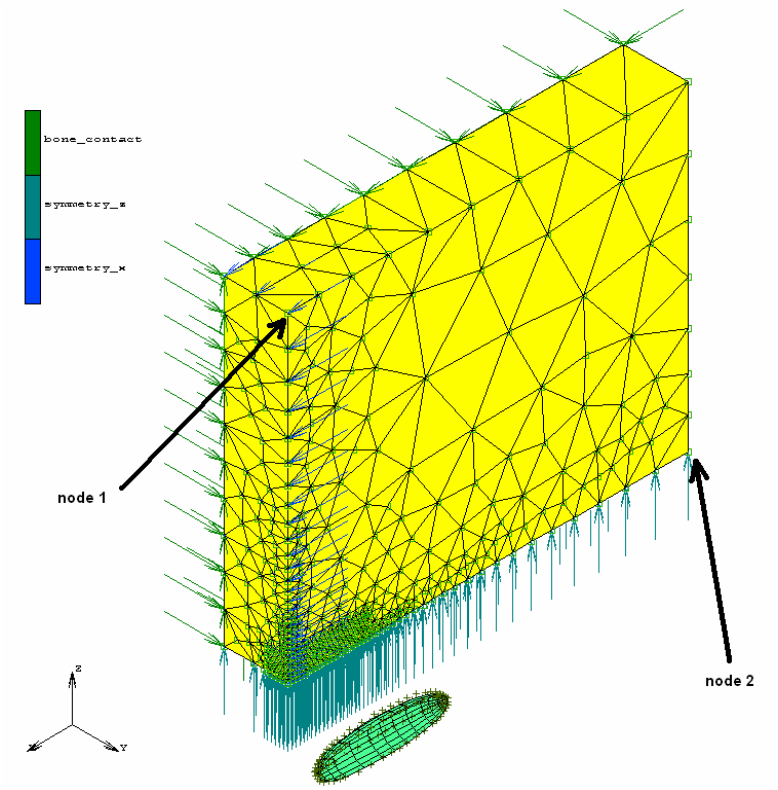

Figure 17 – The Finite Element Model for Model C

Table 2 – Displacement and Principal Strain Values at the Given Nodes for Model C

Node Number	***1***	***2***
Max. Displacement (mm)	3.162E-2	1.565E-2
$\left(\frac{Max.Displacement}{Max.Displacement\ in\ the Model}\right)x100$	0.791 %	0.391 %
Max. Principal Strain	5.678E-4	6.326E-3
$\left(\frac{Max.Principal\ Strain}{Max.Principal\ Strain\ in\ the\ Model}\right)x100$	0.056 %	0.619 %

As seen in Table 2, all the displacement and principal strain values are well below the limits of 3-4 %.

Before deciding this model as completely appropriate for the estimation of the parameters in the subroutine, two more tests have been applied on the model. In these tests, the indenter tip has been rotated 45° and 90° around y-axis and the simulation has also been applied in these orientations (Figures 18 and 19). The displacement and principal strain values at the marked nodes are given in Tables 3 and 4, respectively.

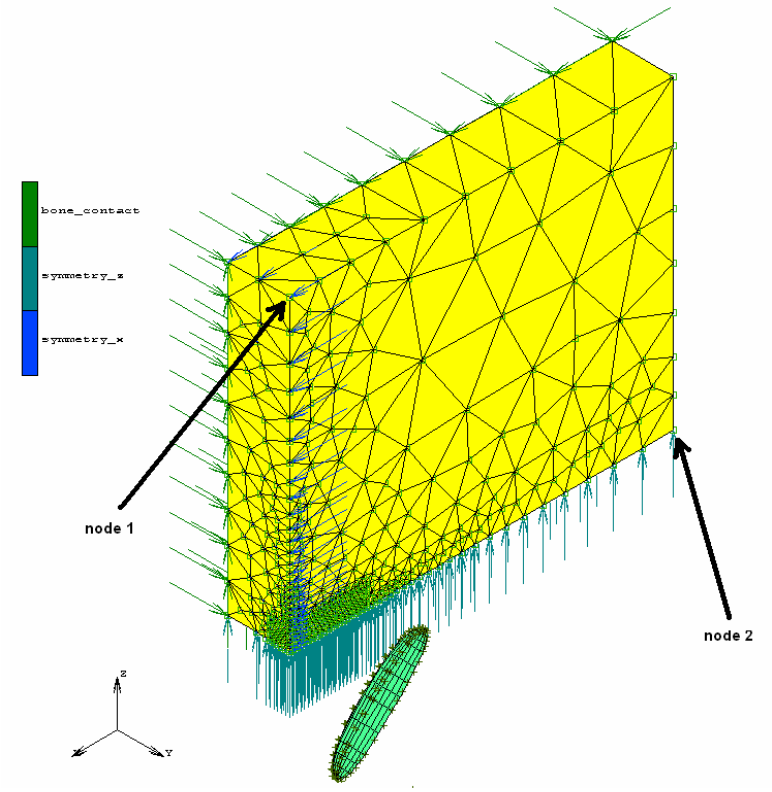

Figure 18 - The Finite Element Model of Model C with 45° Indenter Tip Orientation

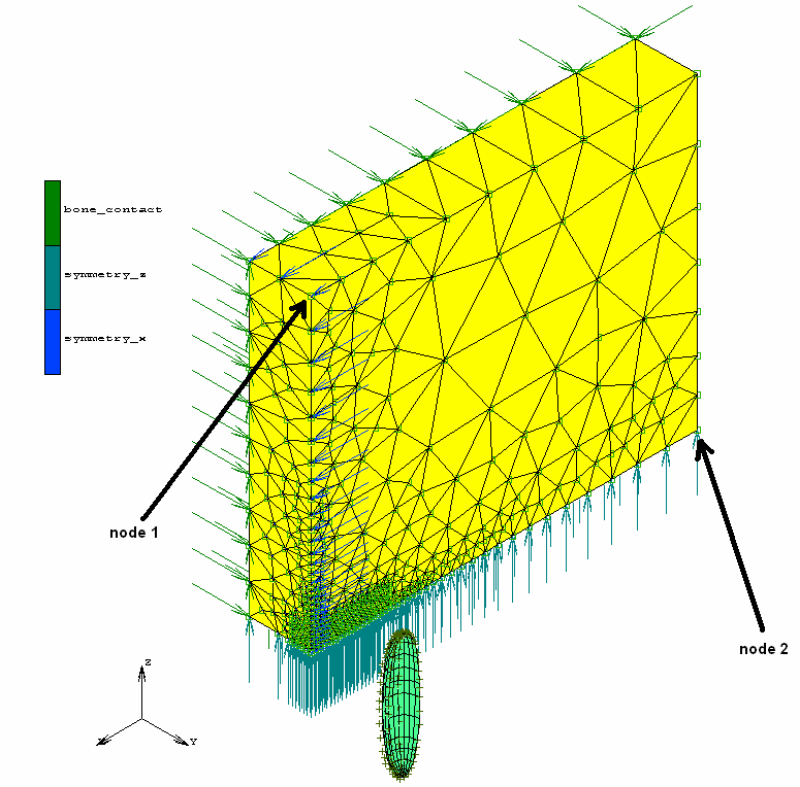

Figure 19 - The Finite Element Model of Model C with 90° Indenter Tip Orientation

Table 3 – Displacement and Principal Strain Values at the Given Nodes for Model C with 45° Indenter Tip Orientation

NodeNumber	***1***	***2***
Max.Displacement (*mm*)	6.401E-2	9.808E-2
$\left(\frac{Max.Displacement}{Max.Displacement\ in\ the Model}\right)x100$	1.6 %	2.452 %
Max.Principal Strain	2.114E-4	3.346E-3
$\left(\frac{Max.Principal\ Strain}{Max.Principal\ Strain\ in\ the\ Model}\right)x100$	0.022 %	0.345 %

Table 4 – Displacement and Principal Strain Values at the Given Nodes for Model C with 90° Indenter Tip Orientation

$Node Number$	***1***	***2***
$Max. Displacement\,(mm)$	1.125E-1	6.506E-2
$\left(\frac{Max. Displacement}{Max. Displacement\ in\ the Model}\right) x100$	2.813 %	1.627 %
$Max. Principal\ Strain$	2.546E-3	2.191E-3
$\left(\frac{Max. Principal\ Strain}{Max. Principal\ Strain\ in\ the\ Model}\right) x100$	0.214 %	0.184 %

In Tables 3 and 4 all the values of displacements and principal strains are seen to be under the limits. So, the tissue can be assumed to have zero displacements and strains at the end of the model axes and this model can be used for the estimation of the parameters in the user subroutine.

The last thing to do is to create different element sizes in the fine mesh region and comparing the results of indenter tip reaction force. The force should converge somewhere, and by also taking the submission time into account, the most appropriate one should be chosen for more accurate results.

So far, the edge length of 0.5 mm has been used for the elements in the fine mesh zone. Four more models will be created with the edge lengths of 0.3, 0.4, 0.6 and 0.7 mm and they will be compared for the best one. The time-indenter tip reaction force curves of these five models are seen in Figure 20.

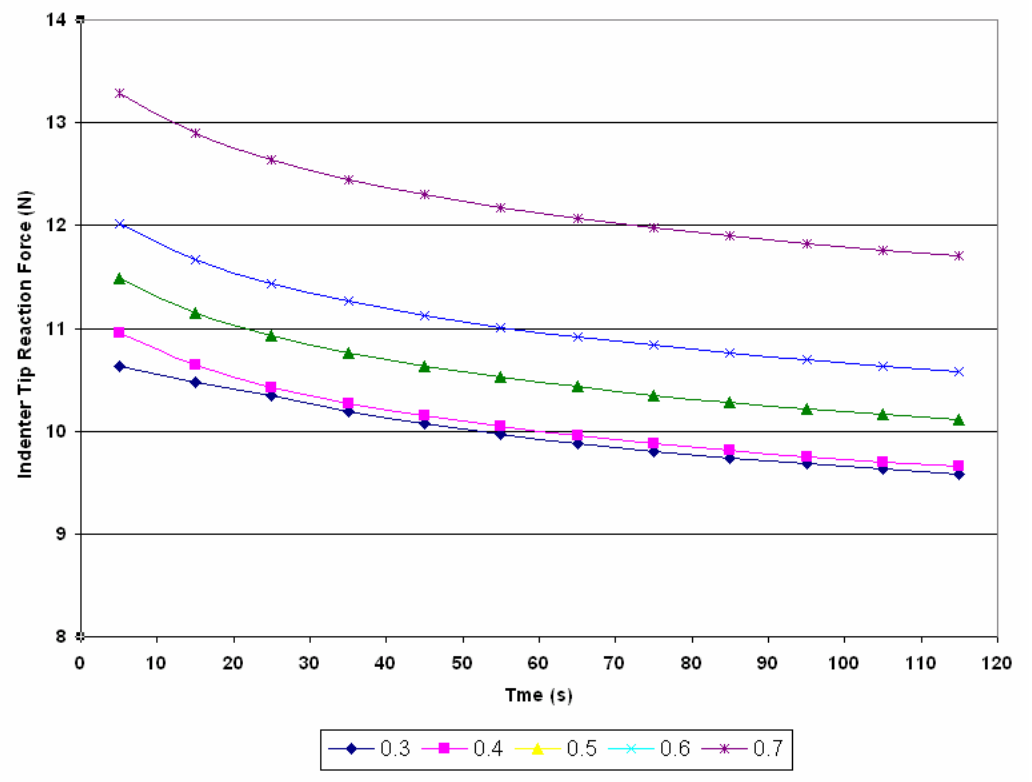

Figure 20 – Time-Indenter Tip Reaction Force Curves for Different Element Edge Lengths in the Fine Mesh Region

As seen in Figure 20, the force values are converging as the element edge lengths are getting smaller. In normal conditions, the best model to be used seems to be the one that has element edge length of 0.3 mm. But, choosing the element edge length of 0.4 mm. instead of 0.3 mm. decreases the submission time about % 60. Since there is not a large difference between these two, the element edge length of 0.4mm is suitable for that study.

As seen in equation (112), quasi-linear viscoelastic model only gives the response of stress with respect to time. But the change of stress with respect to strain is also needed to be able to model hysteresis (Figure 1). The following two methods have been modified from the basic quasi-linear viscoelasticity for this concept.

8.2. Enhanced QLV Modeling by Assuming Soft Tissue as an Isotropic Material

As mentioned before, to be able to obtain stress response with respect to time together with strain, the basic quasi-linear viscoelastic model must be enhanced. This modeling procedure which also assumes the soft tissue as an isotropic material as in the previous one is done as follows;

By using the one dimensional theory of quasi-linear viscoelasticity (presented in Chapter 8.1) the time dependent properties of soft tissue are directly incorporated into a hyperelastic model.

The second Piola-Kirchoff stress written for the one dimensional quasi-linear viscoelasticity, which includes time dependent effects, is (Bischoff, 2006);

$$\sigma_{QLV}(\varepsilon,t)=\int_0^t G(t-\tau)\frac{\partial\sigma^e}{\partial\tau}d\tau \quad \text{.....(115)}$$

where; $G(-)$ is the reduced relaxation function and $\sigma^e(-)$ is the elastic stress function. Note the subscript *'QLV'* to explicitly indicate that this stress includes time dependent behavior according to the quasi-linear viscoelastic theory.

For purposes here, the reduced relaxation function and the elastic stress function used are the same with the ones used in the previous chapter and given by the equations (113) and (114), respectively.

So, the stress versus strain and time relationships along the three material axes can be written as;

$$T_{11}=-p+\frac{a^2\varepsilon_1^2}{8\Lambda}\sigma_{QLV}(\varepsilon,t) \quad \text{.....(116)}$$

$$T_{22} = -p + \frac{b^2 \varepsilon_2^2}{8\Lambda} \sigma_{QLV}(\varepsilon, t) \quad \text{.....(117)}$$

$$T_{33} = -p + \frac{c^2 \varepsilon_3^2}{8\Lambda} \sigma_{QLV}(\varepsilon, t) \quad \text{.....(118)}$$

in which; $\sigma_{QLV}(\varepsilon, t)$ is the quasi-linear viscoelastic stress given by equation (115); p is hydrostatic pressure which is equal zero in our experiment conditions (for more detailed information about hydrostatic pressure, see Appendix E); *a, b* and *c* are unit cell aspect ratios and allow for anisotropic behavior; ε_1, ε_2 and ε_3 are principal strains along three material directions and Λ is fiber contour length determined by the equation;

$$\Lambda = \frac{a^2 + b^2 + c^2}{8} \quad \text{.....(119)}$$

Since isotropic conditions are dealt in this model, we can assume $b = c = a$, so equation (119) becomes;

$$\Lambda = \frac{a^2 + a^2 + a^2}{8} = \frac{3}{8} a^2 \quad \text{.....(120)}$$

With the substitution of this fiber contour length equation into equations (116), (117) and (118), the final form of the model is obtained as;

$$T_{11} = -p + \frac{\varepsilon_1^2}{3} \sigma_{QLV}(\varepsilon, t) \quad \text{.....(121)}$$

$$T_{22} = -p + \frac{\varepsilon_2^2}{3} \sigma_{QLV}(\varepsilon, t) \quad \text{.....(122)}$$

$$T_{33} = -p + \frac{\varepsilon_3^2}{3} \sigma_{QLV}(\varepsilon, t) \quad \text{.....(123)}$$

(The details of derivation of the constitutive equations are presented in Appendix B).

8.2.1. Finite Element Modeling

To be able to model the behavior of soft biological tissue, the parameters of the constitutive equation in the user subroutine must be estimated to simulate the experimental conditions (i.e. indenter reaction force-indenter displacement-time). These parameters are estimated by the inverse finite element modeling of the tissue and the indenter tip. Modeling was done by using the software MSC.Marc.Mentat 2005r2. Enhanced QLV is not available in the material library of the software either. So, a new user subroutine was written (Appendix K). The parameters in this subroutine were given casually and the subroutine has been checked with a simple two dimensional finite element model whether it works correctly (Appendix L). The real values of these material parameters will be estimated by using experimental data. After the verification of the user subroutine, the model was created by using the software MSC.Patran 2004. The rules in Chapter 8.1.1 applies to this model, too.

While modeling, the experiences gained in the previous sections have been used. The modeling has not been started by choosing only the foremost elements of the tissue (in fine mesh zone) as deformable not to cause an unexpected deformation given in Figure 13. Also, fine mesh zone has been selected larger in z direction not to cause sudden change in deformation in z direction as seen in Figure 14.

A. By taking these constraints into account, the modeling has been started with the following dimensions (x-y-z):

Tissue size (mm) : 20-8-20
Fine mesh region (mm) : 10-2.5-3

This geometric model has been created with MSC.Patran and imported into MSC.Mentat to define finite element model. The boundary conditions have been

defined as fixed displacement at the bone contact and symmetry planes in x and z directions (because this is a quarter model of the tissue) (Figure 21)

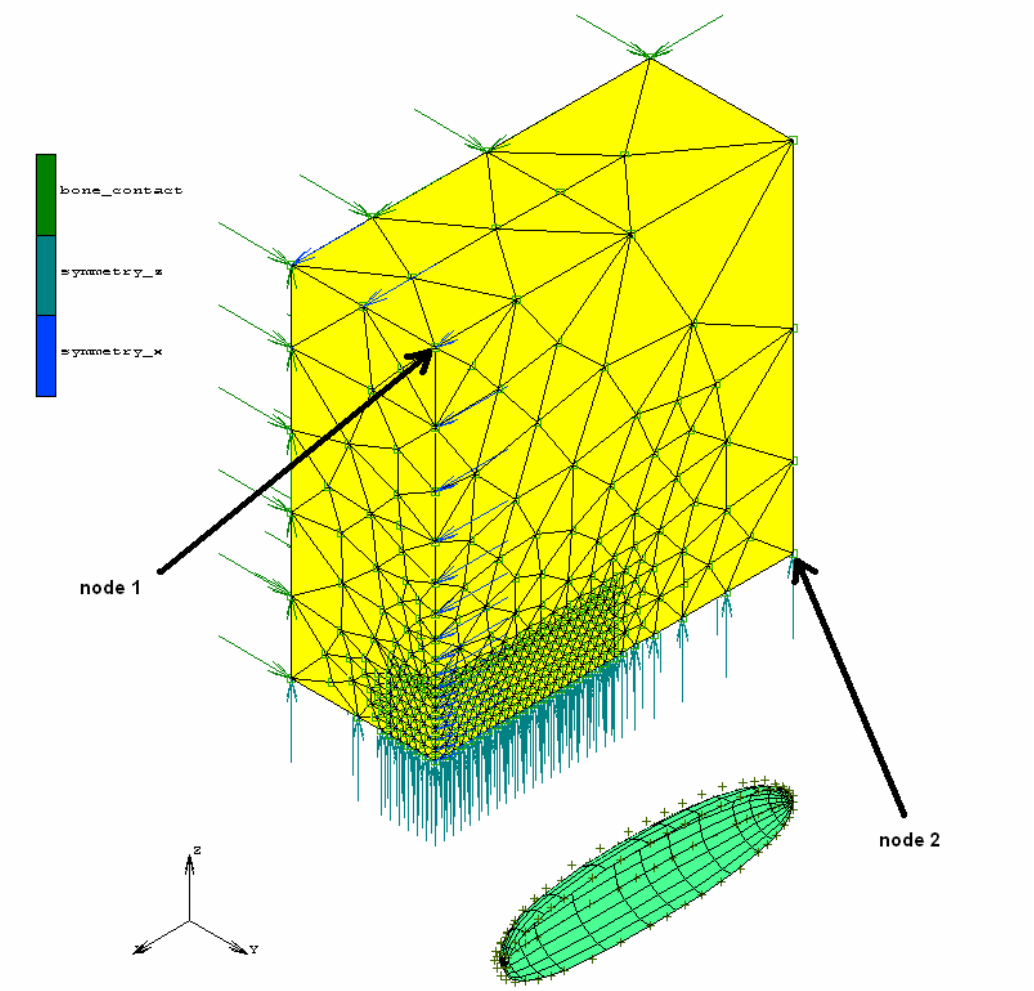

Figure 21 – Boundary Conditions of the Model

Material properties have been chosen as hypoelastic for all materials to be able to use the subroutine written on hypela. As the contact bodies; the surface of the indenter tip was chosen as a rigid body that has a velocity (and also an approach velocity) of

1mm/s in –y direction. The foremost elements of the tissue (in fine mesh zone) have been chosen as deformable and contact situation has been set to *touching*.

Total loadcase time has been set to 4 seconds in 80 equal time steps (increments). So, the rigid indenter tip will indent to the tissue 4 milimeters in total.

Large Displacement and Large Strain-Total Lagrange analysis options have been chosen and the model has been submitted with the user subroutine.

As mentioned before, the displacements, principal strains and principal stresses on the nodes far from the deformation area must be at most the 3-4 % of the total values. The displacements, strains and stresses smaller than that percentage are accepted to be zero during the simulation processes. In this model, two key nodes (marked in Figure 21) have been analyzed whether they have displacements, strains and stresses under desired limits. The results are presented in Table 5.

Table 5 – Displacement, Principal Strain and Principal Stress Values at the Given Nodes for Model A

$Node Number$	***1***	***2***
$Max. Displacement\,(mm)$	6.653E-2	0.3399
$\left(\frac{Max. Displacement}{Max. Displacement\ in\ the Model}\right) x100$	3.08 %	8.498%
$Max. Principal\ Stress\,(MPa)$	1.097E-6	1.976E-2
$\left(\frac{Max. Principal\ Stress}{Max. Principal\ Stress\ in\ the\ Model}\right) x100$	1.191E-6 %	0.021 %
$Max. Principal\ Strain$	8.324E-3	4.565E-2
$\left(\frac{Max. Principal\ Strain}{Max. Principal\ Strain\ in\ the\ Model}\right) x100$	1.755 %	5.703 %

As seen in Table 5, the values of principal stresses are under the limits but the values of displacements and principal strains could not stay under the limits of 3-4 % in some conditions. For example the maximum principal strain at the node 2 is 5.703 % of the maximum value in the model. These values are not acceptable and so, the model must be enlarged in x and z directions. The enlargement in the x direction should be more, because the values at the node 2 on the x-axis are deviating from the limits more than the values at the node 1 on the z-axis. As a result, one more model has been created by multiplying the lengths z-axis with 2 and x-axis with 2.5.

B. To decrease the values of displacements and strains at the nodes mentioned before, the new model has been created with the following dimensions (x-y-z) (Figure 17);

Tissue size (mm) : 50-8-40
Fine mesh region (mm) : 10-2.5-3

As seen in Figure 17, this tissue is much larger than the previous ones. Now, the displacements and principal strains can be checked whether they were within the limits. The results are presented in Table 6.

Table 6 – Displacement, Principal Strain and Principal Stress Values at the Given Nodes for Model B

$Node Number$	***1***	***2***
$Max. Displacement\,(mm)$	5.941E-2	0.1118
$\left(\frac{Max. Displacement}{Max. Displacement\ in\ the Model}\right) x100$	1.485 %	2.795 %
$Max. Principal\ Stress\,(MPa)$	9.543E-9	2.267E-5
$\left(\frac{Max. Principal\ Stress}{Max. Principal\ Stress\ in\ the\ Model}\right) x100$	5.441E-9 %	1.292E-5 %
$Max. Principal\ Strain$	3.864E-3	1.043E-2
$\left(\frac{Max. Principal\ Strain}{Max. Principal\ Strain\ in\ the\ Model}\right) x100$	0.383 %	1.034 %

As seen in Table 6, all the displacement, principal strain and principal stress values are within the limits of 3-4 %.

Before deciding this model as completely appropriate for the estimation of the parameters in the subroutine, two more tests have been applied on the model. In these tests, the indenter tip has been rotated 45° and 90° around y-axis and the simulation has also been applied in these orientations (Figures 18 and 19). The displacement, principal stress and principal strain values at the marked nodes are presented in Tables 7 and 8, respectively.

Table 7 – Displacement, Principal Strain and Principal Stress Values at the Given Nodes for Model B with 45° Indenter Tip Orientation

$Node Number$	***1***	***2***
$Max. Displacement\,(mm)$	0.1366	0.1222
$\left(\frac{Max. Displacement}{Max. Displacement\ in\ the Model}\right) x100$	3.415 %	3.055 %
$Max. Principal\ Stress\,(MPa)$	7.827E-8	8.756E-6
$\left(\frac{Max. Principal\ Stress}{Max. Principal\ Stress\ in\ the\ Model}\right) x100$	1.734E-8 %	1.939E-6 %
$Max. Principal\ Strain$	7.973E-3	9.874E-3
$\left(\frac{Max. Principal\ Strain}{Max. Principal\ Strain\ in\ the\ Model}\right) x100$	0.805 %	0.996 %

Table 8– Displacement, Principal Strain and Principal Stress Values at the Given Nodes for Model B with 90° Indenter Tip Orientation

$Node Number$	***1***	***2***
$Max. Displacement\,(mm)$	3.565E-2	7.367E-2
$\left(\frac{Max. Displacement}{Max. Displacement\ in\ the Model}\right) x100$	0.892 %	1.842 %
$Max. Principal\ Stress\,(MPa)$	2.507E-8	3.084E-6
$\left(\frac{Max. Principal\ Stress}{Max. Principal\ Stress\ in\ the\ Model}\right) x100$	4.023E-9 %	4.949E-7 %
$Max. Principal\ Strain$	1.516E-3	6.023E-3
$\left(\frac{Max. Principal\ Strain}{Max. Principal\ Strain\ in\ the\ Model}\right) x100$	0.126 %	0.499 %

In Tables 7 and 8 all the values of displacements, principal strains and principal stresses are seen to be under the limits. So, the tissue can be assumed to have zero displacements, principal strains and principal stresses at the end of the model axes and this model can be used for the estimation of the parameters in the user subroutine.

The last thing to do is to create different element sizes in the fine mesh zone and comparing the results of indenter tip reaction force. The force should converge somewhere, and by also taking the submission time into account, the most appropriate one should be chosen for more accurate results.

So far, the edge length of 0.5 mm has been used for the elements in the fine mesh zone. Four more models will be created with the element edge lengths of 0.3, 0.4, 0.6 and 0.7 mm and they will be compared for the best one. The time-indenter tip reaction force curves of these five models are seen in Figure 22.

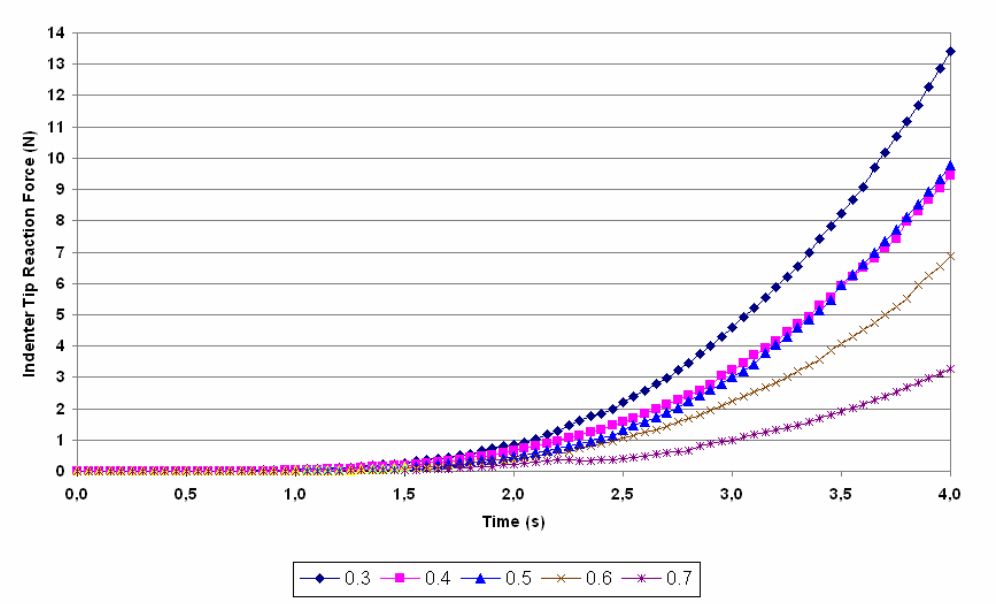

Figure 22 – Time-Indenter Tip Reaction Force Curves for Different Element Edge Lengths in the More Intensive Element Area

As seen in the Figure 22, the force values were converging until the edge length of 0.4 mm. The 0.7 mm. edge length elements are not suitable, because it does not give a good response as seen in the figure. This can be because of nonlinearities in the system, the difference between the two axes lengths of the fine mesh zone or the anisotropic shape of the indenter tip. The 0.3 mm. edge length elements are not converging and also it takes more than half an hour to conclude the submission of that model. As a result, the best edge length for the materials in the fine mesh zone can be chosen as 0.4 mm. In that model, there are 17612 elements and the submission takes about 14 minutes. This model is presented in Figure 23.

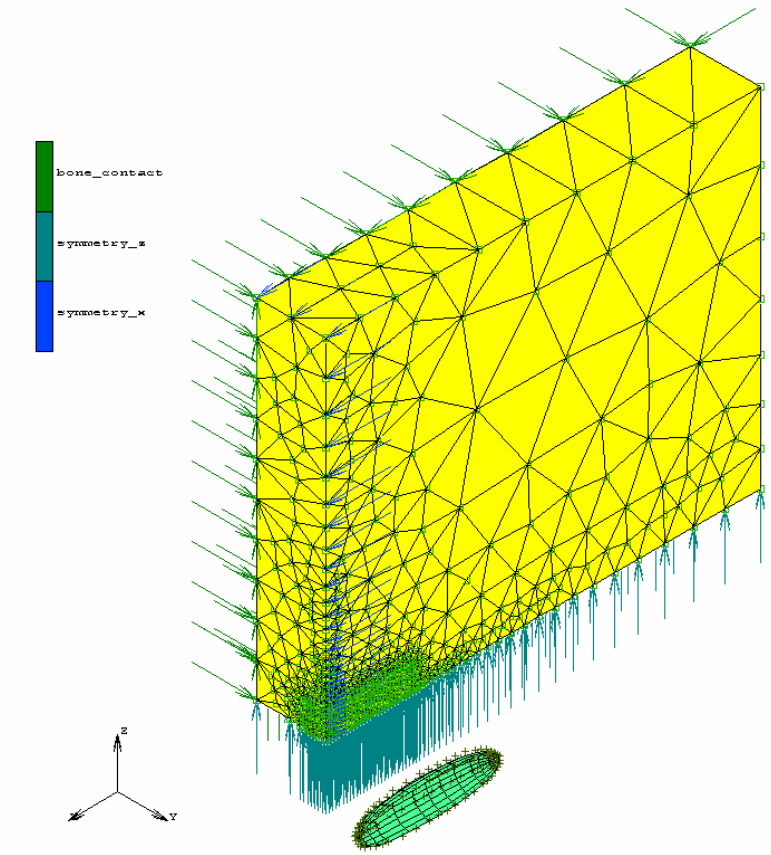

Figure 23- The Last Shape of the Model

As seen in the equations from (121) to (123), this modeling gives the response of stress with respect to time and strain. But there is no term modeling anisotropy despite the fact that soft tissues are much likely to be anisotropic. The following last model assumes soft tissues as anisotropic and enhances the model one more step.

8.3. Enhanced QLV Modeling by Assuming Soft Tissue as an Anisotropic Material

The final model within the context of this thesis is the one that is modified by using the model in Chapter 8.2. This time, the soft tissue is assumed to be anisotropic. There is a little change in the final form of the constitutive equations.

Representing constitutive equations of this model had been given in the previous section as;

$$T_{11} = -p + \frac{a^2 \varepsilon_1^2}{8\Lambda} \sigma_{QLV}(\varepsilon, t) \quad \text{.....(124)}$$

$$T_{22} = -p + \frac{b^2 \varepsilon_2^2}{8\Lambda} \sigma_{QLV}(\varepsilon, t) \quad \text{.....(125)}$$

$$T_{33} = -p + \frac{c^2 \varepsilon_3^2}{8\Lambda} \sigma_{QLV}(\varepsilon, t) \quad \text{.....(126)}$$

However, this time anisotropic conditions are dealt with and equation (120) cannot be used. Fiber contour length is calculated with equation (119). By taking the unit cell aspect ratios different from each other, one can also make this model consider the anisotropy in tissue. (The derivation of the constitutive equations is presented Appendix C).

8.3.1. Finite Element Modeling

The user subroutine developed to model anisotropy (Appendix M) consists of three more material parameters (for detailed information see Appendix C). The same procedure was used here for creating the model and compiling the subroutine. The parameters in the subroutine were assigned casually and the subroutine has been checked with a simple two dimensional finite element model whether it works correctly (Appendix N). The values of these material parameters will be estimated by using experimental data and inverse finite element modeling.

After the verification of the user subroutine, the model is created while considering the rules given in Chapter 8.1.1. However, there is one exception, instead of taking the limits of displacements, principal strains and principal stresses on the nodes far from the deformation area 3-4 % of the total values, for this model they were assumed to be under the limit of 1 % which is stricter than the previous ones.

While modeling, the experiences gained in Chapter 8.1.1 have been used here, too. The modeling has not been started by choosing only the foremost elements of the tissue (in fine mesh zone) as deformable not to cause an unexpected deformation as seen in Figure 13. Also, the fine mesh zone has been taken larger in z direction not to cause sudden change in deformation in z direction as seen in Figure 14.

A. By taking these constraints into account, the modeling has been started with the following dimensions (x-y-z):

Tissue size (mm) : 20-8-20
Fine mesh region (mm) : 10-2.5-3

The boundary conditions have been defined as fixed displacement in three mutually perpendicular at the bone contact and symmetry planes in x and z directions (because this is a quarter model of the tissue) (Figure 21)

Material properties have been chosen as hypoelastic for all materials to be able to use the subroutine hypela.

As the contact bodies; the surface of the indenter tip has been chosen as rigid body that has a velocity (and also an approach velocity) of 1mm/s in –y direction. The foremost elements of the tissue (in fine mesh zone) have been chosen as deformable body and contact situation has been set to *touching*.

Total loadcase time has been set to 4 seconds in 80 equal time steps (increments). So, the rigid indenter tip will indent to the tissue 4 milimeters in total.

Large displacement and large strain-total Lagrange analysis options have been chosen and the model has been submitted with the user subroutine.

As mentioned before, the displacements, principal strains and principal stresses on the nodes far from the deformation area must be at most the 1 % of the total values. The displacements, strains and stresses smaller than that percentage are accepted to be zero during the simulation processes. In this model, two key nodes (marked in Figure 21) have been analyzed whether they have displacements, strains and stresses under desired limits. The results are presented in Table 9.

Table 9 – Displacement, Principal Strain and Principal Stress Values at the Given Nodes for Model A

$Node Number$	***1***	***2***
$Max. Displacement\,(mm)$	2.143E-2	7.217E-2
$\left(\frac{Max. Displacement}{Max. Displacement\ in\ the Model}\right) x100$	0.536 %	1.804 %
$Max. Principal\ Stress\,(MPa)$	1.592E-4	1.833E-2
$\left(\frac{Max. Principal\ Stress}{Max. Principal\ Stress\ in\ the\ Model}\right) x100$	2.726E-4 %	0.031 %
$Max. Principal\ Strain$	2.163E-3	1.022E-2
$\left(\frac{Max. Principal\ Strain}{Max. Principal\ Strain\ in\ the\ Model}\right) x100$	1.023 %	4.834 %

As seen in Table 9, the values of principal stresses are under the limits but the values of displacements and principal strains could not stay under the limit of 1 % in some conditions. For example the maximum principal strain at the node 2 is 4.834 % of the maximum value in the model. These values are not acceptable and so, the model must be enlarged in x and z directions. The enlargement in the x direction should be more, because the values at the node 2 on the x-axis are deviating from the limits more than the values at the node 1 on the z-axis. As a result, one more model has been created by multiplying the lengths of z-axis with 2 and x-axis with 2.5.

B. To decrease the values of displacements and strains at the nodes mentioned before, the new model has been created with the following dimensions (x-y-z) (Figure 17);

Tissue size(mm) : 50-8-40

Fine mesh region (mm) : 10-2.5-3

As presented in Figure 17, this tissue is larger than the previous ones. Now, the displacements and principal strains can be checked whether they exceed the limits. The results are given in Table 10.

Table 10 – Displacement, Principal Strain and Principal Stress Values at the Given Nodes for Model B

$Node Number$	***1***	***2***
$Max. Displacement\,(mm)$	2.106E-2	2.43E-2
$\left(\frac{Max. Displacement}{Max. Displacement\ in\ the Model}\right) x100$	0.527 %	0.608 %
$Max. Principal\ Stress\,(MPa)$	4.326E-5	1.026E-4
$\left(\frac{Max. Principal\ Stress}{Max. Principal\ Stress\ in\ the\ Model}\right) x100$	5.797E-5 %	1.375E-4 %
$Max. Principal\ Strain$	1.39E-3	2.379E-3
$\left(\frac{Max. Principal\ Strain}{Max. Principal\ Strain\ in\ the\ Model}\right) x100$	0.545 %	0.933 %

As seen in Table 10, all the displacement, principal strain and principal stress values are within the limit of 1 %.

Before deciding this model as completely appropriate for the estimation of the parameters in the subroutine, two more tests have been applied on the model. In these tests, the indenter tip has been rotated 45° and 90° around y-axis and the simulation has also been applied in these orientations (Figures 18 and 19). The displacement, principal stress and principal strain values at the marked nodes are given in Tables 11 and 12.

Table 11 – Displacement, Principal Strain and Principal Stress Values at the Given Nodes for Model B with 45° Indenter Tip Orientation

$Node Number$	***1***	***2***
$Max. Displacement\,(mm)$	1.944E-2	2.466E-2
$\left(\frac{Max. Displacement}{Max. Displacement\ in\ the Model}\right) x100$	0.486 %	0.617 %
$Max. Principal\ Stress\,(MPa)$	1.418E-4	6.034E-5
$\left(\frac{Max. Principal\ Stress}{Max. Principal\ Stress\ in\ the\ Model}\right) x100$	4.348E-5 %	1.85E-5 %
$Max. Principal\ Strain$	1.062E-3	2.058E-3
$\left(\frac{Max. Principal\ Strain}{Max. Principal\ Strain\ in\ the\ Model}\right) x100$	0.591 %	1.145 %

Table 12 – Displacement, Principal Strain and Principal Stress Values at the Given Nodes for Model B with 90° Indenter Tip Orientation

$Node Number$	***1***	***2***
$Max. Displacement\,(mm)$	3.667E-3	1.24E-2
$\left(\frac{Max. Displacement}{Max. Displacement\ in\ the Model}\right) x100$	0.092 %	0.31 %
$Max. Principal\ Stress\,(MPa)$	2.929E-6	1.356E-5
$\left(\frac{Max. Principal\ Stress}{Max. Principal\ Stress\ in\ the\ Model}\right) x100$	6.083E-7 %	2.816E-6 %
$Max. Principal\ Strain$	2.125E-4	1.086E-3
$\left(\frac{Max. Principal\ Strain}{Max. Principal\ Strain\ in\ the\ Model}\right) x100$	0.109 %	0.558 %

In Tables 11 and 12 all the values of displacements, principal strains and principal stresses are seen to be under the limits. Only the principle strain at the node 2 at the indenter tip orientation of 45° is a little bit larger than % 1, but this is tolerable. So, the tissue can be assumed to have zero displacements, principal strains and principal stresses at the end of the model axes and this model can be used for the estimation of the parameters in the user subroutine.

The last thing to do is to create different mesh sizes in the fine mesh zone and compare the results of indenter tip reaction force. The force should converge somewhere, and by also taking the submission time into account, the most appropriate one should be chosen for more accurate results.

So far, the edge length of 0.5 mm has been used for the elements in the fine mesh zone. Four more models will be created with the edge lengths of 0.3, 0.4, 0.6 and 0.7 mm and they will be compared for the convergence. The time-indenter tip reaction force curves of these five models are seen in the Figure 24.

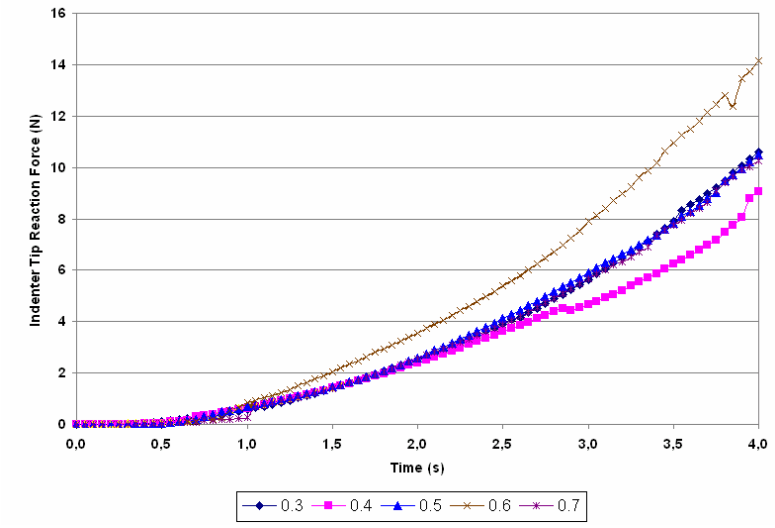

Figure 24 – Time-Indenter Tip Reaction Force Curves for Different Element Edge Lengths in the Fine Mesh Region

In Figure 24, the change of the indenter tip reaction with time is seen. Three of these curves are very close to each other. These are the ones having the element edge lengths of 0.3, 0.5 and 0.7mm. The one having the element edge length of 0.6 mm is starting diverging at about first second. And the one having the element edge length of 0.4 mm is giving bad results between third and fourth seconds of the analysis time. So, these two are not good enough to be used. The other two curves representing the element edges of 0.3 and 0.7 mm. are also giving some bad responses that can be seen by looking carefully. This can be due to node separations at those increments as a result of tetrahedral meshing. Sudden changes in the reaction forces can also happen because of anisotropy. Different directions of the tissue have different stiffness and that can cause different sudden increases or decreases along those directions. Also it is more advantageous to use 0.5 mm instead of 0.3 mm edge length. Because the submission of 0.3 mm is lasting more than one hour, whereas the 0.5 mm is lasting in about twelve minutes and they yield nearly the same result (convergence is satisfied). As a result, the best element edge length for the elements in the fine mesh zone has been chosen as 0.5 mm. This version of the model is presented in Figure 25.

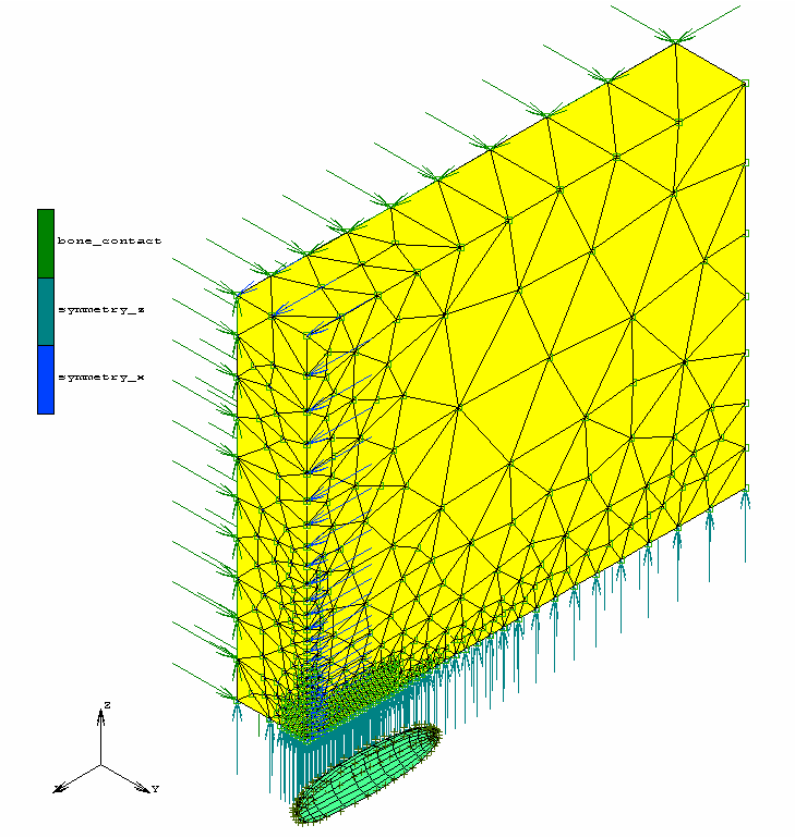

Figure 25- The Model with the Elements of 0.5 mm Edge Length

So far, the thickness of the tissue has been assumed as 8 mm for decreasing the calculation load of the finite element model. It was also observed that for the maximum displacement, maximum principal strain and maximum principal stress values to be assumed as disappeared (to have values within the limits), the tissue should be modeled with the lengths of 50 mm (6.25 times greater than the tissue thickness) in x direction and 40 mm (5 times greater than the tissue thickness) in z direction. In the real case (where the experiments were performed), the thickness of the tissue was about 40 mm. So, in that last step of the finite element model creation process, the model will be drawn with its real dimensions (250-40-200 mm). Since this model is five times greater than the previous one in all the material axes, the maximum displacement, maximum principal strain and maximum principal stress

values cannot be larger than the previous model. But, against all the possibilities, they will be calculated and the results will be presented in Table 13. The last version of the finite element model can be seen in Figure 26.

Table 13 – Displacement, Principal Strain and Principal Stress Values at the Given Nodes for the Last Version of the Model

$Node Number$	***1***	***2***
$Max. Displacement\,(mm)$	1.112E-2	1.51E-2
$\left(\frac{Max. Displacement}{Max. Displacement\ in\ the Model}\right) x100$	0.278 %	0.378 %
$Max. Principal\ Stress\,(MPa)$	1.842E-5	7.664E-5
$\left(\frac{Max. Principal\ Stress}{Max. Principal\ Stress\ in\ the\ Model}\right) x100$	2.468E-5 %	1.027E-4 %
$Max. Principal\ Strain$	9.937E-4	1.88E-3
$\left(\frac{Max. Principal\ Strain}{Max. Principal\ Strain\ in\ the\ Model}\right) x100$	0.39 %	0.737 %

Table 13 summarizes the values of the maximum displacement, maximum principal strain and maximum principal stress values at nodes 1 and 2 which have been calculated by the third material model. The results of these material models are very close to each other, so, to obtain the values within the limits for this model is sufficient. As seen in the table, all the values of displacements, principal strains and principal stresses are under the limits. So, the tissue can be assumed to have zero displacements, principal strains and principal stresses at the end of the model axes and this final finite element model can be used for the estimation of the parameters in the user subroutine.

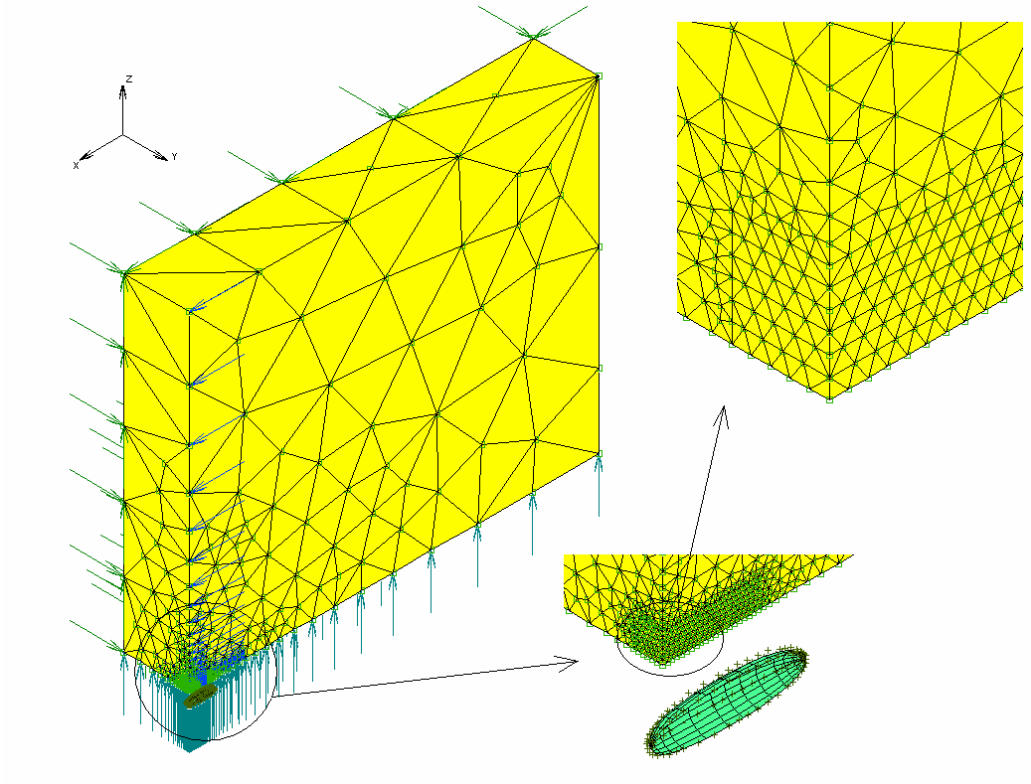

Figure 26- The Last Version of the Finite Element Model

CHAPTER 9

RESULTS

In this chapter, the results obtained by submitting the finite element model which was created in Chapter 8 will be presented. Each finite element model was submitted with the relevant material model (presented in detail in Appendices I, K and M, respectively). The constants in these material models were changed and best fit between the experimental data and the finite element solution was tried to be found. These procedures will be presented in the following subsections in detail.

9.1. Simulation of Experimental Data with the QLV Model by Assuming Soft Tissue as an Isotropic Material

The simulation process was started with the quasi-linear isotropic material model. The material model for this simulation was presented in Appendix I. This material model was independent of strain. It involved the experiment time only, so, this model was only able to simulate relaxation and creep behaviors but not cyclic loading. Details are presented in the following subsections.

9.1.1. Simulation of Relaxation Behavior

Relaxation experiment data was available as indicated with the continuous line in Figure 27. This data was obtained by indenting (by the elliptic indenter tip with the dimensions of 8-2-2 mm in x, y and z axes, respectively) the soft tissue (forearm, medial part) which had a thickness of about 40 mm. The soft tissue was indented 20

mm (50 % of its thickness) with the indenter speed of 1 mm/s in 20 seconds. Then, this displacement was kept constant during 120 seconds and the relaxation behavior was observed.

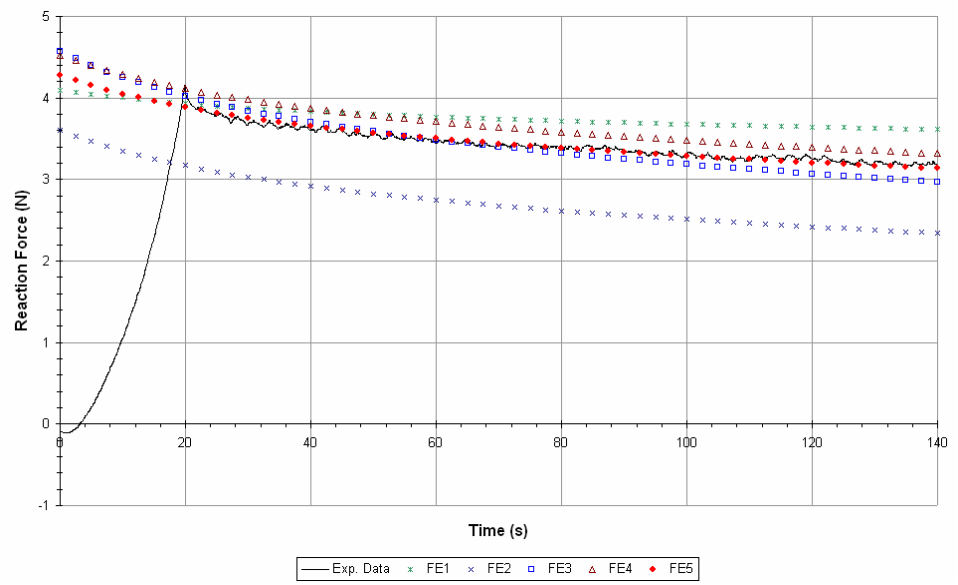

Figure 27 – Relaxation Curves for the Simulation of the First Model

For the simulation of the experimental data, five finite element (FE) trials were performed which can be seen in Figure 27. The normalized sums of square errors (NSSE) for each trial were presented in Figure 28.

In the first FE trial, the base material model (subroutine) which was presented in Appendix I was used. This trial was able to simulate the magnitude of the reaction force at the beginning of the relaxation period, but, the total amount of relaxation, which can be thought as the difference of reaction forces between the 20^{th} and 140^{th} seconds, was seemed to be larger in the experimental data. The NSSE for this simulation was calculated as 31.82 %. The majority of this error was due to the deficiency in the amount of total relaxation magnitude which causes the long term

relaxation magnitude to deviate from the experimental data more and more as time passes.

To increase the amount of total relaxation magnitude, the relaxation amplitude constant (C) in the material model was increased. So, in the second FE trial, the relaxation amplitude constant was taken to be 8 instead of 0.08. This procedure increased the magnitude of both short term and long term amounts of relaxation. But the increase in the long term relaxation amount was more than the short term relaxation amount. This caused the total relaxation amount to increase as seen in Figure 27. This FE trial was seemed to give reaction force magnitudes which are much less then the experimental data. A careful examination of the curve reveals that the curvature of this curve is similar to the experimental data curve than the previous trial. The NSSE for this simulation was calculated as 169.33 %. The majority of this error was due to the deviation of the magnitudes of the reaction forces from the experimental data.

After obtaining the sufficient amount of total relaxation, the magnitudes of reaction forces should have been approached to the ones in the experimental data. To do that, the short term relaxation constant (τ_1) in the material model was increased. So, in the third FE trial, the short term relaxation constant was taken to be 4 seconds instead of 0.8 seconds. As seen in Figure 27, by increasing the short term relaxation constant, the decrease in the relaxation magnitude could be obtained. The decrease of the short term relaxation period magnitude was a little bit larger than the decrease of the long term relaxation period magnitude. This was due to the fact that the short term relaxation constant was changed and so, short term relaxation behavior was affected more. The fitting between the FE trial 3 and the experimental data seemed to be better than the previous ones. In this trial, the NSSE was 4.46 % (see Figure 28). This was due to having relaxation magnitude less than the experimental data in the short term relaxation period and having relaxation magnitude more than the experimental data in the long term relaxation period.

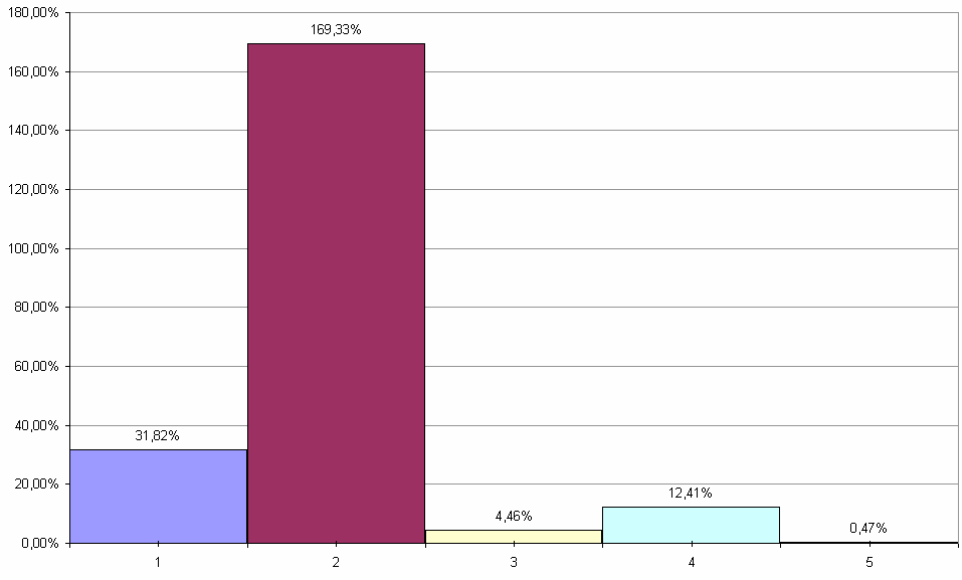

Figure 28 – Normalized Sums of Square Errors for the Relaxation Simulation of the First Model

To overcome the deviations in the long and short term relaxation periods, long and short term relaxation constants in the material model should have been changed appropriately. First, to obtain better fit in the long term relaxation period, the long term relaxation constant (τ_2) was changed in the fourth FE trial. The constant was increased from 1400 seconds to 10000 seconds. This increase caused the long term relaxation amount to decrease. As seen in the Figure 27, this FE trial had less relaxation amount than the previous one in the long term relaxation period. Now, the curvature of the FE trial 4 response seemed to be much similar to the experimental data. Last thing to do was to have more relaxation amount in the short term relaxation period. This could be achieved in the fifth FE trial by decreasing the short term relaxation constant from 4 seconds to 2.5 seconds. As seen in Figure 27, a great fit between the experimental data and finite element trial could be obtained after this trial. The proof of this great fit is the value of NSSE which was calculated as 0.47 %. The constants used in each finite element trial are summarized in Table 14.

Table 14 – Constants of the First Material Model (equation A59) Used in the Relaxation Simulation

Trial	A	B	C	τ_1	τ_2
FE1	1.96E-38	42	0.08	0.8	1400
FE2	1.96E-38	42	8.0	0.8	1400
FE3	1.96E-38	42	8.0	4.0	1400
FE4	1.96E-38	42	8.0	4.0	10000
FE5	1.96E-38	42	8.0	2.5	10000

9.1.2. Simulation of Creep Behavior

Creep experiment data was available as indicated with the continuous line in Figure 29. This data was obtained by indenting (by the elliptic indenter tip with the dimensions of 8-2-2 mm in x, y and z axes, respectively) the soft tissue (forearm, medial part) which had a thickness of about 40 mm. The soft tissue was indented 22.5 mm (56.25 % of its thickness) with the indenter speed of 1 mm/s in 22.5 seconds until the reaction force reached to 5 N. Then, this reaction force which occurred at the end of the loading period was kept constant during 120 seconds and the creep behavior was observed.

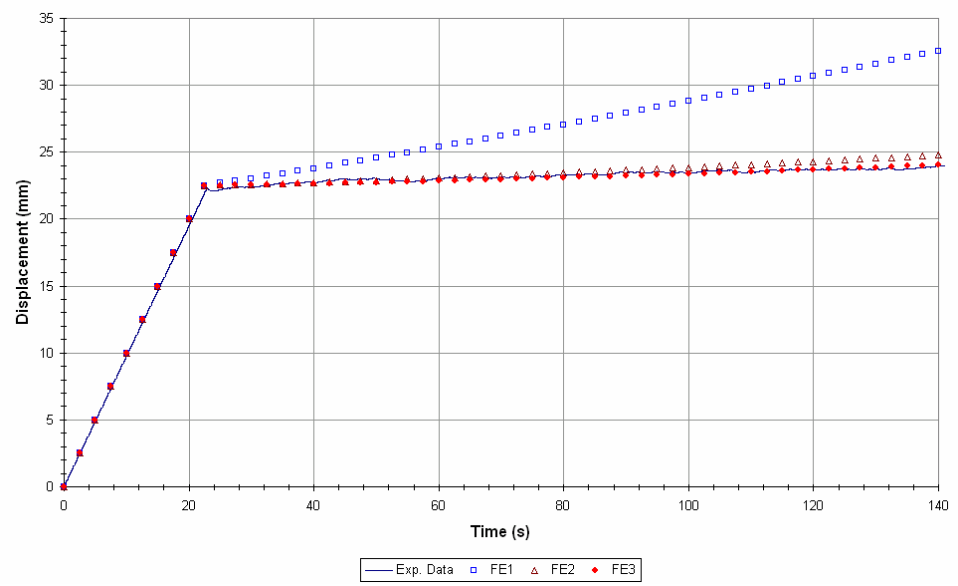

Figure 29 - Creep Curves for the Simulation of the First Model

For the simulation of the experimental data, three finite element (FE) trials were performed which can be seen in Figure 29. The normalized sums of square errors (NSSE) for each trial were presented in Figure 30.

In the first FE trial, the material model which had been used for the last FE trial of the relaxation simulation procedure was used. This trial has given rather large magnitudes of displacement responses, i.e. the creep response occurred much more than the experimental data. This trial, which had the NSSE value of 190.05 % (Figure 30), can be seen in Figure 29.

The total amount of creep response was then tried to be decreased by increasing the elastic constant (*A*) from 1.96E-38 MPa to 4E-38 MPa in the second trial. This procedure decreased the magnitude of creep response and made it approached to the experimental data. After this second trial, the NSSE value appeared as 1.58 % which means that the second trial gives much accurate responses than the first one.

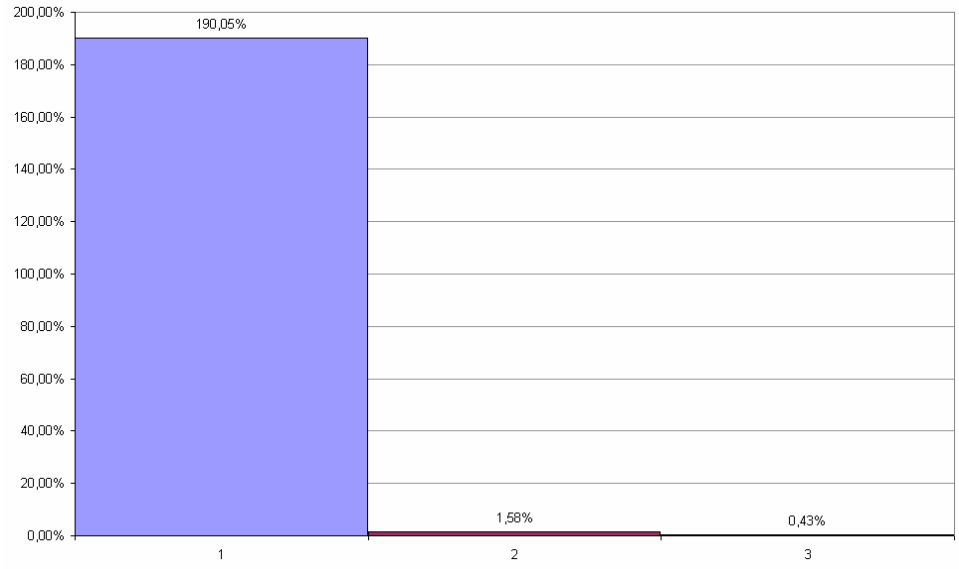

Figure 30 - Normalized Sums of Square Errors for the Creep Simulation of the First Model

To increase the accuracy of the simulation further, i.e. to decrease the value of NSSE, one more FE trial was performed. In this last trial (FE3), the elastic constant was increased a little bit more and it was made 4.455E-38 MPa. This procedure decreased the magnitude of creep response a little bit more and made it approached to the experimental data. After this third trial, the NSSE value appeared as 0.43 % which proves that there occurred a great fit between the finite element solution and the experimental data. The constants used in each finite element trial are summarized in Table 15.

Table 15 – Constants of the First Material Model (equation A59) Used in the Creep Simulation

Trial	A	B	C	τ_1	τ_2
FE1	1.96E-38	42	8.0	2.5	10000
FE2	4.0E-38	42	8.0	2.5	10000
FE3	4.455E-38	42	8.0	2.5	10000

9.2. Simulation of Experimental Data with the Enhanced QLV Model by Assuming Soft Tissue as an Isotropic Material

The simulation process was carried on with the enhanced quasi-linear isotropic material model. The material model for this simulation was presented in Appendix K. This material model was dependent on both experiment time and strain, so, it was able to simulate relaxation and creep behaviors together with cyclic loading. Details are presented in the following subsections.

9.2.1. Simulation of Relaxation Behavior

Relaxation experiment data was available as indicated with the continuous line in Figure 31. This data was obtained by indenting (by the elliptic indenter tip with the dimensions of 8-2-2 mm in x, y and z axes, respectively) the soft tissue (forearm, medial part) which had a thickness of about 40 mm. The soft tissue was indented 20 mm (50 % of its thickness) with the indenter speed of 1 mm/s in 20 seconds. Then, this displacement was kept constant during 120 seconds and the relaxation behavior was observed.

For the simulation of the experimental data, six finite element (FE) trials were performed which can be seen in Figure 31. The normalized sums of square errors (NSSE) for each trial were presented in Figure 32.

In the first FE trial, the base material model (subroutine) which was presented in Appendix K was used. This trial was not able to simulate the magnitude of the reaction force at the beginning of the relaxation period. The reaction force for this simulation was starting from about 4.8 N, whereas the reaction force of the experimental data was starting from somewhere close to 4 N. (see Figure 31) The great majority of the NSSE of 399.29 % for this simulation was arising from this force difference. So, in the second FE trial, the short term relaxation constant (τ_1) was decreased from 8 seconds to 0.8 seconds. As seen in Figure 31, by decreasing the value of the short term relaxation constant, the reaction force at the beginning of the relaxation period could be simulated. This can also be seen from the value of NSSE which decreased to 30.45 % in one step. The majority of this error was due to the deficiency in the amount of total relaxation magnitude which causes the long term relaxation magnitude to deviate from the experimental data more and more as time passes.

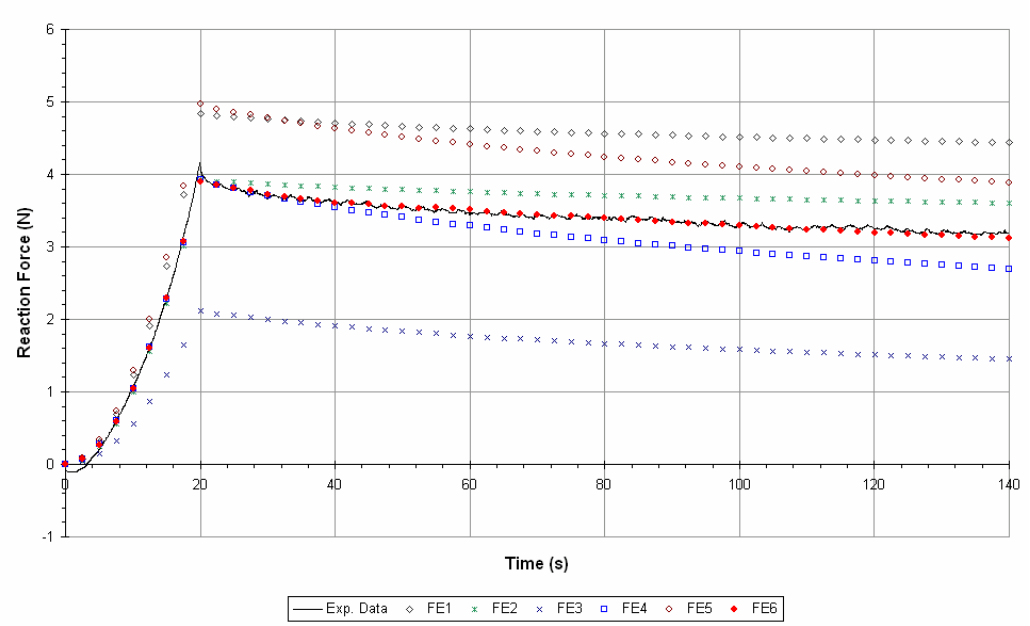

Figure 31 – Relaxation Curves for the Simulation of the Second Model

To increase the amount of total relaxation magnitude, the relaxation amplitude constant (C) in the material model was increased from 0.08 to 0.8 in the third FE trial. This procedure increased the magnitude of both short term and long term amounts of relaxation. The increase in the long term relaxation amount was more than the short term relaxation amount. This caused the total relaxation amount to increase as seen in Figure 31. This FE trial was seemed to yield reaction force magnitudes which are much less then the experimental data. A careful examination of the curve reveals that the curvature of this curve is similar to the experimental data curve than the previous trial. The NSSE for this simulation was calculated as 877.42 %. The majority of this error was due to the deviation of the magnitudes of the reaction forces from the experimental data.

For increasing the reaction force same magnitude for all of the simulation points, i.e. for decreasing the amount of total relaxation magnitude, the elastic constant (A) was increased from 9E-35 MPa to 1.67E-34 MPa in the fourth trial. After this trial, the simulation response of the reaction force was shifted upwards as seen in Figure 31. This process decreased the NSSE to 28.41 %.

In the fifth FE trial, for decreasing the amount of relaxation in the long term relaxation period more than the short term relaxation period, the long term relaxation constant (τ_2) was increased from 140 seconds to 1400 seconds. Because, choosing a greater long term relaxation constant causes the long term relaxation to occur later. Consequently, this process caused the long term relaxation to decrease more than the short term relaxation.

In the last FE trial, the short term relaxation constant was decreased one more step and was made 0.3 seconds to catch the experimental data. After that step, there occurred a great fit between the experimental data and simulation response which was proved by the NSSE value of 0.6 % given in Figure 32. The constants used in each finite element trial are summarized in Table 16.

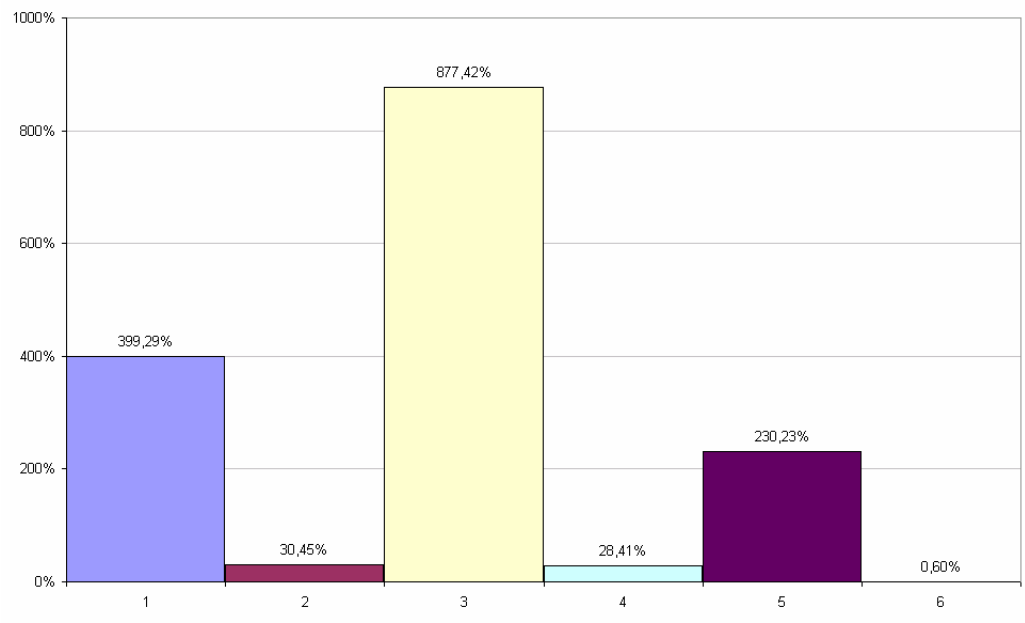

Figure 32 - Normalized Sums of Square Errors for the Relaxation Simulation of the Second Model

Table 16 – Constants of the Second Material Model (equation B21) Used in the Relaxation Simulation

Trial	A	B	C	τ_1	τ_2	a	b	c
FE1	9.0E-35	42	0.08	8.0	140	0.8	0.8	0.8
FE2	9.0E-35	42	0.08	0.8	140	0.8	0.8	0.8
FE3	9.0E-35	42	0.8	0.8	140	0.8	0.8	0.8
FE4	1.67E-34	42	0.8	0.8	140	0.8	0.8	0.8
FE5	1.67E-34	42	0.8	0.8	1400	0.8	0.8	0.8
FE6	1.67E-34	42	0.8	0.3	1400	0.8	0.8	0.8

9.2.2. Simulation of Creep Behavior

Creep experiment data was available as indicated with the continuous line in Figure 33. This data was obtained by indenting (by the elliptic indenter tip with the dimensions of 8-2-2 mm in x, y and z axes, respectively) the soft tissue (forearm, medial part) which had a thickness of about 40 mm. The soft tissue was indented 22.5 mm (56.25 % of its thickness) with the indenter speed of 1 mm/s in 22.5 seconds until the reaction force reached to 5 N. Then, this reaction force which occurred at the end of the loading period was kept constant during 120 seconds and the creep behavior was observed.

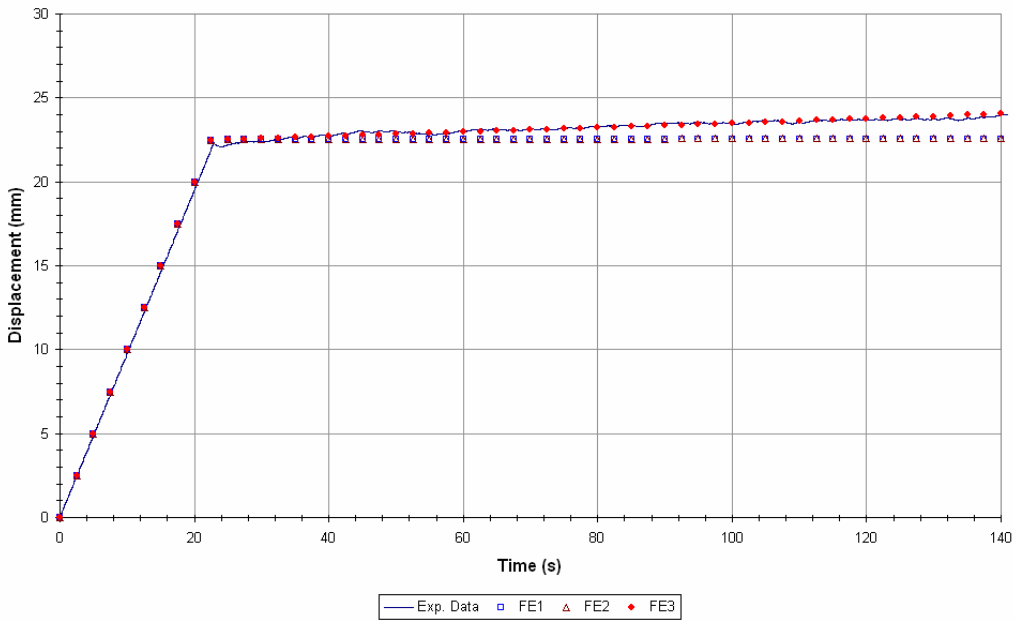

Figure 33 - Creep Curves for the Simulation of the Second Model

For the simulation of the experimental data, three finite element (FE) trials were performed which can be seen in Figure 33. The normalized sums of square errors (NSSE) for each trial were presented in Figure 34.

In the first FE trial, the material model which had been used for the last FE trial of the relaxation simulation procedure was used. This trial has given a little bit smaller magnitudes of displacement responses, i.e. the creep response occurred less than the experimental data. This trial, which had the NSSE value of 6.36 % (Figure 34), can be seen in Figure 33.

The total amount of creep response was then tried to be increased by decreasing the elastic constant (A) from 1.67E-34 MPa to 1.67E-35 MPa in the second trial. This procedure increased the magnitude of creep response and made it approached to the experimental data. After this second trial, the NSSE value appeared as 5.52 % which means that the second trial gives more accurate responses than the first one.

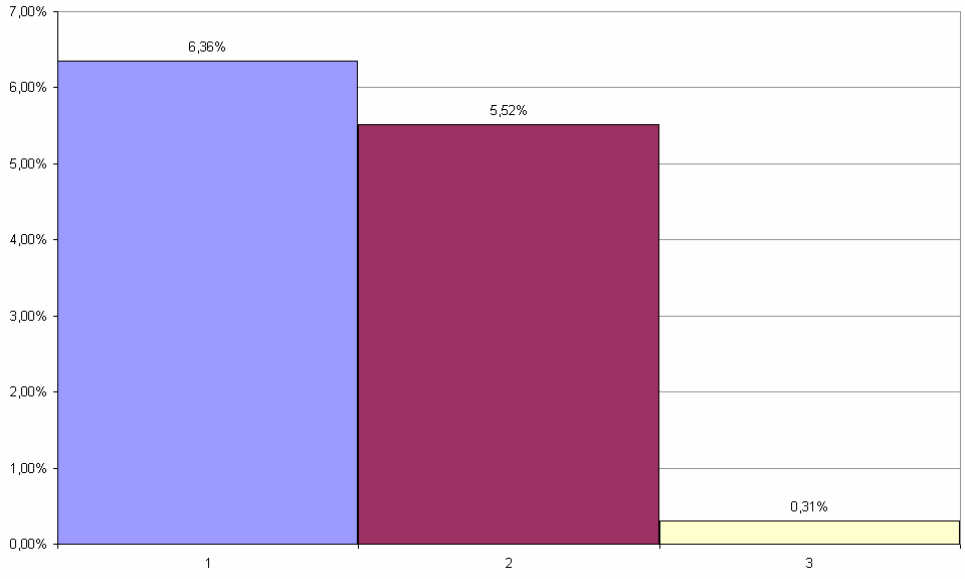

Figure 34 - Normalized Sums of Square Errors for the Creep Simulation of the Second Model

To increase the accuracy of the simulation further, i.e. to decrease the value of NSSE, one more FE trial was performed. In this last trial (FE3), the elastic constant was decreased a little bit more and it was made 1.31E-36 MPa. This procedure increased the magnitude of creep response a little bit more and made it approached to the experimental data. After this third trial, the NSSE value appeared as 0.31 % which proves that there occurred a great fit between the finite element solution and the experimental data. The constants used in each finite element trial are summarized in Table 17.

Table 17 – Constants of the Second Material Model (equation B21) Used in the Creep Simulation

Trial	A	B	C	τ_1	τ_2	a	b	c
FE1	1.67E-34	42	0.8	0.3	1400	0.8	0.8	0.8
FE2	1.67E-35	42	0.8	0.3	1400	0.8	0.8	0.8
FE3	1.31E-36	42	0.8	0.3	1400	0.8	0.8	0.8

9.2.3. Simulation of Hysteresis Behavior

Hysteresis experiment data was available as indicated with the continuous lines in Figure 35 and Figure 39. This data was obtained by loading (by the elliptic indenter tip with the dimensions of 8-2-2 mm in x, y and z axes, respectively) the soft tissue (forearm, medial part) which had a thickness of about 40 mm. The soft tissue was loaded 15 mm (37.5 % of its thickness) with the indenter speed of 4 mm/s in 3.75 seconds. Then, the tissue was unloaded with the same speed and the indenter tip returned to its original position when the experiment time is 7.5 seconds. Within this one cycle of loading and unloading, the change of reaction force with respect to time (Figure 35) and with respect to displacement (Figure 39) was observed.

For the simulation of the experimental data, five finite element (FE) trials were performed which can be seen in Figure 35 and Figure 39. The normalized sums of square errors (NSSE) for each trial of the reaction force simulation with respect to time were presented in Figure 36, Figure 37 and Figure 38 for loading and unloading periods, for loading period only and for unloading period only, respectively. The NSSE values for each trial of the reaction force simulation with respect to displacement were presented in Figure 40, Figure 41 and Figure 42 for loading and unloading periods, for loading period only and for unloading period only, respectively.

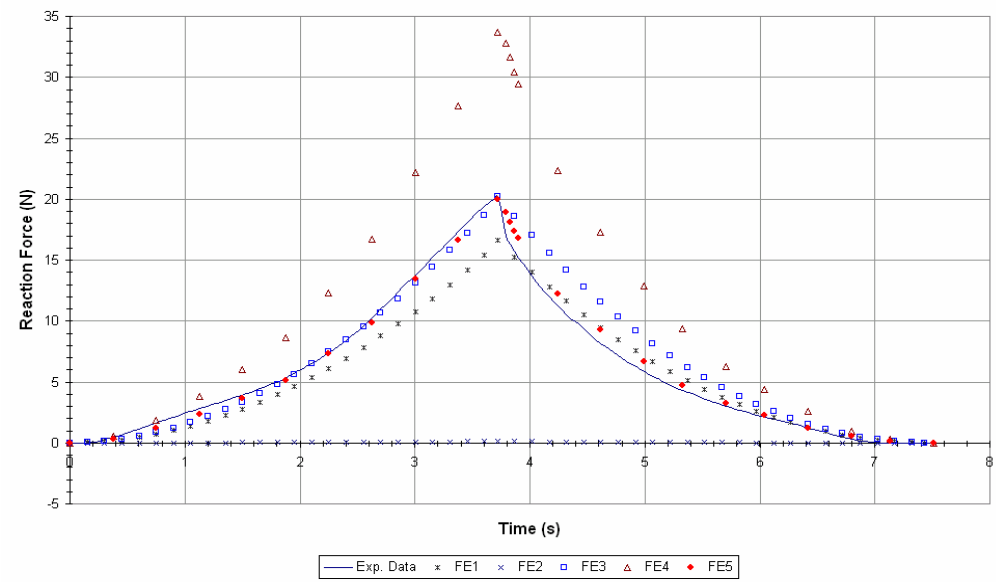

Figure 35 – Hysteresis (Time - Reaction Force) Curves for the Simulation of the Second Model

In the first finite element trial, the material model, which had been used in the last step of the simulation of relaxation behavior for this model was used. This model was not very successful in simulating the material behavior both in loading and unloading periods of the simulation as seen in Figures 35 and 39. The NSSE values

of 27.35 % given in Figure 36 and 27.1 % given in Figure 40 were the proof of that. But, by a more detailed examination of Figure 35, one can see that the simulation of the unloading period was better than the simulation of the loading period. The proof of that is given in Figure 37 and Figure 38 which presents the NSSE values in loading as 23.92 % and in unloading as 3.43 %. This can also be seen from Figure 41 and Figure 42 with the NSSE values of 22.49 % in loading and 4.61 % in unloading, respectively.

For the second FE trial of the simulation of hysteresis behavior, the material model, which had been used in the last step of the simulation of creep behavior for this model was used. This model presented very small values of the reaction force response during the experiment time (see Figure 35) which resulted in very large NSSE values as given in the Figures 36, 37 and 38. For increasing these reaction force values, the elastic material constant (A) was increased from 1.31E-36 MPa to 2.033E-34 MPa in the third trial. This model was not very successful in simulating the material behavior both in loading and unloading periods of the simulation like the first one as seen in Figure 35. The NSSE value of 29.53 % given in Figure 36 and 33.31 % given in Figure 40 were the proof of that. But, by a more detailed examination of Figure 35, one can see this time that the simulation of the loading period was better than the simulation of the unloading period. The proof of that is given in the Figure 37 and Figure 38 which presents the NSSE values in loading as 1.97 % and in unloading as 27.56 %. This can also be seen from Figure 41 and Figure 42 with the NSSE values of 1.71 % in loading and 31.6 % in unloading, respectively.

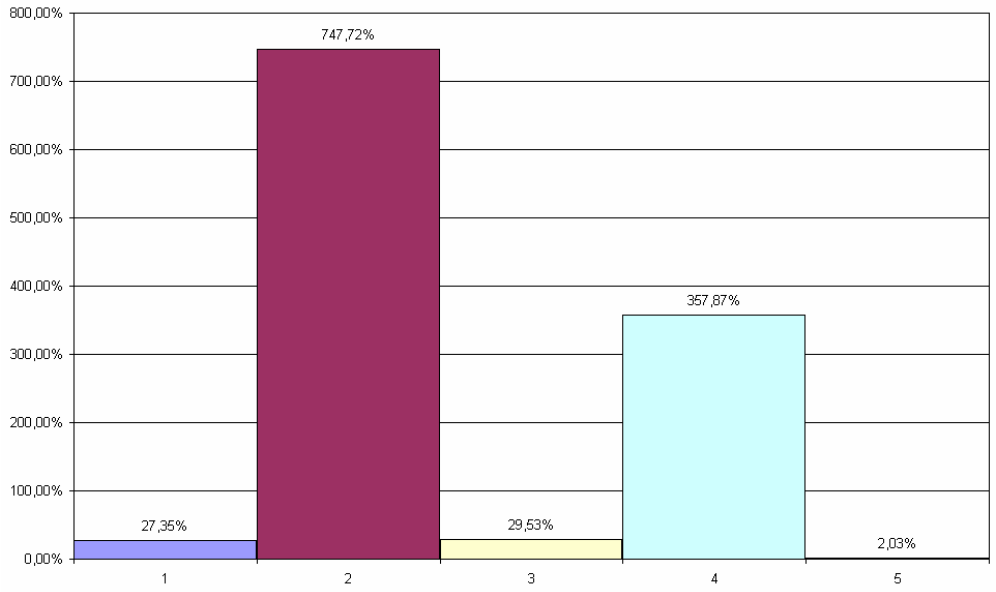

Figure 36 – Normalized Sums of Square Errors for the Hysteresis (Time - Reaction Force) Simulation of the Second Model in Loading and Unloading

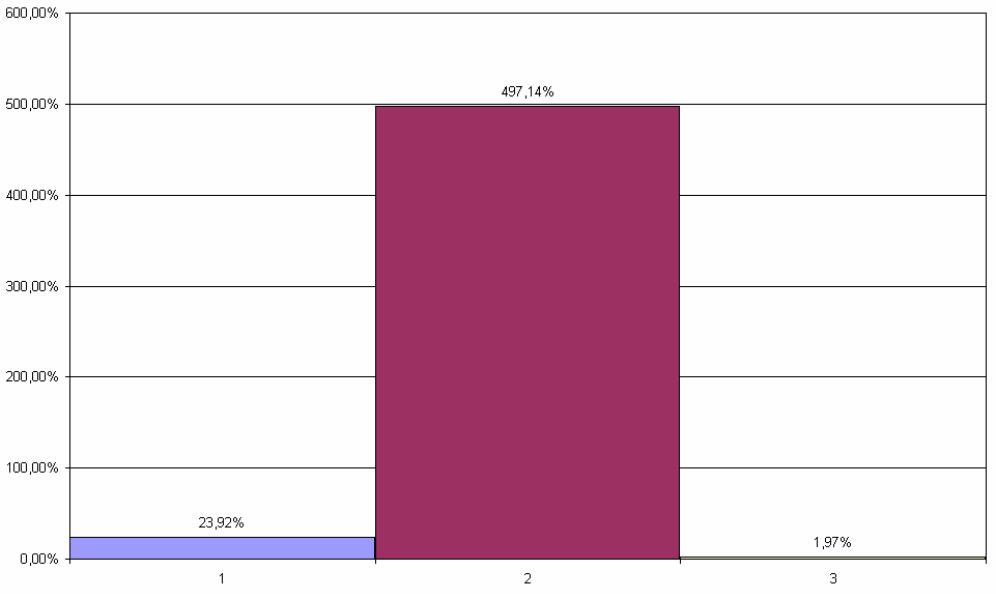

Figure 37 - Normalized Sums of Square Errors for the Hysteresis (Time - Reaction Force) Simulation of the Second Model in Loading

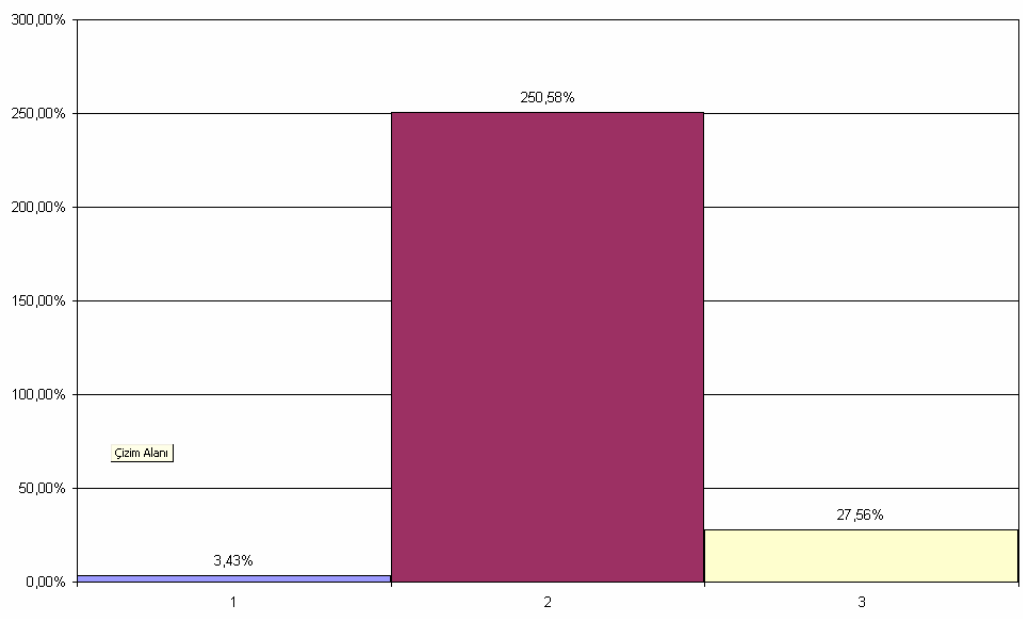

Figure 38 - Normalized Sums of Square Errors for the Hysteresis (Time - Reaction Force) Simulation of the Second Model in Unloading

The main source of these errors was thought to be due to the data acquisition speed of the experiment apparatus. By a carefully examination of Figure 35 and Figure 39, one can see the strangeness at the transition periods between the loading and the unloading periods. The indenter tip was stopped about 0.15 seconds after the loading period, and then started the unloading period. During this short experiment time, a sudden relaxation happened in the tissue. So, for being able to simulate this behavior, the simulation procedure was changed for the fourth and fifth trials as follows:

The soft tissue was loaded 15 mm (37.5 % of its thickness) with the indenter speed of 4 mm/s in 3.75 seconds. Then, this displacement was kept constant during 0.15 seconds to allow for the relaxation behavior. Later, the tissue was unloaded and the indenter tip returned to its original position when the experiment time is 7.5 seconds.

In the fourth FE trial, the short term relaxation constant was decreased from 0.3 second to 0.03 second to be able to simulate that sudden decrease in the reaction force. The relaxation behavior between the loading and the unloading periods was seemed to be simulated which can be seen from Figure 35 and Figure 39. But this time, the magnitude of the reaction forces appeared as larger than the experimental data. The NSSE value of 357.87 % given in Figure 36 and 293.81 % given in Figure 40 are the proof of that. To decrease the magnitude of the reaction force, the elastic material constant (A) was increased once more from 2.033E-34 MPa to 3.21E-33 MPa in the last FE trial. After that trial, a good fit between the experimental data and the finite element simulation could be obtained (see Figures 35 and 39), with the NSSE value of 2.03 % in the simulation of reaction force with respect to experiment time (see Figure 36) and with the NSSE value of 0.58 % in the simulation of the reaction force with respect to displacement (see Figure 40). The constants used in each finite element trial are summarized in Table 18.

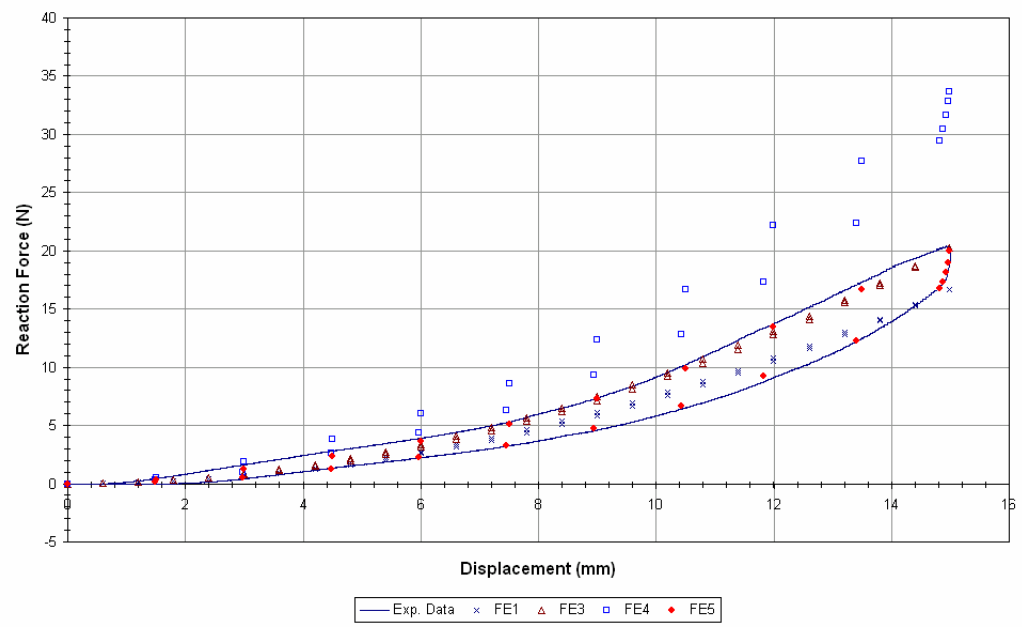

Figure 39 - Hysteresis (Displacement - Reaction Force) Curves for the Simulation of the Second Model

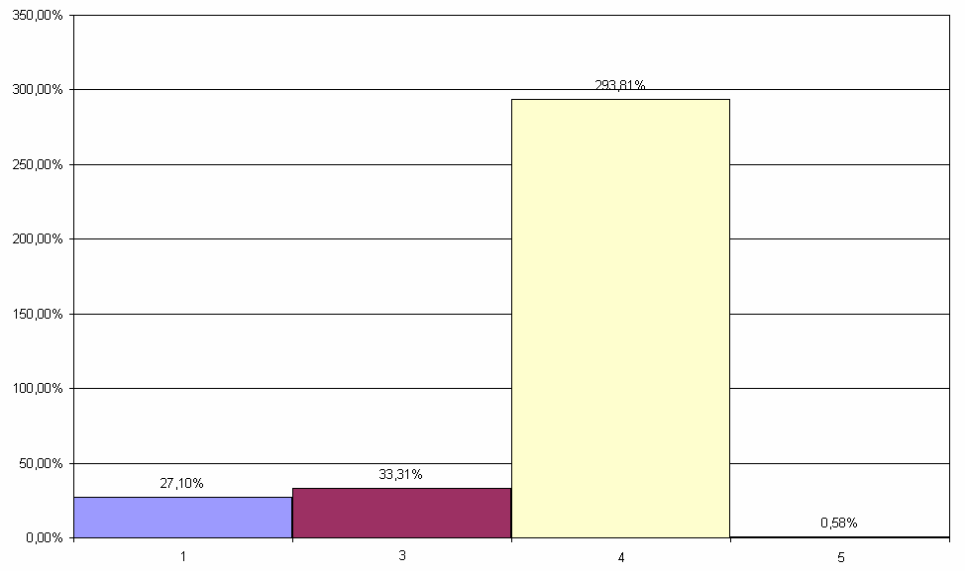

Figure 40 – Normalized Sums of Square Errors for the Hysteresis (Displacement - Reaction Force) Simulation of the Second Model in Loading and Unloading

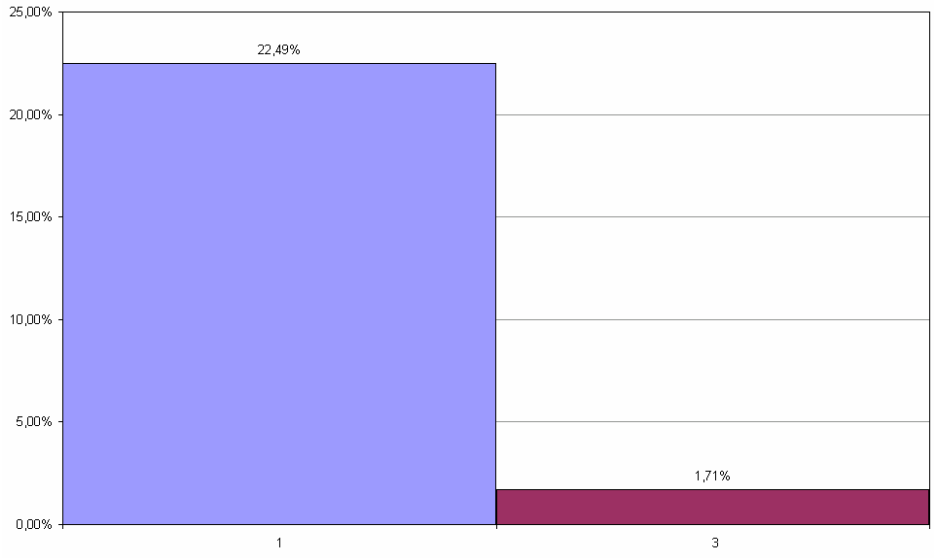

Figure 41 – Normalized Sums of Square Errors for the Hysteresis (Displacement - Reaction Force) Simulation of the Second Model in Loading

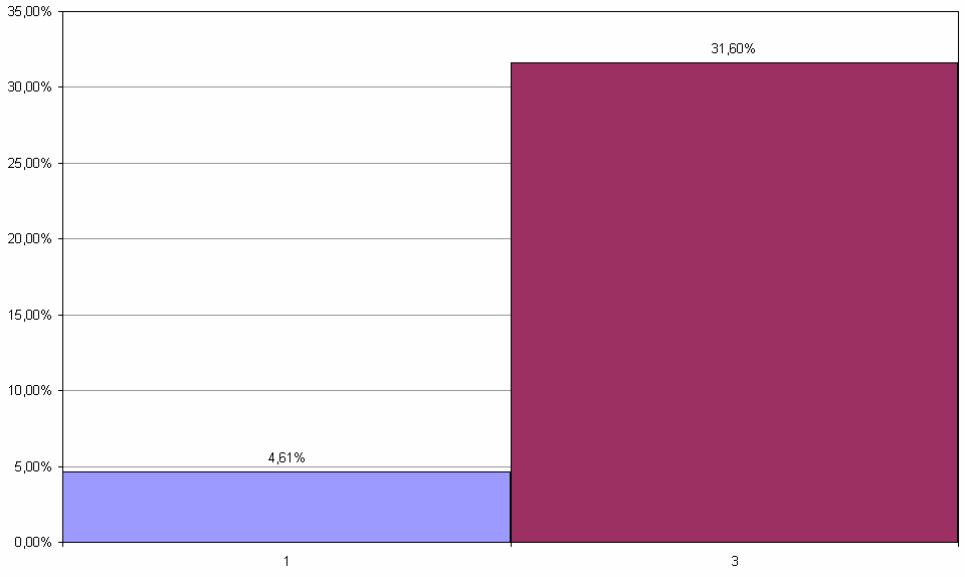

Figure 42 – Normalized Sums of Square Errors for the Hysteresis (Displacement - Reaction Force) Simulation of the Second Model in Unloading

Table 18 – Constants of the Second Material Model (equation B21) Used in the Hysteresis Simulation

Trial	A	B	C	τ_1	τ_2	a	b	c
FE1	1.67E-34	42	0.8	0.3	1400	0.8	0.8	0.8
FE2	1.31E-36	42	0.8	0.3	1400	0.8	0.8	0.8
FE3	2.033E-34	42	0.8	0.3	1400	0.8	0.8	0.8
FE4	2.033E-34	42	0.8	0.03	1400	0.8	0.8	0.8
FE5	3.21E-33	42	0.8	0.03	1400	0.8	0.8	0.8

9.2.4. Simulation of Preconditioning (Mullin's Effect) Behavior

Preconditioning experiment data was available as indicated with the continuous line in Figure 43. This data was obtained by loading (by the elliptic indenter tip with the dimensions of 8-2-2 mm in x, y and z axes, respectively) the soft tissue (forearm, medial part) which had a thickness of about 40 mm. The soft tissue was loaded 15 mm (37.5 % of its thickness) with the indenter speed of 4 mm/s in 3.75 seconds. Then, this displacement was kept constant during 0.15 seconds to allow for the relaxation behavior like in the hysteresis simulation. Later, the tissue was unloaded and the indenter tip returned to its original position when the experiment time is 7.5 seconds. This loading and unloading cycle was repeated ten times and the change of reaction force with respect to time (Figure 43) was observed.

The simulation of the experimental data was performed with the material model which had been used in the last trial for the simulation of the hysteresis behavior of this model. This simulation is concluded with the NSSE value of 3.69 % which can be assumed as acceptable for the preconditioning behavior. The constants used in the finite element trial are summarized in Table 19.

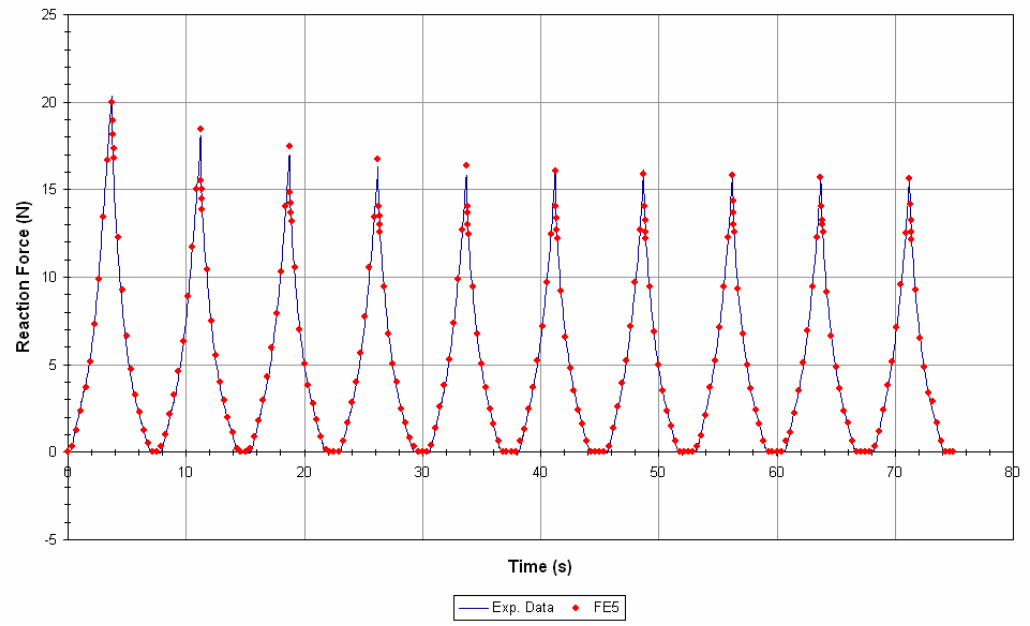

Figure 43 - Preconditioning (Mullin's Effect) Curves for the Simulation of the Second Model

Table 19 – Constants of the Second Material Model (equation B21) Used in the Preconditioning Simulation

Trial	A	B	C	τ_1	τ_2	a	b	c
FE5	3.21E-33	42	0.8	0.03	1400	0.8	0.8	0.8

9.3. Simulation of Experimental Data with the Enhanced QLV Model by Assuming Soft Tissue as an Anisotropic Material

The last simulation process was performed with the enhanced quasi-linear anisotropic material model. The material model for this simulation was presented in

Appendix M. This material model was dependent on both experiment time and strain, so, it was able to simulate relaxation and creep behaviors together with cyclic loading. Difference of this model from the previous one is the fact that this model was created as anisotropic. The relaxation, creep and cyclic loading behaviors of the soft tissue was tried to be simulated by this anisotropic material model in this step.

9.3.1. Simulation of Relaxation Behavior

Relaxation experiment data was available as indicated with the continuous line in Figure 44. This data was obtained by indenting (by the elliptic indenter tip with the dimensions of 8-2-2 mm in x, y and z axes, respectively) the soft tissue (forearm, medial part) which had a thickness of about 40 mm. The soft tissue was indented 20 mm (50 % of its thickness) with the indenter speed of 1 mm/s in 20 seconds. Then, this displacement was kept constant during 120 seconds and the relaxation behavior was observed.

For the simulation of the experimental data, six finite element (FE) trials were performed which can be seen in Figure 44. The normalized sums of square errors (NSSE) for each trial were presented in Figure 45.

In the first FE trial, the base material model (subroutine) which was presented in Appendix M was used. This trial was not able to simulate the magnitude of the reaction force at the beginning of the relaxation period. The reaction force for this simulation was starting from about 4.2 N, whereas the reaction force of the experimental data was starting from somewhere close to 4 N. The great majority of the NSSE of 86.86 % for this simulation was arising from this force difference. So, in the second FE trial, the short term relaxation constant (τ_1) was decreased from 8 seconds to 4 seconds. As seen in Figure 44, by decreasing the value of the short term relaxation constant, the reaction force at the beginning of the relaxation period could be simulated. This can also be seen from the value of NSSE which decreased to 46.91 % in one step. The majority of this error was due to the deficiency in the

amount of total relaxation magnitude which causes the long term relaxation magnitude to deviate from the experimental data more and more as time passes.

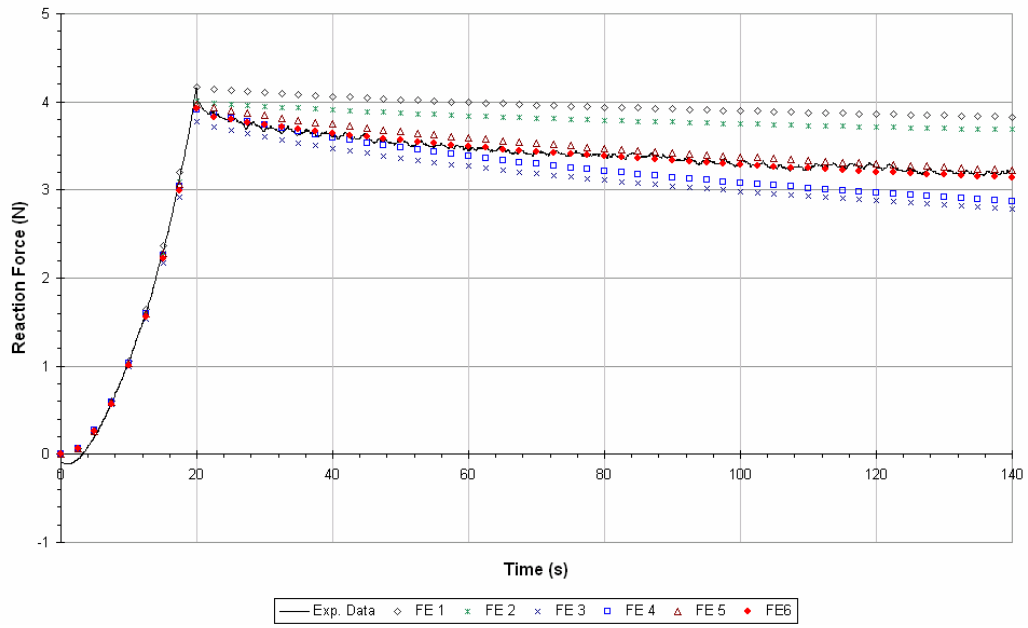

Figure 44 – Relaxation Curves for the Simulation of the Third Model

To increase the amount of total relaxation magnitude, the relaxation amplitude constant (C) in the material model was increased from 0.08 to 8 in the third FE trial. This procedure increased the magnitude of both short term and long term amounts of relaxation. The increase in the long term relaxation amount was more than the short term relaxation amount. This caused the total relaxation amount to increase as seen in Figure 44. In the fourth FE trial, the short term relaxation constant (τ_1) was increased from 4 seconds to 5 seconds to shift the left hand side of the relaxation curve upwards. As expected, also the right hand side of the relaxation curve was shifted by increasing the short term relaxation constant, but this is not as much as the increase of the left hand side. So, after this trial, the short term relaxation was

seemed to be simulated better (see Figure 44) which was proved with the NSSE value of 10.87 % given in Figure 45.

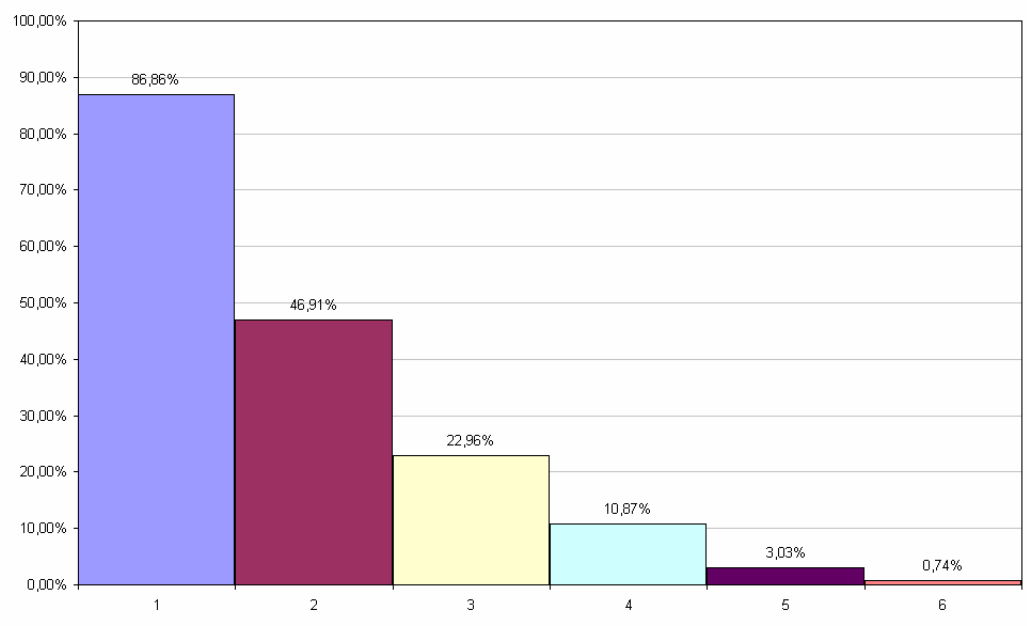

Figure 45 - Normalized Sums of Square Errors for the Relaxation Simulation of the Third Model

In the fifth FE trial, for decreasing the amount of relaxation in the long term relaxation period more than the short term relaxation period, i.e. for shifting the right hand side of the relaxation curve upwards more than the left hand side, the long term relaxation constant (τ_2) was increased from 1400 seconds to 14000 seconds. Because, choosing a greater long term relaxation constant causes the long term relaxation to occur later. Consequently, this process caused the long term relaxation to decrease more than the short term relaxation.

In the last FE trial, the short term relaxation constant was decreased back to 4 seconds to match the experimental data. After that step, there occurred a great fit

between the experimental data and simulation response which was proved by the NSSE value of 0.74 % given in Figure 45. The constants used in each finite element trial are summarized in Table 20.

Table 20 – Constants of the Third Material Model (equation C19) Used in the Relaxation Simulation

Trial	A	B	C	τ_1	τ_2	a	b	c
FE1	7.6E-37	42	0.08	8.0	1400	0.7	0.8	0.9
FE2	7.6E-37	42	0.08	4.0	1400	0.7	0.8	0.9
FE3	7.6E-37	42	8.0	4.0	1400	0.7	0.8	0.9
FE4	7.6E-37	42	8.0	5.0	1400	0.7	0.8	0.9
FE5	7.6E-37	42	8.0	5.0	14000	0.7	0.8	0.9
FE6	7.6E-37	42	8.0	4.0	14000	0.7	0.8	0.9

9.3.2. Simulation of Creep Behavior

Creep experiment data was available as indicated with the continuous line in Figure 46. This data was obtained by indenting (by the elliptic indenter tip with the dimensions of 8-2-2 mm in x, y and z axes, respectively) the soft tissue (forearm, medial part) which had a thickness of about 40 mm. The soft tissue was indented 22.5 mm (56.25 % of its thickness) with the indenter speed of 1 mm/s in 22.5 seconds until the reaction force reached to 5 N. Then, this reaction force which occurred at the end of the loading period was kept constant during 120 seconds and the creep behavior was observed.

For the simulation of the experimental data, three finite element (FE) trials were performed which can be seen in Figure 46. The normalized sums of square errors (NSSE) for each trial were presented in Figure 47.

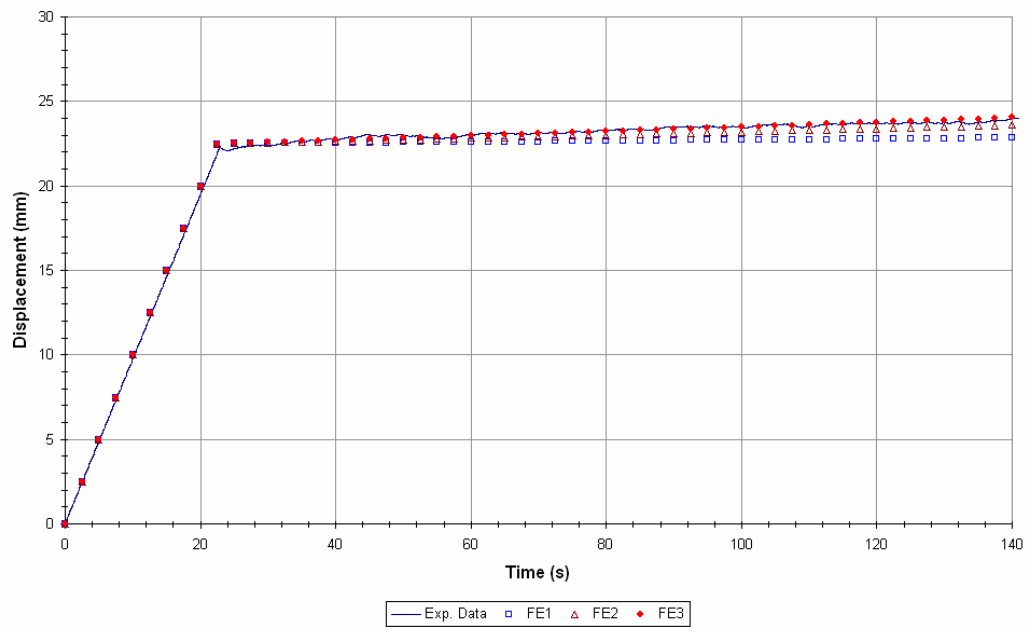

Figure 46 - Creep Curves for the Simulation of the Third Model

In the first FE trial, the material model which had been used for the last FE trial of the relaxation simulation procedure was used. This trial has given a little bit smaller magnitudes of displacement responses, i.e. the creep response occurred less than the experimental data. This trial, which had the NSSE value of 3.98 % (Figure 47), can be seen in Figure 46.

The total amount of creep response was then tried to be increased by decreasing the elastic constant (*A*) from 7.6E-37 MPa to 3.4E-37 MPa in the second trial. This procedure increased the magnitude of creep response and made it approached to the

experimental data. After this second trial, the NSSE value appeared as 0.79 % which means that the second trial gives more accurate responses than the first one.

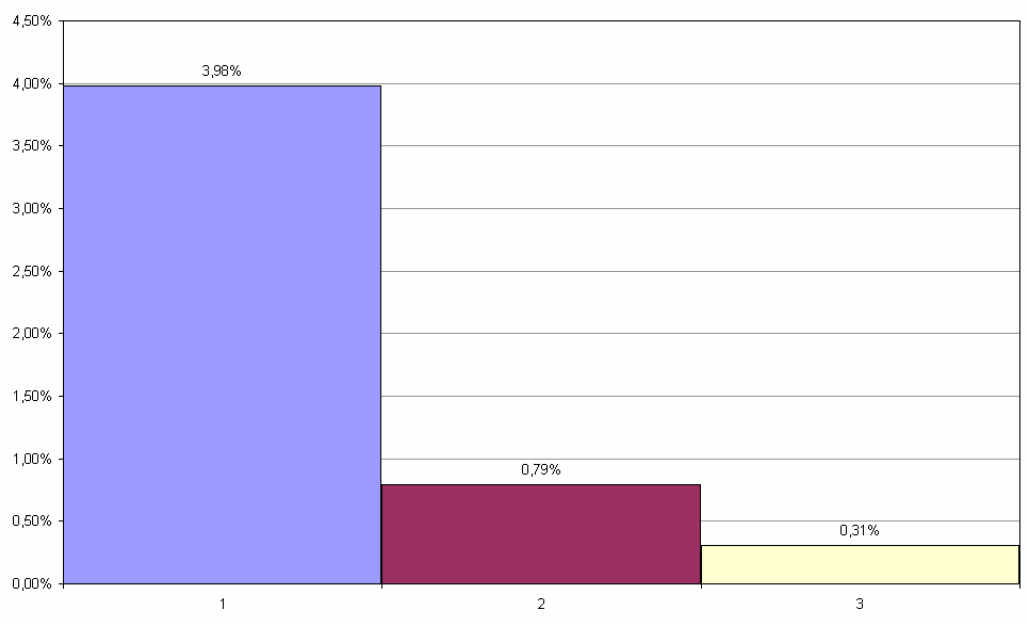

Figure 47 - Normalized Sums of Square Errors for the Creep Simulation of the Third Model

To increase the accuracy of the simulation further, i.e. to decrease the value of NSSE, one more FE trial was performed. In this last trial (FE3), the elastic constant was decreased a little bit more and it was made 2.55E-37 MPa. This procedure increased the magnitude of creep response a little bit more and made it approached to the experimental data. After this third trial, the NSSE value appeared as 0.31 % which proves that there occurred a great fit between the finite element solution and the experimental data. The constants used in each finite element trial are summarized in Table 21.

Table 21 – Constants of the Third Material Model (equation C19) Used in the Creep Simulation

Trial	A	B	C	τ_1	τ_2	a	b	c
FE1	7.6E-37	42	8.0	4.0	14000	0.7	0.8	0.9
FE2	3.4E-37	42	8.0	4.0	14000	0.7	0.8	0.9
FE3	2.55E-37	42	8.0	4.0	14000	0.7	0.8	0.9

9.3.3. Simulation of Hysteresis Behavior

Hysteresis experiment data was available as indicated with the continuous lines in Figure 48 and Figure 52. This data was obtained by loading (by the elliptic indenter tip with the dimensions of 8-2-2 mm in x, y and z axes, respectively) the soft tissue (forearm, medial part) which had a thickness of about 40 mm. The soft tissue was loaded 15 mm (37.5 % of its thickness) with the indenter speed of 4 mm/s in 3.75 seconds. Then, the tissue was unloaded with the same speed and the indenter tip returned to its original position when the experiment time is 7.5 seconds. Within this one cycle of loading and unloading, the change of reaction force with respect to time (Figure 48) and with respect to displacement (Figure 52) was observed.

For the simulation of the experimental data, five finite element (FE) trials were performed which can be seen in Figure 48 and Figure 52. The normalized sums of square errors (NSSE) for each trial of the reaction force simulation with respect to time were presented in Figure 49, Figure 50 and Figure 51 for loading and unloading periods, for loading period only and for unloading period only, respectively. The NSSE values for each trial of the reaction force simulation with respect to displacement were presented in Figure 53, Figure 54 and Figure 55 for loading and unloading periods, for loading period only and for unloading period only, respectively.

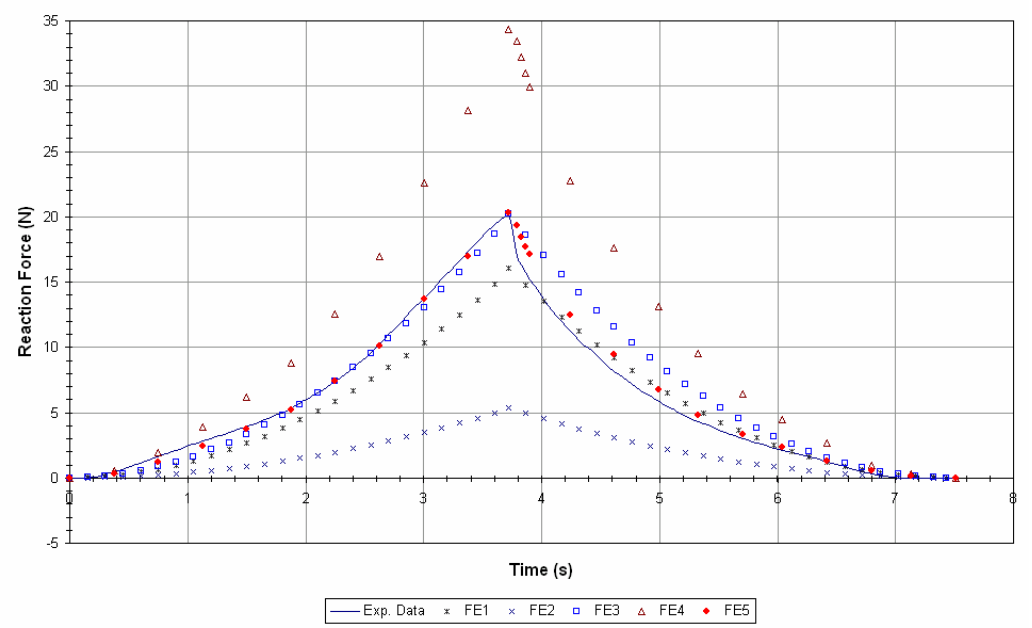

Figure 48 – Hysteresis (Time - Reaction Force) Curves for the Simulation of the Third Model

In the first finite element trial, the material model, which had been used in the last step of the simulation of relaxation behavior for this model was used. This model was not very successful in simulating the material behavior both in loading and unloading periods of the simulation as seen in Figures 48 and 52. The NSSE values of 32.66 % given in Figure 49 and 31.7 % given in Figure 53 were the proof of that. A more detailed examination of Figure 48, one can see that the simulation of the unloading period was better than the simulation of the loading period. The proof of that is given in Figure 50 and Figure 51 which presents the NSSE values in loading as 30.41 % and in unloading as 2.26 %. This can also be seen from Figure 54 and Figure 55 with the NSSE values of 28.75 % in loading and 2.96 % in unloading, respectively.

For the second FE trial of the simulation of hysteresis behavior, the material model, which had been used in the last step of the simulation of creep behavior for this

model was used. This model presented very small values of the reaction force response during the experiment time (see Figure 48) which resulted in very large NSSE values as given in the Figures 49, 50 and 51. For increasing these reaction force values, the elastic material constant (*A*) was increased from 2.55E-37 MPa to 9.58E-37 MPa in the third trial. This model was not very successful in simulating the material behavior both in loading and unloading periods of the simulation like the first one as seen in Figure 48. The NSSE value of 29.86 % given in Figure 49 and 33.64 % given in Figure 53 were the proof of that. A more detailed examination of Figure 48, one can see this time that the simulation of the loading period was better than the simulation of the unloading period. The proof of that is given in the Figure 50 and Figure 51 which presents the NSSE values in loading as 2.06 % and in unloading as 27.8 %. This can also be seen from Figure 54 and Figure 55 with the NSSE values of 1.78 % in loading and 31.86 % in unloading, respectively.

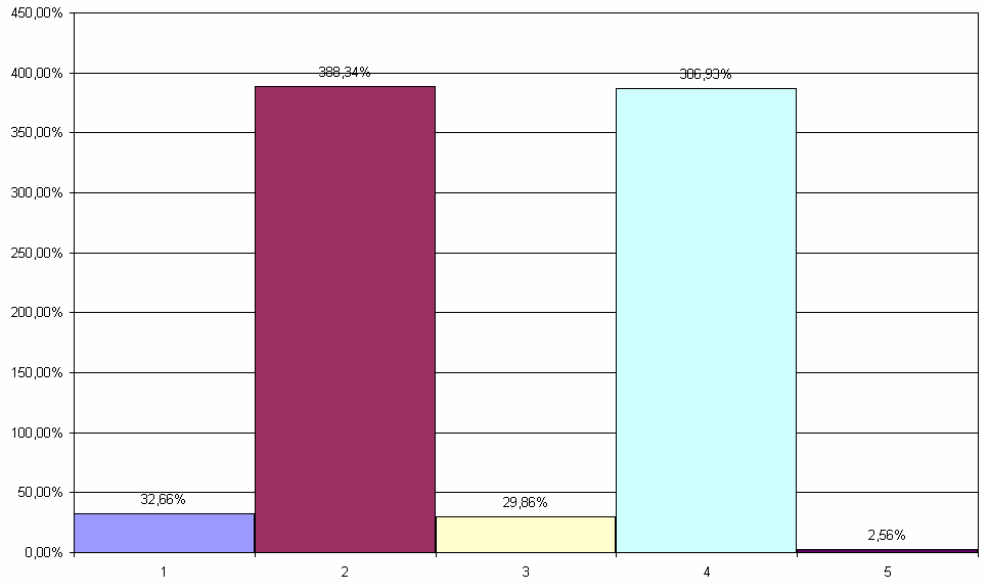

Figure 49 – Normalized Sums of Square Errors for the Hysteresis (Time - Reaction Force) Simulation of the Third Model in Loading and Unloading

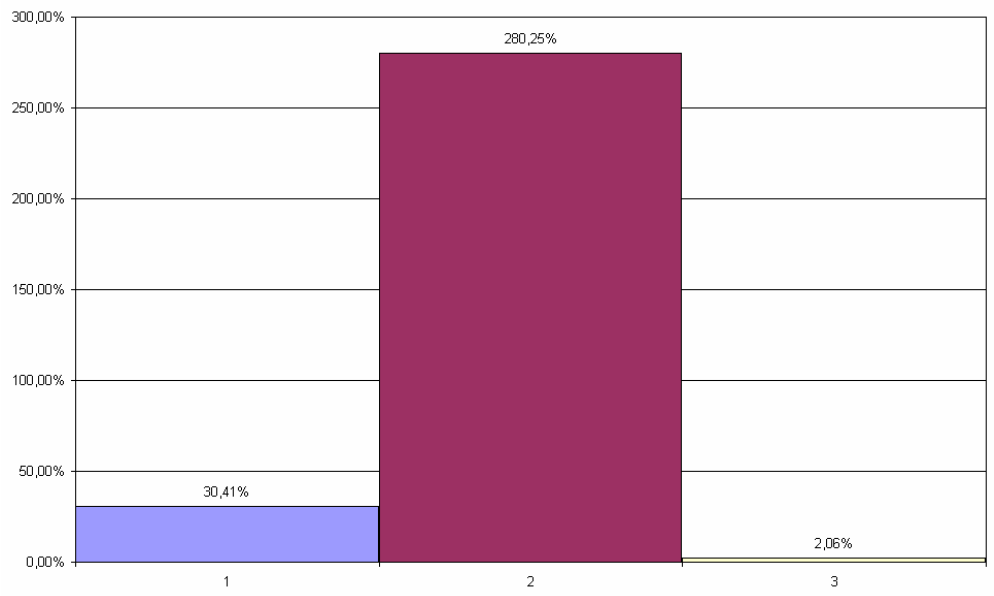

Figure 50 - Normalized Sums of Square Errors for the Hysteresis (Time - Reaction Force) Simulation of the Third Model in Loading

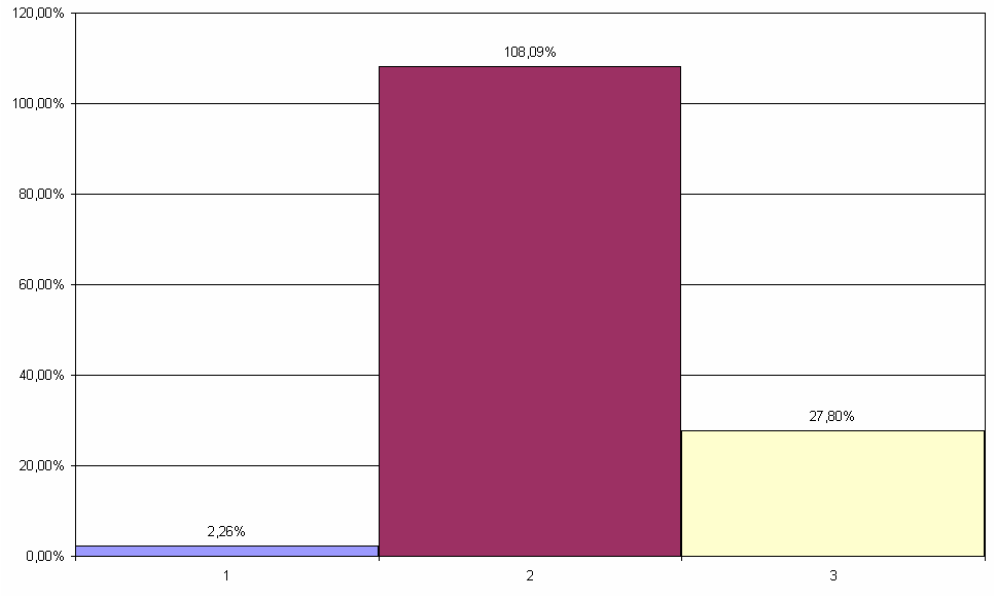

Figure 51 - Normalized Sums of Square Errors for the Hysteresis (Time - Reaction Force) Simulation of the Third Model in Unloading

The main source of these errors was thought to be due to the data acquisition speed of the experiment apparatus. By a carefully examination of Figure 48 and Figure 52, one can see the strangeness at the transition periods between the loading and the unloading periods. The indenter tip was stopped about 0.15 seconds after the loading period, and then started the unloading period. During this short time, a sudden relaxation happened in the tissue. So, for being able to simulate this behavior, the simulation procedure was changed for the fourth and fifth trials as follows:

The soft tissue was loaded 15 mm (37.5 % of its thickness) with the indenter speed of 4 mm/s in 3.75 seconds. Then, this displacement was kept constant during 0.15 seconds to allow for the relaxation behavior. Later, the tissue was unloaded and the indenter tip returned to its original position when the experiment time is 7.5 seconds.

In the fourth FE trial, the short term relaxation constant was decreased from 4 seconds to 0.02 second to be able to simulate that sudden decrease in the reaction force. The relaxation behavior between the loading and the unloading periods was seemed to be simulated which can be seen from Figure 48 and Figure 52. But this time, the magnitude of the reaction forces appeared as larger than the experimental data. The NSSE value of 386.93 % given in Figure 49 and 362.12 % given in Figure 53 are the proof of that. To decrease the magnitude of the reaction force, the elastic material constant (A) was increased once more from 9.58E-37 MPa to 1.61E-36 MPa in the last FE trial. After that trial, a good fit between the experimental data and the finite element simulation could be obtained (see Figures 48 and 52), with the NSSE value of 2.56 % in the simulation of reaction force with respect to experiment time (see Figure 49) and with the NSSE value of 2.93 % in the simulation of the reaction force with respect to displacement (see Figure 53). The constants used in each finite element trial are summarized in Table 22.

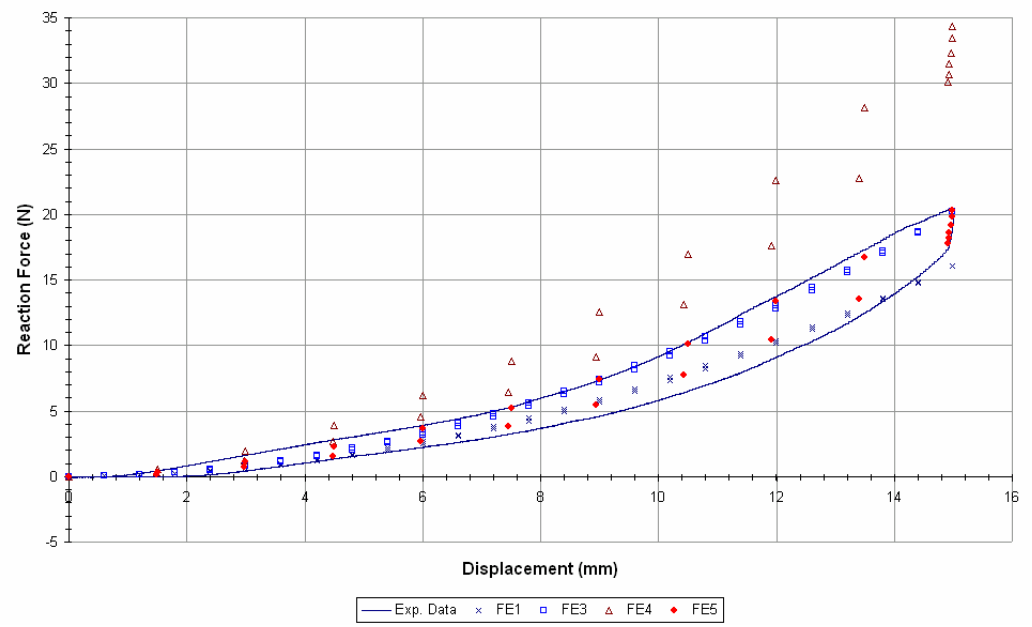

Figure 52 - Hysteresis (Displacement - Reaction Force) Curves for the Simulation of the Third Model

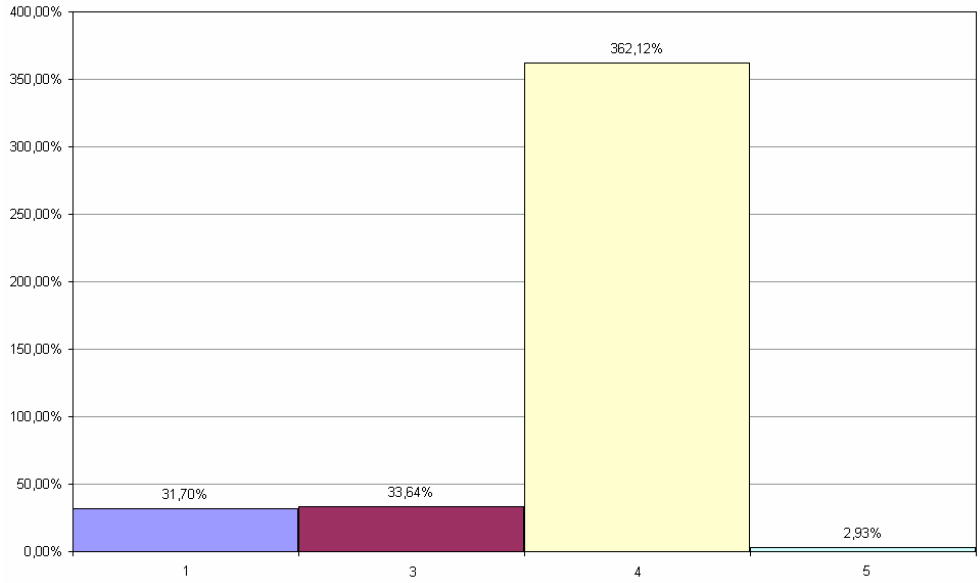

Figure 53 – Normalized Sums of Square Errors for the Hysteresis (Displacement - Reaction Force) Simulation of the Third Model in Loading and Unloading

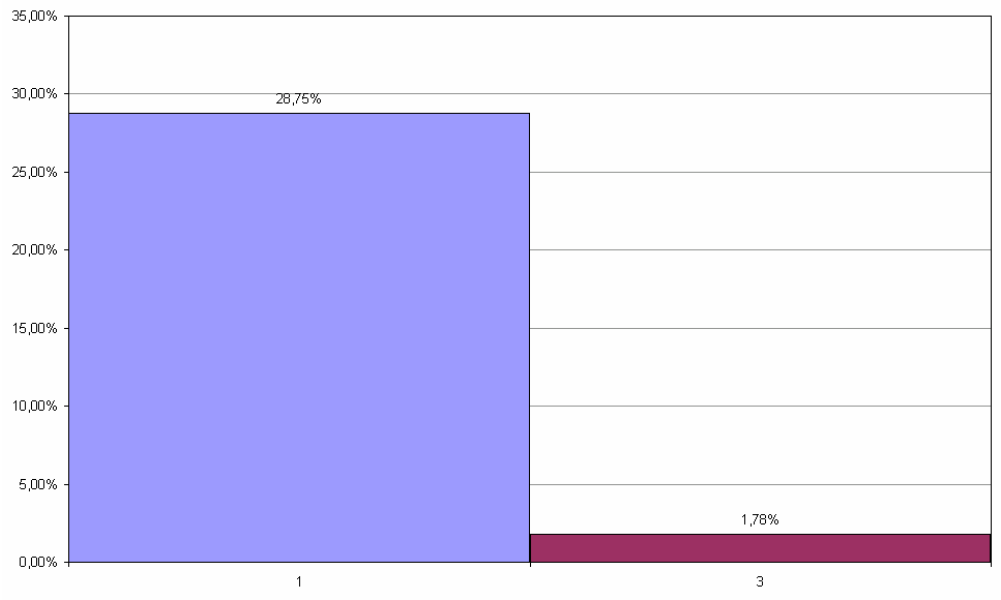

Figure 54 – Normalized Sums of Square Errors for the Hysteresis (Displacement - Reaction Force) Simulation of the Third Model in Loading

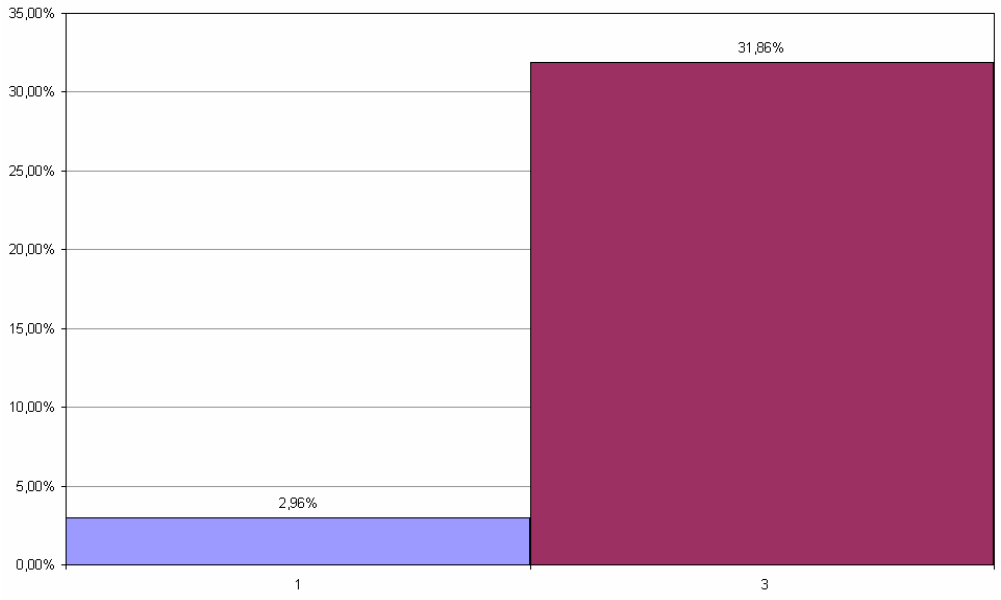

Figure 55 – Normalized Sums of Square Errors for the Hysteresis (Displacement - Reaction Force) Simulation of the Third Model in Unloading

Table 22 – Constants of the Third Material Model (equation C19) Used in the Hysteresis Simulation

Trial	A	B	C	τ_1	τ_2	a	b	c
FE1	7.6E-37	42	8.0	4.0	14000	0.7	0.8	0.9
FE2	2.55E-37	42	8.0	4.0	14000	0.7	0.8	0.9
FE3	9.58E-37	42	8.0	4.0	14000	0.7	0.8	0.9
FE4	9.58E-37	42	8.0	0.02	14000	0.7	0.8	0.9
FE5	1.61E-36	42	8.0	0.02	14000	0.7	0.8	0.9

9.3.4. Simulation of Preconditioning (Mullin's Effect) Behavior

Preconditioning experiment data was available as indicated with the continuous line in Figure 56. This data was obtained by loading (by the elliptic indenter tip with the dimensions of 8-2-2 mm in x, y and z axes, respectively) the soft tissue (forearm, medial part) which had a thickness of about 40 mm. The soft tissue was loaded 15 mm (37.5 % of its thickness) with the indenter speed of 4 mm/s in 3.75 seconds. Then, this displacement was kept constant during 0.15 seconds to allow for the relaxation behavior like in the hysteresis simulation. Later, the tissue was unloaded and the indenter tip returned to its original position when the experiment time is 7.5 seconds. This loading and unloading cycle was repeated ten times and the change of reaction force with respect to time (Figure 56) was observed.

The simulation of the experimental data was performed with the material model which had been used in the last trial for the simulation of the hysteresis behavior of this model. This simulation is concluded with the NSSE value of 3.89 % which can be assumed as acceptable for the preconditioning behavior. The constants used in the finite element trial are summarized in Table 23.

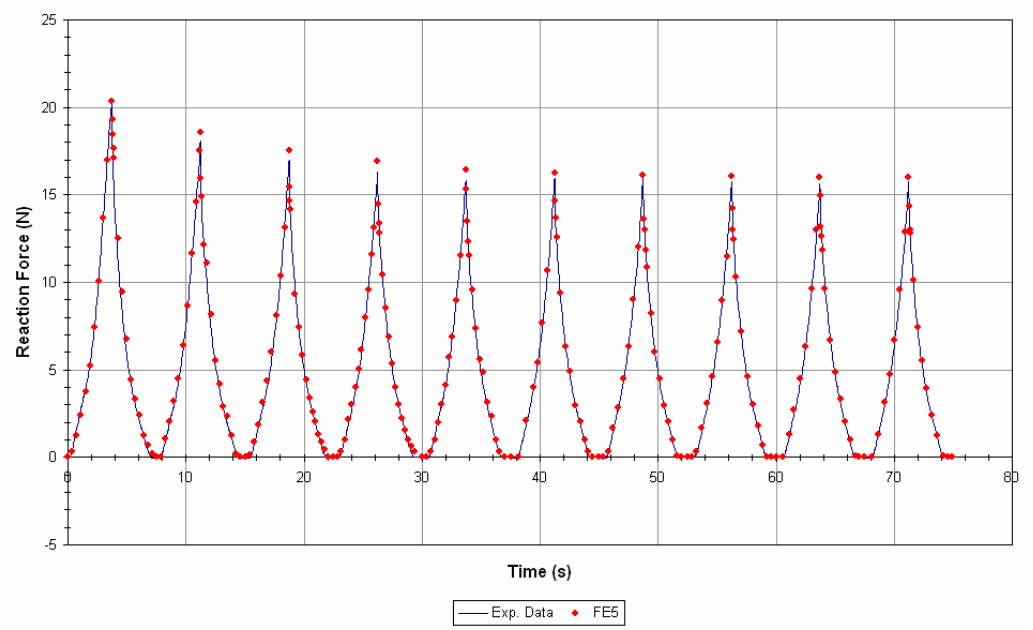

Figure 56 - Preconditioning (Mullin's Effect) Curves for the Simulation of the Third Model

Table 23 – Constants of the Third Material Model (equation C19) Used in the Preconditioning Simulation

Trial	A	B	C	τ_1	τ_2	a	b	c
FE5	1.61E-36	42	8.0	0.02	14000	0.7	0.8	0.9

CHAPTER 10

CONCLUSIONS

For the simulation of the soft tissue mechanical behaviors like relaxation, creep, hysteresis and preconditioning three models were proposed. The finite element models have also been constructed and the constants in these material models were found by using inverse finite element method.

The first model was created to simulate the relaxation and the creep behaviors of biological soft tissues. Since this model was not dependent on the strain, it was not able to simulate hysteresis and preconditioning.

For the relaxation simulation of this model, five finite element solutions were tried. After iterations, the normalized sum of square errors was appeared to be 0.47 % which proves that this simulation is rather accurate and acceptable.

For the creep simulation of the first model, three finite element solutions were tried. The initial guess for material parameters were the values obtained from the relaxation simulation. After two iterations, the normalized sum of square errors was appeared to be 0.43 % which proves that this simulation is rather accurate and acceptable.

As a conclusion, it is possible to say that the first (quasi-linear viscoelastic) model which assumes soft tissue as an isotropic material is very successful in simulating the relaxation and the creep behaviors. By changing only one of the constants, both of the characteristic soft tissue behaviors could be simulated. The simulation of relaxation could be concluded with the NSSE value of 0.47 % while the simulation

of creep could be concluded with the NSSE value of 0.43 %. The change in the coefficient was 127.3 % which includes the contribution of experimental errors as well.

The main shortcoming of the first model used in this study was the fact that it was not dependent on the strain which makes it impossible to simulate hysteresis and preconditioning behaviors. To overcome this shortcoming and be able to simulate both hysteresis and preconditioning together with relaxation and creep, the second and third quasi-linear viscoelastic models were proposed. The second material model is isotropic and the third one is anisotropic.

The second model was proposed to simulate the relaxation and the creep behaviors together with the cyclic loading behavior of biological soft tissues. Since this model was dependent on the strain together with the experiment time, it was able to simulate relaxation and creep behaviors together with cyclic loading.

For the relaxation simulation of this model, six finite element solutions were tried. In the first trial, the base model written in Appendix K was used. After five iterations, the normalized sum of square errors was appeared to be 0.6 % which proves that this simulation is rather accurate and acceptable.

For the creep simulation of the second model, three finite element solutions were tried. The initial guess for material parameters were the values obtained from the relaxation simulation. After three iterations, the normalized sum of square errors was appeared to be 0.31 % which proves that this simulation is rather accurate and acceptable.

For the hysteresis simulation of the second model, five finite element solutions were tried. In the first and second trials, the material models, which had been used in the last step of the relaxation simulation and in the last step of the creep simulation, were used, respectively. For the third trial, the elastic constant was increased to obtain larger reaction force responses than the second trial. In the fourth and fifth trials, the

simulation procedure was changed a little bit to obtain results as in the experiments. The short term relaxation constant was decreased in the fourth trial to be able to obtain sudden relaxation response as in the experiment between loading and unloading periods. In the last trial, the elastic constant was increased once more to obtain a better fit between the experimental data and the finite element solution. After the last finite element trial, the normalized sum of square errors was appeared to be 2.03 % for the simulation of the reaction force with respect to experiment time and 0.58 % for the simulation of the reaction force with respect to indenter tip displacement. These results prove that this simulation is rather accurate and acceptable for a hysteresis simulation.

For the preconditioning simulation of the second model, the last material model which had been used in the simulation of the hysteresis behavior of this model was used. The normalized sum of square errors was appeared to be 3.69 % for the simulation of the reaction force with respect to experiment time. This result proves that this simulation is rather accurate and acceptable for a preconditioning simulation.

As a conclusion, it is possible to say that the second (enhanced quasi-linear viscoelastic) model which assumes soft tissue as an isotropic material is very successful in simulating the relaxation and the creep behaviors. It can also be assumed as successful in simulating the hysteresis and preconditioning behaviors. Because, all these characteristic behaviors of soft biological tissue were tried to be simulated by only one material model. By changing the constants in the proper way, this material model could successfully be used for the simulation of the mechanical behaviors of the soft biological tissue.

The main shortcoming of the second model used in this study was the fact that it was not an anisotropic model despite the fact that the original structure of the soft tissues is much likely to anisotropic. To overcome this situation and simulating the material constants by using an anisotropic model the third model was proposed.

The third model was created to simulate the relaxation and the creep behaviors together with the cyclic loading behavior of biological soft tissues buy using an anisotropic material model. Since this model was dependent on the strain together with the experiment time like the second model, it was also able to simulate relaxation and creep behaviors together with cyclic loading.

For the relaxation simulation of this model, six finite element solutions were tried. In the first trial, the base model written in Appendix M was used. After five iterations, the normalized sum of square errors was appeared to be 0.74 % which proves that this simulation is rather accurate and acceptable.

For the creep simulation of the third model, three finite element solutions were tried. The initial guess for material parameters were the values obtained from the relaxation simulation. After three iterations, the normalized sum of square errors was appeared to be 0.31 % which proves that this simulation is rather accurate and acceptable.

For the hysteresis simulation of the third model, five finite element solutions were tried. In the first and second trials, the material models, which had been used in the last step of the relaxation simulation and in the last step of the creep simulation, were used, respectively. For the third trial, the elastic constant was increased to obtain larger reaction force responses than the second trial. In the fourth and fifth trials, the simulation procedure was changed a little bit to obtain results as in the experiments. The short term relaxation constant was decreased in the fourth trial to be able to obtain sudden relaxation response as in the experiment between loading and unloading periods. In the last trial, the elastic constant was increased once more to obtain a better fit between the experimental data and the finite element solution. After the last finite element trial, the normalized sum of square errors was appeared to be 2.56 % for the simulation of the reaction force with respect to experiment time and 2.93 % for the simulation of the reaction force with respect to indenter tip displacement. These results prove that this simulation is rather accurate and acceptable for a hysteresis simulation.

For the preconditioning simulation of the third model, the last material model which had been used in the simulation of the hysteresis behavior of this model was used. The normalized sum of square errors was appeared to be 3.89 % for the simulation of the reaction force with respect to experiment time. This result proves that this simulation is rather accurate and acceptable for a preconditioning simulation.

As a conclusion, it is possible to say that the third (enhanced quasi-linear viscoelastic) model which assumes soft tissue as an anisotropic material is very successful in simulating the relaxation and the creep behaviors. It can also be assumed as successful in simulating the hysteresis and preconditioning behaviors. Because, all these characteristic behaviors of soft biological tissue were tried to be simulated by only one material model and with minimal change in material parameters. By changing the constants in the proper way, this material model could successfully be used for the simulation of the mechanical behaviors of the soft biological tissue.

Is is also possible to simulate the experimental data by using another sets of constants within the material models. An alternative simulation of the relaxation behavior with the third model is presented in Appendix S. Here, the constants in the material model were given different values than the original simulation and the experimental data could also be simulated by these constants with the NSSE value of 0.63 %.

If one examines the history of soft tissue simulation studies, he would not be able to find any model which can simulate all the characteristic behaviors of soft tissues. So far, many scientists have worked on soft tissue simulation. Some of them could only simulate the relaxation behavior and some others could simulate the creep response by using the relaxation data. Some tried to fit soft tissue responses to mathematical series and some tried to decrease the number of constants in these formulations. This study was able to simulate all the characteristic behaviors of soft biological tissues with only one constitutive equation by some little changes in the material constants. By using these models, interaction between residual limb tissue and prosthetic socket

can be simulated which can be used for the future design of prosthetic socket. The interactions between feet and shoes of a person who has diabetes can be simulated which can be utilized for the future design of diabetic shoe. Also the interactions between bed and body of the person who has paralysis can be simulated which can be used for the future design of beds.

The finite element models created for these three material models were not able to run in short times. One of the reasons of that was the type of analysis. In these models, there applied a contact analysis instead of determining a loading type and contact analyses last in much larger times than other linear analyses in finite element softwares because of geometric nonlinearities. Another reason of these long simulation times was the number of elements in the model. Especially for having good convergence in the contact area, this area was modeled as a fine mesh area with smaller and constant length elements which caused the number of element in the model to be about 27000. The more elements in the finite element analyses always mean the longer simulation times. One other reason of the long simulation times was the fact that the material models used for these analyses were not available in the material library of the finite element software. So, they were needed to be written by a compiler and compiled during each simulation which caused the simulation times to become much longer. Also using these nonlinear material models with large strain and large displacement conditions makes the simulation times much longer. The technological constraints can also be assumed as the reason of these long submission times. The computer with which these finite element analyses were performed had a single-cored processor with the CPU speed of 3.0 GHz. It had 1024 MB memory and 120 GB of hard disc space. These specifications are far from the ones of a finite element computer and cause the simulation times to increase further.

Consequently, these presented results of the finite element models could be obtained after very long simulation times. For relaxation and creep, the simulation times reached to one hour. For hysteresis simulations, the simulation times were about one and a half hours and for preconditioning these were almost sixteen hours. However, some of these simulations could not be concluded due to convergence errors because

of the structure of the model. To overcome this situation, a better finite element model can be created for working on a computer which has better specifications than the current one. This model can have more elements which are consequently smaller than the current one. Also creating these elements in the same size and creating them as hexahedral instead of tetrahedral can give more accurate results in the simulations. After creating that kind of model and being able to run it faster, more simulations could me performed by changing the constants in the material models again and again which helps the user to understand the effect of these constant better.

Consequently, three material models were created and they were used in the simulations of three finite element models. The first one was able to simulate relaxation and creep but not cyclic loading. To also be able to simulate cyclic loading, the second model was created, but this model was not anisotropic like real soft biological tissues. To also include the anisotropy within the finite element analysis, the third material model was created. All these finite element model simulations proved that these material models are successful in simulating the mechanical behavior of soft biological tissues.

By implementing the suggestions given for the future analyses of these material models, more accurate and acceptable results with smaller values of NSSE can be obtained. Also by using the experimental data obtained from other soft tissues of human body can be used to be simulated by these material models and the results can be compared.

BIBLIOGRAPHY

Abramowitch, S. D., Woo, S. L.-Y., *An Improved Method to Analyze the Stress Relaxation of Ligaments Following a Finite Ramp Time Based on the Quasi-Linear Viscoelastic Theory,* J. Biomechanical Engineering, vol. 126, pp. 92-97, 2004.

Barry, S. I., Mercer, G. N., *Flow and Deformation in Poroelasticity-I Unusual Exact Solutions,* Mathematical and Computer Modeling, vol. 30, pp. 23-29, 1999.

Bernstein, B., Kearsley, E. A., Zapas, L. S., *A Study of Stress Relaxation with Finite Strains,* Trans. Soc. Rheol., vol.7, pp. 391-410, 1963.

Bischoff, J. E, Arruda, E. M., Grosh, K., *Finite Element Modeling of Human Skin Using an Isotropic, Nonlinear Elastic Constitutive Model,* Journal of Biomechanics, vol. 33, pp. 645-652, 2000.

Bischoff, J. E, Arruda, E. M., Grosh, K., *A Rheological Network Model for the Continuum Anisotropic and Viscoelastic Behavior of Soft Tissue,* Biomechan Model Mechanobiol, vol. 3, pp. 56-65, 2004.

Bischoff, J. E., *Static Indentation of Anisotropic Biomaterials Using Axially Asymmetric Indenters - a Computational Study,* Journal of Biomechanical Engineering, vol. 126, pp. 498-505, 2004.

Bischoff, J. E., *Reduced Parameter Formulation for Incorporating Fiber Level Viscoelasticity into Tissue Level Biomechanical Models,* Annals of Biomedical Engineering, vol. 34, pp. 1164-1172, 2006.

Cheng, L., Xia, X., Yu, W., Scriven, L. E., Gerberich, W., *Flat-Punch Indentation of Viscoelastic Materials,* Journal of Polymer Science: Part B: Polymer Physics, vol. 38, pp. 10-22, 2000.

Choi, A. P. C., Zheng Y. P., *Estimation of Young's Modulus and Poisson's Ratio of Soft Tissue from Indentation Using Two Different-sized Indentors: Finite Element*

Analysis of the Finite Deformation Effect, Med. Biol. Eng. Comput., vol. 43, pp. 258-264, 2005.

Commean, P. K., Smith, K. E., Vannier, M. W., Szabo, B. A., Actis, R. L., *Finite Element Modeling and Experimental Verification of Lower Extremity Shape Change Under Load,* J. Biomechanics, vol. 30, pp. 531-536, 1997.

Cowin, S. C., *Anisotropic Poroelasticity: Fabric Tensor Formulation*, Mechanics of Materials, vol. 36, pp. 665-677, 2004.

Dehoff, P. H., *On the Nonlinear Viscoelastic Behavior of Soft Biological Tissues,* J. Biomechanics, vol. 11, pp. 35-40, 1978.

Delingette, H., *Toward Realistic Soft-Tissue Modeling in Medical Simulation,* Proceedings of the IEEE, vol. 86, pp. 512-523, 1998.

Deng, B., Hubbard, R., *Measuring and Modeling Force-Deflection Responses of Human Thighs in Seated Posture,* Advances in Biomechanics, vol. 28, pp. 101-102, 1994.

Dortmans, L. J. M. G., Sauren, A. A. H. J., Rousseau, E. P. M., *Parameter Estimation Using the Quasi-Linear Viscoelastic Model Proposed by Fung,* J. Biomechanical Engineering, vol. 106, pp. 198-203, 1984.

Drozdov, A. D., *A Model for the Viscoelastic Behavior of Polymers at Finite Strains,* Archive of Applied Mechanics, vol. 68, pp. 308-322, 1998.

Drozdov, A. D., Ghristiansen, J. deC., *Constitutive Equations for the Nonlinear Viscoelastic and Viscoplastic Behavior of Thermoplastic Elastomers,* International Journal of Engineering Science, vol. 44, pp. 205-226, 2006.

Drozdov, A. D., Kalamkarov, A. L., *A Constitutive Model for Nonlinear Viscoelastic Behavior of Polymers,* Polymer Engineering and Science, vol. 36, pp. 1907-1919, 1996.

Fung, Y. C., *Foundations of Solid Mechanics,* Prentice-Hall, Englewood Cliffs, NJ., pp. 436-439, 1965.

Fung, Y. C., *Elasticity of Soft Tissues in Simple Elongation,* Am. J. Physiology, vol. 213, pp. 1532-1544, 1967.

Fung, Y. C., *Biomechanics – Its Scope, History and Some Problems of Continuum Mechanics in Physiology,* Applied Mechanics, vol. 21, pp. 1-20, 1969.

Fung, Y. C., *Biorheology of Soft Tissues,* Biorheology J., vol. 10, pp. 139-155, 1973.

Fung, Y. C., *On Mathematical Models of Stress-Strain Relationship for Living Soft Tissues,* Mechanika Polymerov USSR, vol. 10, pp. 850-867, 1975.

Fung, Y. C., *On Pseudo-elasticity of Living Tissues*, Mechanics Today J., vol. 5, pp. 487-504, 1980.

Fung, Y. C., *Structure and Stress-Strain Relationship of Soft Tissues,* Am. Zool., vol. 24, pp. 13-22, 1984.

Fung, Y. C., *Biomechanics: Mechanical Properties of Living Tissues,* Springer-Verlag, Second Edition, pp. 23-65, 1993.

Fung, Y. C., *A First Course in Continuum Mechanics,* Prentice Hall, Third Edition, 1994.

Fung, Y. C., Perrone, N., Anliker, M., *Stress-Strain History Relations of Soft Tissues in Simple Elongation,* Biomechanics: Its Foundations and Objectives, chapter 7, pp. 181-208, Prentice-Hall, 1970.

Fung, Y. C., Fronek, K. and Paticucci, P., *On Pseudo-elasticity of Arteries and the Choice of its Mathematical Expression,* Amer. J. of Physiology, vol. 237, pp. 620-631, 1979.

Gou, P. E., *Strain Energy Function for Biological Tissues,* J. Biomechanics, vol. 3, pp. 547-550, 1970.

Gradshteyn, I. S., Ryzhik, I. M., *Table of Integrals, Serials and Products*, Academic Press, 4^{th} edition, 1965.

Grashow, J. S., Sacks, M. S., Liao, J., Yoganathan, A. P., *Planar Biaxial Creep and Stress Relaxation of the Mitral Valve Anterior Leaflet,* Annals of Biomedical Engineering, vol. 34, pp. 1509-1518, 2006.

Green, A. E., Adkins, J. E., *Large Elastic Deformations and Nonlinear Continuum Mechanics,* Oxford University Press, pp. 1-33, 96-123, 1960.

Green, A. E., Zerna, W., *Theoretical Elasticity,* Oxford University Press, pp. 80-113, 1960.

Henry, W., Haslach, Jr., *Nonlinear Viscoelastic, Thermodynamically Consistent, Models for Biological Soft Tissue,* Biomechan Model Mechanobiol, vol. 3, pp. 172-189, 2005.

Holt, B., Tripathi, A., Morgan, J., *Viscoelastic Response of Human Skin to Low Magnitude Physiologically Relevant Shear*, Journal of Biomechanics, DOI:10.1016/j.jbiomech.2008.06.008, 2008.

Hoppin, F. G., Lee, G. C. and Dawson, S. V., *Properties of Lung Parenchyma in Distortion,* J. Applied Physiology, vol. 39, pp. 742-751, 1975.

Kaliske, M., Rothert, H. *Formulation and Implementation of Three-Dimensional Viscoelasticity at Small and Finite Strains,* Computational Mechanics, vol. 19, pp. 228-239, 1997.

Kauer, M., Vuskovic, V., Dual, J., Szekely, G., Bajka, M., *Inverse Finite Element Characterization of Soft Tissues,* Medical Image Analysis, vol. 6, pp. 275-287, 2002.

Khan, A., Zhang, H., *Finite Deformation of a Polymer: Experiments and Modeling,* International Journal of Plasticity, vol. 17, pp. 1167-1188, 2001.

Kim, J. H., Jeong, S. J., Lee, H. J., Han, S. W., Choi, B. I., Park, S. H., Yang, D. Y., *Linear Analysis of the Viscoelastic Response of Polymer Micro-Pillars Using the Open-Loop Flat Punch Indentations Test,* Philosophical Magazine, vol. 86, pp. 5679-5690, 2006.

Korhonen, R. K., Saarakkala, S., Toyras, J., Laasanen, M. S., Kiviranta, I., Jurvelin, J. S., *Experimental and Numerical Validation for the Novel Configuration of an Arthroscopic Indentation Instrument*, Phys. Med. Biol., vol. 48, pp. 1565–1576, 2003.

Kraft, M., Meissner, J., Kaschta J., *Linear Viscoelastic Characterization of Polymer Melts with Long Relaxation Times,* Macromolecules, vol. 32, pp. 751-757, 1999.

Kroon, M., Holzapfel, G.A., *A New Constitutive Model for Multi-layered Collagenous Tissues*, Journal of Biomechanics, DOI:10.1016/j.jbiomech.2008.05.033, 2008.

Laible, J. P., Pflaster, D., Simon, B. R., Krag, M. H., Pope, M., Haugh, L. D., *A Dynamic Material Parameter Estimation Procedure for Soft Tissue Using a Poroelastic Finite Element Model,* Journal of Biomechanical Engineering, vol. 116, pp. 19-29, 1994.

Ledoux, W. R., Blevins, J. J., *The Compressive Material Properties of the Plantar Soft Tissue,* Journal of Biomechanics, vol. 40, pp. 2975-2981, 2007.

Lee, A., McKenna, G. B., *Anomalous Aging in Two-Phase Systems: Creep and Stress Relaxation Differences in Rubber-Toughened Epoxies,* J. Polym. Sci. B: Polym. Phys., vol. 35, pp. 1167-1174, 1997.

Lei, F., Szeri, A. Z., *Inverse Analysis of Constitutive Models: Biological Soft Tissues,* Journal of Biomechanics, vol. 40, pp. 936-940, 2007.

Lianis, G., *Constitutive Equations for Viscoelastic Solids under Large Deformation,* A&ES Report No.63-5, Perdue University, 1963.

Malvern, L. E., *Introduction to the Mechanics of a Continuous Medium,* Prentice-Hall, Inc., pp. 150-172, 220-226, 273-327, 1969.

Maurel, W., Wu, Y., Thalmann, N. M., Thalmar, D., *Biomechanical Models for Soft Tissue Simulation,* Springer-Verlag, 1998.

Mooney, M., *A Theory of Large Elastic Deformation*, J. Applied Physics, vol. 11, pp. 582-592, 1940.

Mow, V. C., *Biphasic Creep and Stress Relaxation of Articular Cartilage in Compression,* Journal of Biomechanical Engineering, vol. 102, pp.73-84, 1980.

Oza, A., Vanderby Jr., R., Lakes, R. S., *Generalized Solution for Predicting Relaxation from Creep in Soft Tissue: Application to Ligament,* International Journal of Mechanical Sciences, vol. 48, pp. 662-673, 2006.

Pena, E., Pena, J. A., Doblare, M., *On Modelling Nonlinear Viscoelastic Effects in Ligaments*, Journal of Biomechanics, DOI:10.1016/j.jbiomech.2008.06.019, 2008.

Petekkaya, A.T., *In Vivo Indenter Experiments on Soft Biological Tissues for Identification of Material Models and Corresponding Parameters,* M.S. Thesis, Middle East Technical University, 2008.

Provenzano, P. P., Lakes, R. S., Corr, D. T., Vanderby, R., *Application of Nonlinear Viscoelastic Models to Describe Ligament Behavior,* Biomechan Model Mechanobiol, vol. 1, pp. 45-57, 2002.

Samani, A., Plewes, D., *A Method to Measure the Hyperelastic Parameters of ex vivo Breast Tissue Samples,* Physics in Medicine and Biology, vol. 49, pp. 4395-4405, 2004.

Samani, A., Plewes, D., *An Inverse Problem Solution for Measuring the Elastic Modulus of Intact ex vivo Breast Tissue Tumours,* Physics in Medicine and Biology, vol. 52, pp. 1247-1260, 2007.

Sanjeevi, R., *A Viscoelastic Model for the Mechanical Properties of Biological Materials*, J. Biomechanics, vol. 15, pp. 107-109, 1982.

Sauren, A. A. H. J., Rousseau, E. P. M., *A Concise Sensitivity Analysis of the Quasi-Linear Viscoelastic Model Proposed by Fung,* J. Biomechanical Engineering, vol. 105, pp. 92-95, 1983.

Schmidth, A., Gaul, L., *Finite Element Formulation of Viscoelastic Constitutive Equations Using Fractional Time Derivatives,* Nonlinear Dynamics, vol. 39, pp. 37-55, 2002.

Schwartz, J. M., Denninger, M., Rancourt, D., Moisan, C., Laurendeau, D., *Modeling Liver Tissue Properties Using a NonLinear Viscoelastic Model for Surgery Simulation,* Medical Image Analysis, vol. 9, pp. 103-112, 2005.

Setyabudhy, R. H., Akram, A., Hubbard, R. P., Beckett, C., Averill, R. C., *Measuring and Modeling of Human Soft Tissue and Seat Interaction*, Society of Automotive Engineers, Inc., pp. 135-142, 1997.

Spilker, R. L., Suh, J. K., *Formulation and Evaluation of a Finite Element Model for the Biphasic Model of Hydrated Soft Tissues,* J. Computers and Structures, vol. 35, pp. 425-439, 1990.

Sun, W., Sacks, M. S., *Multiaxial MechanicalBehavior of Biological Materials,* Annu. Rev. Biomed. Eng., vol. 5, pp. 251-284, 2003.

Suvorora, J. V., Ohlson, N. G., Alexeeva, S. I., *An Approach to the Description of Time-Dependent Materials,* Materials and Design, vol. 24, pp. 293-297, 2003.

Tekkaya, E., *ME413: Introduction to Finite Element Analysis Lecture Notes,* METU, Department of Mechanical Engineering, 2003-2004 Spring Semester.

The Wolfram Functions Site, *ExpIntegralEi*, http://functions.wolfram.com/webMathematica/FunctionEvaluation.jsp?name=ExpIntegralEi , last accessed date: Jan 7th, 2008.

The Wolfram Functions Site, *ExpIntegralEi*, http://functions.wolfram.com/PDF/ExpIntegralEi.pdf , last accessed date: Jan 7th, 2008.

Toms, S. R., Dakin, G. J., Lemons, J. E., Eberhardt, A. W., *Quasi-Linear Viscoelastic Behavior of the Human Periodontal Ligament,* Journal of Biomechanics, vol. 35, pp. 1411-1415, 2002.

Tong, P. and Fung, Y. C., *The Stress-Strain Relationship for the Skin,* J. Biomechanics, vol. 9, pp. 649-657, 1976.

Tönük, E., *Dizaltı Ampute Yumuşak Doku Mekanik Özelliklerinin Araştırılması için Deney Cihazı Tasarımı ve Üretimi*, Makina Tasarım ve İmalat Dergisi Cilt 5, Sayı 1, 42-49, Mayıs 2003.

Tönük, E., *Dizaltı Protez Kullananlarda Yumuşak Doku Mekanik Özelliklerinin Belirlenmesi İçin İndentör,* The Scientific and Technical Research Council of Turkey, MİSAG-183, 2004.

Tönük, E., *Introduction to Biomechanics Lecture Notes*, Middle East Technical University, 2006.

Tönük, E., Silver-Thorn, M. B., *Nonlinear Elastic Material Property Estimation of Lower Extremity Residual Limb Tissues,* IEEE Transactions on Neural Systems and Rehabilitation Engineering, vol. 11, pp. 43-53, 2003.

Tönük, E., Silver-Thorn, M. B., *Nonlinear Viscoelastic Material Property Estimation of Lower Extremity Residual Limb Tissues,* Journal of Biomechanical Engineering, vol. 126, pp. 289-300, 2004.

Vaishnav, R. N., Young, J. T., Janicki, J. S. and Patel, D. J., *Nonlinear Anisotropic Elastic Poperties of the Canine Aorta,* Biophysical J., vol. 12, pp. 1008-1027, 1972.

Vannah, W. M., Childress, D. S., *Indentor Tests and Finite Element Modeling of Bulk Muscular Tissue in Vivo,* Journal of Rehabilitation Research and Development, vol. 33, pp. 239-252, 1996.

Wang, J.-L., Shirazi-Adl, S., Engin, A. E., Parnianpour, M., *Modeling of Viscoelastic Behavior of Soft Tissues: A Parametric Study of Methods Based on Prony Series and Bailey Norton Law*, Advances in Bioengineering, vol. 28, pp. 49-50, 1994.

Wolfram Mathworld Site, Exponential Integral, http://mathworld.wolfram.com/ExponentialIntegral.html , last accessed date: Jan 7 th, 2008.

Xia, H., Song, M., Zhang, Z., Richardson, M., *Microphase Separation, Stress Relaxation, and Creep Behavior of Polyurethane Nanocomposites,* Journal of Applied Polymer Science, vol. 103, pp. 2992-3002, 2007.

Yin, Y., Ling, S-F., Liu, Y., *A Dynamic Indentation Method for Characterizing Soft Incompressible Viscoelastic Materials*, Materials Science and Engineering A, vol. 379, pp. 334–340, 2004.

APPENDIX A

DERIVATION OF THE CONSTITUTIVE EQUATIONS FOR QLV MODELING BY ASSUMING SOFT TISSUE AS AN ISOTROPIC MATERIAL

The time dependent 2^{nd} Piola-Kirchoff stress can be written by using the one dimensional theory of QLV as;

$$\sigma(t)=\int_0^t G(t-\tau)\frac{\partial\sigma^e[\varepsilon(\tau)]}{\partial\tau}d\tau \quad \text{.....(A1)}$$

where; $\sigma(t)$ is QLV stress at any time *t*; $G(-)$ is the reduced relaxation function and $\sigma^e(-)$ is the elastic stress function. Since the elastic stress function is a function of strain and time, equation (A1) can be rewritten as;

$$\sigma(t)=\int_0^t G(t-\tau)\frac{\partial\sigma^e[\varepsilon(\tau)]}{\partial\varepsilon(\tau)}\frac{\partial\varepsilon(\tau)}{\partial\tau}d\tau \quad \text{.....(A2)}$$

where; the term $\frac{\partial\varepsilon(\tau)}{\partial\tau}$ is called *the strain rate* and can be denoted with $\dot{\varepsilon}$ in the loading portion and it is equal to zero in the relaxation portion of the experiment.

For purposes here, the reduced relaxation function was taken to be;

$$G(t)=\frac{1+C[E_1(t/\tau_2)-E_1(t/\tau_1)]}{1+C\ln(\tau_2/\tau_1)} \quad \text{.....(A3)}$$

So;

$$G(t-\tau)=\frac{1+C\left[E_1\left(t-\tau/\tau_2\right)-E_1\left(t-\tau/\tau_1\right)\right]}{1+C\ln\left(\tau_2/\tau_1\right)} \quad \text{.....(A4)}$$

where; C is a material parameter related to the viscous damping; τ_1 and τ_2 are material parameters related to the strain rates over which hysteresis is nearly constant and E_1 is the first exponential integral function which is in the form;

$$E_1(x)=\int_1^{\infty}\frac{e^{-tx}}{t}dt=\int_x^{\infty}\frac{e^{-u}}{u}du \quad \text{.....(A5)}$$

The elastic stress function, $\sigma^e(\varepsilon)$ was assumed to be represented through the nonlinear elastic relationship;

$$\sigma^e(\varepsilon)=A\left(e^{B\varepsilon}-1\right) \quad \text{.....(A6)}$$

where; A and B are material constants.

So, the term $\frac{\partial\sigma^e[\varepsilon(\tau)]}{\partial\varepsilon(\tau)}$ in equation (A2) becomes;

$$\frac{\partial\sigma^e[\varepsilon(\tau)]}{\partial\varepsilon(\tau)}=\frac{\partial}{\partial\varepsilon}\left[A\left(e^{B\varepsilon}-1\right)\right] \quad \text{.....(A7)}$$

$$=ABe^{B\varepsilon} \quad \text{.....(A8)}$$

$$=ABe^{B\dot{\varepsilon}\tau} \quad \text{.....(A9)}$$

Note that, the equation $\varepsilon=\dot{\varepsilon}\tau$ has been used in equation (A9) to make it able to be integrated over time.

Substituting equations (A4) and (A9) into equation (A2), the stress history from 0 to t_0 (beginning of relaxation) and from t_0 to the end of test period can be obtained as;

$$\sigma(0 \le t \le t_0) = \int_0^t \left(\frac{1 + C\left[E_1\left(t - \tau / \tau_2 \right) - E_1\left(t - \tau / \tau_1 \right) \right]}{1 + C \ln(\tau_2 / \tau_1)} \right) ABe^{B\dot{\varepsilon}\tau}\, \dot{\varepsilon}\, d\tau \quad \text{.....(A10)}$$

Note the stress response from t_0 to the end of the experiment includes the stress history up to t_0 plus the stress history from t_0 onward. However, since the strain rate from t_0 onward is zero, we are simply left with;

$$\sigma(t > t_0) = \int_0^{t_0} \left(\frac{1 + C\left[E_1\left(t - \tau / \tau_2 \right) - E_1\left(t - \tau / \tau_1 \right) \right]}{1 + C \ln(\tau_2 / \tau_1)} \right) ABe^{B\dot{\varepsilon}\tau}\, \dot{\varepsilon}\, d\tau \quad \text{.....(A11)}$$

Since this study is dealing with the relaxation part of the experiment, derivation will go on from equation (A11).

Rearranging and simplifying;

$$\sigma(t) = \frac{AB\dot{\varepsilon}}{1 + C \ln(\tau_2 / \tau_1)} \int_0^{t_0} e^{B\dot{\varepsilon}\tau} \left\{ 1 + C\left[E_1\left(t - \tau / \tau_2 \right) - E_1\left(t - \tau / \tau_1 \right) \right] \right\} d\tau \quad \text{.....(A12)}$$

$$= \frac{AB\dot{\varepsilon}}{1 + C \ln(\tau_2 / \tau_1)} \left\{ \int_0^{t_0} e^{B\dot{\varepsilon}\tau}\, d\tau + C \int_0^{t_0} e^{B\dot{\varepsilon}\tau} E_1\left(t - \tau / \tau_2 \right) d\tau - C \int_0^{t_0} e^{B\dot{\varepsilon}\tau} E_1\left(t - \tau / \tau_1 \right) d\tau \right\}$$

.....(A13)

$$= \frac{AB\dot{\varepsilon}}{1 + C \ln(\tau_2 / \tau_1)} \left[I_1 + C(I_2 - I_3) \right] \text{.....(A14)}$$

where;

$$I_1 = \int_0^{t_0} e^{B\dot{\varepsilon}\tau}\, d\tau \quad \text{.....(A15)}$$

$$I_2 = \int_0^{t_0} e^{B\dot{\varepsilon}\tau} E_1\left(t - \tau \big/ \tau_2 \right) d\tau \quad \text{.....(A16)}$$

$$I_3 = \int_0^{t_0} e^{B\dot{\varepsilon}\tau} E_1\left(t - \tau \big/ \tau_1 \right) d\tau \quad \text{.....(A17)}$$

<u>*Formula:*</u> $\int e^{ax}\, dx = \frac{1}{a} e^{ax}$ .....(A18)

Substituting equation (A18) into equation (A15), one obtains;

$$I_1 = \int_0^{t_0} e^{B\dot{\varepsilon}\tau}\, d\tau = \frac{1}{B\dot{\varepsilon}}\, e^{B\dot{\varepsilon}\tau}\Big|_{\tau=0}^{t_0} = \frac{1}{B\dot{\varepsilon}} \left(e^{B\dot{\varepsilon}t_0} - 1 \right)$$

$$\Rightarrow \quad I_1 = \frac{e^{B\dot{\varepsilon}t_0} - 1}{B\dot{\varepsilon}} \quad \text{.....(A19)}$$

The first exponential integral function is related to the general exponential integral function with the following formula;

$$E_1(x) = -E_i(-x) \quad \text{.....(A20)}$$

where; $E_1(x)$ is the first exponential integral function and $E_i(x)$ is the general exponential integral function.

Substituting equation (A20) into equations (A16) and (A17), one obtains;

$$I_2 = \int_0^{t_0} e^{B\dot{\varepsilon}\tau} E_1\left(t - \tau \big/ \tau_2 \right) d\tau = -\int_0^{t_0} e^{B\dot{\varepsilon}\tau} E_i\left(-(t-\tau) \big/ \tau_2 \right) d\tau$$

$$\Rightarrow \quad I_2 = -\int_0^{t_0} e^{B\dot{\varepsilon}\tau} E_i\left(\tau - t/\tau_2\right) d\tau \quad \text{.....(A21)}$$

And similarly;

$$\Rightarrow \quad I_3 = -\int_0^{t_0} e^{B\dot{\varepsilon}\tau} E_i\left(\tau - t/\tau_1\right) d\tau \quad \text{.....(A22)}$$

Substituting equations (A19), (A21) and (A22) into equation (A14), one obtains;

$$\sigma(t) = \frac{AB\dot{\varepsilon}}{1 + C\,\ln(\tau_2/\tau_1)} \left\{ \left(\frac{e^{B\dot{\varepsilon}t_0} - 1}{B\dot{\varepsilon}} \right) + C \left[\begin{array}{l} \left(-\int_0^{t_0} e^{B\dot{\varepsilon}\tau} E_i\left(\tau - t/\tau_2\right) d\tau \right) \\ -\left(-\int_0^{t_0} e^{B\dot{\varepsilon}\tau} E_i\left(\tau - t/\tau_1\right) d\tau \right) \end{array} \right] \right\} \quad \text{.....(A23)}$$

$$= \frac{AB\dot{\varepsilon}}{1 + C\,\ln(\tau_2/\tau_1)} \left[\left(\frac{e^{B\dot{\varepsilon}t_0} - 1}{B\dot{\varepsilon}} \right) + C \left(\begin{array}{l} \int_0^{t_0} e^{B\dot{\varepsilon}\tau} E_i\left(\tau - t/\tau_1\right) d\tau \\ -\int_0^{t_0} e^{B\dot{\varepsilon}\tau} E_i\left(\tau - t/\tau_2\right) d\tau \end{array} \right) \right] \quad \text{.....(A24)}$$

$$= \frac{AB\dot{\varepsilon}}{1 + C\,\ln(\tau_2/\tau_1)} \left[\left(\frac{e^{B\dot{\varepsilon}t_0} - 1}{B\dot{\varepsilon}} \right) + C\left(I_4 - I_5\right) \right] \quad \text{.....(A25)}$$

where;

$$I_4 = \int_0^{t_0} e^{B\dot{\varepsilon}\tau} E_i\left(\tau - t/\tau_1\right) d\tau \quad \text{.....(A26)}$$

$$I_5 = \int_0^{t_0} e^{B\dot{\varepsilon}\tau} E_i\left(\tau - t/\tau_2\right) d\tau \quad \text{.....(A27)}$$

Changing variables in equations (A26) and (A27) as;

$$
\begin{aligned}
&x = \tau - t \\
&\tau = 0 \;\Rightarrow x = -t \;\;;\;\; \tau = t_0 \;\Rightarrow x = t_0 - t \\
&\Rightarrow \;\; \tau = x + t \\
&\Rightarrow \;\; d\tau = dx
\end{aligned}
\qquad \text{.....(A28)}
$$

they become;

$$I_4 = \int_{-t}^{t_0 - t} e^{B\dot{\varepsilon}(x+t)} E_i\left(x/\tau_1\right) dx = e^{B\dot{\varepsilon}t} \int_{-t}^{t_0 - t} e^{B\dot{\varepsilon}x} E_i\left(x/\tau_1\right) dx \qquad \text{.....(A29)}$$

$$I_5 = \int_{-t}^{t_0 - t} e^{B\dot{\varepsilon}(x+t)} E_i\left(x/\tau_2\right) dx = e^{B\dot{\varepsilon}t} \int_{-t}^{t_0 - t} e^{B\dot{\varepsilon}x} E_i\left(x/\tau_2\right) dx \qquad \text{.....(A30)}$$

Formula:

$$\int e^{bz} E_i(az)\, dz = \frac{e^{bz} E_i(az) - E_i[(a+b)z]}{b} \qquad \text{.....(A31)}$$

Applying the formula in equation (A31) to equations (A29) and (A30), one obtains;

$$
\begin{aligned}
I_4 &= e^{B\dot{\varepsilon}t} \int_{-t}^{t_0 - t} e^{B\dot{\varepsilon}x} E_i\left(x/\tau_1\right) dx \\
&= e^{B\dot{\varepsilon}t} \left[\frac{e^{B\dot{\varepsilon}x} E_i\left(x/\tau_1\right) - E_i\left[\left(B\dot{\varepsilon} + 1/\tau_1\right)x\right]}{B\dot{\varepsilon}} \right]_{x=-t}^{t_0 - t}
\end{aligned}
\qquad \text{.....(A32)}
$$

and similarly;

$$I_5 = e^{B\dot{\varepsilon}t} \int_{-t}^{t_0 - t} e^{B\dot{\varepsilon}x} E_i\left(x/\tau_2\right) dx$$

$$= e^{B\dot{\varepsilon}t}\left[\frac{e^{B\dot{\varepsilon}x}E_i\left(x/\tau_2\right) - E_i\left[\left(B\dot{\varepsilon} + 1/\tau_2\right)x\right]}{B\dot{\varepsilon}}\right]\Bigg|_{x=-t}^{t_0-t} \quad \text{.....(A33)}$$

Substituting equations (A32) and (A33) into equation (A25), one obtains;

$$\sigma(t) = \frac{AB\dot{\varepsilon}}{1 + C\ln\left(\frac{\tau_2}{\tau_1}\right)}\left\{\left(\frac{e^{B\dot{\varepsilon}t_0} - 1}{B\dot{\varepsilon}}\right) + C\left\{\begin{array}{l} e^{B\dot{\varepsilon}t}\left[\dfrac{e^{B\dot{\varepsilon}x}E_i\left(x/\tau_1\right) - E_i\left[\left(B\dot{\varepsilon} + 1/\tau_1\right)x\right]}{B\dot{\varepsilon}}\right]\Bigg|_{x=-t}^{t_0-t} \\ -e^{B\dot{\varepsilon}t}\left[\dfrac{e^{B\dot{\varepsilon}x}E_i\left(x/\tau_2\right) - E_i\left[\left(B\dot{\varepsilon} + 1/\tau_2\right)x\right]}{B\dot{\varepsilon}}\right]\Bigg|_{x=-t}^{t_0-t} \end{array}\right\}\right\}$$

.....(A34)

$$\sigma(t) = \frac{AB\dot{\varepsilon}}{1 + C\ln\left(\frac{\tau_2}{\tau_1}\right)}\left\{\left(\frac{e^{B\dot{\varepsilon}t_0} - 1}{B\dot{\varepsilon}}\right) + C\left\{\frac{e^{B\dot{\varepsilon}t}}{B\dot{\varepsilon}}\left[\begin{array}{l} e^{B\dot{\varepsilon}x}E_i\left(x/\tau_1\right) - E_i\left[\left(B\dot{\varepsilon} + 1/\tau_1\right)x\right] \\ -e^{B\dot{\varepsilon}x}E_i\left(x/\tau_2\right) + E_i\left[\left(B\dot{\varepsilon} + 1/\tau_2\right)x\right] \end{array}\right]\Bigg|_{x=-t}^{t_0-t}\right\}\right\}$$

.....(A35)

$$\sigma(t) = \frac{AB\dot{\varepsilon}}{1 + C\ln\left(\frac{\tau_2}{\tau_1}\right)}\left\{\left(\frac{e^{B\dot{\varepsilon}t_0} - 1}{B\dot{\varepsilon}}\right) + \frac{C\,e^{B\dot{\varepsilon}t}}{B\dot{\varepsilon}}\left[\begin{array}{l} e^{B\dot{\varepsilon}x}\left[E_i\left(x/\tau_1\right) - E_i\left(x/\tau_2\right)\right] \\ -E_i\left[\left(B\dot{\varepsilon} + 1/\tau_1\right)x\right] \\ +E_i\left[\left(B\dot{\varepsilon} + 1/\tau_2\right)x\right] \end{array}\right]\Bigg|_{x=-t}^{t_0-t}\right\} \quad \text{.....(A36)}$$

$$\sigma(t)=\frac{A}{1+C\ln\left(\frac{\tau_2}{\tau_1}\right)}\left\{\left(e^{B\dot{\varepsilon}t_0}-1\right)+C\,e^{B\dot{\varepsilon}t}\left[\begin{array}{l} e^{B\dot{\varepsilon}x}\left[E_i\left(x/\tau_1\right)-E_i\left(x/\tau_2\right)\right] \\ -E_i\left[\left(B\dot{\varepsilon}+1/\tau_1\right)x\right] \\ +E_i\left[\left(B\dot{\varepsilon}+1/\tau_2\right)x\right]\end{array}\right]_{x=-t}^{t_0-t}\right\}\text{.....(A37)}$$

$$\sigma(t)=\frac{A}{1+C\ln\left(\frac{\tau_2}{\tau_1}\right)}\left\{\left(e^{B\dot{\varepsilon}t_0}-1\right)+C\,e^{B\dot{\varepsilon}t}\left[e^{B\dot{\varepsilon}x}\left(F_1-F_2\right)-F_3+F_4\right]_{x=-t}^{t_0-t}\right\}\text{.....(A38)}$$

where;

$$F_1=E_i\left(x/\tau_1\right)\text{.....(A39)}$$

$$F_2=E_i\left(x/\tau_2\right)\text{.....(A40)}$$

$$F_3=E_i\left[\left(B\dot{\varepsilon}+1/\tau_1\right)x\right]\text{.....(A41)}$$

$$F_4=E_i\left[\left(B\dot{\varepsilon}+1/\tau_2\right)x\right]\text{.....(A42)}$$

The exponential integral function is known by the equations as;

$$E_i(ax)=\begin{cases}\ln|ax|+\gamma+ax+\dfrac{(ax)^2}{2.2!}+\dfrac{(ax)^3}{3.3!}+\dfrac{(ax)^4}{4.4!}+... & for\ |ax|\le 2 \\ e^{ax}\left[\dfrac{1}{ax}+\dfrac{1}{(ax)^2}+\dfrac{2}{(ax)^3}+\dfrac{3!}{(ax)^4}+\dfrac{4!}{(ax)^5}+...\right] & for\ |ax|>2\end{cases}\text{.....(A43)}$$

where; γ is a constant called *Euler-Mascheroni constant* which is equal to 0.5772156649…

By using the appropriate equation in (A43) within the equations from (A39) to (A42) one obtains;

$$F_1 = E_i\left(x/\tau_1\right) = e^{x/\tau_1}\left[\frac{1}{x/\tau_1} + \frac{1}{\left(x/\tau_1\right)^2}\right] = e^{x/\tau_1}\left[\frac{\tau_1}{x} + \left(\frac{\tau_1}{x}\right)^2\right] \quad \text{(A44)}$$

$$F_2 = E_i\left(x/\tau_2\right) = \ln\left|\frac{x}{\tau_2}\right| + \gamma + \frac{x}{\tau_2} \quad \text{(A45)}$$

$$F_3 = E_i\left[\left(B\dot{\varepsilon} + 1/\tau_1\right)x\right] = e^{\left(B\dot{\varepsilon} + 1/\tau_1\right)x}\left[\frac{1}{\left(B\dot{\varepsilon} + 1/\tau_1\right)x} + \frac{1}{\left(\left(B\dot{\varepsilon} + 1/\tau_1\right)x\right)^2}\right]$$

$$= e^{\left(B\dot{\varepsilon} + 1/\tau_1\right)x}\left[\frac{\tau_1}{(B\dot{\varepsilon}\tau_1 + 1)x} + \left(\frac{\tau_1}{(B\dot{\varepsilon}\tau_1 + 1)x}\right)^2\right] \quad \text{(A46)}$$

$$F_4 = E_i\left[\left(B\dot{\varepsilon} + 1/\tau_2\right)x\right] = e^{\left(B\dot{\varepsilon} + 1/\tau_2\right)x}\left[\frac{1}{\left(B\dot{\varepsilon} + 1/\tau_2\right)x} + \frac{1}{\left(\left(B\dot{\varepsilon} + 1/\tau_2\right)x\right)^2}\right]$$

$$= e^{\left(B\dot{\varepsilon} + 1/\tau_2\right)x}\left[\frac{\tau_2}{(B\dot{\varepsilon}\tau_2 + 1)x} + \left(\frac{\tau_2}{(B\dot{\varepsilon}\tau_2 + 1)x}\right)^2\right] \quad \text{(A47)}$$

As seen above, different equations were used for the calculation of exponential integral functions. In equations (A44), (A46) and (A47) the terms of the exponential integral functions are larger than two. So, the second line of the equation (A43) must be used for convergence. On the contrary, the exponential integral term of equation (A45) is smaller than two. So, this time the second line of the equation (A43) must be used for convergence.

In equations (A44) - (A47), only the first two or three terms of the expansion were taken into account. The real forms of those equations have infinite number of terms, but it is impossible to use all these terms in the expansion. So, minimum possible number of terms in the expansions of the exponential integral functions was taken into account not to increase the load of process.

Using the truncated forms of the exponential integral functions bring on a very small error that is acceptable. However, the advantage of using the short forms of the equations reduces the model and allows for the easier and faster calculation of whole model.

Substituting equations between (A44) and (A47) into equation (A38), one obtains;

$$\sigma(t)=\frac{A}{1+C\ln\left(\frac{\tau_2}{\tau_1}\right)}\left\{\left(e^{B\dot{\varepsilon}t_0}-1\right)+Ce^{B\dot{\varepsilon}t}\left[\begin{array}{l} e^{B\dot{\varepsilon}x}\left[e^{x/\tau_1}\left[\frac{\tau_1}{x}+\left(\frac{\tau_1}{x}\right)^2\right]-\left(\ln\left|\frac{x}{\tau_2}\right|+\gamma+\frac{x}{\tau_2}\right)\right] \\ -e^{\left(B\dot{\varepsilon}+1/\tau_1\right)x}\left[\frac{\tau_1}{(B\dot{\varepsilon}\tau_1+1)x}+\left(\frac{\tau_1}{(B\dot{\varepsilon}\tau_1+1)x}\right)^2\right] \\ +e^{\left(B\dot{\varepsilon}+1/\tau_2\right)x}\left[\frac{\tau_2}{(B\dot{\varepsilon}\tau_2+1)x}+\left(\frac{\tau_2}{(B\dot{\varepsilon}\tau_2+1)x}\right)^2\right] \end{array}\right]\Bigg|_{x=-t}^{t_0-t}\right\}$$

……(A48)

$$\sigma(t)=\frac{A}{1+C\ln\left(\frac{\tau_2}{\tau_1}\right)}\left\{\left(e^{B\dot{\varepsilon}t_0}-1\right)+Ce^{B\dot{\varepsilon}t}\left[\begin{array}{l} e^{B\dot{\varepsilon}x}\left[e^{x/\tau_1}\left[\frac{\tau_1}{x}+\left(\frac{\tau_1}{x}\right)^2\right]-\ln\left|\frac{x}{\tau_2}\right|-\gamma-\frac{x}{\tau_2}\right] \\ -e^{B\dot{\varepsilon}x}\left[e^{x/\tau_1}\left[\frac{\tau_1}{(B\dot{\varepsilon}\tau_1+1)x}+\left(\frac{\tau_1}{(B\dot{\varepsilon}\tau_1+1)x}\right)^2\right]\right. \\ \left.-e^{x/\tau_2}\left[\frac{\tau_2}{(B\dot{\varepsilon}\tau_2+1)x}+\left(\frac{\tau_2}{(B\dot{\varepsilon}\tau_2+1)x}\right)^2\right]\right] \end{array}\right]\Bigg|_{x=-t}^{t_0-t}\right\}$$

……(A49)

$$\sigma(t)=\frac{A}{1+C\ln\left(\frac{\tau_2}{\tau_1}\right)}\left\{\left(e^{B\dot{\varepsilon}t_0}-1\right)+Ce^{B\dot{\varepsilon}t}\left[e^{B\dot{\varepsilon}x}\left[\begin{array}{l}e^{x/\tau_1}\left[\frac{\tau_1}{x}+\left(\frac{\tau_1}{x}\right)^2\right]-\ln\left|\frac{x}{\tau_2}\right|-\gamma-\frac{x}{\tau_2}\\-e^{x/\tau_1}\left[\frac{\tau_1}{(B\dot{\varepsilon}\tau_1+1)x}+\left(\frac{\tau_1}{(B\dot{\varepsilon}\tau_1+1)x}\right)^2\right]\\+e^{x/\tau_2}\left[\frac{\tau_2}{(B\dot{\varepsilon}\tau_2+1)x}+\left(\frac{\tau_2}{(B\dot{\varepsilon}\tau_2+1)x}\right)^2\right]\end{array}\right]\right]\Bigg|_{x=-t}^{t_0-t}\right\}$$

……(A50)

$$\sigma(t)=\frac{A}{1+C\ln\left(\frac{\tau_2}{\tau_1}\right)}\left\{\left(e^{B\dot{\varepsilon}t_0}-1\right)+Ce^{B\dot{\varepsilon}(t+x)}\left[\begin{array}{l}e^{x/\tau_1}\left(\frac{\tau_1}{x}\right)\left(1+\frac{\tau_1}{x}\right)-\ln\left|\frac{x}{\tau_2}\right|-\gamma-\frac{x}{\tau_2}\\-e^{x/\tau_1}\left(\frac{\tau_1}{(B\dot{\varepsilon}\tau_1+1)x}\right)\left[1+\frac{\tau_1}{(B\dot{\varepsilon}\tau_1+1)x}\right]\\+e^{x/\tau_2}\left(\frac{\tau_2}{(B\dot{\varepsilon}\tau_2+1)x}\right)\left[1+\frac{\tau_2}{(B\dot{\varepsilon}\tau_2+1)x}\right]\end{array}\right]\Bigg|_{x=-t}^{t_0-t}\right\}$$

……(A51)

$$\sigma(t)=\frac{A}{1+C\ln\left(\frac{\tau_2}{\tau_1}\right)}\left\{\left(e^{B\dot{\varepsilon}t_0}-1\right)+Ce^{B\dot{\varepsilon}(t+x)}\left[\begin{array}{l}e^{x/\tau_1}\left[\left(\frac{\tau_1}{x}\right)\left(1+\frac{\tau_1}{x}\right)-\left(\frac{\tau_1}{(B\dot{\varepsilon}\tau_1+1)x}\right)\left[1+\frac{\tau_1}{(B\dot{\varepsilon}\tau_1+1)x}\right]\right]\\+e^{x/\tau_2}\left(\frac{\tau_2}{(B\dot{\varepsilon}\tau_2+1)x}\right)\left[1+\frac{\tau_2}{(B\dot{\varepsilon}\tau_2+1)x}\right]-\ln\left|\frac{x}{\tau_2}\right|-\gamma-\frac{x}{\tau_2}\end{array}\right]\Bigg|_{x=-t}^{t_0-t}\right\}$$

……(A52)

$$\sigma(t)=\frac{A}{1+C\ln\left(\frac{\tau_2}{\tau_1}\right)}\left\{\left(e^{B\dot{\varepsilon}t_0}-1\right)+C\left\{\begin{array}{l} e^{B\dot{\varepsilon}t_0}\left[e^{{}^{t_0-t}\!/\!_{\tau_1}}\left[\left(\frac{\tau_1}{t_0-t}\right)\left(1+\frac{\tau_1}{t_0-t}\right)-\left(\frac{\tau_1}{(B\dot{\varepsilon}\tau_1+1)(t_0-t)}\right)\left[1+\frac{\tau_1}{(B\dot{\varepsilon}\tau_1+1)(t_0-t)}\right]\right]\right] \\ +e^{{}^{t_0-t}\!/\!_{\tau_2}}\left(\frac{\tau_2}{(B\dot{\varepsilon}\tau_2+1)(t_0-t)}\right)\left[1+\frac{\tau_2}{(B\dot{\varepsilon}\tau_2+1)(t_0-t)}\right]-\ln\left|\frac{t_0-t}{\tau_2}\right|-\gamma-\frac{t_0-t}{\tau_2} \\ -e^{{}^{-t}\!/\!_{\tau_1}}\left[\left(-\frac{\tau_1}{t}\right)\left(1-\frac{\tau_1}{t}\right)-\left(\frac{\tau_1}{(B\dot{\varepsilon}\tau_1+1)(-t)}\right)\left[1+\frac{\tau_1}{(B\dot{\varepsilon}\tau_1+1)(-t)}\right]\right] \\ -e^{{}^{-t}\!/\!_{\tau_2}}\left(\frac{\tau_2}{(B\dot{\varepsilon}\tau_2+1)(-t)}\right)\left[1+\frac{\tau_2}{(B\dot{\varepsilon}\tau_2+1)(-t)}\right]+\ln\left|\frac{-t}{\tau_2}\right|+\gamma-\frac{t}{\tau_2} \end{array}\right\}\right\}$$

……(A53)

$$\sigma(t)=\frac{A}{1+C\ln\left(\frac{\tau_2}{\tau_1}\right)}\left\{\left(e^{B\dot{\varepsilon}t_0}-1\right)+C\left\{\begin{array}{l} e^{B\dot{\varepsilon}t_0}\left[e^{{}^{t_0-t}\!/\!_{\tau_1}}\left[\left(\frac{\tau_1}{t_0-t}\right)\left(1+\frac{\tau_1}{t_0-t}\right)-\left(\frac{\tau_1}{(B\dot{\varepsilon}\tau_1+1)(t_0-t)}\right)\left[1+\frac{\tau_1}{(B\dot{\varepsilon}\tau_1+1)(t_0-t)}\right]\right]\right] \\ +e^{{}^{t_0-t}\!/\!_{\tau_2}}\left(\frac{\tau_2}{(B\dot{\varepsilon}\tau_2+1)(t_0-t)}\right)\left[1+\frac{\tau_2}{(B\dot{\varepsilon}\tau_2+1)(t_0-t)}\right]-\ln\left(\frac{t-t_0}{\tau_2}\right)-\gamma-\frac{t_0-t}{\tau_2} \\ +e^{{}^{-t}\!/\!_{\tau_1}}\left[\left(\frac{\tau_1}{t}\right)\left(1-\frac{\tau_1}{t}\right)-\left(\frac{\tau_1}{(B\dot{\varepsilon}\tau_1+1)t}\right)\left[1-\frac{\tau_1}{(B\dot{\varepsilon}\tau_1+1)t}\right]\right] \\ +e^{{}^{-t}\!/\!_{\tau_2}}\left(\frac{\tau_2}{(B\dot{\varepsilon}\tau_2+1)t}\right)\left[1-\frac{\tau_2}{(B\dot{\varepsilon}\tau_2+1)t}\right]+\ln\left(\frac{t}{\tau_2}\right)+\gamma-\frac{t}{\tau_2} \end{array}\right\}\right\}$$

……(A54)

$$\sigma(t)=\frac{A}{1+C\ln\left(\frac{\tau_2}{\tau_1}\right)}\left\{\left(e^{B\dot{\varepsilon}t_0}-1\right)+C\left\{\begin{array}{l} e^{\left(B\dot{\varepsilon}+\frac{1}{\tau_1}\right)t_0-\frac{t}{\tau_1}}\left[\left(\frac{\tau_1}{t_0-t}\right)\left(1+\frac{\tau_1}{t_0-t}\right)-\left(\frac{\tau_1}{(B\dot{\varepsilon}\tau_1+1)(t_0-t)}\right)\left[1+\frac{\tau_1}{(B\dot{\varepsilon}\tau_1+1)(t_0-t)}\right]\right] \\ +e^{\left(B\dot{\varepsilon}+\frac{1}{\tau_2}\right)t_0-\frac{t}{\tau_2}}\left(\frac{\tau_2}{(B\dot{\varepsilon}\tau_2+1)(t_0-t)}\right)\left[1+\frac{\tau_2}{(B\dot{\varepsilon}\tau_2+1)(t_0-t)}\right] \\ -e^{B\dot{\varepsilon}t_0}\left[\ln\left(\frac{t-t_0}{\tau_2}\right)+\gamma+\frac{t_0-t}{\tau_2}\right]+\ln\left(\frac{t}{\tau_2}\right)+\gamma-\frac{t}{\tau_2} \\ +e^{{}^{-t}\!/\!_{\tau_1}}\left[\left(\frac{\tau_1}{t}\right)\left(1-\frac{\tau_1}{t}\right)-\left(\frac{\tau_1}{(B\dot{\varepsilon}\tau_1+1)t}\right)\left[1-\frac{\tau_1}{(B\dot{\varepsilon}\tau_1+1)t}\right]\right] \\ +e^{{}^{-t}\!/\!_{\tau_2}}\left(\frac{\tau_2}{(B\dot{\varepsilon}\tau_2+1)t}\right)\left[1-\frac{\tau_2}{(B\dot{\varepsilon}\tau_2+1)t}\right] \end{array}\right\}\right\}$$

……(A55)

$$\sigma(t)=\frac{A}{1+C\ln\left(\frac{\tau_2}{\tau_1}\right)}\left\{\left(e^{B\dot{\varepsilon}t_0}-1\right)+C\left\{\begin{array}{l} e^{-\frac{t}{\tau_1}}\left[e^{\left(B\dot{\varepsilon}+\frac{1}{\tau_1}\right)t_0}\left[\left(\frac{\tau_1}{t_0-t}\right)\left(1+\frac{\tau_1}{t_0-t}\right)-\left(\frac{\tau_1}{(B\dot{\varepsilon}\tau_1+1)(t_0-t)}\right)\left[1+\frac{\tau_1}{(B\dot{\varepsilon}\tau_1+1)(t_0-t)}\right]\right]\right. \\ \qquad \left.+\left(\frac{\tau_1}{t}\right)\left(1-\frac{\tau_1}{t}\right)-\left(\frac{\tau_1}{(B\dot{\varepsilon}\tau_1+1)t}\right)\left[1-\frac{\tau_1}{(B\dot{\varepsilon}\tau_1+1)t}\right]\right] \\ +e^{-\frac{t}{\tau_2}}\left[e^{\left(B\dot{\varepsilon}+\frac{1}{\tau_2}\right)t_0}\left(\frac{\tau_2}{(B\dot{\varepsilon}\tau_2+1)(t_0-t)}\right)\left[1+\frac{\tau_2}{(B\dot{\varepsilon}\tau_2+1)(t_0-t)}\right]\right. \\ \qquad \left.+\left(\frac{\tau_2}{(B\dot{\varepsilon}\tau_2+1)t}\right)\left[1-\frac{\tau_2}{(B\dot{\varepsilon}\tau_2+1)t}\right]\right] \\ -e^{B\dot{\varepsilon}t_0}\left[\ln\left(\frac{t-t_0}{\tau_2}\right)+\gamma+\frac{t_0-t}{\tau_2}\right]+\ln\left(\frac{t}{\tau_2}\right)+\gamma-\frac{t}{\tau_2} \end{array}\right\}$$

……(A56)

$$\sigma(t)=q_1\left\{q_5+C\left\{\begin{array}{l} e^{-\frac{t}{\tau_1}}\left[q_9\left[\left(\frac{\tau_1}{t_0-t}\right)\left(\frac{q_{13}-t}{t_0-t}\right)-\left(\frac{\tau_1}{q_{15}-q_{14}t}\right)\left[\frac{q_{16}-q_{14}t}{q_{15}-q_{14}t}\right]\right]+\left(\frac{\tau_1}{t}\right)\left(1-\frac{\tau_1}{t}\right)-\left(\frac{\tau_1}{q_{14}t}\right)\left[1-\frac{\tau_1}{q_{14}t}\right]\right] \\ +e^{-\frac{t}{\tau_2}}\left[q_{12}\left(\frac{\tau_2}{q_{18}-q_{17}t}\right)\left[\frac{q_{19}-q_{17}t}{q_{18}-q_{17}t}\right]+\left(\frac{\tau_2}{q_{17}t}\right)\left[1-\frac{\tau_2}{q_{17}t}\right]\right]-q_4\left[q_{20}+\ln(t-t_0)-\frac{t}{\tau_2}\right]+q_{21}+\ln t-\frac{t}{\tau_2} \end{array}\right\}\right\}$$

……(A57)

where;

$$q_1=\frac{A}{1+C\ln(\tau_2/\tau_1)} \qquad q_{12}=e^{\left(B\dot{\varepsilon}+\frac{1}{\tau_2}\right)t_0}=e^{q_{11}}$$

$$q_2=B\dot{\varepsilon} \qquad q_{13}=t_0+\tau_1$$

$$q_3=B\dot{\varepsilon}t_0=q_2t_0 \qquad q_{14}=B\dot{\varepsilon}\tau_1+1=q_2\tau_1+1$$

$$q_4=e^{B\dot{\varepsilon}t_0}=e^{q_3} \qquad q_{15}=(B\dot{\varepsilon}\tau_1+1)t_0=q_{14}t_0$$

$$q_5=e^{B\dot{\varepsilon}t_0}-1=q_4-1 \qquad q_{16}=(B\dot{\varepsilon}\tau_1+1)t_0+\tau_1=q_{15}+\tau_1$$

$$q_6=e^{B\dot{\varepsilon}t_0}+1=q_4+1 \qquad q_{17}=B\dot{\varepsilon}\tau_2+1=q_2\tau_2+1$$

$$q_7=B\dot{\varepsilon}+\frac{1}{\tau_1}=q_2+\frac{1}{\tau_1} \qquad q_{18}=(B\dot{\varepsilon}\tau_2+1)t_0=q_{17}t_0$$

$$q_8=\left(B\dot{\varepsilon}+\frac{1}{\tau_1}\right)t_0=q_7t_0 \qquad q_{19}=(B\dot{\varepsilon}\tau_2+1)t_0+\tau_2=q_{18}+\tau_2$$

$$q_9 = e^{\left(B\dot{\varepsilon}+\frac{1}{\tau_1}\right)t_0} = e^{q_8} \qquad q_{20} = \gamma + \frac{t_0}{\tau_2} - \ln\tau_2$$

$$q_{10} = B\dot{\varepsilon} + \frac{1}{\tau_2} = q_2 + \frac{1}{\tau_2} \qquad q_{21} = \gamma - \ln\tau_2$$

$$q_{11} = \left(B\dot{\varepsilon} + \frac{1}{\tau_2}\right)t_0 = q_{10}\,t_0$$

$$\sigma(t) = q_1\left\{q_5 + C\left\{e^{-\frac{t}{\tau_1}}\left[q_9\left(q_{22}-q_{23}\right)+q_{24}-q_{25}\right] + e^{-\frac{t}{\tau_2}}\left(q_{12}\,q_{26}+q_{27}\right) - q_4\,q_{28}+q_{29}\right\}\right\} \text{.....(A58)}$$

where;

$$q_{22} = \left(\frac{\tau_1}{t_0 - t}\right)\left(\frac{q_{13}-t}{t_0-t}\right) \qquad q_{26} = \left(\frac{\tau_2}{q_{18}-q_{17}\,t}\right)\left[\frac{q_{19}-q_{17}\,t}{q_{18}-q_{17}\,t}\right]$$

$$q_{23} = \left(\frac{\tau_1}{q_{15}-q_{14}\,t}\right)\left[\frac{q_{16}-q_{14}\,t}{q_{15}-q_{14}\,t}\right] \qquad q_{27} = \left(\frac{\tau_2}{q_{17}\,t}\right)\left[1-\frac{\tau_2}{q_{17}\,t}\right]$$

$$q_{24} = \left(\frac{\tau_1}{t}\right)\left(1-\frac{\tau_1}{t}\right) \qquad q_{28} = q_{20} + \ln\left(t-t_0\right) - \frac{t}{\tau_2}$$

$$q_{25} = \left(\frac{\tau_1}{q_{14}\,t}\right)\left[1-\frac{\tau_1}{q_{14}\,t}\right] \qquad q_{29} = q_{21} + \ln t - \frac{t}{\tau_2}$$

Rearranging and simplifying, the final form of the equation can be obtained as;

$$\sigma(t) = q_1\left[q_5 + C\left(e^{-\frac{t}{\tau_1}}\,q_{30} + e^{-\frac{t}{\tau_2}}\,q_{31} + q_{32}\right)\right] \text{.....(A59)}$$

where;

$$q_{30} = q_9\left(q_{22}-q_{23}\right)+q_{24}-q_{25}$$

$$q_{31} = q_{12}\,q_{26} + q_{27}$$

$$q_{32} = q_{29} - q_4\,q_{28}$$

APPENDIX B

DERIVATION OF THE CONSTITUTIVE EQUATIONS FOR ENHANCED QLV MODELING BY ASSUMING SOFT TISSUE AS AN ISOTROPIC MATERIAL

The stress history equation can be written by using the one dimensional theory of QLV as;

$$\sigma_{QLV}(\varepsilon,t)=\int_0^t G(t-\tau)\frac{\partial\sigma^e}{\partial\tau}d\tau \quad \text{.....(B1)}$$

where; $\sigma_{QLV}(\varepsilon,t)$ is QLV stress at any time t and strain ε; $G(-)$ is the reduced relaxation function and $\sigma^e(-)$ is the elastic stress function. Since the elastic stress function is a function of strain and time, equation (B1) can be rewritten as;

$$\sigma_{QLV}(\varepsilon,t)=\int_0^t G(t-\tau)\frac{\partial\sigma^e[\varepsilon(\tau)]}{\partial\varepsilon(\tau)}\frac{\partial\varepsilon(\tau)}{\partial\tau}d\tau \quad \text{.....(B2)}$$

where; the term $\frac{\partial\varepsilon(\tau)}{\partial\tau}$ is called *the strain rate* and can be denoted with $\dot{\varepsilon}$ in the loading portion and it is equal to zero in the relaxation portion of the experiment.

For purposes here, the reduced relaxation function was taken to be;

$$G(t)=\frac{1+C[E_1(t/\tau_2)-E_1(t/\tau_1)]}{1+C\ln(\tau_2/\tau_1)} \quad \text{.....(B3)}$$

So;

$$G(t-\tau)=\frac{1+C\left[E_1\left(t-\tau/\tau_2\right)-E_1\left(t-\tau/\tau_1\right)\right]}{1+C\ln\left(\tau_2/\tau_1\right)} \quad \text{.....(B4)}$$

where; C is a material parameter related to the viscous damping; τ_1 and τ_2 are material parameters related to the strain rates over which hysteresis is nearly constant and E_1 is the first exponential integral function which is in the form;

$$E_1(x)=\int_1^{\infty}\frac{e^{-tx}}{t}dt=\int_x^{\infty}\frac{e^{-u}}{u}du \quad \text{.....(B5)}$$

The elastic stress function $\sigma^e(\varepsilon)$ in equation (B2) is the following nonlinear function;

$$\sigma^e(\varepsilon)=A\left(e^{B\varepsilon}-1\right) \quad \text{.....(B6)}$$

where; A and B are material constants.

So, the term $\frac{\partial\sigma^e[\varepsilon(\tau)]}{\partial\varepsilon(\tau)}$ in equation (B2) becomes;

$$\frac{\partial\sigma^e[\varepsilon(\tau)]}{\partial\varepsilon(\tau)}=\frac{\partial}{\partial\varepsilon}\left[A\left(e^{B\varepsilon}-1\right)\right] \quad \text{.....(B7)}$$

$$=ABe^{B\varepsilon} \quad \text{.....(B8)}$$

$$=ABe^{B\dot{\varepsilon}\tau} \quad \text{.....(B9)}$$

Note that, the equation $\varepsilon=\dot{\varepsilon}\tau$ has been used in equation (B9) to make it able to be integrated over time.

Substituting equations (B4) and (B9) into equation (B2), the stress history from 0 to t_0 (beginning of relaxation) and from t_0 to the end of test period can be obtained as;

$$\sigma_{QLV}\left(0 \le t \le t_0, \varepsilon\right) = \int_0^t \left(\frac{1 + C\left[E_1\left(t - \tau / \tau_2 \right) - E_1\left(t - \tau / \tau_1 \right) \right]}{1 + C \ln\left(\tau_2 / \tau_1 \right)} \right) ABe^{B\dot{\varepsilon}\tau} \dot{\varepsilon}\, d\tau \text{ .....(B10)}$$

Note the stress response from t_0 to the end of the experiment includes the stress history up to t_0 plus the stress history from t_0 onward. However, since the stretch rate from t_0 onward is zero, we are simply left with;

$$\sigma_{QLV}\left(t > t_0, \varepsilon\right) = \int_0^{t_0} \left\{ \frac{1 + C\left[E_1\left(t - \tau / \tau_2 \right) - E_1\left(t - \tau / \tau_1 \right) \right]}{1 + C \ln\left(\tau_2 / \tau_1 \right)} \right\} ABe^{B\dot{\varepsilon}\tau} \dot{\varepsilon}\, d\tau \text{ .....(B11)}$$

Since this study is dealing with the relaxation part of the experiment, derivation will go on from equation (B11).

Rearranging and abbreviating;

$$\sigma_{QLV} = \frac{AB\dot{\varepsilon}}{1 + C \ln\left(\tau_2 / \tau_1 \right)} \int_0^{t_0} e^{B\dot{\varepsilon}\tau} \left\{ 1 + C\left[E_1\left(t - \tau / \tau_2 \right) - E_1\left(t - \tau / \tau_1 \right) \right] \right\} d\tau$$

.....(B12)

Concluding the intermediate operations on equation (B12) as in the Appendix A, finally one obtains;

$$\sigma_{QLV} = q_1 \left[q_5 + C\left(e^{-\frac{t}{\tau_1}} q_{30} + e^{-\frac{t}{\tau_2}} q_{31} + q_{32} \right) \right] \text{.....(B13)}$$

where;

$$q_1 = \frac{A}{1 + C\ln(\tau_2/\tau_1)} \qquad q_5 = e^{B\dot{\varepsilon}t_0} - 1 = q_4 - 1$$

$$q_2 = B\dot{\varepsilon} \qquad q_6 = e^{B\dot{\varepsilon}t_0} + 1 = q_4 + 1$$

$$q_3 = B\dot{\varepsilon}t_0 = q_2 t_0 \qquad q_7 = B\dot{\varepsilon} + \frac{1}{\tau_1} = q_2 + \frac{1}{\tau_1}$$

$$q_4 = e^{B\dot{\varepsilon}t_0} = e^{q_3} \qquad q_8 = \left(B\dot{\varepsilon} + \frac{1}{\tau_1}\right)t_0 = q_7 t_0$$

$$q_9 = e^{\left(B\dot{\varepsilon} + \frac{1}{\tau_1}\right)t_0} = e^{q_8} \qquad q_{21} = \gamma - \ln\tau_2$$

$$q_{10} = B\dot{\varepsilon} + \frac{1}{\tau_2} = q_2 + \frac{1}{\tau_2} \qquad q_{22} = \left(\frac{\tau_1}{t_0 - t}\right)\left(\frac{q_{13} - t}{t_0 - t}\right)$$

$$q_{11} = \left(B\dot{\varepsilon} + \frac{1}{\tau_2}\right)t_0 = q_{10}t_0 \qquad q_{23} = \left(\frac{\tau_1}{q_{15} - q_{14}t}\right)\left[\frac{q_{16} - q_{14}t}{q_{15} - q_{14}t}\right]$$

$$q_{12} = e^{\left(B\dot{\varepsilon} + \frac{1}{\tau_2}\right)t_0} = e^{q_{11}} \qquad q_{24} = \left(\frac{\tau_1}{t}\right)\left(1 - \frac{\tau_1}{t}\right)$$

$$q_{13} = t_0 + \tau_1 \qquad q_{25} = \left(\frac{\tau_1}{q_{14}t}\right)\left[1 - \frac{\tau_1}{q_{14}t}\right]$$

$$q_{14} = B\dot{\varepsilon}\tau_1 + 1 = q_2\tau_1 + 1 \qquad q_{26} = \left(\frac{\tau_2}{q_{18} - q_{17}t}\right)\left[\frac{q_{19} - q_{17}t}{q_{18} - q_{17}t}\right]$$

$$q_{15} = (B\dot{\varepsilon}\tau_1 + 1)t_0 = q_{14}t_0 \qquad q_{27} = \left(\frac{\tau_2}{q_{17}t}\right)\left[1 - \frac{\tau_2}{q_{17}t}\right]$$

$$q_{16} = (B\dot{\varepsilon}\tau_1 + 1)t_0 + \tau_1 = q_{15} + \tau_1 \qquad q_{28} = q_{20} + \ln(t - t_0) - \frac{t}{\tau_2}$$

$$q_{17} = B\dot{\varepsilon}\tau_2 + 1 = q_2\tau_2 + 1 \qquad q_{29} = q_{21} + \ln t - \frac{t}{\tau_2}$$

$$q_{18} = (B\dot{\varepsilon}\tau_2 + 1)t_0 = q_{17}t_0 \qquad q_{30} = q_9(q_{22} - q_{23}) + q_{24} - q_{25}$$

$$q_{19} = (B\dot{\varepsilon}\tau_2 + 1)t_0 + \tau_2 = q_{18} + \tau_2 \qquad q_{31} = q_{12}\,q_{26} + q_{27}$$

$$q_{20} = \gamma + \frac{t_0}{\tau_2} - \ln\tau_2 \qquad q_{32} = q_{29} - q_4\,q_{28}$$

So far, the same model as in the previous one (Appendix A) have been used. To enhance this formulation, it was multiplied with strain and other constants allow for anisotropic behavior. That is;

$$T_{11} = -p + \frac{a^2 \varepsilon_1^2}{8\Lambda} \sigma_{QLV} \quad \text{.....(B14)}$$

$$T_{22} = -p + \frac{b^2 \varepsilon_2^2}{8\Lambda} \sigma_{QLV} \quad \text{.....(B15)}$$

$$T_{33} = -p + \frac{c^2 \varepsilon_3^2}{8\Lambda} \sigma_{QLV} \quad \text{.....(B16)}$$

where; T_{11}, T_{22} and T_{33} are stresses along the three material axes; p is hydrostatic pressure which is equal zero in our experiment conditions (for detailed information about hydrostatic pressure, see Appendix E); ε_1, ε_2 and ε_3 are principal strains along three material directions; σ_{QLV} is the quasi-linear viscoelastic stress calculated by the equation (B13) and Λ is fiber contour length known by the equation;

$$\Lambda = \frac{a^2 + b^2 + c^2}{8} \quad \text{.....(B17)}$$

where; *a, b* and *c* are material parameters that reflect the unit cell dimensions and allow for anisotropic behavior. But, this formulation does not deal with anisotropy. For isotropic case, $b = c = a$. Consequently, Λ can be taken as one material parameter only (not depending on the three parameters *a, b* and *c* individually). So, equation (B17) becomes;

$$\Lambda = \frac{a^2 + a^2 + a^2}{8} = \frac{3}{8} a^2 \quad \text{.....(B18)}$$

With the substitution of this fiber contour length equation into equations (B14), (B15) and (B16), the final form of the model is obtained as;

$$T_{11} = -p + \frac{a^2 \varepsilon_1^2}{8\Lambda} \sigma_{QLV} = \frac{a^2 \varepsilon_1^2}{8\left(\frac{3}{8} a^2\right)} \sigma_{QLV} \quad \text{.....(B19)}$$

$$\Rightarrow T_{11} = \frac{\varepsilon_1^2}{3} \sigma_{QLV} \quad \text{.....(B20)}$$

And similarly;

$$\Rightarrow T_{22} = \frac{\varepsilon_2^2}{3} \sigma_{QLV} \quad \text{.....(B21)}$$

$$\Rightarrow T_{33} = \frac{\varepsilon_3^2}{3} \sigma_{QLV} \quad \text{.....(B22)}$$

Purely quasi-linear viscoelastic model (formulated in Appendix A) is capable of simulating relaxation and creep behaviors. As a result of multiplication with the square of strain, we hope this model to simulate cyclic loading (hysteresis) and also preconditioning together with relaxation and creep.

APPENDIX C

DERIVATION OF THE CONSTITUTIVE EQUATIONS FOR ENHANCED QLV MODELING BY ASSUMING SOFT TISSUE AS AN ANISOTROPIC MATERIAL

The stress history equation can be written by using the one dimensional theory of QLV as;

$$\sigma_{QLV}(\varepsilon,t)=\int_0^t G(t-\tau)\frac{\partial\sigma^e}{\partial\tau}d\tau \quad \text{.....(C1)}$$

where; $\sigma_{QLV}(\varepsilon,t)$ is QLV stress at any time t and strain ε; $G(-)$ is the reduced relaxation function and $\sigma^e(-)$ is the elastic stress function. Since the elastic stress function is a function of strain and time, equation (C1) can be rewritten as;

$$\sigma_{QLV}(\varepsilon,t)=\int_0^t G(t-\tau)\frac{\partial\sigma^e[\varepsilon(\tau)]}{\partial\varepsilon(\tau)}\frac{\partial\varepsilon(\tau)}{\partial\tau}d\tau \quad \text{.....(C2)}$$

where; the term $\frac{\partial\varepsilon(\tau)}{\partial\tau}$ is called *the strain rate* and can be denoted with $\dot{\varepsilon}$ in the loading portion and it is equal to zero in the relaxation portion of the experiment.

For purposes here, the reduced relaxation function was taken to be;

$$G(t)=\frac{1+C\left[E_1(t/\tau_2)-E_1(t/\tau_1)\right]}{1+C\ln(\tau_2/\tau_1)} \quad \text{.....(C3)}$$

So;

$$G(t-\tau)=\frac{1+C\left[E_1\left(t-\tau/\tau_2\right)-E_1\left(t-\tau/\tau_1\right)\right]}{1+C\ln\left(\tau_2/\tau_1\right)} \quad \text{.....(C4)}$$

where; C is a material parameter related to the viscous damping; τ_1 and τ_2 are material parameters related to the strain rates over which hysteresis is nearly constant and E_1 is the first exponential integral function which is in the form;

$$E_1(x)=\int_1^\infty \frac{e^{-tx}}{t}dt=\int_x^\infty \frac{e^{-u}}{u}du \quad \text{.....(C5)}$$

The elastic stress function $\sigma^e(\varepsilon)$ in equation (C2) is the following nonlinear function;

$$\sigma^e(\varepsilon)=A\left(e^{B\varepsilon}-1\right) \quad \text{.....(C6)}$$

where; A and B are material constants.

So, the term $\frac{\partial\sigma^e[\varepsilon(\tau)]}{\partial\varepsilon(\tau)}$ in equation (C2) becomes;

$$\frac{\partial\sigma^e[\varepsilon(\tau)]}{\partial\varepsilon(\tau)}=\frac{\partial}{\partial\varepsilon}\left[A\left(e^{B\varepsilon}-1\right)\right] \quad \text{.....(C7)}$$

$$=ABe^{B\varepsilon} \quad \text{.....(C8)}$$

$$=ABe^{B\dot{\varepsilon}\tau} \quad \text{.....(C9)}$$

Note that, the equation $\varepsilon=\dot{\varepsilon}\tau$ has been used in equation (C9) to make it able to be integrated over time.

Substituting equations (C4) and (C9) into equation (C2), the stress history from 0 to t_0 (beginning of relaxation) and from t_0 to the end of test period can be obtained as;

$$\sigma_{QLV}\left(0 \le t \le t_0, \varepsilon\right) = \int_0^t \left(\frac{1 + C\left[E_1\left(t - \tau / \tau_2 \right) - E_1\left(t - \tau / \tau_1 \right) \right]}{1 + C \ln\left(\tau_2 / \tau_1 \right)} \right) ABe^{B\dot{\varepsilon}\tau} \dot{\varepsilon}\, d\tau \text{ .....(C10)}$$

Note the stress response from t_0 to the end of the experiment includes the stress history up to t_0 plus the stress history from t_0 onward. However, since the stretch rate from t_0 onward is zero, we are simply left with;

$$\sigma_{QLV}\left(t > t_0, \varepsilon\right) = \int_0^{t_0} \left\{ \frac{1 + C\left[E_1\left(t - \tau / \tau_2 \right) - E_1\left(t - \tau / \tau_1 \right) \right]}{1 + C \ln\left(\tau_2 / \tau_1 \right)} \right\} ABe^{B\dot{\varepsilon}\tau} \dot{\varepsilon}\, d\tau \text{ .....(C11)}$$

Since this study is dealing with the relaxation part of the experiment, derivation will go on from equation (C11).

Rearranging and abbreviating;

$$\sigma_{QLV} = \frac{AB\dot{\varepsilon}}{1 + C \ln\left(\tau_2 / \tau_1 \right)} \int_0^{t_0} e^{B\dot{\varepsilon}\tau} \left\{ 1 + C\left[E_1\left(t - \tau / \tau_2 \right) - E_1\left(t - \tau / \tau_1 \right) \right] \right\} d\tau \ldots$$

.....(C12)

Concluding the intermediate operations on equation (C12) as in the Appendix A, finally one obtains;

$$\sigma_{QLV} = q_1 \left[q_5 + C\left(e^{-\frac{t}{\tau_1}} q_{30} + e^{-\frac{t}{\tau_2}} q_{31} + q_{32} \right) \right] \text{.....(C13)}$$

where;

$$q_1 = \frac{A}{1 + C\ln(\tau_2/\tau_1)} \qquad q_5 = e^{B\dot{\varepsilon}t_0} - 1 = q_4 - 1$$

$$q_2 = B\dot{\varepsilon} \qquad q_6 = e^{B\dot{\varepsilon}t_0} + 1 = q_4 + 1$$

$$q_3 = B\dot{\varepsilon}t_0 = q_2 t_0 \qquad q_7 = B\dot{\varepsilon} + \frac{1}{\tau_1} = q_2 + \frac{1}{\tau_1}$$

$$q_4 = e^{B\dot{\varepsilon}t_0} = e^{q_3} \qquad q_8 = \left(B\dot{\varepsilon} + \frac{1}{\tau_1}\right)t_0 = q_7 t_0$$

$$q_9 = e^{\left(B\dot{\varepsilon} + \frac{1}{\tau_1}\right)t_0} = e^{q_8} \qquad q_{21} = \gamma - \ln\tau_2$$

$$q_{10} = B\dot{\varepsilon} + \frac{1}{\tau_2} = q_2 + \frac{1}{\tau_2} \qquad q_{22} = \left(\frac{\tau_1}{t_0 - t}\right)\left(\frac{q_{13} - t}{t_0 - t}\right)$$

$$q_{11} = \left(B\dot{\varepsilon} + \frac{1}{\tau_2}\right)t_0 = q_{10}t_0 \qquad q_{23} = \left(\frac{\tau_1}{q_{15} - q_{14}t}\right)\left[\frac{q_{16} - q_{14}t}{q_{15} - q_{14}t}\right]$$

$$q_{12} = e^{\left(B\dot{\varepsilon} + \frac{1}{\tau_2}\right)t_0} = e^{q_{11}} \qquad q_{24} = \left(\frac{\tau_1}{t}\right)\left(1 - \frac{\tau_1}{t}\right)$$

$$q_{13} = t_0 + \tau_1 \qquad q_{25} = \left(\frac{\tau_1}{q_{14}t}\right)\left[1 - \frac{\tau_1}{q_{14}t}\right]$$

$$q_{14} = B\dot{\varepsilon}\tau_1 + 1 = q_2\tau_1 + 1 \qquad q_{26} = \left(\frac{\tau_2}{q_{18} - q_{17}t}\right)\left[\frac{q_{19} - q_{17}t}{q_{18} - q_{17}t}\right]$$

$$q_{15} = (B\dot{\varepsilon}\tau_1 + 1)t_0 = q_{14}t_0 \qquad q_{27} = \left(\frac{\tau_2}{q_{17}t}\right)\left[1 - \frac{\tau_2}{q_{17}t}\right]$$

$$q_{16} = (B\dot{\varepsilon}\tau_1 + 1)t_0 + \tau_1 = q_{15} + \tau_1 \qquad q_{28} = q_{20} + \ln(t - t_0) - \frac{t}{\tau_2}$$

$$q_{17} = B\dot{\varepsilon}\tau_2 + 1 = q_2\tau_2 + 1 \qquad q_{29} = q_{21} + \ln t - \frac{t}{\tau_2}$$

$$q_{18} = (B\dot{\varepsilon}\tau_2 + 1)t_0 = q_{17}t_0 \qquad q_{30} = q_9(q_{22} - q_{23}) + q_{24} - q_{25}$$

$$q_{19} = (B\dot{\varepsilon}\tau_2 + 1)t_0 + \tau_2 = q_{18} + \tau_2 \qquad q_{31} = q_{12}\,q_{26} + q_{27}$$

$$q_{20} = \gamma + \frac{t_0}{\tau_2} - \ln\tau_2 \qquad q_{32} = q_{29} - q_4\,q_{28}$$

This is the quasi-linear part of the model. To enhance this formulation, it was multiplied with strain and other constants allow for anisotropic behavior. That is;

$$T_{11} = -p + \frac{a^2 \varepsilon_1^2}{8\Lambda} \sigma_{QLV} \quad \text{.....(C14)}$$

$$T_{22} = -p + \frac{b^2 \varepsilon_2^2}{8\Lambda} \sigma_{QLV} \quad \text{.....(C15)}$$

$$T_{33} = -p + \frac{c^2 \varepsilon_3^2}{8\Lambda} \sigma_{QLV} \quad \text{.....(C16)}$$

where; T_{11}, T_{22} and T_{33} are stresses along the three material axes; p is hydrostatic pressure which is equal zero in our experiment conditions (for detailed information about hydrostatic pressure, see Appendix E); ε_1, ε_2 and ε_3 are principal strains along three material directions; σ_{QLV} is the quasi-linear viscoelastic stress calculated by the equation (C13) and Λ is fiber contour length known by the equation;

$$\Lambda = \frac{a^2 + b^2 + c^2}{8} \quad \text{.....(C17)}$$

where; *a, b* and *c* are material parameters that reflect the unit cell dimensions and allow for anisotropic behavior. Consequently, two more constants were needed to be used than the previous one to take anisotropy into account. After final abbreviations, equations (C14), (C15) and (C16) can be written as;

$$T_{11} = \frac{a^2 \varepsilon_1^2}{8\Lambda} \sigma_{QLV} \quad \text{.....(C18)}$$

$$T_{22} = \frac{b^2 \varepsilon_2^2}{8\Lambda} \sigma_{QLV} \quad \text{.....(C19)}$$

$$T_{33} = \frac{c^2 \varepsilon_3^2}{8\Lambda} \sigma_{QLV} \quad \text{.....(C20)}$$

Purely quasi-linear viscoelastic model (formulated in Appendix A) is capable of simulating relaxation and creep behaviors. As a result of multiplication with the square of strain, we hope this model to simulate cyclic loading (hysteresis) and also preconditioning together with relaxation and creep. Also by using the constants *a, b* and *c* different than each other, we hope to model anisotropy of the soft biological tissues.

APPENDIX D

REDUCED RELAXATION FUNCTION

For simulation purposes of the soft biological tissues, the most commonly used method is quasi-linear viscoelasticity. According to this method, a reduced relaxation function is multiplied with the derivative of the elastic stress function with respect to time and the whole expression is integrated over time.

In this section, two forms of the reduced relaxation function will be expressed. The first one has six material parameters but easy to be formulated; and the second one has only three material parameters but cannot be formulated as easy as the former one.

The first form of the reduced relaxation function is;

$$G(t) = a e^{-bt} + c e^{-dt} + f e^{-ht} \quad \text{.....(D1)}$$

where; a and b represent the short term behavior; c and d represent the intermediate term behavior; f and h represent the long term behavior of the soft biological tissue. For the graphical illustration of the 6-parameter reduced relaxation function and effects of changing these constants on it, see Figures D1 – D7. In these curves, the responses calculated by the reduced relaxation function after a ramp strain is seen.

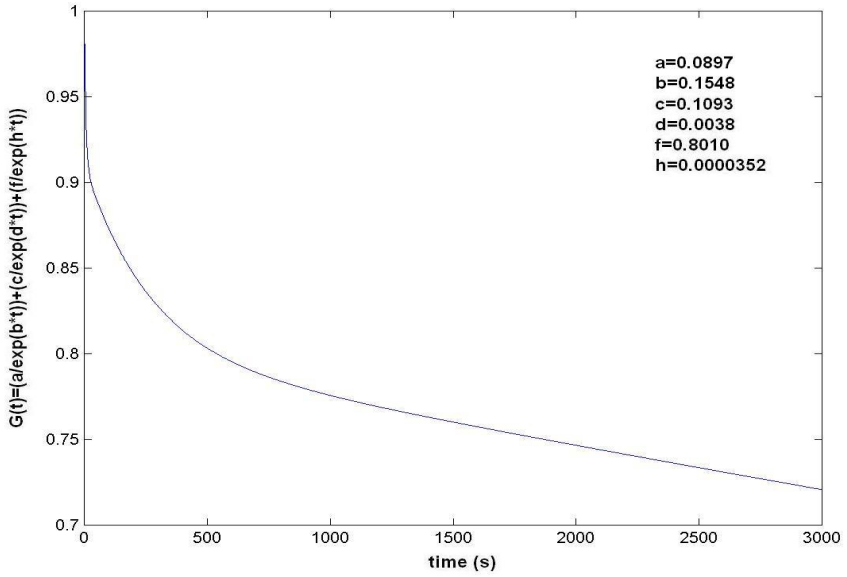

Figure D1 – 6-Parameter Reduced Relaxation Function

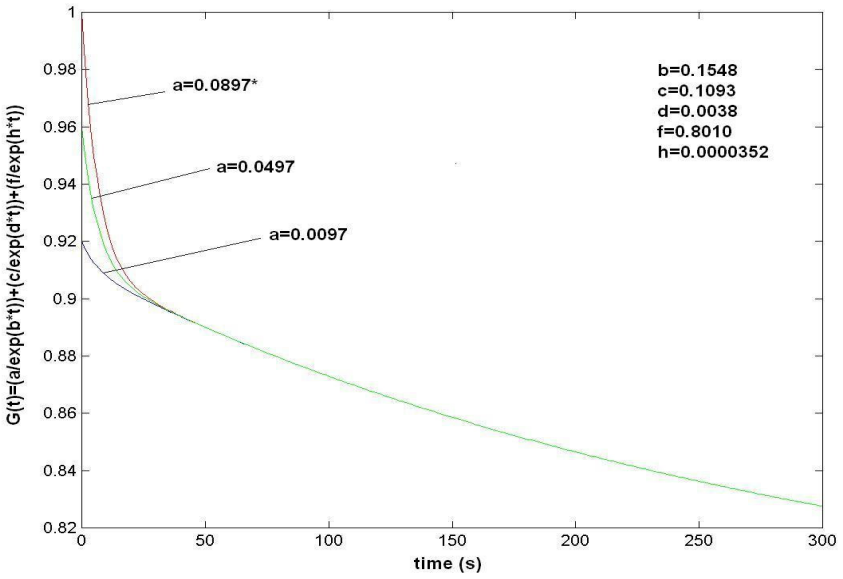

Figure D2 – Effect of Changing the Constant '*a*' on 6-Parameter Reduced Relaxation Function

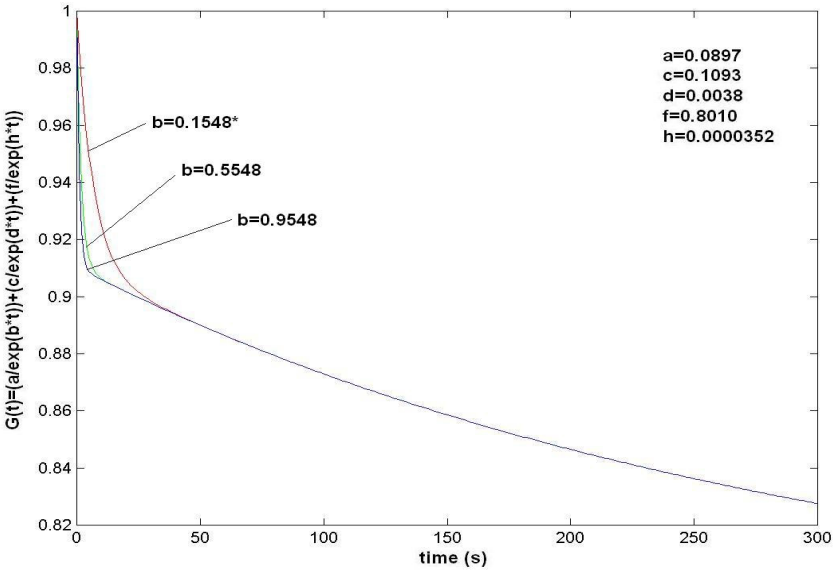

Figure D3 – Effect of Changing the Constant '*b*' on 6-Parameter Reduced Relaxation Function

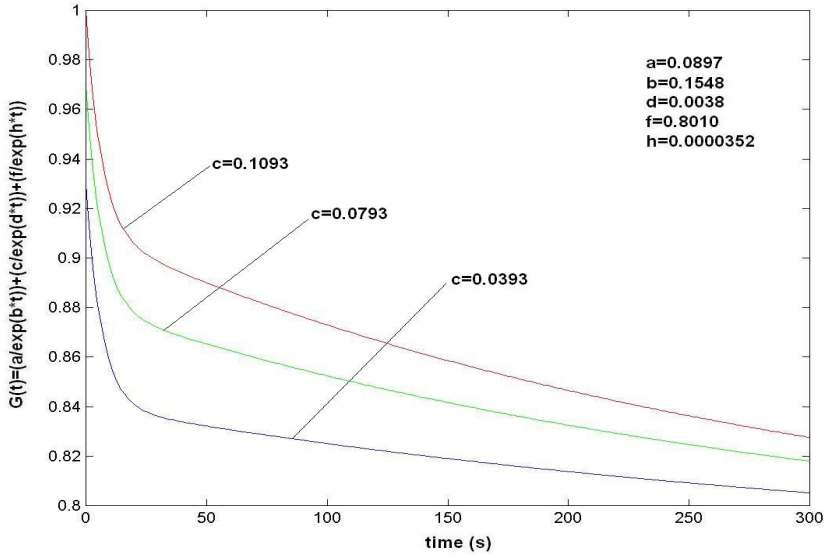

Figure D4 – Effect of Changing the Constant '*c*' on 6-Parameter Reduced Relaxation Function

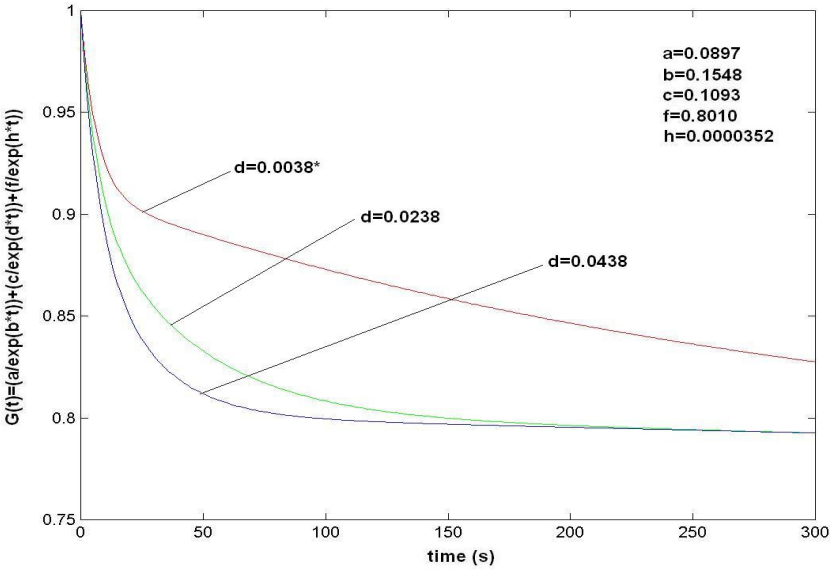

Figure D5 – Effect of Changing the Constant '*d*' on 6-Parameter Reduced Relaxation Function

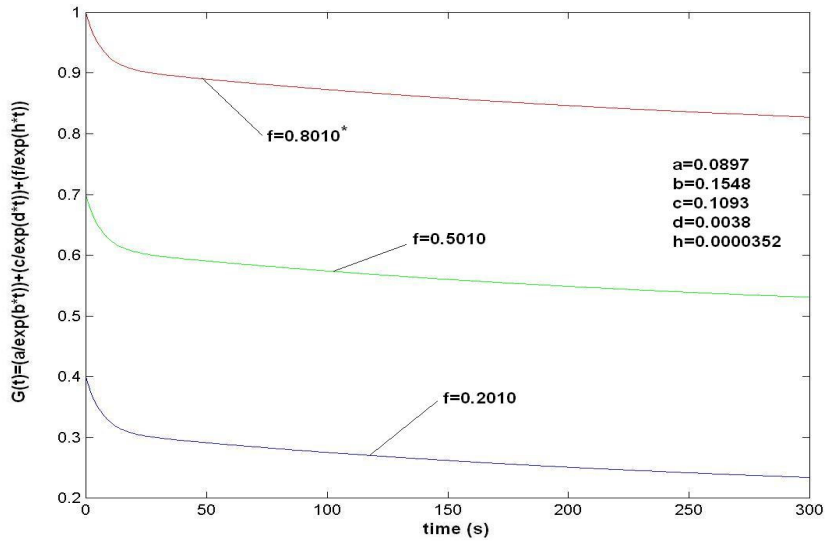

Figure D6 – Effect of Changing the Constant '*f*' on 6-Parameter Reduced Relaxation Function

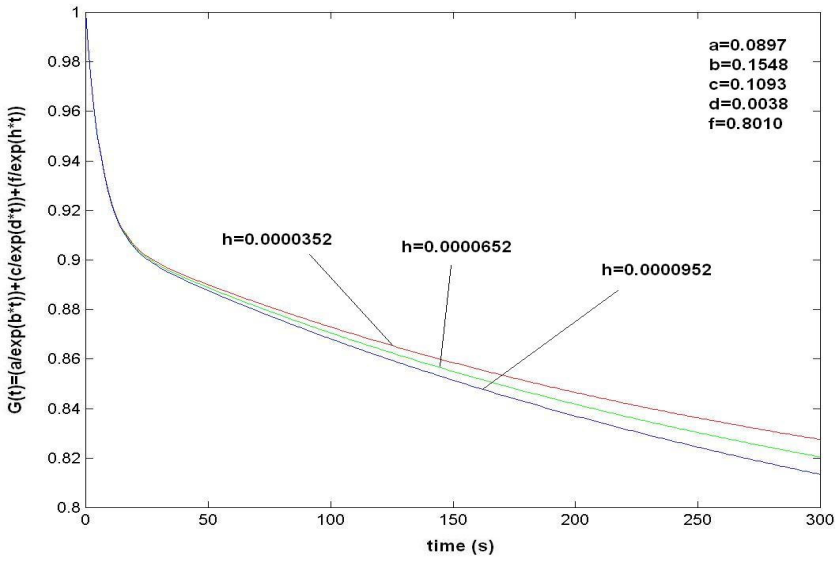

Figure D7 – Effect of Changing the Constant '*h*' on 6-Parameter Reduced Relaxation Function

In Figure D1, the base response of the reduced relaxation function is seen. The parameters are as they are given in the figure and none of them has been changed. In the following figures, only one of the parameters is changed while the others are kept constant, and the effect of changing this parameter is observed.

In Figure D2, the effect of changing the short term constant (*a*) on the reduced relaxation function is seen. Increasing the value of the short term constant causes the sudden relaxation to decrease. Figure D3 shows the effect of changing the short term exponential constant (*b*) on the reduced relaxation function. The sudden relaxation period decreases while the short term exponential constant increases.

In Figure D4, the effect of changing the intermediate term constant (*c*) on the reduced relaxation function is seen. Increasing the value of the intermediate term constant causes the intermediate relaxation to increase, too. Figure D5 shows the effect of changing the intermediate term exponential constant (*d*) on the reduced

relaxation function. The intermediate relaxation period decreases while the intermediate term exponential constant increases.

In Figure D6, the effect of changing the long term constant (*f*) on the reduced relaxation function is seen. Increasing the value of the long term constant causes the all relaxation curve to be shifted upward. Finally, Figure D7 shows the effect of changing the long term exponential constant (*h*) on the reduced relaxation function. The long relaxation period decreases while the long term exponential constant increases.

This 6-parameter reduced relaxation function has so many constants which is not a desirable condition. So, it has not been preferred within the concept of this thesis. Instead, a 3-parameter reduced relaxation function has been used. As previously mentioned, it is harder to formulate this reduced relaxation function, but it requires less material parameters.

This second form of the reduced relaxation function is;

$$G(t) = \frac{1 + C\left[E_1(t/\tau_2) - E_1(t/\tau_1)\right]}{1 + C\,\ln(\tau_2/\tau_1)} \qquad \text{(D2)}$$

where; C is a material parameter related to the viscous damping; τ_1 and τ_2 are material parameters related to the strain rates over which hysteresis is nearly constant and E_1 is the first exponential integral function which is in the form;

$$E_1(x) = \int_1^{\infty} \frac{e^{-tx}}{t}\,dt = \int_x^{\infty} \frac{e^{-u}}{u}\,du \qquad \text{(D3)}$$

For the graphical illustration of the 3-parameter reduced relaxation function and effects of changing these constants on it, see Figures D8 – D11. In these curves, the responses calculated by the reduced relaxation function after a ramp strain is seen.

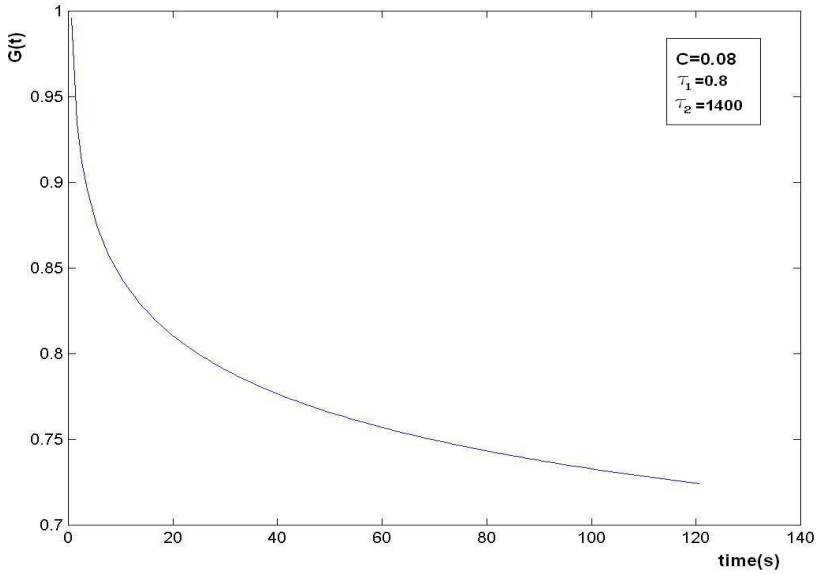

Figure D8 – 3-Parameter Reduced Relaxation Function

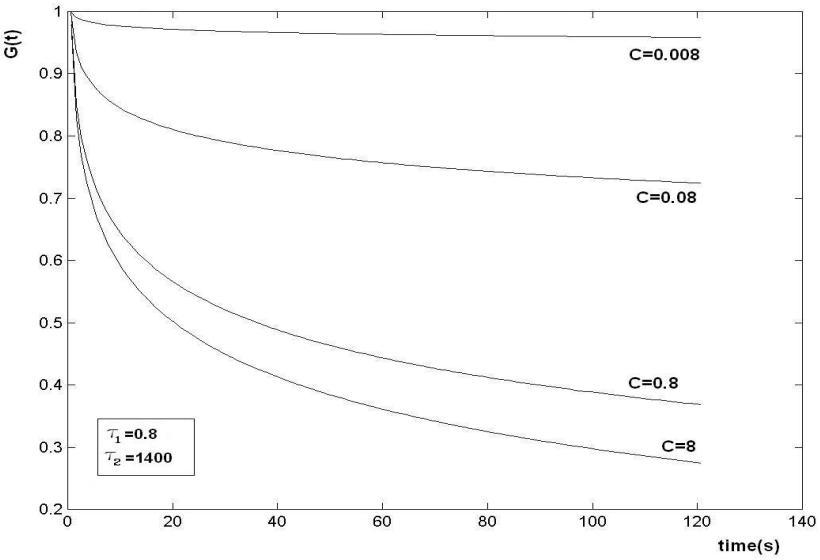

Figure D9 – Effect of Changing the Constant *'C'* on 3-Parameter Reduced Relaxation Function

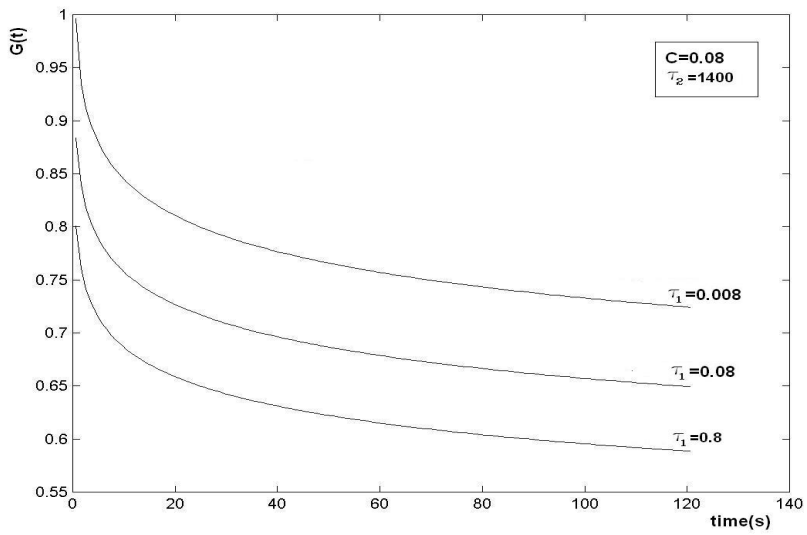

Figure D10 – Effect of Changing the Constant 'τ_1' on 3-Parameter Reduced Relaxation Function

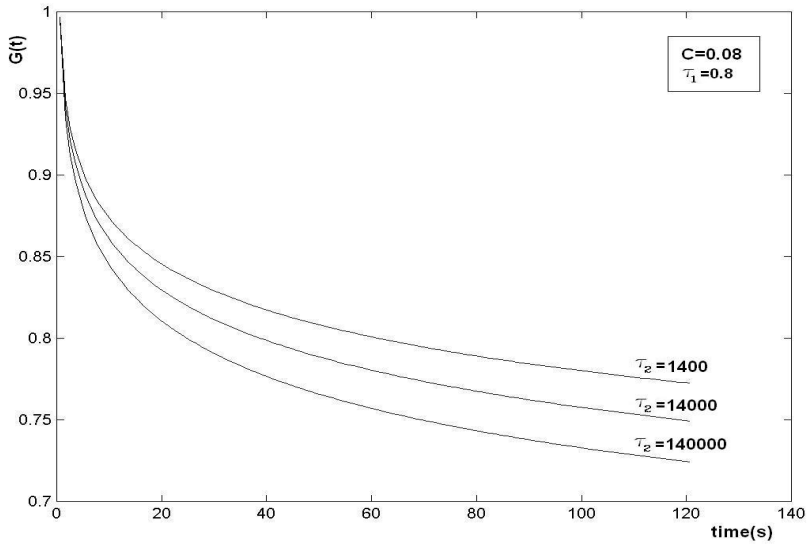

Figure D11 – Effect of Changing the Constant 'τ_2' on 3-Parameter Reduced Relaxation Function

In Figure D8, the base response of the reduced relaxation function is seen. The parameters are as they are given in the figure and none of them has been changed. In the following figures, only one of the parameters is changed while the others are kept constant, and the effect of changing this parameter is observed.

In Figure D9, the effect of changing the viscous damping parameter (C) on the reduced relaxation function is seen. As seen, increasing the value of the viscous damping constant causes all the relaxation amplitude to increase, too. Figure D10 shows the effect of changing the short term constant (τ_1) on the reduced relaxation curve. Increasing the value of the short term constant causes the all relaxation curve to be shifted downwards. Finally, in Figure D11 the effect of changing the long term constant (τ_2) on the reduced relaxation curve is seen. Increasing the value of the long term relaxation constant causes the long term relaxation to increase, too.

This 3-parameter reduced relaxation function has been used to model the time dependent response of a variety of biomaterials including ligament, bladder, and aortic valve (Dehoff, 2006).

APPENDIX E

HYDROSTATIC PRESSURE

Hydrostatic pressure, which appears in hydrostatic state of stress, is the pressure at a given depth in a static liquid. This pressure comes into being as a result of the weight of the liquid acting on a unit area plus any pressure acting on the surface of the liquid.

$$P = P_{atm} + \rho g h \quad \text{.....(E1)}$$

where; P_{atm} is the atmospheric pressure; ρ is the density of the liquid; g is the gravitational acceleration and h is the distance below the surface of the liquid. The term $\rho g h$ is called the gage pressure which is due to the liquid alone.

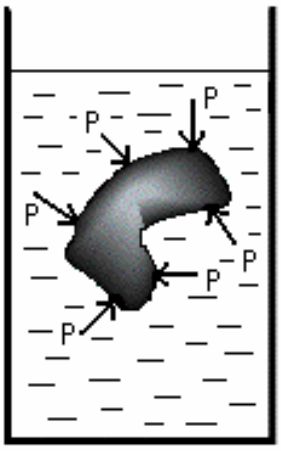

Figure E1 – Hydrostatic Pressure

The hydrostatic state of stress is also called the *spherical* state of stress. In that case, all the principal stresses are equal to the negative of the pressure and there is no shear stress on any plane, and any three mutually perpendicular directions may be selected as the principal directions (Malvern, 1969).

Pressure is not really a vector even though it looks like a vector in Figure E1. The arrows indicate the direction of the force that the pressure would exert on a surface it is contact with.

The hydrostatic pressure at a given depth is independent of direction; it is the same in all directions. This is another statement of the fact that the pressure is not a vector and thus has no direction associated with it when it is not in contact with some surface.

The pressure on a submerged object is always perpendicular to the surface at each point on the surface.

Hydrostatic state of stress is the only kind of stress that can exist in a fluid at rest. In some of soft tissue experiment procedures, the experiment is performed on the tissue when it is immersed into a liquid. In these conditions, the stress created by the liquid must be taken into account in the calculation the total stress. In the experiments performed within the context of this research, there was not such a case (no such an experiment condition like immersed into a liquid), so there was no hydrostatic stress other than the atmospheric pressure. However, since the tissue is always under atmospheric pressure, this state may assumed to be the reference state.

APPENDIX F

EXPERIMENTAL APPARATUS: INDENTER

One of the most important aspects of the modeling of soft biological tissues is the way the soft tissue experiments are performed. There are many types of experiments performed on the soft tissues. Uniaxial or multiaxial tensile experiments, compression experiments and indenter experiments are some examples of these. All these experimental procedures have some advantages and disadvantages. The most appropriate one for the specific study must be chosen.

In this thesis, the data obtained by an indenter experiment was used to obtain material coefficients. In an indenter experiment, an indenter tip is pushed into the soft tissue by a step motor and the displacement of the tip is recorded together with the reaction force applied by the tissue on it (Figure F1). The indenter used in this study can perform in vivo experiments and supply tissue reaction force-tissue displacement-time data as stored in the computer. This apparatus can be used within a wide range of cyclic indentation speeds (0.1–14 mm/s). Nonlinear elastic and viscoelastic properties of soft tissues, mechanical energy lost in each loading and anisotropy in the plane of skin can be observed (Petekkaya, 2008).

Three types of experiments can be performed by this apparatus. The first one of these is the *cyclic loading*. In cyclic loading experiments, the tissue is loaded until the desired displacement is accessed and then the loading is cut out. This procedure is repeated 10 times at a specific constant speed, because approximately in the first five cycles pre-conditioning (Mullin's effect) are observed, consequently they are omitted. After the sixth cycle, repeatable results can be accessed. By cyclic loading

experiments; data about displacement - reaction force curve and orientation reaction of the soft tissue and mechanical energy lost during one cycle can be acquired.

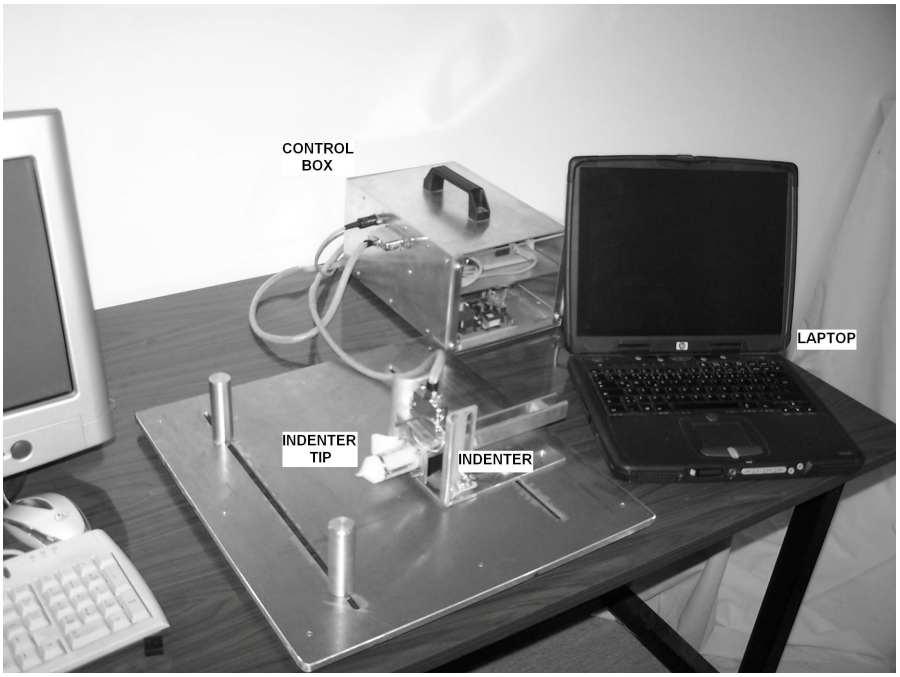

Figure F1 – Soft Tissue Experiment System

The other type of experiment that can be performed is *relaxation* In relaxation experiments, the soft tissue can be subjected to a wide range of speeds of initial loading, after the desired displacement (or load) is reached, the deformation is kept constant (*i.e.* the motor is stopped) and the decrease of tissue reaction force (relaxation) can be observed. Relaxation experiments inform us about viscoelastic characteristics of the soft tissue.

The last type of experiment that can be performed with the apparatus we used is *creep.* In creep experiments, as similar to the relaxation experiments the soft tissue can be subjected to a wide range of speed of initial loading, after the desired tissue

reaction force is reached this force is kept constant and displacement of the tissue (creep) is observed.. Creep experiments also inform us about viscoelastic characteristics of the soft tissue.

The experiment apparatus used for collecting data for modeling the mechanical behavior of soft tissues has the following features:

- The system is computer-controlled and the experiment results are stored in a computer.
- The soft tissue can be loaded as displacement-controlled or speed-controlled.
- Cyclic loading, relaxation and creep experiments can be performed at different speeds.
- The soft tissue can be loaded by different indenter tips having different geometries.
- It has a simple design that allows use in clinical environment.
- It allows modifications on the device or experimental protocols.

The system is shown schematically at Figure F2. There are three main parts interacting with each other: laptop computer (which controls the system and stores the collected data), control box (which has electronic units inside it) and experiment unit (which performs soft tissue experiments).

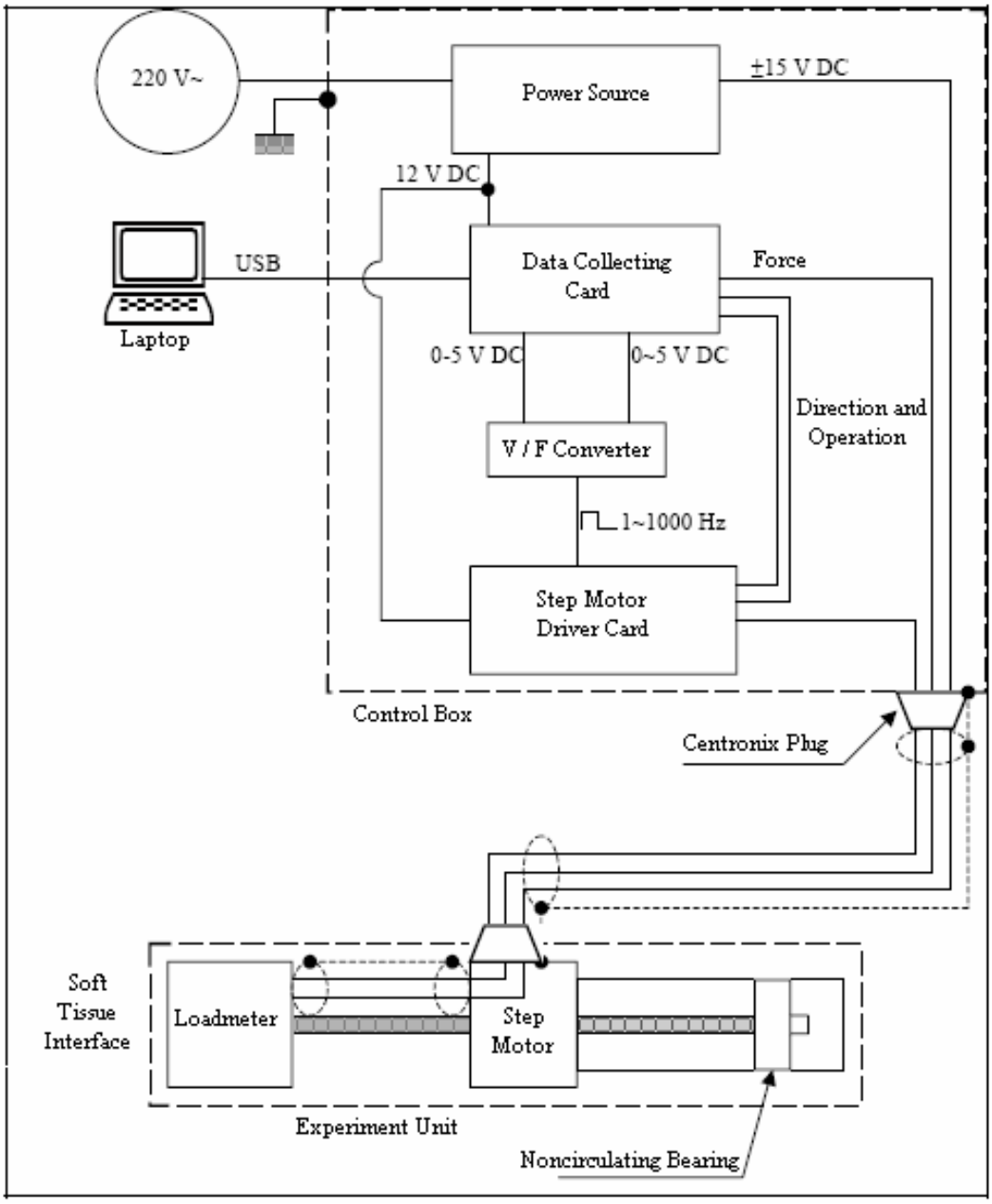

Figure F2 - Soft Tissue Experiment System Sketch

(adopted from *Dizaltı Ampute Yumuşak Doku Mekanik Özelliklerinin Araştırılması için Deney Cihazı Tasarımı ve Üretimi*, Tönük, E., 2008)

APPENDIX G

INVERSE FINITE ELEMENT MODELING

Finite element analyses have been used for the simulation of many mechanical problems for many years. For most of the actual complex engineering problems it is not possible to obtain exact results. Therefore, the physical natures of the problems are approximated to obtain an acceptable solution, i.e. acceptable accuracy in reasonable time and reasonable cost. This is the main concept of finite element analysis.

Finite element models have also been used widely to compute soft-tissue deformations under mechanical constraints. They are well suited to compute accurate and complex deformations. Also visualization of finite elements is well suited for graphics hardware.

A major impediment to building the accurate soft-tissue models is the lack of quantitative mechanical information suitable for finite element computation. The required information not only refers to the inner mechanical property of a given soft tissue but also includes contact with the surrounding tissues. In terms of computation, the former corresponds to the constitutive law of motion linking the stress tensor with the strain tensor, whereas the latter corresponds to the boundary conditions (Kauer et al, 2002).

Finite-element based material identification methods have been used by many investigators to estimate material coefficients for biological tissues. These “inverse methods” assume a constitutive equation for the respective material and estimate the

material coefficient(s) by simulating force-deformation-time characteristics with a computer model (Kauer et all, 2002, Tönük et al, 2003, Fulin et all, 2007).

In this study, a nonlinear finite-element analysis was used to simulate hysteresis, preconditioning, relaxation and creep data obtained during in vivo indentation. The finite element models facilitated estimation of an appropriate set of nonlinear viscoelastic material parameters of quasi-linear viscoelastic formulation, enhanced quasi-linear viscoelastic isotropic formulation and enhanced quasi-linear viscoelastic anisotropic formulation for bulk soft tissue.

Identification of Material Characteristics by Inverse Finite Element Method

It is not possible to implement standard material experiments on some materials. One of the methods to identify the coefficients of the constitutive equations for those materials is "inverse finite element" method. The following study is an example of that. In the study, the experiment results performed on the lower extremity residual limb tissue used for identification of nonlinear elastic and viscoelastic behavior of soft biological tissues.

Soft tissue experiments were performed with two similar soft tissue systems. The first one is a system that has a cylindrical indenter tip of 2.5 mm radius presented by Vetrano et all in 1997. The second system has three cylindrical indenter tips of 3, 5 and 7.5 mm radii and one spherical indenter tip of 15 mm. radius presented by Tönük, 2003. Both systems can perform cyclic loading, relaxation and creep experiments on soft tissues and both can acquire force-displacement-time data from these experiments.

The finite element model of the tissue has been created as close as possible to the real tissue to identify the soft tissue material parameters. An axisymmetric finite element model has been used, because loading conditions and the situation of the soft tissue is like that.

The meshing of the soft tissue is done with gradually changing the mesh size in finite element model. The indenter tip and bone contact of soft tissue have been modeled with two different rigid surfaces (Figure G1). The contact surface between the indenter tip and the soft tissue has been modeled with a fine mesh than the other part of the soft tissue, because stress-strain change is maximum at that surface. The aim of that is to prevent calculation errors that can occur during deformation due to large displacements. As boundary conditions, the soft tissue displacement perpendicular to the symmetry axis has been set to 'fixed' and by assuming that the soft tissue is completely stuck on the bone, the contact between the bone and the soft tissue has been set to 'fixed' in all directions.

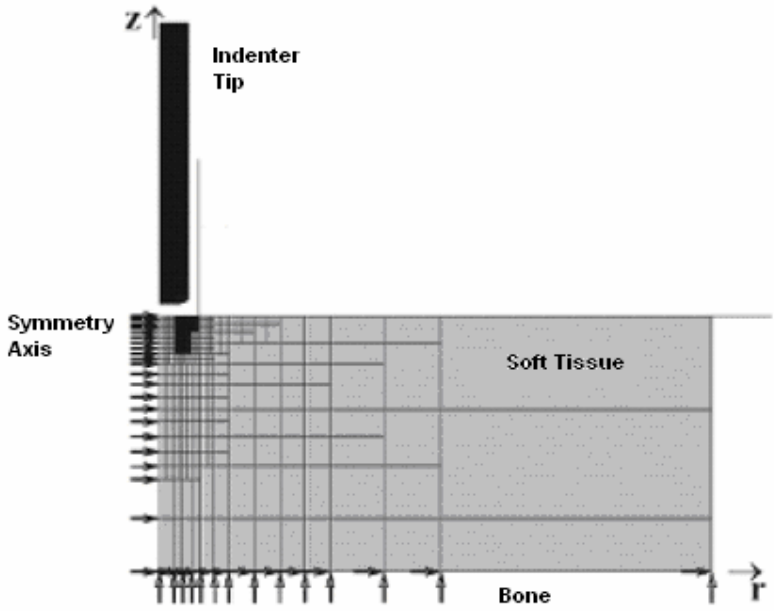

Figure G1 – Finite Element Model

(adopted from *Dizaltı Ampute Yumuşak Doku Mekanik Özelliklerinin Araştırılması için Deney Cihazı Tasarımı ve Üretim*i, Tönük, E., 2003)

As soft tissue material model James-Green-Simpson (third degree Mooney) has been chosen. This is an empirical material model and has been used to model the behavior of polymeric materials for long years. Because of the fact that the material model is empirical, the parameters do not posess any physical meanings. The constitutive equation of the model is given by;

$$W = C_{10}(I_1 - 3) + C_{01}(I_2 - 3) + C_{11}(I_1 - 3)(I_2 - 3) + C_{20}(I_1 - 3)^2 + C_{30}(I_1 - 3)^3 \text{ ……...(G1)}$$

where; I_1 and I_2 are first and second invariants of the Green's finite strain tensor and C_{ij} are material constants to be determined. For axisymmetric models of incompressible materials, equation (G1) can be reduced to (Tönük et all, 2003);

$$W = C_I(I - 3) + C_J(I - 3)^2 + C_K(I - 3)^3 \text{ ……(G2)}$$

where;
$$C_I = C_{10} + C_{01}$$
$$C_J = C_{11} + C_{20}$$
$$C_K = C_{30}$$

For the cyclic loading experiments, inverse finite element analysis has been started with the initial values of $C_I = C_J = C_K = 1$ kPa. Indentation of the soft tissue by the indenter tip has been simulated with computer and soft tissue reaction force results have been compared with the ones obtained by experiments. These simulation results have been changed with respect to the difference between the simulation and experiment results. The results and material constants are given in Figure G2 and table G1, respectively.

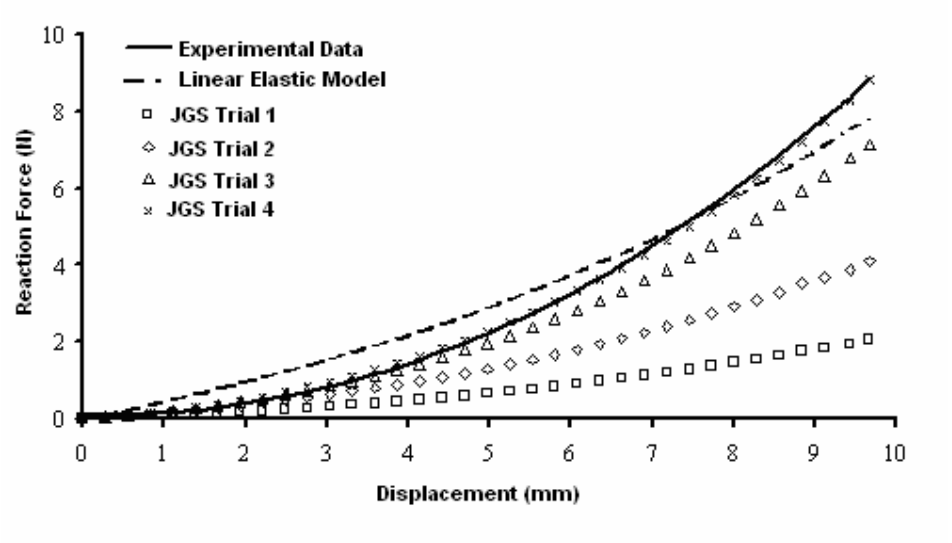

Figure G2 – Identification of the Parameters of James-Green-Simpson Material by Finite Element Method

(adopted from *Dizaltı Ampute Yumuşak Doku Mekanik Özelliklerinin Araştırılması için Deney Cihazı Tasarımı ve Üretim*i, Tönük, E., 2003)

Table G1 – Material Constants Used in the Simulations and Sum of Error Squares

(adopted from *Dizaltı Ampute Yumuşak Doku Mekanik Özelliklerinin Araştırılması için Deney Cihazı Tasarımı ve Üretim*i, Tönük, E., 2003)

	[MPa]			**[-]**
Trial	**C_I**	**C_J**	**C_K**	**Sum of Error Squares**
1	0,001	0,001	0,001	412,28%
2	0,002	0,002	0,002	188,82%
3	0,002	0,01	0,002	24,46%
4	0,002	0,015	0,002	0,41%

In this experiment, only nonlinear characteristic of the material has been taken into account, viscoelastic characteristic has been ignored. For modeling the data obtained by relaxation and creep experiments, the relaxation form of the James-Green-Simpson model given in equation (G3) (available in MSC.Marc) is used;

$$W(t) = W_0\left[1 - \delta_1\left(1 - e^{\left(\frac{-t}{\tau_1}\right)}\right) - \delta_2\left(1 - e^{\left(\frac{-t}{\tau_2}\right)}\right)\right] \text{.....(G3)}$$

where; W_0 is instantaneous strain energy function and can be denoted as in equation (G2) for axisymmetric problem; δ_1 and τ_1 are short time relaxation magnitude and time constant; δ_2 and τ_2 are long time relaxation magnitude and time constant, respectively.

For the initial values of time constants and relaxation magnitudes, the function given in equation (G4) is applied to the experimental data. By performing relaxation experiments, the constants C_I, C_J ve C_K (and W_0) are obtained as in the cyclic loading experiments.

$$F(t) = F_0\left[1 - \delta_1\left(1 - e^{\left(\frac{-t}{\tau_1}\right)}\right) - \delta_2\left(1 - e^{\left(\frac{-t}{\tau_2}\right)}\right)\right] \text{.....(G4)}$$

To fit the finite element results with the experiment results, magnitudes of relaxation have been changed. This can be seen in Figure G3.

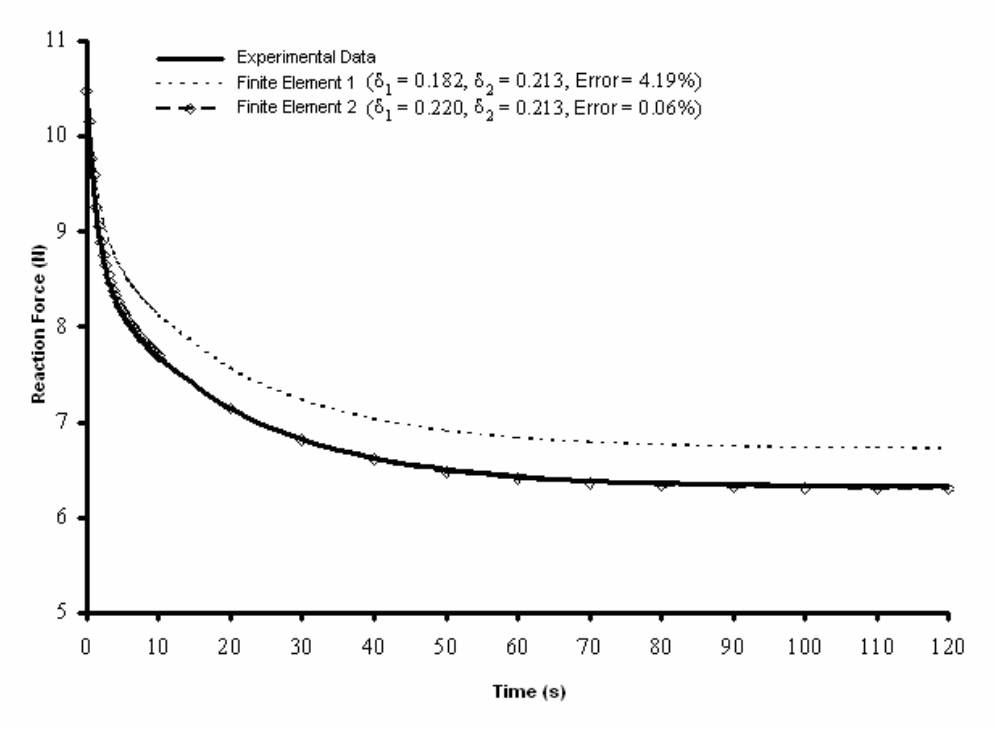

Figure G3 – Identification of Viscoelastic Material Constants for Relaxation (adopted from *Dizaltı Ampute Yumuşak Doku Mekanik Özelliklerinin Araştırılması için Deney Cihazı Tasarımı ve Üretim*i, Tönük, E., 2003)

In creep experiments, the function given in equation (G5) is applied to the experimental data.

$$d(t) = d_0\left[1+\delta_1'\left(1-e^{\left(\frac{-t}{\tau_1'}\right)}\right)+\delta_2'\left(1-e^{\left(\frac{-t}{\tau_2'}\right)}\right)\right] \quad \text{.....(G5)}$$

where; δ_1' and τ_1' are short time creep magnitude and time constant; δ_2' and τ_2' are long time creep magnitude and time constant, respectively. These can be expressed in terms of relaxation constants assuming linear viscoelastic behavior as follows;

$$\delta_1 = \frac{\delta_1'}{1+\delta_1'+\delta_2'} \quad \text{.....(G6)}$$

$$\delta_2 = \frac{\delta_2'}{1+\delta_1'+\delta_2'} \quad \text{.....(G7)}$$

$$\tau_1 = (1-\delta_1-\delta_2)\tau_1' \quad \text{.....(G8)}$$

$$\tau_2 = (1-\delta_1-\delta_2)\tau_2' \quad \text{.....(G9)}$$

To fit the finite element results with the experiment results, magnitudes of creep have been changed. This can be seen in figure G4.

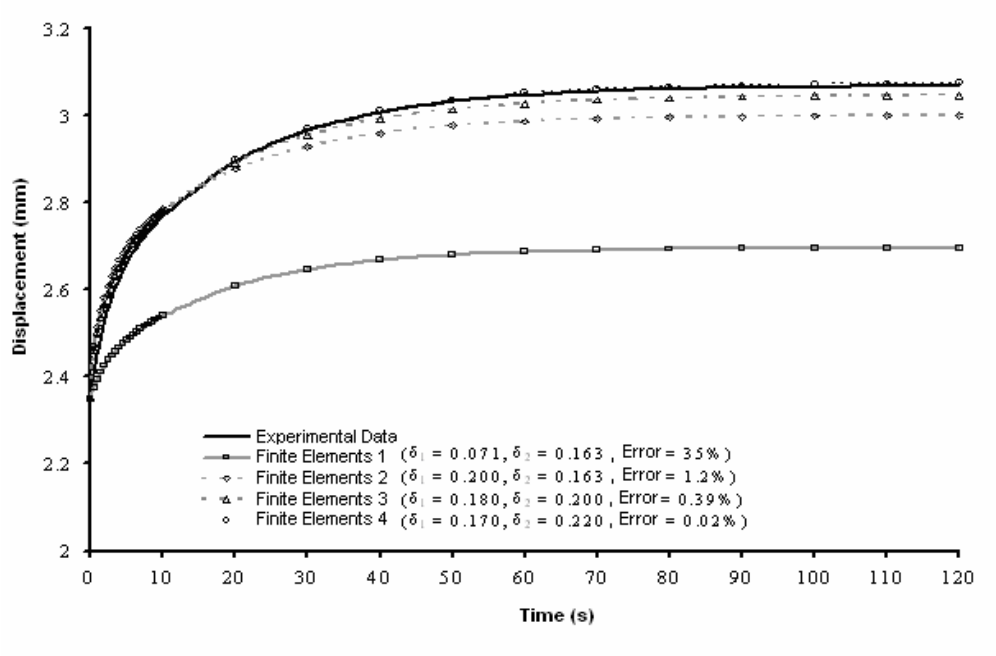

Figure G4 – Identification of Viscoelastic Material Constants for Creep
(adopted from *Dizaltı Ampute Yumuşak Doku Mekanik Özelliklerinin Araştırılması için Deney Cihazı Tasarımı ve Üretim*i, Tönük, E., 2003)

In inverse finite element methods, the first thing to do is to create the model, and then the constitutive equation which represents the material behavior is chosen. The initial guess of the material coefficients are selected arbitrarily. The model is submitted with these initial guess constants and results are compared with

experimental data. By changing the values of material coefficients, the best fit between the simulation and the experimental data is tried to be found. When this simulation becomes accurate enough with selected coefficients, the model is assumed to represent the behavior of the material. In this study, the constants of nonlinear and viscoelastic soft tissues have been identified by using experimental data by inverse finite element method.

However, inverse finite element method has two disadvantages:

- The material model must represent the behavior of that material especially for the ones which can not be represented by a linear elastic model.
- Because of the fact that the material is not linear, finite element model can be divergent. Also, for some material models, due to nonlinearities in the model, uniqueness of the coefficients may not be guaranteed.

APPENDIX H

USER SUBROUTINE TEMPLATE *(hypela.f)*

```
      subroutine hypela(d,g,e,de,s,temp,dtemp,ngens,n,nn,kc,mats,
     * ndi,nshear)
c* * * * * *
c
c     user subroutine to define young's modulus and poisson's ratio
c     as function of stress in non-linear elastic small strain
c     material.
c
c     d        stress strain law to be formed by user
c     g        change in stress due to temperature effects
c     e        total strain
c     de       increment of strain
c     s        stress - should be updated by user
c     temp     state variables
c     dtemp    increment of state variables
c     ngens    size of stress - strain law
c     n        element number
c     nn       integration point number
c     kc       layer number
c     mats     material i.d.
c     ndi      number of direct components
c     nshear   number of shear components
c
c* * * * * *
      implicit real*8 (a-h,o-z)
      dimension e(*),de(*),temp(*),dtemp(*),g(*),d(ngens,ngens),s(*)
      dimension n(2),et(6)
c
      return
      end
```

APPENDIX I

USER SUBROUTINE FOR QLV MODELING BY ASSUMING SOFT TISSUE AS AN ISOTROPIC MATERIAL

```
      subroutine hypela(d,g,e,de,s,temp,dtemp,ngens,n,nn,kc,mats,
     * ndi,nshear)
c* * * * * *
c
c     user subroutine to define young's modulus and poisson's ratio
c     as function of stress in non-linear elastic small strain
c     material.
c
c     d        stress strain law to be formed by user
c     g        change in stress due to temperature effects
c     e        total strain
c     de       increment of strain
c     s        stress - should be updated by user
c     temp     state variables
c     dtemp    increment of state variables
c     ngens    size of stress - strain law
c     n        element number
c     nn       integration point number
c     kc       layer number
c     mats     material i.d.
c     ndi      number of direct components
c     nshear   number of shear components
c
c* * * * * *
      implicit real*8 (a-h,o-z)
          include '../marc_working_directory/concom'
          include '../marc_working_directory/creeps'
c         ******
c
c         By including the common blocks concom and creeps, we include these
c         variables into the subroutine:
c
c         cptim: time at beginning of increment
c         timinc: time increment
```

```
c       ncycle: number of increment
c
c       ******
      dimension e(3),de(3),temp(1),dtemp(1),g(1),d(ngens,ngens),s(3)
      dimension n(2),et(3),ets(3)
c       ******
c
c       Since, this is a three dimensional model, we need three dimensional strain,
c       strain increment and stress values. This is done by setting these variables
c       three dimensional with dimension command.
c
c       ******
        if (ncycle.eq.0) t=cptim+20.0d0
        if (ncycle.eq.0) et(1)=e(1)
        if (ncycle.eq.0) et(2)=e(2)
        if (ncycle.eq.0) et(3)=e(3)
        if (ncycle.gt.0) t=cptim+20.0d0+timinc
        if (ncycle.gt.0) et(1)=e(1)+de(1)
        if (ncycle.gt.0) et(2)=e(2)+de(2)
        if (ncycle.gt.0) et(3)=e(3)+de(3)
c       ******
c
c       To eliminate the errors (like dividing by zero or logarithm of zero) in the
c       calculation of some constants like q28 and q29, a new constant is created as
c       t0=18.4 and time of simulation is set to start from 20.
c
c       ******
        ets(1)=et(1)**2.0d0
        ets(2)=et(2)**2.0d0
        ets(3)=et(3)**2.0d0
c
        a=1.96d-38
        b=4.2d1
        c=8.0d-2
        T1=8.0d-1
        T2=1.4d3
        t0=1.84d1
        epsdat=2.5d-2
c       ******
c
c       Constants in the subroutine are as they are explained in chapter A
c
c       The user subroutine is written in double precision to be able to obtain more
c       accurate results.
c
c       ******
        q1=a/(1.0d0+c*log(T2/T1))
```

```
      q2=b*epsdat
      q3=q2*t0
      q4=exp(q3)
      q5=q4-1.0d0
      q6=q4+1.0d0
      q7=q2+(1.0d0/T1)
      q8=q7+t0
      q9=exp(q8)
      q10=q2+(1.0d0/T2)
      q11=q10*t0
      q12=exp(q11)
      q13=t0+T1
      q14=q2*T1+1.0d0
      q15=q14*t0
      q16=q15+T1
      q17=q2*T2+1.0d0
      q18=q17*t0
      q19=q18+T2
      q20=0.57722d0-log(T2)+(t0/T2)
      q21=log(T2)-0.57722d0
c
      q22=(T1/(t0-t))*((q13-t)/(t0-t))
      q23=(T1/(q15-q14*t))*((q16-q14*t)/(q15-q14*t))
      q24=(T1/t)*(1.0d0-(T1/t))
      q25=(T1/q14*t)*(1.0d0-(T1/q14*t))
      q26=(T2/(q18-q17*t))*((q19-q17*t)/(q18-q17*t))
      q27=(T2/q17*t)*(1.0d0-(T2/q17*t))
      q28=q20+log(t-t0)-(t/T2)
      q29=q21+(t/T2)-log(t)
      q30=q9*(q22-q23)+q24-q25
      q31=q12*q26+q27
      q32=q4*q28+q29
c
      sig=q1*(q5+c*((exp(-t/T1)*q30)+(exp(-t/T2)*q31)-q32))
c
      do 100 i=1,ngens
        do 110 j=1,ngens
          d(i,j)=0.0d0
110     continue
100   continue
c     ******
c
c     Since there are no shear stresses in our experiment, the values of
c      d(1,2)=d(2,1), d(1,3)=d(3,1) and d(2,3)=d(3,2) of the tangent stiffness are set
c      to zero.
c
c     ******
```

```
        d(1,1)=sig
        d(2,2)=d(1,1)
        d(3,3)=d(1,1)
c
        do 120 k=1,3
          s(k)=d(k,k)*ets(k)
120     continue
c       ******
c
c       This quasi-linear viscoelastic formulation is expected to simulate the stress
c       relaxation and creep behaviors of soft biological tissues with time. So, the
c       constitutive equations of stresses were written in term of the only independent
c       variable time. Other constants are calculated by using the material
c       parameters.
c
c       ******
    return
    end
```

This user subroutine allows the user to implement arbitrary material models in conjunction with the hypoelastic model definition option in MSC.Marc. MSC.Marc supplies hypela total mechanical strain (mechanical strain = total strain - thermal strain), the increment of mechanical strain, and other information. Stress, total mechanical strain and state variable arrays at the beginning of the increment (t = n) are passed to hypela with the incremental strain. The user is expected to calculate stresses S, tangent stiffness D, and state variables (if present) that correspond to the current strain at the end of the increment (t = n + 1).

.

APPENDIX J

VERIFICATION OF THE SUBROUTINE IN APPENDIX I

WITH A SIMPLE 3D MODEL

For the verification of the subroutine written in Appendix I, the three dimensional model seen in the Figure J1 was created. This specimen was 100 mm long with square cross section of 5 x 5 mm and had the material properties of hypoelastic materials in Mentat. The model had eight nodes, four of which are seen on the right hand side having fixed displacement boundary conditions along three material axes. Other four nodes are seen on the left hand side and three of them are linked (nodal tie) to the other one on which a position controlled boundary condition was applied. These nodes are only exposed to position controlled boundary condition for this model (as explained in section J.1) to prove that the subroutine is able to simulate relaxation and creep since, this material is expected to simulate relaxation and creep behaviors.

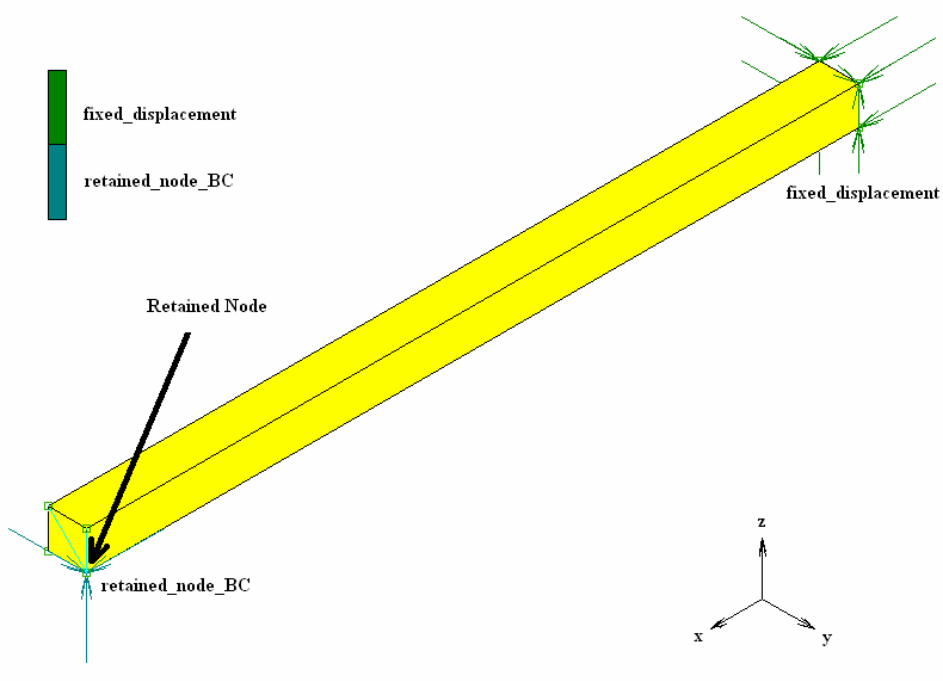

Figure J1 – Simple Three Dimensional Model

J.1. Verification of Relaxation Simulation

For the verification of the subroutine in relaxation simulation, the retained node of the specimen was applied to a displacement controlled boundary condition. It was firstly applied to tension and the specimen was lengthened 5 mm in five seconds which was applied in 50 time steps (increments) in x-direction. Then, the specimen was kept at that deformation for 120 seconds in 30 time steps to observe stress relaxation behavior (Figure J2). This model was submitted with the large displacement and large strain - total Lagrange analysis options by using the subroutine given in the Appendix I.

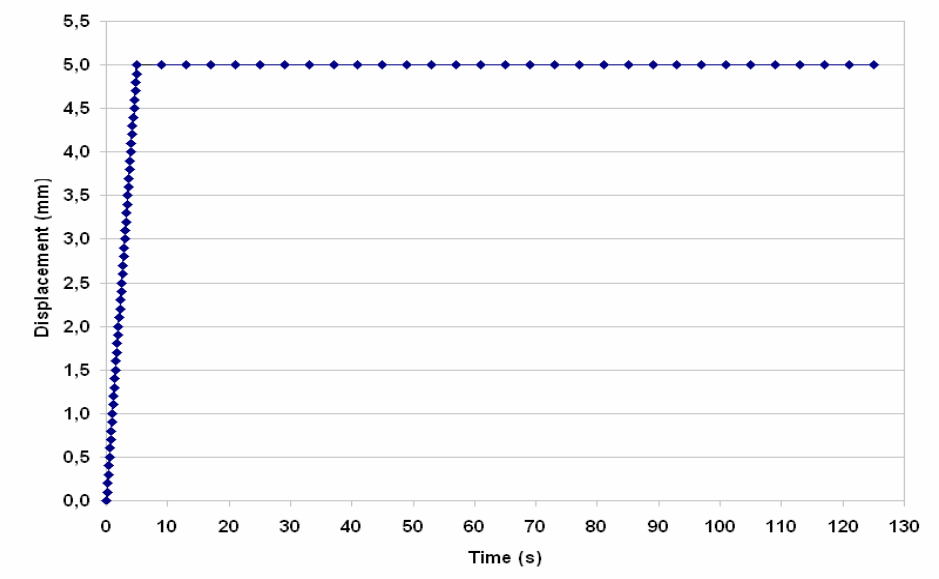

Figure J2 – Change of Displacement of the Retained Node with Time

Figure J3 and J4 show the decrease of reaction force and stress with time, respectively. These decreases occurred while the displacement was kept constant. So, this simple simulation proves that the subroutine written in Appendix I is working properly while simulating relaxation.

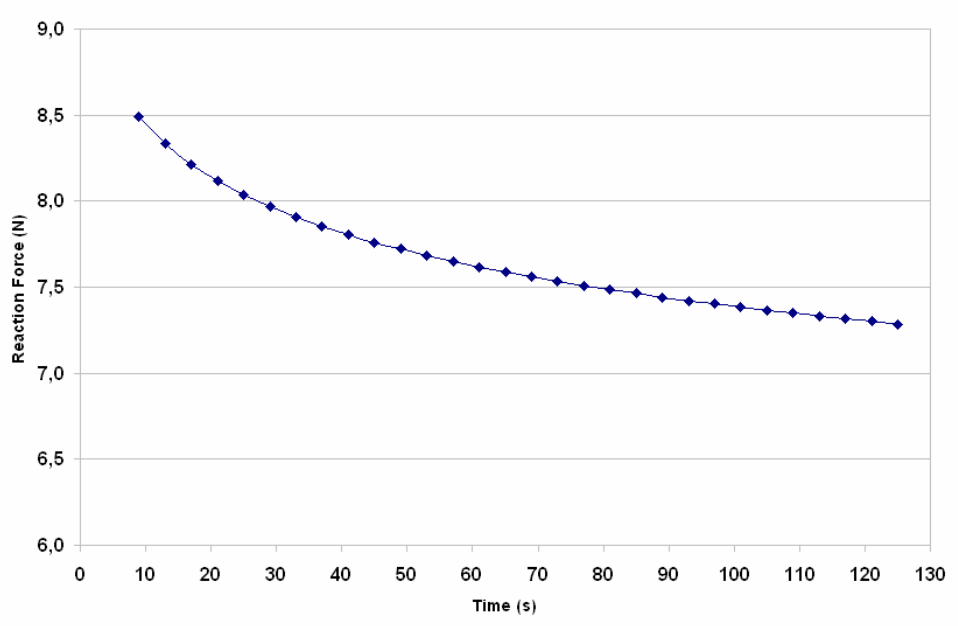

Figure J3 – Decrease of Reaction Force with Time

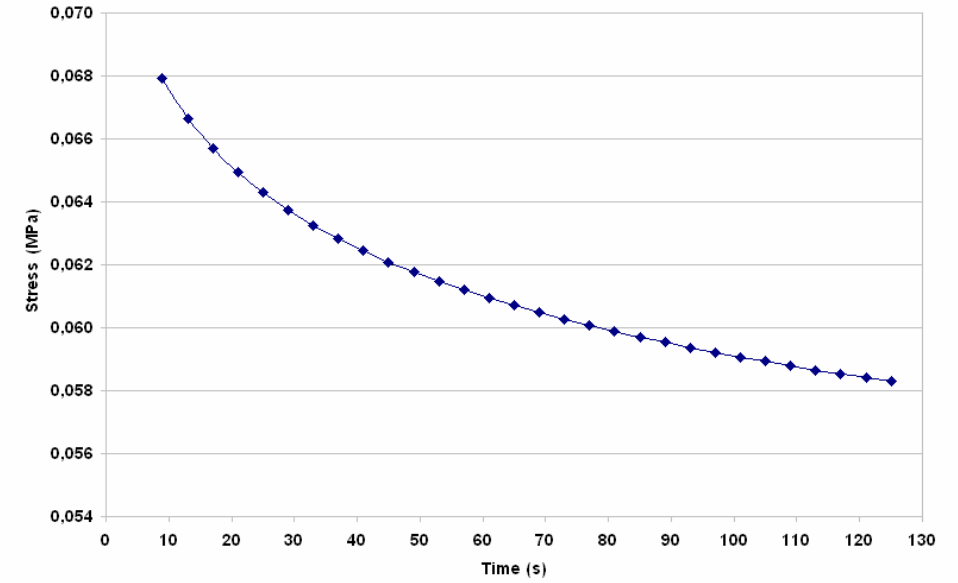

Figure J4 – Decrease of Stress (Relaxation) with Time

J.2. Verification of Creep Simulation

For the verification of the subroutine in creep simulation, the retained node of the specimen was applied to displacement and load controlled boundary conditions. It was firstly applied to tension and the specimen was stretched 5 mm in five seconds which was applied in 50 time steps (increments) in x-direction. Then, the reaction force (in x-direction) occurred at fifth second was kept being applied constantly for 120 more seconds in 30 increments and change of displacement with time was observed. This model was submitted with the large displacement and large strain - total Lagrange analysis options by using the subroutine given in the Appendix I.

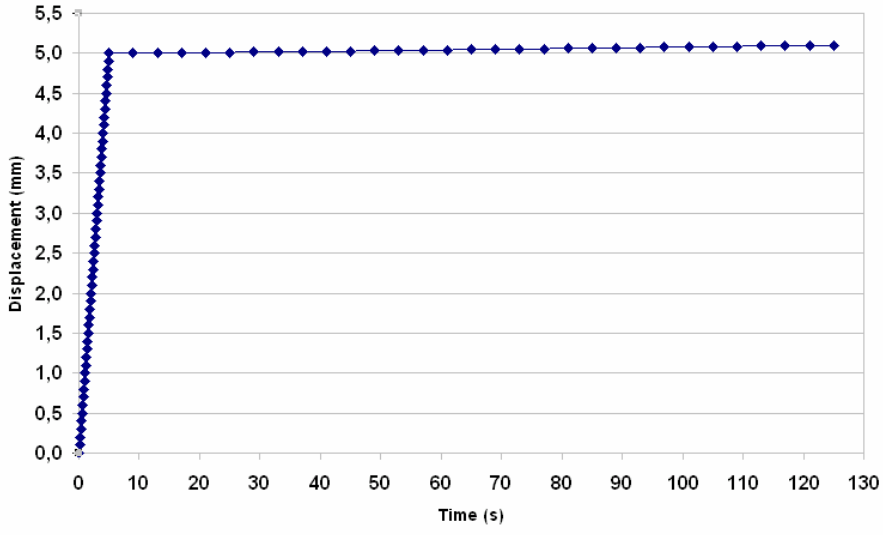

Figure J5 – Increase of Displacement (Creep) with Time

Figure J5 shows the increase of displacement with time. This increase occurred while the reaction force was kept constant. So, this simple simulation proves that the subroutine written in Appendix I is working properly while simulating creep behavior. The next job to do is to implement this subroutine to the original soft tissue model and to estimate the real values of the parameters in it.

APPENDIX K

USER SUBROUTINE FOR ENHANCED QLV MODELING BY ASSUMING SOFT TISSUE AS AN ISOTROPIC MATERIAL

```
      subroutine hypela(d,g,e,de,s,temp,dtemp,ngens,n,nn,kc,mats,
     * ndi,nshear)
c* * * * * *
c
c     user subroutine to define young's modulus and poisson's ratio
c     as function of stress in non-linear elastic small strain
c     material.
c
c     d        stress strain law to be formed by user
c     g        change in stress due to temperature effects
c     e        total strain
c     de       increment of strain
c     s        stress - should be updated by user
c     temp     state variables
c     dtemp    increment of state variables
c     ngens    size of stress - strain law
c     n        element number
c     nn       integration point number
c     kc       layer number
c     mats     material i.d.
c     ndi      number of direct components
c     nshear   number of shear components
c
c* * * * * *
      implicit real*8 (a-h,o-z)
          include '../marc_working_directory/concom'
          include '../marc_working_directory/creeps'
c         ******
c
c         By including the common blocks concom and creeps, we include these
c         variables into the subroutine:
c
c         cptim: time at beginning of increment
c         timinc: time increment
c         ncycle: number of increment
```

```
c
c       ******
      dimension e(3),de(3),temp(1),dtemp(1),g(1),d(ngens,ngens),s(3)
      dimension n(2),et(3),ets(3)
c       ******
c
c       Since, this is a three dimensional model, we need three dimensional strain,
c       strain increment and stress values. This is done by setting these variables
c       three dimensional with dimension command.
c
c       ******
        if (ncycle.eq.0) t=cptim+20.0d0
        if (ncycle.eq.0) et(1)=e(1)
        if (ncycle.gt.0) t=cptim+20.0d0+timinc
        if (ncycle.gt.0) et(1)=e(1)+de(1)
c       ******
c
c       To eliminate the errors (like dividing by zero or logarithm of zero) in the
c       calculation of some constants like q28 and q29, a new constant is created as
c       t0=18.4 and time of simulation is set to start from 20.
c
c       ******
        et(2)=et(1)
        et(3)=et(1)
c       ******
c
c       It can also be seen in this subroutine that, since this is an isotropic
c       formulation, all the principal strains must be equal to each other. This was
c       obtained by equating the strains along three material axes.
c
c       ******
        ets(1)=et(1)**2.0d0
        ets(2)=ets(1)
        ets(3)=ets(1)
c
        a=9.0d-35
        b=4.2d1
        c=8.0d-2
        T1=8.0d0
        T2=1.4d2
        t0=1.84d1
        epsdat=2.5d-2
        a1=b1
        b1=8.0d-1
        c1=b1
c       ******
c
```

```
c       Constants in the subroutine are as they are explained in chapter B
c
c       The user subroutine is written in double precision to be able to obtain more
c       accurate results.
c
c       ******
        qlam=(a1*a1+b1*b1+c1*c1)/8.0d0
        q1=a/(1.0d0+c*log(T2/T1))
        q2=b*epsdat
        q3=q2*t0
        q4=exp(q3)
        q5=q4-1.0d0
        q6=q4+1.0d0
        q7=q2+(1.0d0/T1)
        q8=q7+t0
        q9=exp(q8)
        q10=q2+(1.0d0/T2)
        q11=q10*t0
        q12=exp(q11)
        q13=t0+T1
        q14=q2*T1+1.0d0
        q15=q14*t0
        q16=q15+T1
        q17=q2*T2+1.0d0
        q18=q17*t0
        q19=q18+T2
        q20=0.57722d0-log(T2)+(t0/T2)
        q21=log(T2)-0.57722d0
c
        q22=(T1/(t0-t))*((q13-t)/(t0-t))
        q23=(T1/(q15-q14*t))*((q16-q14*t)/(q15-q14*t))
        q24=(T1/t)*(1.0d0-(T1/t))
        q25=(T1/q14*t)*(1.0d0-(T1/q14*t))
        q26=(T2/(q18-q17*t))*((q19-q17*t)/(q18-q17*t))
        q27=(T2/q17*t)*(1.0d0-(T2/q17*t))
        q28=q20+log(t-t0)-(t/T2)
        q29=q21+(t/T2)-log(t)
        q30=q9*(q22-q23)+q24-q25
        q31=q12*q26+q27
        q32=q4*q28+q29
c
        sig=q1*(q5+c*((exp(-t/T1)*q30)+(exp(-t/T2)*q31)-q32))
        p=sig/(8.0d0*qlam)
c
        do 100 i=1,ngens
          do 110 j=1,ngens
            d(i,j)=0.0d0
```

```
110       continue
100     continue
c       ******
c
c       Since there are no shear stresses in our experiment, the values of
c        d(1,2)=d(2,1), d(1,3)=d(3,1) and d(2,3)=d(3,2) of the tangent stiffness are set
c        to zero.
c
c       ******
        d(1,1)=p*a1**2.0d0
        d(2,2)=p*b1**2.0d0
        d(3,3)=p*c1**2.0d0
c
        do 120 k=1,3
          s(k)=d(k,k)*ets(k)
120     continue
c       ******
c
c       This enhanced quasi-linear viscoelastic formulation is expected to simulate
c       the hysteresis, preconditioning, stress relaxation and creep behaviors of soft
c       biological tissues. So, the constitutive equations of stresses were written in
c       terms of the two independent variables strain and time. Other constants are
c       calculated by using the material parameters.
c
c       ******
    return
    end
```

This user subroutine allows the user to implement arbitrary material models in conjunction with the hypoelastic model definition option in MSC.Marc. MSC.Marc supplies hypela total mechanical strain (mechanical strain = total strain - thermal strain), the increment of mechanical strain, and other information. Stress, total mechanical strain and state variable arrays at the beginning of the increment (t = n) are passed to hypela with the incremental strain. The user is expected to calculate stresses S, tangent stiffness D, and state variables (if present) that correspond to the current strain at the end of the increment (t = n + 1).

APPENDIX L

VERIFICATION OF THE SUBROUTINE IN APPENDIX K WITH A SIMPLE 3D MODEL

For the verification of the subroutine written in Appendix K, the three dimensional model seen in the Figure L1 was created. This specimen was 100 mm long with square cross section of 5 x 5 mm and has the material properties of hypoelastic materials in Mentat. The model had eight nodes, four of which are seen on the right hand side having fixed displacement boundary conditions along three material axes. Other four nodes are seen on the left hand side and three of them are linked (nodal tie) to the other one on which a position or load controlled boundary condition was applied. These nodes were exposed to different position or load controlled conditions (as explained in the following sections in detail) to prove that the subroutine is able to simulate hysteresis, preconditioning, relaxation and creep since, this subroutine is expected to simulate all these behaviors.

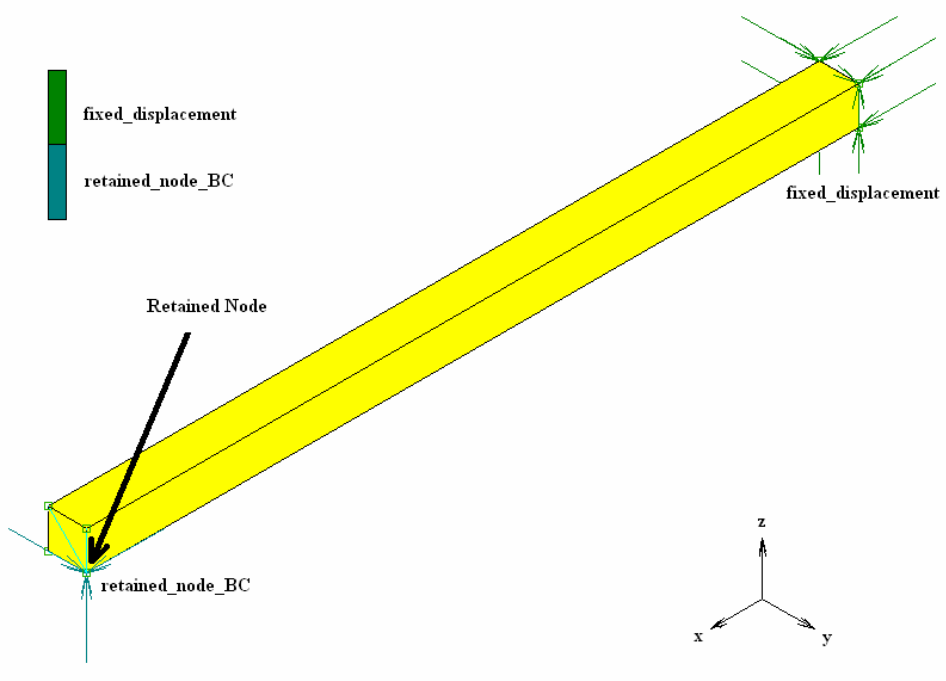

Figure L1 – Simple Three Dimensional Model

L.1. Verification of Relaxation Simulation

For the verification of the subroutine in relaxation simulation, the retained node of the specimen was applied to a displacement controlled boundary condition. It was firstly applied to tension and the specimen was lengthened 5 mm in five seconds which was applied in 50 time steps (increments) along x-direction. Then, the specimen was kept at that deformation for 120 seconds in 30 time steps to observe stress relaxation behavior (Figure L2). This model was submitted with the large displacement and large strain - total Lagrange analysis options by using the subroutine given in the Appendix K.

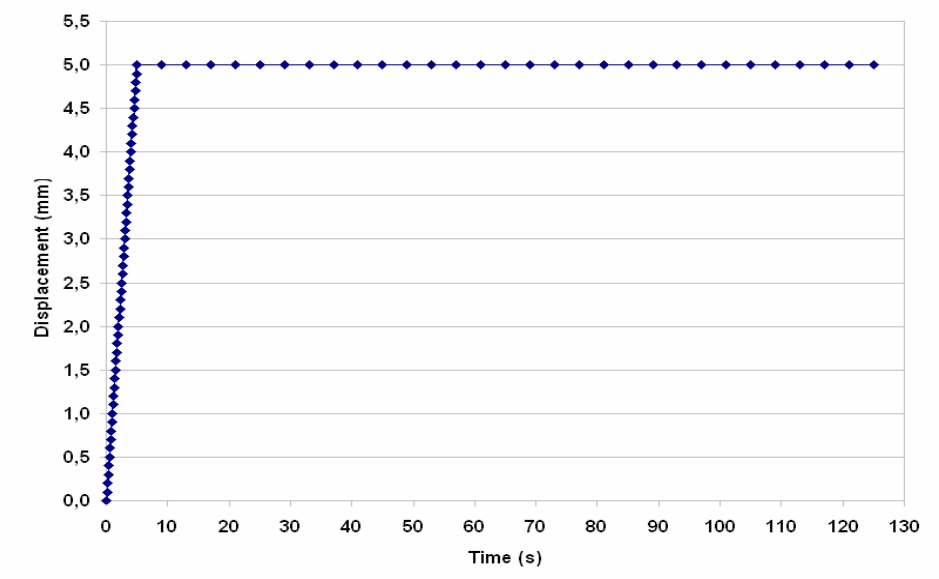

Figure L2 – Change of Displacement of the Retained Node with Time

Figures L3 and L4 show the decrease of reaction force and stress with time, respectively. These decreases occurred while the displacement was kept constant. So, this simple simulation proves that the subroutine written in Appendix K is working properly while simulating relaxation behavior.

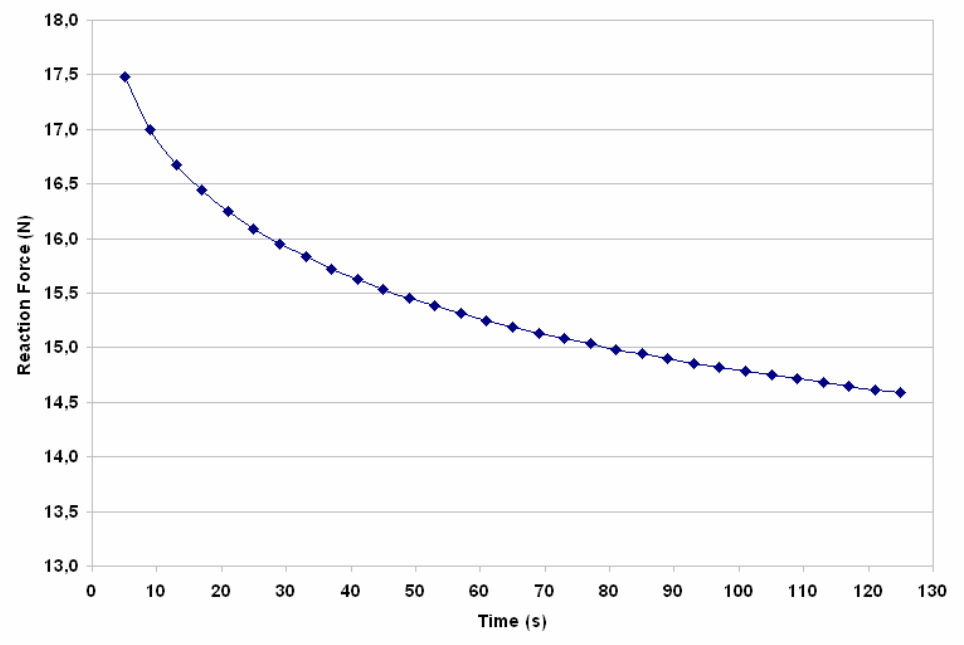

Figure L3 – Decrease of Reaction Force with Time

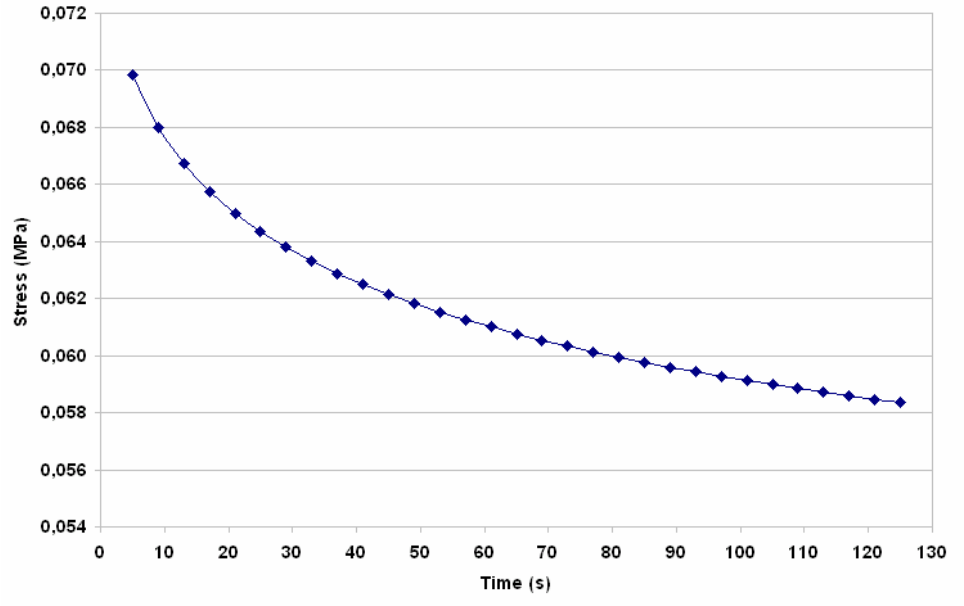

Figure L4 – Decrease of Stress with Time (Relaxation)

L.2. Verification of Creep Simulation

For the verification of the subroutine in creep simulation, the retained node of the specimen was applied to a displacement and then a load controlled boundary condition. The specimen was stretched 5 mm in five seconds which was applied in 50 time steps (increments) in x-direction. Then, the reaction force (in x-direction) occurred at fifth second was kept being applied constantly for 120 more seconds in 30 increments and change of displacement with time was observed. This model was submitted with the large displacement and large strain - total Lagrange analysis options by using the subroutine given in the Appendix K.

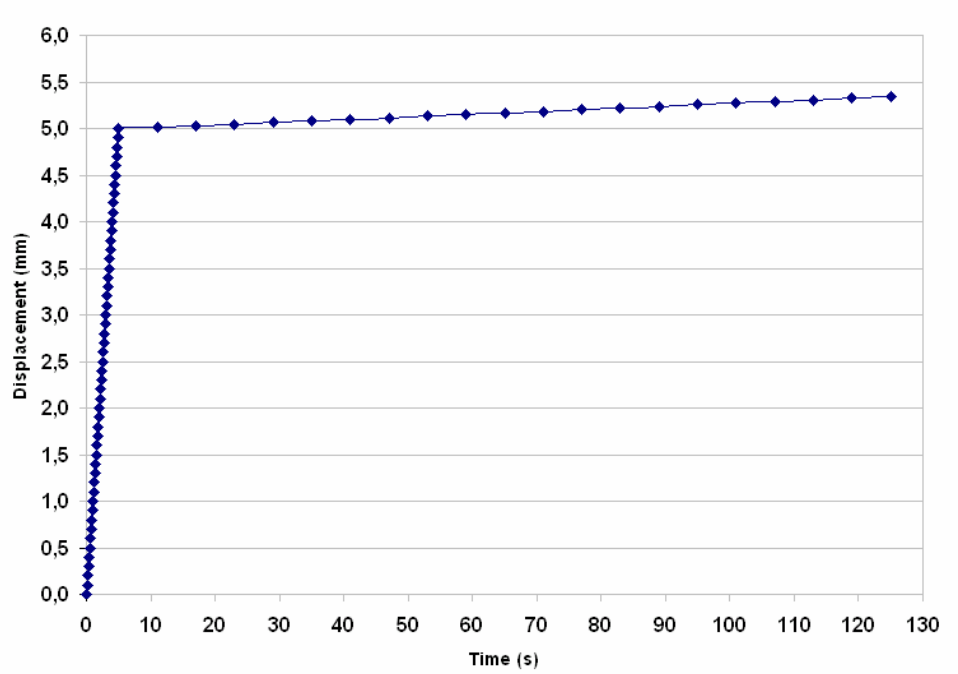

Figure L5 – Increase of Displacement with Time (Creep)

Figure L5 shows the increase of displacement with time. This increase occurred while the reaction force was kept constant. So, this simple simulation proves that the

subroutine written in Appendix K is working properly while simulating creep behavior.

L.3. Verification of Hysteresis Simulation

For the verification of the subroutine in hysteresis simulation, the retained node of the specimen was applied to a displacement controlled boundary condition. It was firstly applied to tension and the specimen was stretched 5 mm in five seconds which was applied in 25 time steps (increments) along x-direction. Then, the specimen was returned to its original shape with the application of compression with the same rate as tension. The difference between reaction force versus time curves and strain versus stress curves (hysteresis) in loading (tension) and unloading (compression) were observed. This model was submitted with the large displacement and Large Strain - Total Lagrange analysis options by using the subroutine given in the Appendix K.

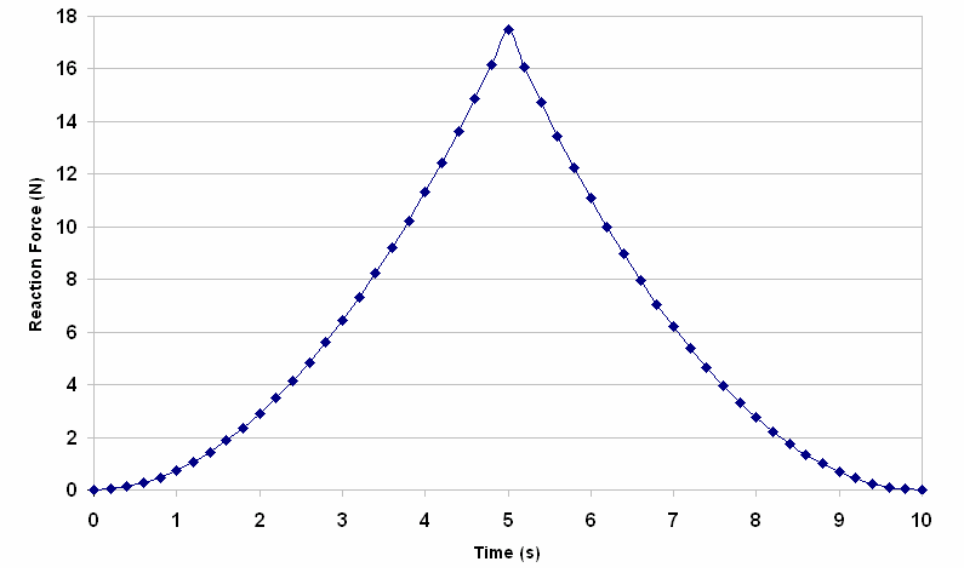

Figure L6 – Difference between Reaction Force vs. Time Curves

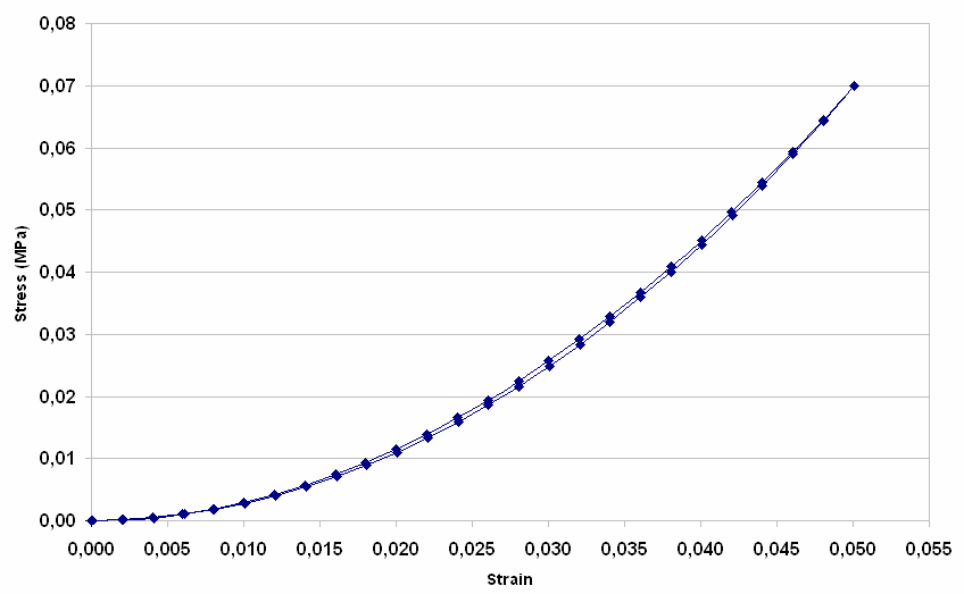

Figure L7 – Difference between Strain vs. Stress Curves (Hysteresis)

Figures L6 and L7 show the difference between reaction force versus time curves and strain versus stress curves (hysteresis) in loading and unloading, respectively. Loading and unloading curves are not the same in Figure L6, but the difference can be seen much clearly in Figure L7. This difference between two curves is called hysteresis and appears as energy loss during cyclic loading. So, this simple simulation proves that the subroutine written in Appendix K is working properly while simulating hysteresis behavior.

L.4. Verification of Preconditioning (Mullin's Effect) Simulation

For the verification of the subroutine in preconditioning simulation, the retained node of the specimen was applied a displacement controlled boundary condition. Displacement was applied and the specimen was stretched 5 mm in five seconds which was applied in 50 time steps (increments) along x-direction. Then, the specimen was returned to its original length with the application of displacement

with the same rate as tension. This cycle was repeated ten times and the difference between reaction force versus time curves and strain versus stress curves in loading (tension) and unloading (compression) in these cycles were observed. This model was submitted with the large displacement and Large Strain - Total Lagrange analysis options by using the subroutine given in the Appendix K.

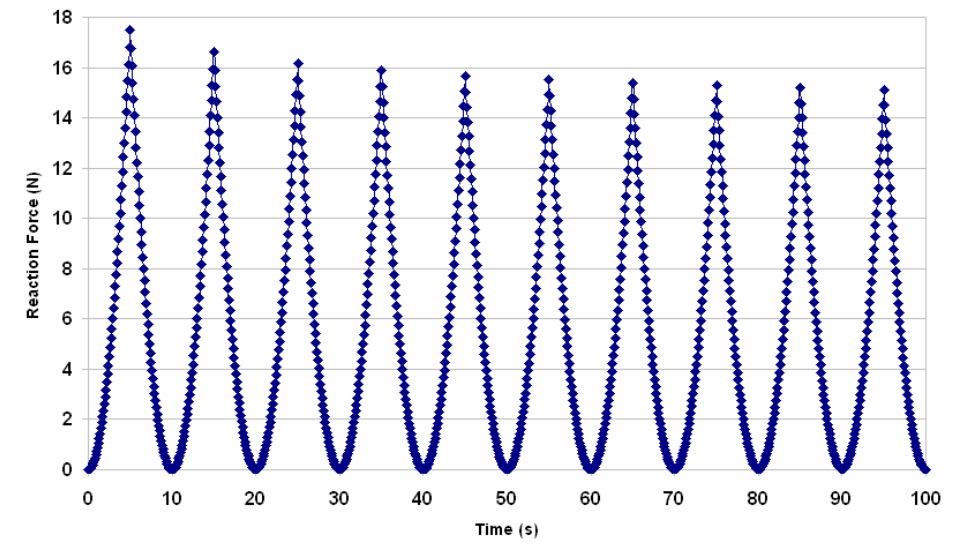

Figure L8 – Difference between Reaction Force vs. Time Curves (Preconditioning)

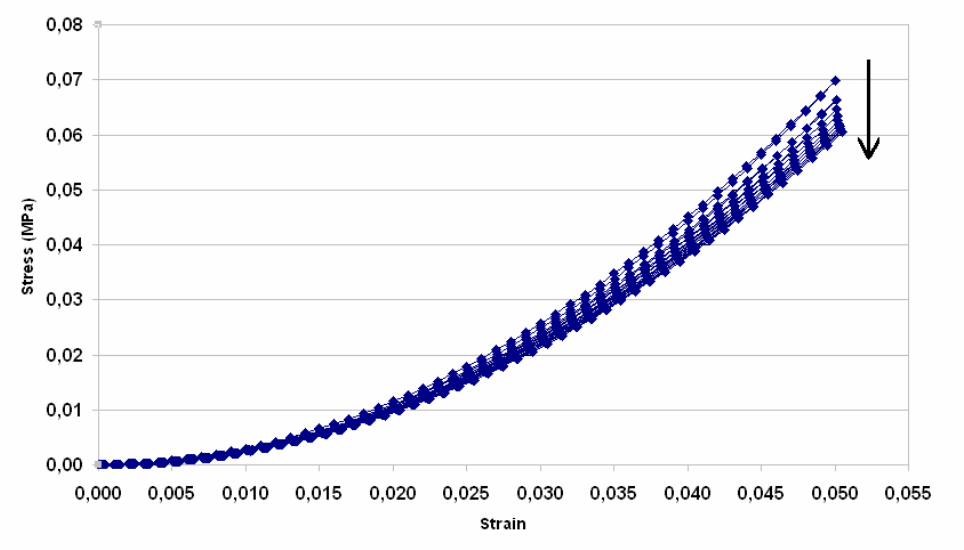

Figure L9 – Difference between Strain vs. Stress Curves (Preconditioning)

Figures L8 and L9 show the difference between reaction force versus time curves and strain versus stress curves in loading and unloading. These curves are becoming repeatable after about seventh or eighth cycle which is called as preconditioning. So, this simple simulation proves that the subroutine written in Appendix K is working properly while simulating preconditioning behavior.

So far, it was proved that the subroutine written in Appendix K is able to simulate all the behaviors. The next job to do is to implement this subroutine to the original soft tissue model and to estimate the real values of the parameters in it.

APPENDIX M

USER SUBROUTINE FOR ENHANCED QLV MODELING BY ASSUMING SOFT TISSUE AS AN ISOTROPIC MATERIAL

```
      subroutine hypela(d,g,e,de,s,temp,dtemp,ngens,n,nn,kc,mats,
     * ndi,nshear)
c* * * * * *
c
c     user subroutine to define young's modulus and poisson's ratio
c     as function of stress in non-linear elastic small strain
c     material.
c
c     d        stress strain law to be formed by user
c     g        change in stress due to temperature effects
c     e        total strain
c     de       increment of strain
c     s        stress - should be updated by user
c     temp     state variables
c     dtemp    increment of state variables
c     ngens    size of stress - strain law
c     n        element number
c     nn       integration point number
c     kc       layer number
c     mats     material i.d.
c     ndi      number of direct components
c     nshear   number of shear components
c
c* * * * * *
      implicit real*8 (a-h,o-z)
          include '../marc_working_directory/concom'
          include '../marc_working_directory/creeps'
c         ******
c
c         By including the common blocks concom and creeps, we include these
c         variables into the subroutine:
c
c         cptim: time at beginning of increment
c         timinc: time increment
c         ncycle: number of increment
```

```
c
c       ******
      dimension e(3),de(3),temp(1),dtemp(1),g(1),d(ngens,ngens),s(3)
      dimension n(2),et(3),ets(3)
c       ******
c
c       Since, this is a three dimensional model, we need three dimensional strain,
c       strain increment and stress values. This is done by setting these variables
c       three dimensional with dimension command.
c
c       ******
        if (ncycle.eq.0) t=cptim+20.0d0
        if (ncycle.eq.0) et(1)=e(1)
        if (ncycle.eq.0) et(2)=e(2)
        if (ncycle.eq.0) et(3)=e(3)
        if (ncycle.gt.0) t=cptim+20.0d0+timinc
        if (ncycle.gt.0) et(1)=e(1)+de(1)
        if (ncycle.gt.0) et(2)=e(2)+de(2)
        if (ncycle.gt.0) et(3)=e(3)+de(3)
c       ******
c
c       To eliminate the errors (like dividing by zero or logarithm of zero) in the
c       calculation of some constants like q28 and q29, a new constant is created as
c       t0=18.4 and time of simulation is set to start from 20.
c
c       ******
        ets(1)=et(1)**2.0d0
        ets(2)=et(2)**2.0d0
        ets(3)=et(3)**2.0d0
c
        a=7.6d-37
        b=4.2d1
        c=8.0d-2
        T1=8.0d0
        T2=1.4d3
        t0=1.84d1
        epsdat=2.5d-2
        a1=7.0d-1
        b1=8.0d-1
        c1=9.0d-1
c       ******
c
c       Constants in the subroutine are as they are explained in chapter C
c
c       The user subroutine is written in double precision to be able to obtain more
c       accurate results.
c
```

```
c       ******
        qlam=(a1*a1+b1*b1+c1*c1)/8.0d0
        q1=a/(1.0d0+c*log(T2/T1))
        q2=b*epsdat
        q3=q2*t0
        q4=exp(q3)
        q5=q4-1.0d0
        q6=q4+1.0d0
        q7=q2+(1.0d0/T1)
        q8=q7+t0
        q9=exp(q8)
        q10=q2+(1.0d0/T2)
        q11=q10*t0
        q12=exp(q11)
        q13=t0+T1
        q14=q2*T1+1.0d0
        q15=q14*t0
        q16=q15+T1
        q17=q2*T2+1.0d0
        q18=q17*t0
        q19=q18+T2
        q20=0.57722d0-log(T2)+(t0/T2)
        q21=log(T2)-0.57722d0
c
        q22=(T1/(t0-t))*((q13-t)/(t0-t))
        q23=(T1/(q15-q14*t))*((q16-q14*t)/(q15-q14*t))
        q24=(T1/t)*(1.0d0-(T1/t))
        q25=(T1/q14*t)*(1.0d0-(T1/q14*t))
        q26=(T2/(q18-q17*t))*((q19-q17*t)/(q18-q17*t))
        q27=(T2/q17*t)*(1.0d0-(T2/q17*t))
        q28=q20+log(t-t0)-(t/T2)
        q29=q21+(t/T2)-log(t)
        q30=q9*(q22-q23)+q24-q25
        q31=q12*q26+q27
        q32=q4*q28+q29
c
        sig=q1*(q5+c*((exp(-t/T1)*q30)+(exp(-t/T2)*q31)-q32))
        p=sig/(8.0d0*qlam)
c
        do 100 i=1,ngens
          do 110 j=1,ngens
            d(i,j)=0.0d0
110       continue
100     continue
c       ******
c
c       Since there are no shear stresses in our experiment, the values of
```

```
c        d(1,2)=d(2,1), d(1,3)=d(3,1) and d(2,3)=d(3,2) of the tangent stiffness are set
c        to zero.
c
c       ******
        d(1,1)=p*a1**2.0d0
        d(2,2)=p*b1**2.0d0
        d(3,3)=p*c1**2.0d0
c
        do 120 k=1,3
          s(k)=d(k,k)*ets(k)
120     continue
c       ******
c
c       This enhanced quasi-linear viscoelastic formulation is expected to simulate
c       the hysteresis, preconditioning, stress relaxation and creep behaviors of soft
c       biological tissues. So, the constitutive equations of stresses were written in
c       terms of the two independent variables strain and time. Other constants are
c       calculated by using the material parameters.
c
c       ******
    return
    end
```

This user subroutine allows the user to implement arbitrary material models in conjunction with the hypoelastic model definition option in MSC.Marc. MSC.Marc supplies hypela total mechanical strain (mechanical strain = total strain - thermal strain), the increment of mechanical strain, and other information. Stress, total mechanical strain and state variable arrays at the beginning of the increment (t = n) are passed to hypela with the incremental strain. The user is expected to calculate stresses S, tangent stiffness D, and state variables (if present) that correspond to the current strain at the end of the increment (t = n + 1).

APPENDIX N

VERIFICATION OF THE SUBROUTINE IN APPENDIX M WITH A SIMPLE 3D MODEL

For the verification of the subroutine written in Appendix M, the three dimensional model seen in the Figure N1 was created. This specimen was 100 mm long with square cross section of 5 x 5 mm and had the material properties of hypoelastic materials in Mentat. The model had eight nodes, four of which are seen on the right hand side having fixed displacement boundary conditions along three material axes. Other four nodes are seen on the left hand side and three of them are linked (nodal tie) to the other one on which a position or load controlled boundary condition was applied. These nodes were exposed to different position or load controlled conditions (as explained in the following sections in detail) to prove that the subroutine is able to simulate hysteresis, preconditioning, relaxation and creep since, this subroutine is expected to simulate all these behaviors.

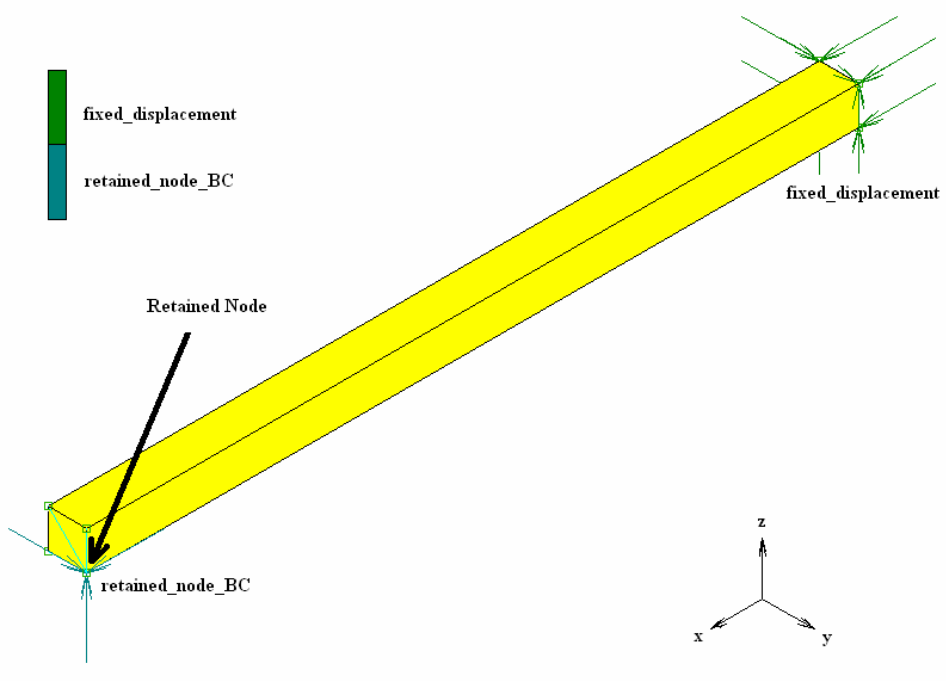

Figure N1 – Simple Three Dimensional Model

N.1. Verification of Relaxation Simulation

For the verification of the subroutine in relaxation simulation, the retained node of the specimen was applied to a displacement controlled boundary condition. It was firstly applied to tension and the specimen was lengthened 5 mm in five seconds which was applied in 50 time steps (increments) along x-direction. Then, the specimen was kept at that deformation for 120 seconds in 30 time steps to observe stress relaxation behavior (Figure N2). This model was submitted with the large displacement and large strain - total Lagrange analysis options by using the subroutine given in the Appendix M.

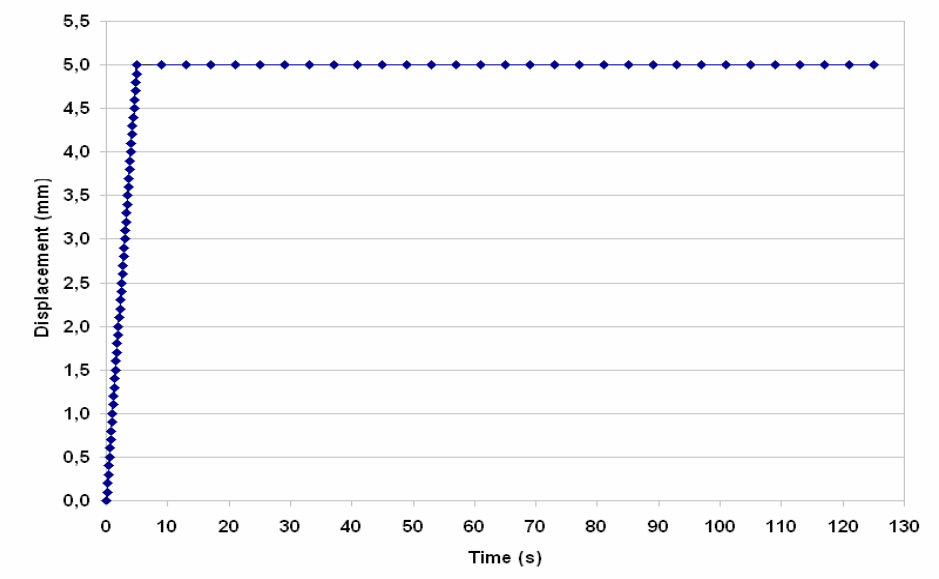

Figure N2 – Change of Displacement of the Retained Node with Time

Figures N3 and N4 show the decrease of reaction force and stress with time, respectively. These decreases occurred while the displacement was kept constant. So, this simple simulation proves that the subroutine written in Appendix M is working properly while simulating relaxation behavior.

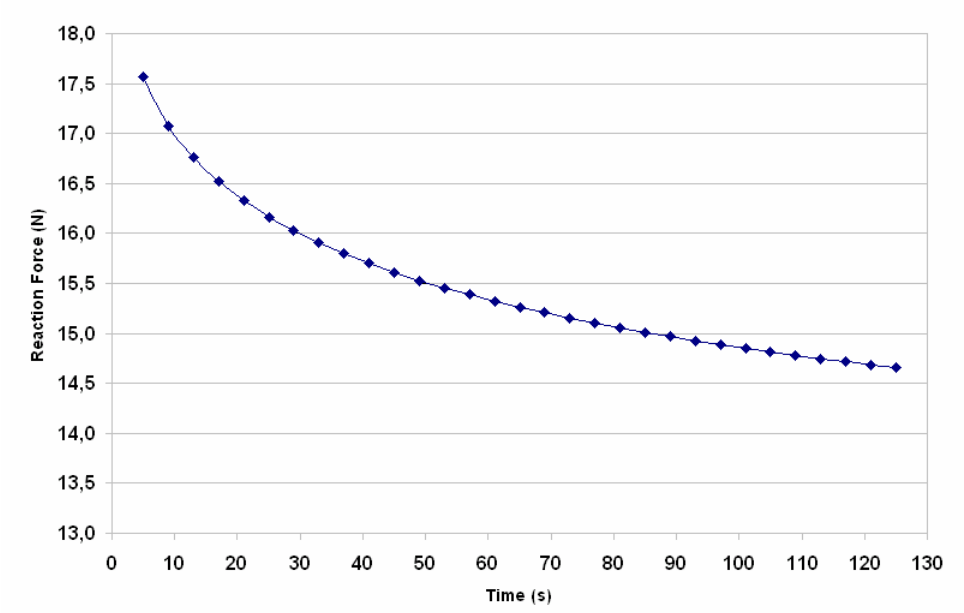

Figure N3 – Decrease of Reaction Force with Time

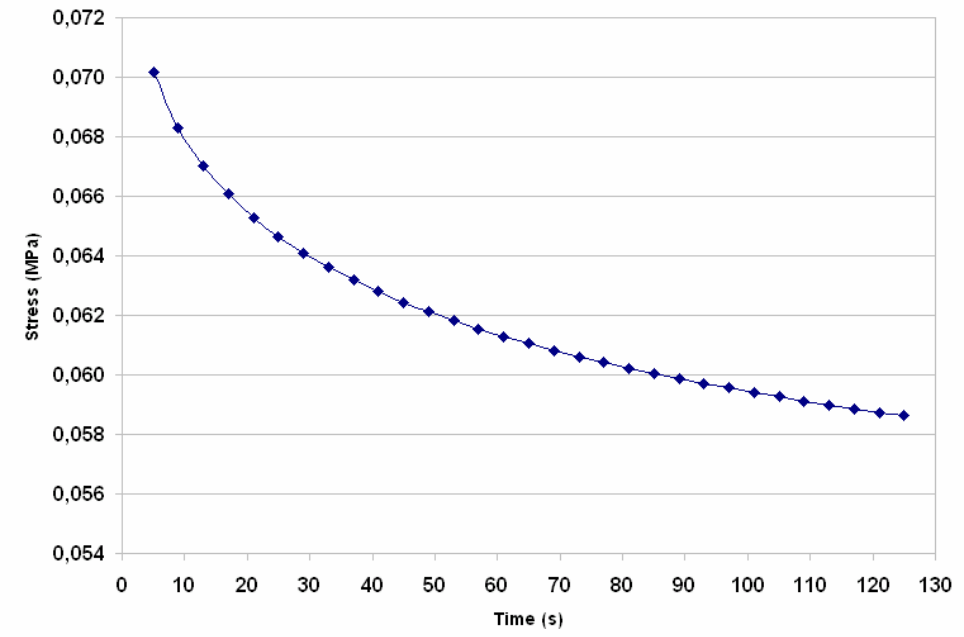

Figure N4 – Decrease of Stress (Relaxation) with Time

N.2. Verification of Creep Simulation

For the verification of the subroutine in creep simulation, the retained node of the specimen was applied to displacement and load controlled boundary conditions. It was firstly applied to tension and the specimen was lengthened 5 mm in five seconds which was applied in 50 time steps (increments) in x-direction. Then, the reaction force (in x-direction) occurred at fifth second was kept being applied constantly for 120 more seconds in 30 increments and change of displacement with time was observed. This model was submitted with the large displacement and large strain - total Lagrange analysis options by using the subroutine given in the Appendix M.

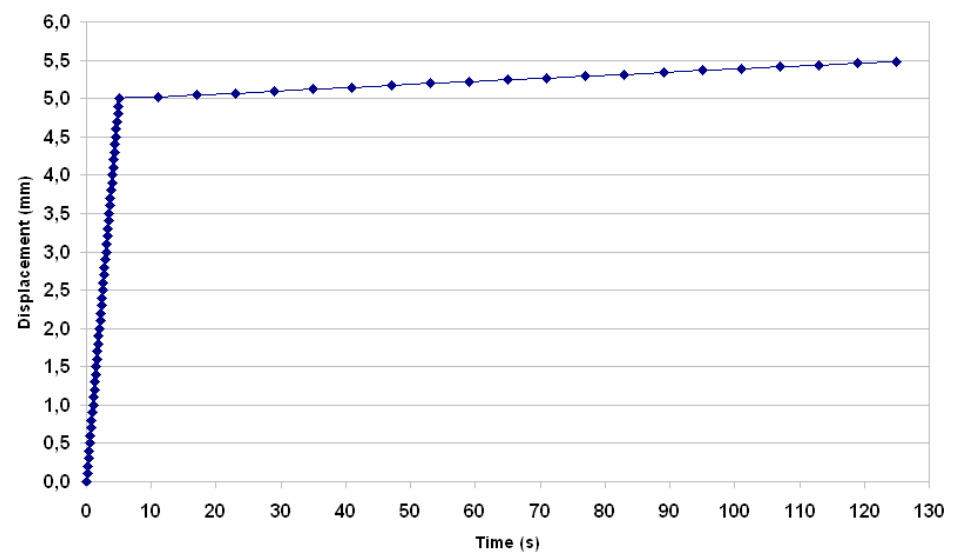

Figure N5 – Increase of Displacement (Creep) with Time

Figure N5 shows the increase of displacement with time. This increase occurred while the reaction force was kept constant. So, this simple simulation proves that the subroutine written in Appendix M is working properly while simulating creep behavior.

N.3. Verification of Hysteresis Simulation

For the verification of the subroutine in hysteresis simulation, the retained node of the specimen was applied to a displacement controlled boundary condition. It was firstly applied to tension and the specimen was lengthened 5 mm in five seconds which was applied in 25 time steps (increments) along x-direction. Then, the specimen was returned to its original shape with the application of compression with the same rate as tension. The difference between reaction force versus time curves and strain versus stress curves (hysteresis) in loading (tension) and unloading (compression) were observed. This model was submitted with the large displacement and large strain - total Lagrange analysis options by using the subroutine given in the Appendix M.

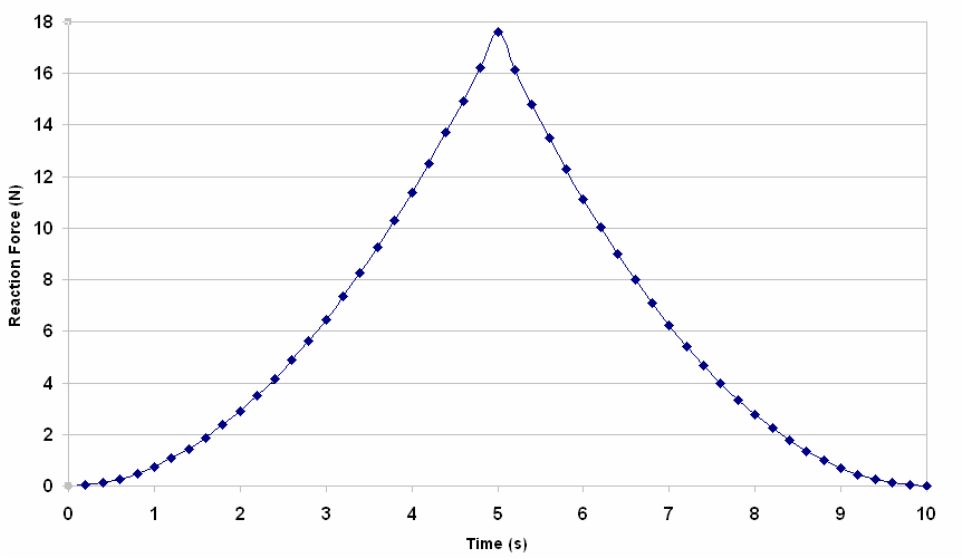

Figure N6 – Difference between Reaction Force vs. Time Curves

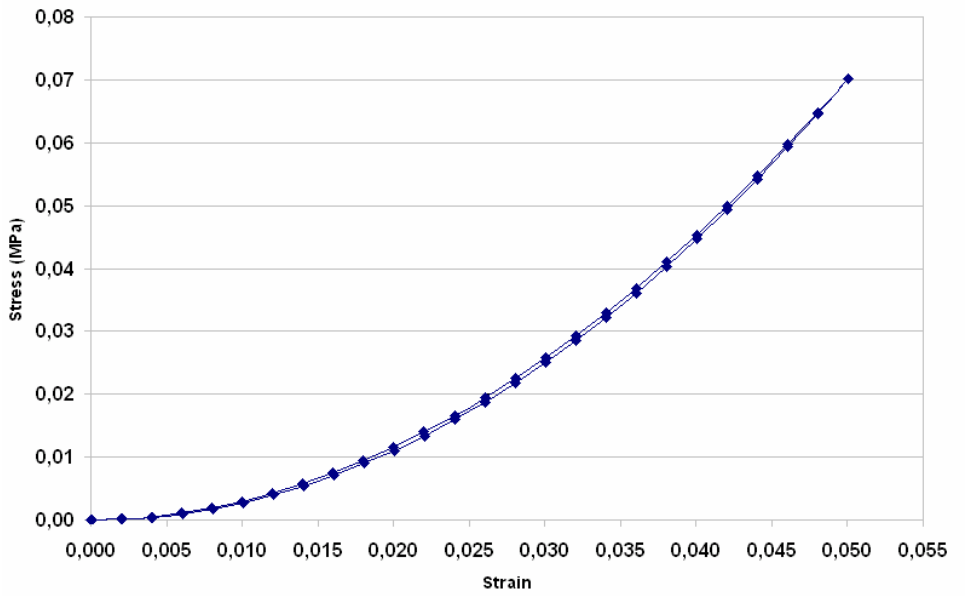

Figure N7 – Difference between Strain vs. Stress Curves (Hysteresis)

Figures N6 and N7 show the difference between reaction force versus time curves and strain versus stress curves (hysteresis) in loading and unloading, respectively. Loading and unloading curves are not the same in Figure N6, but the difference can be seen much clearly in Figure N7. This difference between two curves is called hysteresis and appears as energy loss during cyclic loading. So, this simple simulation proves that the subroutine written in Appendix M is working properly while simulating hysteresis behavior.

N.4. Verification of Preconditioning (Mullin's Effect) Simulation

For the verification of the subroutine in preconditioning simulation, the retained node of the specimen was applied to a displacement controlled boundary condition. It was firstly applied to tension and the specimen was lengthened 5 mm in five seconds which was applied in 50 time steps (increments) along x-direction. Then, the specimen was returned to its original shape with the application of compression with

the same rate as tension. This cycle is repeated ten times and the difference between reaction force versus time curves and strain versus stress curves in loading (tension) and unloading (compression) in these cycles were observed. This model was submitted with the large displacement and Large Strain - Total Lagrange analysis options by using the subroutine given in the Appendix M.

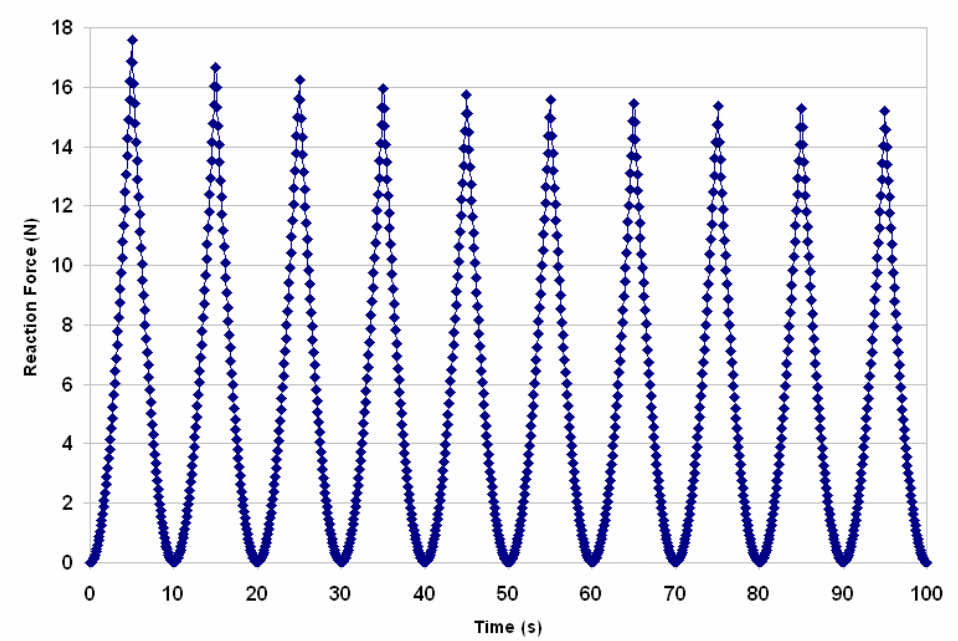

Figure N8 – Difference between Reaction Force vs. Time Curves (Preconditioning)

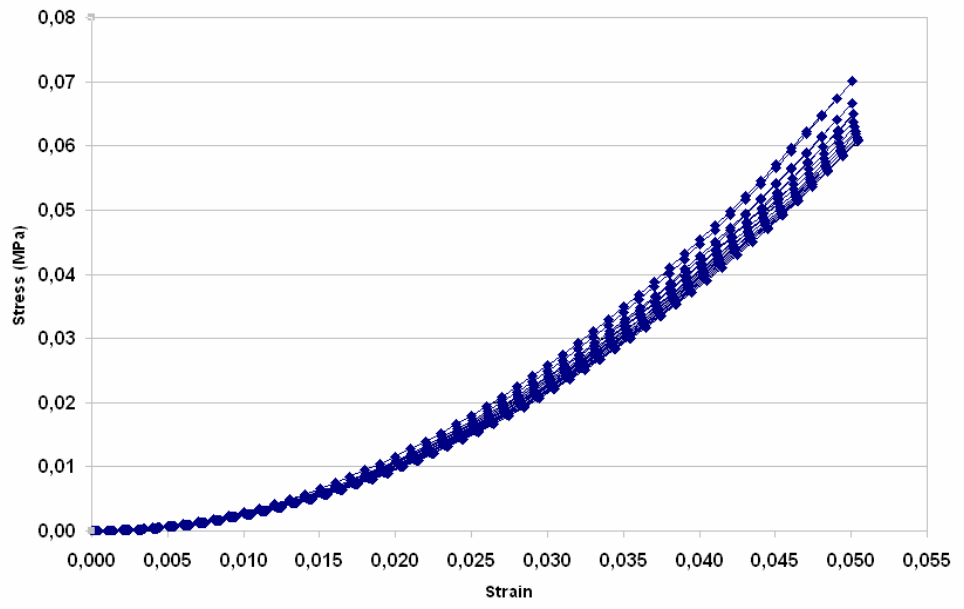

Figure N9 – Difference between Strain vs. Stress Curves (Preconditioning)

Figures N8 and N9 show the difference between reaction force versus time curves and strain versus stress curves in loading and unloading. These curves are becoming repeatable after about seventh or eighth cycle which is called as preconditioning. So, this simple simulation proves that the subroutine written in Appendix M is working properly while simulating preconditioning behavior.

So far, it was proved that the subroutine written in Appendix M is able to simulate all the behaviors. The next job to do is to implement this subroutine to the original soft tissue model and to estimate the real values of the parameters in it.

APPENDIX O

CHAPTER IN A BOOK "ORTOPEDİ BİYOMEKANİĞİ"

editors: İ. D. Akçalı, M. Gülşen, K. Ün, to be published in 2009

O.1. Yumuşak Doku Mekanik Modelleri

O.1.1. Giriş

İskelet sisteminin üzeri bir yumuşak doku tabakasıyla kaplı olduğu için insan bedeninin dış dünya ile olan mekanik etkileşimi hemen her zaman yumuşak dokular aracılığıyla olmaktadır. Öte yandan insan bedenini oluşturan dokulardan, kemik dışında kalan hemen tüm dokular yumuşak doku olarak adlandırılmaktadır. Yumuşak dokuların çeşitli kuvvetler altında nasıl bir mekanik davranış göstereceğinin önceden kestirilebilmesi veya mekanik davranışın bilgisayarda andırımının (simülasyonunun) yapılabilmesi için yumuşak doku mekanik davranışının ayrıntılı olarak bilinmesi ve bu davranışı temsil edecek bünye denklemleri ile bu denklemlere ait katsayıların belirlenmesi gerekir. Protez kovanı ile amputasyon güdüğü arasındaki mekanik etkileşimi bilgisayarda modelleyebilmek amacıyla güdük üzerindeki yumuşak dokuların modellenmesi [1-9], yemek borusunun modellenmesi [10], eklem kıkırdağının modellenmesi [11], bağlar ve kirişlerin modellenmesi [12], yumuşak doku mekanik davranışının bilinmesinin gerekliliğini gösteren bazı örneklerdir. Bu bölümün amacı, okurlarda yumuşak doku mekanik davranışının modellenmesi ve bu davranışın belirlenmesi ile ilgili yaygın olarak kullanılan yöntemler hakkında bir farkındalık yaratmak ve araştırmacılara ilgili kaynaklara yönetmektir.

Mekanik açıdan, mühendislik malzemeleri ile karşılaştırıldığında, yumuşak dokuların davranışları daha karmaşıktır. Bu karmaşıklığın nedenleri arasında dokunun iki fazlı (katı ve sıvı) [13] veya kimi yazarlara göre daha fazla fazlı (katı ve iyonik çözeltiler

gibi) [14] olmasının yanı sıra kollajen, elastin gibi farklı ve karmaşık yapıtaşlarından oluşmuş olmasının [15, 16] da etkisi vardır. Yaşayan ve koşullara göre kendini uyarlayan biyolojik dokuların mekanik özelliklerinin de gerek çevreyle mekanik etkileşim sonucu, gerekse diğer etmenler nedeniyle zaman içinde değişmesi kaçınılmazdır. Öte yandan, biyolojik malzemelerin mekanik özelliklerinin çeşitli sınıflamalar kullanılarak çizelgeler halinde sunulmaya çalışılması da mühendislik malzemeleri kadar kesin ve güvenilir sonuçlar vermemiştir. Özellikle yumuşak dokularda, kullanılacak bünye denklemi konusunda araştırmacılar arasında genel kabul gören bir yaklaşım henüz yoktur. Araştırmacıların önemli bir bölümü, dokuların mekanik özelliklerinin kişiden kişiye önemli değişiklikler gösterdiğini ve gerçeğe yakın modelleme yapılabilmesi için geometrik (anatomik) özelliklerle birlikte kişiye özgü olarak belirlenmesi gerektiğini öne sürmüştür [7-9]. Yine yumuşak doku mekanik özellikleri üzerinde deneğin yaşının [17-20] ve sağlık durumunun [21-24] önemli etkisi olduğu şeklinde görüşler de vardır.

Biyolojik dokuların yumuşak ve sert doku olarak ayrılması, mekanik davranışlar açısından da olanaklıdır. Kemik gibi sert dokular katı cisimler mekaniği kuramında "küçük gerinme" kuramına büyük ölçüde uydukları için gerek bünye denklemlerinin ve bu denklemlere ait katsayıların elde edilmesi, gerekse bilgisayar andırımları yumuşak dokulara göre daha kolaydır. Ancak unutulmamalıdır ki görece kolay bu yaklaşımda sert dokular çoğunlukla tek bir malzemeden oluşmuş sürekli bir ortam olarak modellenmektedir ve bu yaklaşımla ilgili kısıtlamaların dikkate alınması önemlidir. Öte taraftan, yumuşak doku olarak adlandırılan, kemik dışında kalan dokularda gerinmeler nadiren "küçük gerinme" kuramı ile modellenebilecek büyüklükte olur. Çoğu durumda, daha genel, karmaşık ve doğrusal olmayan "büyük gerinme" kuramının kullanılması gerekli olur. Ayrıca, doğrusal elastik malzeme modelleri (Hooke bünye denklemleri) de yumuşak dokuların mekanik davranışını modellemede çoğu zaman yetersiz kalır. Yine yumuşak dokularda, genellikle mühendislik malzemelerinde yok sayılabilecek düzeyde görülen alışma etkisi (*preconditioning, Mullin's effect*, malzemenin ilk birkaç yüklemede daha direngen davranması, sonraki yüklemelerde direngenliğinin azalarak tekrar edilebilir bir gerilme-gerinim özelliğine kavuşması, Şekil O1), yükün artma ve azalma yönlerinde

görülen iki farklı direngenlik (ve bir yükleme-yük azaltma çeviriminde yok sayılamayacak düzeyde mekanik enerji kaybı, Şekil O2), sabit yer değiştirme (veya gerinme) altında tepki kuvvetinin (gerilmenin) azalması yani gevşeme (Şekil O3), sabit kuvvet (veya gerilme) altında yer değiştirmenin (veya gerinmenin) artması yani sünme (Şekil O4) etkilerinin görüldüğü birçok çalışmada belirtilmiştir [15].

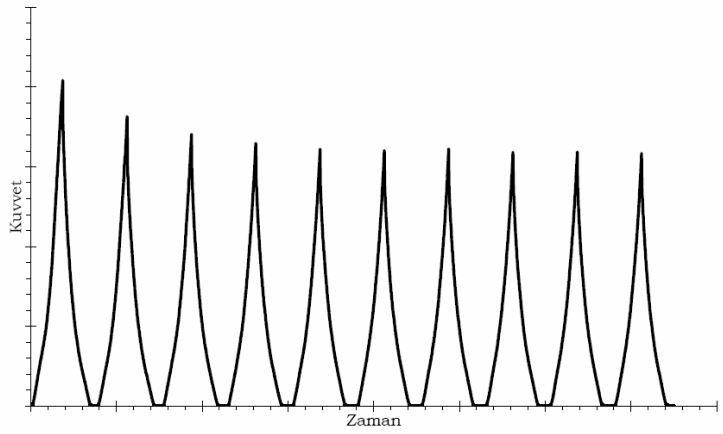

Şekil O1 - Yumuşak Dokunun Peşpeşe Yapılan Yüklemelerde Gösterdiği Alışma Etkisi

Şekil O2 - Yumuşak Dokunun Gerinmenin Artması ve Azalması Yönündeki Davranışı

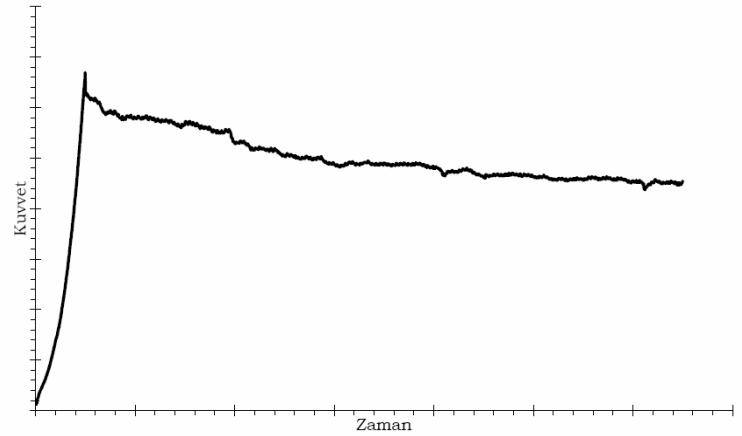

Şekil O3 - Yumuşak Dokunun Sabit Gerinmede Gevşeme Davranışı

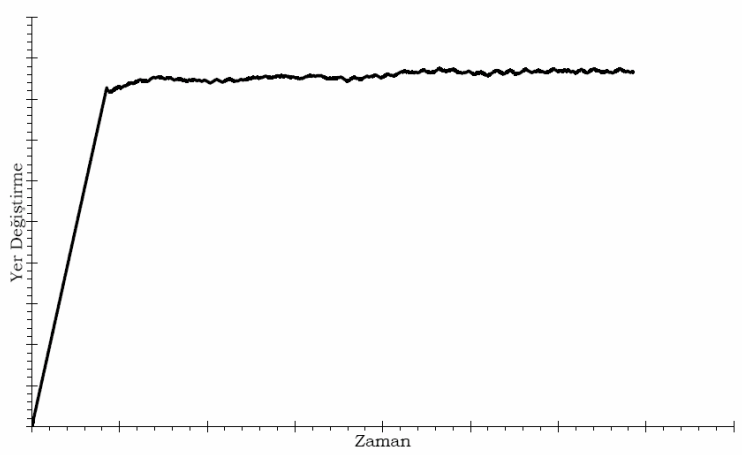

Şekil O4 - Yumuşak Dokunun Sabit Gerilmede Sünme Davranışı

O.1.2. Yumuşak Doku Deneyleri

Tüm malzemelerde olduğu gibi yumuşak dokuların mekanik davranışının belirlenmesi ve bünye denklemlerinin oluşturulması için kullanılan yöntem deneyseldir. Yumuşak doku mekanik davranışını belirlemek için değişik deney yöntemleri vardır. Her bir yöntemin kendisine özgü üstünlükleri ve zayıflıkları bulunmaktadır. Bu üstünlük ve zayıflıklardan çalışma için önemli olanları

değerlendirilerek en uygun deney yöntemine karar verilmelidir. Bu deneylerden elde edilen mekanik yanıtlar arasında farklar olduğu karşılaştırmalı çalışmalar yapan çeşitli yazarlar tarafından rapor edilmiştir [25-27].

O.1.2.1. Eks-Vivo (Laboratuvar) Deneyleri

Deney yapılacak doku yerinden çıkartılır ve laboratuvar ortamında,yaşam koşullarının benzetildiği bir ortamda, doku cansız bir durumda iken deney yapılır [27]. Deneyler laboratuvar ortamında yapıldığı için hem deney örneğinin geometrisi gerçeğe yakın olarak belirlenebilir, hem de deneyden daha iyi veriler elde edilebilir. Ancak doku kendi fizyolojik ortamından çıkartıldığı ve canlılığını yitirdiği için hem mekanik özelliklerinde bazı değişiklikler olabildiği gibi, doku fizyolojik mekanik gerilmeden arındırılmış olduğu için elde edilen mekanik yanıt dokunun kendi fizyolojik ortamındakinden farklı olabilir [28]. Buna karşın dokunun yaşam koşullarının benzetilmesi deney verilerinin ölü koşullarla karşılaştırıldığında daha iyi olmasını sağlamaktadır.

O.1.2.2. İn-Vitro (Laboratuvar) Deneyleri

İn-vitro deneyler de eks-vivo deneylerde olduğu gibi doku bulunduğu ortamdan çıkarılarak cansız bir durumda iken yapılır. Ancak dokunun yaşam koşulları benzetilmeye çalışılmaz. İn-vitro deneylerde özellikle yumuşak dokuların canlılığını yitirmesinden dolayı mekanik malzeme özelliklerinin önemli ölçüde değiştiği kanısı yaygındır [27].

O.1.2.3. İn-Situ (Cansız Denek Üzerinde) Deneyler

İn-situ deneylerde yumuşak doku yerinde incelenir. Ancak organ canlı değildir. İn-situ deneyler taze dondurulmuş veya fikse edilmiş kadavralarda da yapılabilir [26].

Her durumda, incelenen doku canlılığını yitirmiş olacağı için mekanik özelliklerinin değiştiği düşünülmektedir. Öte taraftan, çoğunlukla deney örneğinin düzgün bir geometriye sahip olması sağlanamaz ve sınır koşulları tam olarak belirlenemez.

O.1.2.4. İn-Vivo (Canlı Denek Üzerinde) Deneyler

İn-vivo deneyler, doku denek üzerinde kendi fizyolojik koşullarındayken ve denek canlıyken yapılır. Girişimsel ve girişimsel olmayan iki yöntem vardır. İn-vivo deneylerin üstün yönü, üzerinde deney yapılacak doku ile çevre dokuların mekanik etkileşimlerinin deney sırasında da var olması ve dokunun canlı olması yoluyla, dokunun gerçek davranışına en yakın yanıtı vermesidir. Ancak, deneğin canlı olması nedeniyle etik kurallara uygun, deneğe zarar vermeyecek biçimde yapılmasına özen gösterilmelidir. Öte yandan, deney örneğinde düzgün bir geometri sağlamak olanaklı olmadığı gibi, deney bölgesindeki sınır koşullarını da gerçeğe yakın olarak belirleyebilmek her zaman olası değildir.

O.1.2.4.1. Girişimsel İn Vivo Deneyler

Girişimsel yöntemde dokuya kuvvet uygulanarak bu kuvvet sonucu dokuda oluşan yer değiştirme zaman bilgisiyle birlikte kaydedilir [29].

O.1.2.4.2. Girişimsel Olmayan İn Vivo Deneyler

Girişimsel olmayan yöntemde dışarıdan dokuya bir yer değiştirme uygulanır ve doku içinde oluşan yer değiştirmeler tıbbi görüntüleme yöntemleriyle (manyetik rezonansla görüntüleme [22], ultrasonografi v.b.) ölçülür ve buradan da doku üzerinde oluşan gerinmeler hesaplanır [30].

O.1.2.5. Yumuşak Doku Mekanik Malzeme Deney Sistemleri

Yumuşak doku deneyleri standart malzeme deney sistemleri üzerinde yapılabileceği gibi, yumuşak doku deneyleri yapmak için özel olarak tasarlanmış sistemler de vardır. Bu bölümde her iki tip sistemden de kısaca söz edilecektir.

O.1.2.5.1. Tek Eksenli Çekme Deneyleri

Tek eksenli çekme deneyleri için uygun kapasitedeki bir çekme cihazı ile dokunun cihaza bağlanmasına uygun çeneler veya dokunun dikilebileceği uygun bir aparat yeterlidir. Genellikle kesit alanı dikdörtgen olan, düzgün geometrideki deney örnekleri hazırlanır. Zaman zaman cihazın çene yer değiştirmesi dokudaki uzama olarak kabul edilir, zaman zaman da doku üzerinde alınan iki referans noktasının yer değiştirmesi ölçülerek dokudaki uzama ve gerinme buradan hesaplanır. Tek eksenli çekme deneyleri yumuşak doku mekanik özelliklerinin belirlenmesinde kullanılsa da [31,32], Fung [15] tarafından yumuşak doku mekanik özelliklerini belirlemek için yeterli olmadığı belirtilmiştir.

O.1.2.5.2. Çift Eksenli Çekme Deneyleri

Çift eksenli çekme deneylerinde genellikle bu iş için özel olarak tasarlanmış bir deney sistemi aracılığıyla deney örneği birbirine dik iki eksende birden çekilir [33]. Her iki eksende de dokuya uygulanan kuvvet ve hareket eden çenelerin yer değiştirmesi ölçülür. Dokuda oluşan gerinmelerin hesaplanması için genellikle doku üzerine yüksüzken çizilen referans noktalarının hareketi izlenir. Buradan yer değiştirmeler ve gerinmeler hesaplanır. Çift eksenli deneylerde sınır koşullarını kontrol etmek tek eksenli deneylerden daha zordur.

O.1.2.5.3. Emme Kabı Deneyleri

Çekme deneyleri için deney örneğinin organizmadan izole edilmesinin zorunluluğu nedeniyle deneylerin yerinde yapılabilmesi amacıyla geliştirilmiş bir yöntemdir. Temel olarak üzerinde deney yapılacak doku üzerine geometrisi bilinen bir kap yerleştirilip kabın içindeki hava boşaltılır ve dokuda oluşan şekil değiştirme ölçülür. Alexander [34] ve diğer araştırmacılar tarafından kullanılan yöntem dokunun mekanik özellikleri hakkında fikir verse de önemli kısıtlamaları vardır

.

O.1.2.5.4. Germe Deneyleri

Germe deneyleri de çekme deneyleri gibi yapılır. Ancak germe deneylerindeki fark, dokunun çekme cihazının çenelerine bağlanması yerine doku boyutlarından daha büyük plakalara yapıştırılmasıdır. Germe deneylerinde kuvvet doku kalınlığının normaline dik yönde uygulanır. İn vitro yapılabildiği gibi [35] in vivo da [36] yapılabilmektedir. Tek eksenli olduğu için dokunun mekanik özellikleri hakkında kapsamlı bilgi vermediği düşünülmektedir [15].

O.1.2.5.5. Basma Deneyleri

Basma deneyleri de germe deneylerine benzer biçimde ancak çenelere ait yüzeylerin dokuyu sıkıştırmasıyla yapılır. Basma deneylerinde doku serbest bırakılabilir ve basmanın etkisiyle yanal yönlerde genleşir (*unconfined test*) veya yanal yüzlerin genleşmesi kısıtlanabilir (*confined test*) [37]. Bu durumda doku sıvısının deney bölgesini terk edebilmesi için çenelerden birisi geçirgen yapılır.

O.1.2.5.6. İndentör Deneyleri

Yumuşak doku deneylerinde yaygın olarak kullanılan yöntemlerden birisidir. Tercih edilen geometrideki indentör ucu ile yumuşak doku bastırılırken ucun yer

değiştirmesi ve dokunun uca uyguladığı tepki kuvveti zamanla birlikte kaydedilir. Böylece in vivo yumuşak doku deneyleri de yapılabilir. Değişik indentör ucu geometrileri ile yumuşak dokunun serbest yüzeyi üzerinde bulunan anizotropinin de belirlenebileceği kuramsal olarak gösterilmiştir [38]. Ancak, bu deneylerle yumuşak dokuda bulunan tüm anizotropinin belirlenebilmesi olası değildir.

O.1.2.6. Yumuşak Doku Mekanik Malzeme Modelleri

O.1.2.6.1. Bünye Denklemleri

Bünye denklemleri, ilgilenilen malzemenin gerilme-gerinme (veya çoğu zaman gerilme-gerinme-zaman) ilişkisini genel bir üç boyutlu gerilme altında veren denklemdir. Herhangi bir yapısal analiz yapılmadan önce, yapıyı oluşturan tüm malzemelerin bünye denklemlerinin bilinmesi zorunludur. Çevremizdeki çok farklı malzemeler için çok farklı bünye denklemleri bulunmaktadır. Uzun yıllardan beri kullanılagelen mühendislik malzemeleri için mekanik davranışlarını oldukça geniş koşullarda büyük bir hassasiyetle modelleyebilecek bünye denklemleri oluşturulmuş olmakla birlikte biyolojik malzemeler için genel kabul görmüş bünye denklemleri daha azdır. Bunun iki nedeninden birisi biyolojik dokularda deney yapmanın güçlüğü, diğeri ise yumuşak dokuların gösterdiği karmaşık mekanik yanıtın bir denklem ile ifade edilmesidir [39].

Çevremizdeki çok değişik malzemelerin önemli bir bölümünü üç ideal malzeme modeli (veya bunların bir bileşimi) ile belirli bir hassasiyette modelleyebiliriz. Bu üç ideal malzeme modeli ağdalı olmayan akışkan, doğrusal (Newton) ağdalı akışkan ve doğrusal elastik (Hooke) katı modelleridir. Ancak biyolojik dokuların önemli bir bölümü, fizyolojik koşullar altında, bu ideal modeller veya bunların bir bileşimi kullanılarak istenen hassasiyette modellenemez [15].

Bünye denklemleri malzemenin fiziksel yapısıyla ilgili olduğu için belirli bir koordinat takımına bağlı değildir ve deneylerle belirlenir. Esnemez katı cisim

biyomekaniği dışında, biyomekaniğin her alanında bünye denklemlerinin belirlenmesine gereksinim duyulur. Bünye denklemlerinin bilinmediği durumlarda biyomekanik niceliksel olamaz ancak niteliksel olabilir. Biyolojik yapılar için bünye denklemlerinin belirlenebilmesi için öncelikle yeterli miktarda verinin sistematik olarak toplanması gereklidir. Aksi durumda yapılan mekanik analizler ve biyomekanik kestirimler dokunun gerçek davranışını istenen hassasiyette modelleyemeyecektir [28].

O.1.2.6.2. Yalancı Elastik Malzeme Modelleri

Yumuşak doku davranışı, çok küçük gerinmeler dışında doğrusal olmaktan uzaktır. Deney sırasında gerinmenin artışı sırasında izlenen kuvvet-yer değiştirme (veya gerilme-gerinme) eğrisi ile gerinmenin azalması yönünde izlenen kuvvet-yer değiştirme (veya gerilme-gerinme) eğrisi birbirinden belirli biçimde farklıdır (Şekil O2). Eğrinin şeklinin belirli frekans bantlarında belirgin biçimde değişmediği gösterilmiştir [28]. Bu nedenle basit bir yaklaşımla, gerinmenin artması yönünde bir elastik malzeme katsayısı seti, azalması yönünde başka bir elastik malzeme katsayısı seti kullanılmaktadır. Dokunun gerçek davranışı elastik olarak modellenemeyeceği için bu modele yalancı-elastik (*pseudoelastic*) denmiştir. Ancak yalancı-elastik malzeme modelleri zamana bağımlı davranışı gözardı ettiği için kullanım alanı sınırlıdır [40]. Yumuşak dokunun artan gerinimle birlikte artan direngenliği (veya teğet elastik modülü) başlangıçta yumaklanmış olarak duran kollajen ve elastin moleküllerinin artan gerinim ile açılmaları ve gerilmeleri ile ilintili olduğu düşünülmektedir [40]. Yumuşak dokunun doğrusal olmayan davranışını modellemek için yaygın olarak kullanılan yöntemlerden birisi de gerinme enerjisi (yoğunluğu) fonksiyonudur. Gerinme enerjisi fonksiyonu kullanılarak büyük gerinmeler için Kirchoff gerilmeleri Green gerinmeleri cinsinden şu şekilde ifade edilebilir:

$$S_{ij} = \frac{\partial(\rho_0 W)}{\partial E_{ij}}$$

Burada ρ_0 malzemenin ilk durumda (şekil değiştirmemiş durumda) kütle yoğunluğudur. Burada kullanılan gerinme enerjisi fonksiyonu termodinamik olarak anlamlı bir fonksiyon değildir, çünkü yumuşak dokunun alışma etkisi dışında işlemin gerinmenin artma veya azalma yönünde olmasına bağlı olarak katsayıları değişmektedir. Bununla beraber, bir yalancı-gerinme enerjisi fonksiyonunun varlığı problemin matematik olarak tanımlanmasını büyük ölçüde kolaylaştırmaktadır. Burada sözü edilen fonksiyonların bazı dokular için 1.5 bazıları içinse 2'ye kadar çıkabilen uzama oranları (son, şekil değiştirmiş uzunluğun ilk uzunluğa oranı) için gerçek doku ile uyumlu sonuç vermeleri beklenmektedir [39]. Literatürde özellikle yumuşak doku modellemek için, veya başka amaçlarla geliştirilmiş ama yumuşak dokuyu da başarıyla modelleyebilecek, değişik gerinme enerjisi fonksiyonları vardır. Bu fonksiyonların hemen tümü görüngüsel (*phenomenological*) olup dokuda görülen gerinmenin artışı ile direngenlikte meydana gelen artmanın mekanik nedenlerini modellememektedir.

Vaishnav [41] tarafından kullanılan gerinme enerjisi fonksiyonu damarlar gibi silindirik yapılar içindir, silindirik koordinat sisteminde ifade edilmiştir ve bir polinom biçimindedir:

$$\rho_0 W = A E_{\theta\theta}{}^2 + B E_{\theta\theta} E_{zz} + C E_{zz}{}^2 + D E_{\theta\theta}{}^3 + E E_{\theta\theta}{}^2 E_{zz} + F E_{\theta\theta} E_{zz}{}^2 + G E_{zz}{}^3$$

Burada A, B, C, D, E, F ve G malzeme sabitleri olup deneysel verinin fonksiyon tarafından kestirilen davranışa uyumunu sağlayacak biçimde belirlenir.

Fung [42] tarafından önerilen fonksiyon ise üstel biçimdedir:

$$\rho_0 W = \frac{C}{2} \exp[a_1 E_{\theta\theta}{}^2 + a_2 E_{zz}{}^2 + 2 a_4 E_{\theta\theta} E_{zz}]$$

Burada C, a_1, a_2 ve a_4 malzeme sabitleridir. Cilt için Tong [39] tarafından önerilen fonksiyon ise;

$$\rho_0 W = f(\alpha, E) + C\exp[F(a, E)]$$

$$f(\alpha, E) = \alpha_1 E_{11}{}^2 + \alpha_2 E_{22}{}^2 + 2\alpha_4 E_{11} E_{22} + \alpha_3 (E_{12} + E_{21})^2$$

$$F(a, E) = a_1 E_{11}{}^2 + a_2 E_{22}{}^2 + 2a_4 E_{11} E_{22} + a_3 (E_{12} + E_{21})^2$$

biçimindedir. Burada $C, \alpha_1, \alpha_2, \alpha_3, \alpha_4, a_1, a_2, a_3$ ve a_4 malzeme sabitleri, X_1 ve X_2 cildi oluşturan düzlem üzerindeki birbirine dik iki koordinat eksenidir.

Tong [39] daha yüksek mertebeden terimler içermesi için denklemin aşağıdaki biçimini de denemiştir:

$$F(a, E) = a_1 E_{11}{}^2 + a_2 E_{22}{}^2 + 2a_4 E_{11} E_{22} + a_3 (E_{12} + E_{21})^2 + \gamma_1 E_{11}{}^3 + \gamma_2 E_{22}{}^3 + \gamma_4 E_{11}{}^2 E_{22} + \gamma_5 E_{11} E_{22}{}^2$$

burada γ_1, γ_2, γ_4, γ_5 ek malzeme sabitleridir.

Akciğer özekdokusu için Hoppin [43] tarafından önerilen fonksiyon ise aşağıda sunulmuştur:

$$\rho_0 W = \sum_{i=1}^{4} a_i (\lambda_1^{2i} + \lambda_2^{2i} + \lambda_3^{2i}) + \sum_{i=1}^{2} b_i (\lambda_1^{2i}\lambda_2^{2i} + \lambda_2^{2i}\lambda_3^{2i} + \lambda_1^{2i}\lambda_3^{2i}) + c_1 \lambda_1^2 \lambda_2^2 \lambda_3^2$$

$$+ \sum_{i=2}^{3} c_i (\lambda_1^{2i}\lambda_2^2 + \lambda_2^{2i}\lambda_3^2 + \lambda_3^{2i}\lambda_1^2 + \lambda_1^2\lambda_2^{2i} + \lambda_2^2\lambda_3^{2i} + \lambda_3^2\lambda_1^{2i})$$

Burada a_i, b_i ve c_i malzeme sabitleridir ve fonksiyon genel bir üç boyutlu gerilme durumu için geçerlidir. Ancak bu biçimin en büyük kısıtlaması malzemenin eşyönlü (izotropik) olduğu varsayımıdır. Bu varsayımı kaldırmak için önerilen biçim ise

$$\rho_0 W = C\exp[a_1 E_{11}^2 + a_2 E_{22}^2 + 2a_4 E_{11} E_{22}] + \text{permütasyon ile simetrik terimler}$$

Mezenter ve kaslar için önerilen gerinme enerjisi fonksiyonu ise [42, 44] şöyledir:

$$\frac{dT}{dE} = \alpha T + \beta$$

Burada T birim alandaki çekme kuvveti, E gerinme, α ve β ise malzeme sabitleridir. Bu denklem gerilmesiz duruma çok yakın durumlar için iyi sonuç vermese de diğer tüm gerilmelerde istenen hassasiyette kestirim yapabilmektedir.

Alt ekstremite yumuşak dokularının modellenebilmesi için Money [45] tarafından önerilen ve daha sonra değişik araştırmacılar tarafından terim sayısı arttırılarak daha çok kauçuk ve polimerik malzemelerin modellenmesinde yararlanılan malzeme modeli kullanılmıştır. Bu model

$$W = \sum_{i+j=1}^{N} C_{ij} (I_1 - 3)^i (I_2 - 3)^i$$

biçiminde ifade edilir. Burada I_1 ve I_2 Green-Lagrange büyük gerinme tensörünün ilk iki değişmezi (*invariant*), C_{ij} ise malzeme sabitleridir. N sayısının aldığı değere bağlı olarak malzeme modeli isimlendirilir. Bu biçimdeki bir model Tönük [7] tarafından kullanılmış olan James-Green-Simpson modelinin eksenel simetrik ve sıkıştırılamaz malzemelere uygulanmış tipidir.

$$W = C_I (I - 3) + C_J (I - 3)^2 + C_K (I - 3)^3$$

Burada I sıkıştırılamaz malzeme için eksenel simetrik Green-Lagrange gerinme tensörünün tek bağımsız değişmezidir.

O.1.2.6.3. Viskoelastik Malzeme Modelleri

Viskoelastik malzemeler katılarla ağdalı sıvıların özelliklerini bir arada gösteren malzemelerdir. Bu malzemeler, katı ve sıvı özelliklerinin baskınlığına göre katıya

daha yakın veya sıvıya daha yakın davranabilirler. Viskoelastik malzemelerin tipik özellikleri, histerezis (malzemenin gerinmesi ve ardından ilk durumuna döndürülmesi sonucu belirgin biçimde mekanik enerji kaybı, gerinme artarken direngenliği daha yüksek azalırken düşük olması, Şekil O2'deki gibi), gevşeme (sabit gerinmede gerilmenin azalması, Şekil O3), sünme (sabit gerilmede gerinmenin artması, Şekil O4) ve gerinme hızına bağlı davranıştır.

En temel iki tip viskoelastik malzeme modeli Maxwell ve Voigt modelleri olup tek boyutlu mekanik model olarak Şekil O5'deki gibi gösterilebilir. Burada yay, elastik davranışı; amortisör ise ağdalı davranışı temsil etmektedir. Maxwell modeli viskoelastik akışkanları modellemekte uygundur. Voigt modelinin tepkisi gerçek viskoelastik katılarla uyuşmadığı için en basit viskoelastik katı modeli için üç elemanlı (bazen Kelvin modeli olarak anılır) model (Şekil O6) önerilmiştir [46-52].

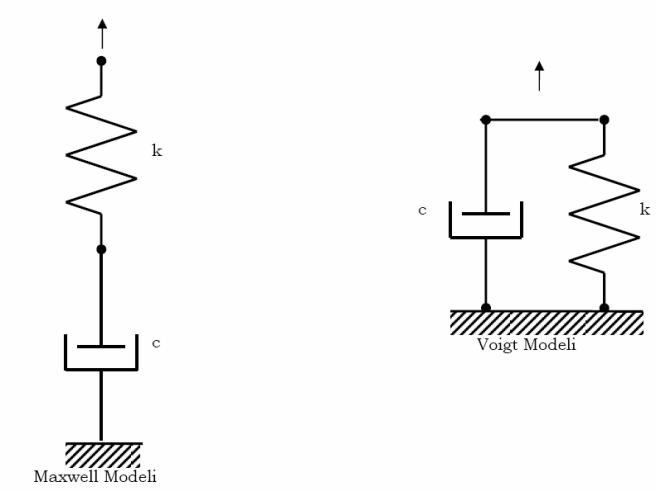

Şekil O5 - Temel Viskoelastik Malzeme Modellerinin Tek Boyutlu Mekanik Modelleri

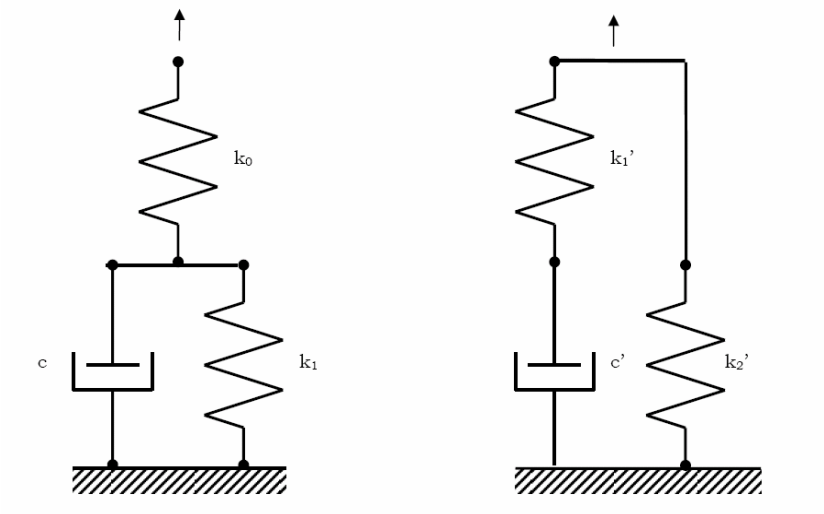

Şekil O6 - Üç elemanlı (Kelvin) Viskoelastik Malzeme Modelinin İki Farklı Gösterimi

Üç elemanlı modelde gerçek viskoelastik katılarda görülen anlık elastik yanıt görülebilmektedir. Bu modellerde gevşeme ve sünme davranışı tek bir üstel ifade ile temsil edilmektedir ve çoğu gerçek viskoelastik katının davranışı bu temsile uymamaktadır. Örneğin dizaltı amputasyon güdükleri üzerinde indentör ile yapılan deneylerden elde edilen yumuşak doku verisinde kısa ve uzun süreli iki sünme davranışı için üç elemanlı model yerine Şekil O7' de gösterilen beş elemanlı bir model kullanılmıştır [8].

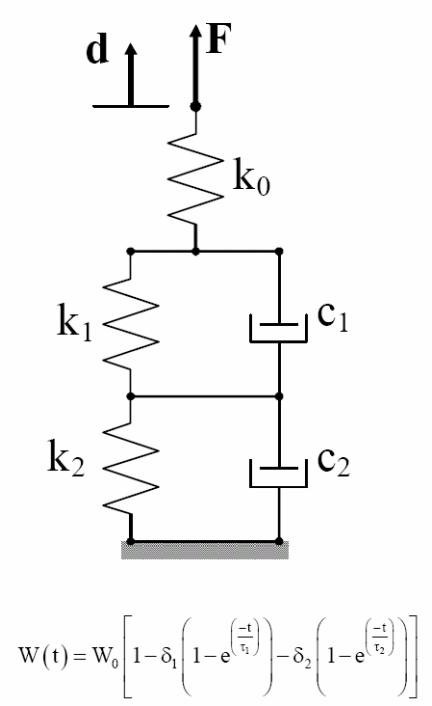

Şekil O7 - Beş Elemanlı Viskoelastik Katı Modeli ve Bünye Denklemi

Bu modelde doğrusal olmayan davranış için bir gerinme enerjisi fonksiyonu (W_0) kullanılmıştır. Modelde iki gevşeme oranı (δ_1 ve δ_2) ile iki gevşeme zaman sabiti (τ_1 ve τ_2) kullanılmıştır. Bu tür modeller gerçek davranışı modellemek üzere Prony serisi olarak genellenebilir:

$$W(t) = W_0\left[1-\sum_{i=1}^{n}\delta_i\left(1-e^{\left(\frac{-t}{\tau_i}\right)}\right)\right]$$

Bu tür modellerde iki temel kısıt, doku davranışının viskoelastik olduğu varsayımı ve elde edilen bünye denklemlerinin cebirsel değil diferansiyel olmasıdır. Yapılan deneylerde, viskoelastik malzeme varsayımının dar bir hız aralığında (veya frekansta) iyi sonuç verse de aralığın genişlemesi ile model hassasiyetinin düştüğü gösterilmiştir [15]. Öte yandan, malzemenin bünye denkleminin cebirsel yerine

diferansiyel olması, elastik malzemeye göre daha karmaşık bir bünye denkleminin çözülmesi gereği, sistem denklemlerini daha da karmaşık hale getirecektir.

Schwartz [53] tarafından önerilen doğrusal elastik tensör-kütle yönteminde elde edilen tensör denklemleri gerçek zamanlı çözümlemeye izin verecek denli hızlı çözülebilmektedir.

Sanjeevi [54] ise oluşan gerilmeyi elastik ve ağdalı etkilerden olmak üzere ayrı ayrı incelemiştir.

DeHoff [55] ise Haut ve Little denklemlerini kullanarak kollajenin viskoelastik davranışını kestirmiştir.

Fung [15] tarafından önerilen ve yumuşak doku modellemesi konusunda çok bilinen bir standart model olan yalancı-doğrusal viskoelastik teori (*quasi-linear viscoelastic theory*) doğrusal olmayan, zaman ve yükleme geçmişine bağlı yumuşak doku mekanik davranışını modellemek üzere pek çok araştırmacı tarafından başarı ile kullanılmıştır. Bu kurama göre gerilim ile gerinim arasındaki ilişki şu şekilde genel bir formül ile gösterilebilir:

$$\sigma(t) = G(t) * \sigma^{e}(\varepsilon)$$

Burada $\sigma(t)$ gerilimin zamana bağlı değişimini, $G(t)$ indirgenmiş gevşeme fonksiyonunu ve $\sigma^{e}(\varepsilon)$ anlık elastik gerilim tepkisi fonksiyonunu ifade eder. Farklı $G(t)$ ve $\sigma^{e}(\varepsilon)$ fonksiyonları kullanılarak farklı modellerin elde edilebilmesiyle birlikte literatürde en fazla kullanılanları şu şekildedir;

$$G(t) = \frac{1 + C\left[E_1(t/\tau_2) - E_1(t/\tau_1)\right]}{1 + C\,\ln(\tau_2/\tau_1)}$$

$$\sigma^{(e)}(\varepsilon) = A\left(e^{B\varepsilon} - 1\right)$$

Buradaki indirgenmiş gevşeme fonksiyonu içerisinde üç parametre bulunmaktadır. Bunlardan τ_1 ile τ_2 sırasıyla kısa ve uzun dönem gevşeme davranışlarını kontrol ederken, *C* parametresi de gevşemenin genliğini belirlemektedir. İfade içerisindeki E_1 birinci üstel integral fonksiyonudur ve şu şekilde tanımlanır:

$$\mathrm{E_1(y)} = \int_{\mathrm{y}}^{\infty} \frac{\mathrm{e^{-z}}}{\mathrm{z}} \mathrm{dz}$$

Anlık elastik gerilim tepkisi fonksiyonunu içerisindeki iki parametre *(A, B)* ile birlikte toplam beş parametreli bir model oluşmaktadır.

Bu denklemler kullanılarak elde edilen model ise şu şekildedir;

$$\sigma(t) = \int_{\tau=0}^{t} G(t-\tau) \frac{\partial \sigma^{(e)}(\varepsilon)}{\partial \varepsilon} \frac{\partial \varepsilon}{\partial \tau} d\tau$$

Yumuşak doku mekanik yanıtını modellemede kullanılan bir başka yöntem ise Bailey Norton yasası ve Prony serisi yaklaşımıdır:

$$\sigma = \int_{0}^{\mathrm{t}} \mathrm{E_R(t,\varepsilon)} \frac{\mathrm{d\varepsilon}}{\mathrm{dt}} \mathrm{dt}$$

$$\mathrm{E_R(t)} = \mathrm{k_0} + \sum_{\mathrm{i=1}}^{\ell} \mathrm{k_i e^{-t/\tau_i}}$$

$$\mathrm{E_R(t,\varepsilon)} = \mathrm{k_0 \varepsilon} + \sum_{\mathrm{i=1}}^{\ell} \mathrm{k_i e^{-t/\tau_i}}$$

Burada $E_R(t)$ doğrusal, $E_R(t,\varepsilon)$ ise doğrusal olmayan gevşeme fonksiyonlarıdır.

$$\dot{\varepsilon} = \dot{\varepsilon}_{\mathrm{cr}} + \dot{\varepsilon}_{\mathrm{el}}$$

ifadesi ise Bailey Norton yasasıdır.

O.1.2.6.4 Gözenekli-Elastik Malzeme Modelleri

Gözenekli-elastik (*poroelastik*) malzeme modelleri, gözenekli bir elastik katı ortam içerisinde sıvı akışını modelleyen yaklaşımdır ve biyomekanikte zaman zaman yumuşak doku ve özellikle de eklem kıkırdaklarının modellenmesi için kullanılır. Katı üzerinde oluşan gerinmeler nedeniyle sıvı üzerinde oluşan basınç farkları sonucunda sıvı akışı olmaktadır [56]. Yumuşak dokunun iki fazlı modellenmesine yönelik Zhu [57] tarafından hazırlanan çalışmada modelleme ile ilgili ayrıntılar verilmiştir. Ün [58, 59] tarafından yumuşak doku mekanik davranışının modellenmesinde sonlu elemanlar andırımı kullanılmıştır. Ancak gerek modeldeki karmaşıklık gerekse model katsayılarının elde edilmesine yönelik zorluklar nedeniyle bugüne kadar yaygın kullanım alanı bulamamıştır.

O.1.2.7 Yumuşak Doku Malzeme Sabitlerinin Belirlenmesi (Yumuşak Doku Mekanik Karakterizasyonu)

Bünye denklemlerindeki malzeme sabitlerinin belirlenebilmesi, ancak ilgili malzemeler üzerinde ayrıntılı deneyler yapmakla olasıdır. Yapılan deneylerin cinsine göre, eğer kontrollü ortamda ve basit bir geometrili deney örneği kullanılıyorsa cebirsel denklemlerle dokunun gerilme-gerinme-zaman özellikleri (bünye denklemi katsayıları) elde edilebilir. Ancak geometri karmaşıksa (örneğin indentör deneylerinde olduğu gibi indentör ucunun dokuyla teması, büyük yer değiştirmeler gibi) evrik yöntemlere (genellikle evrik sonlu elemanlar yöntemi) başvurulur.

O.1.2.7.1 Analitik Yaklaşımlar

Deney yapılan geometrinin basit olduğu veya basit geometrilerle modellenebildiği (genellikle yarı-sonsuz ortam) ve bununla beraber malzemenin bünye denkleminin de görece basit olduğu (genellikle doğrusal elastik veya doğrusal viskoelastik malzeme) ve tüm bunlara ek olarak gerinmelerin ve yer değiştirmelerin küçük olduğu çok

kısıtlı sayıdaki yumuşak doku deneyleri için mekanik davranış, içerisinde malzeme sabitinin de bulunduğu tek bir analitik denklem ile ifade edilebilmektedir. Bu durumda, analitik denklemden malzeme sabiti çözülerek deney sonucuna bağlı olarak sayısal değer kolaylıkla elde edilebilir [60, 61]. Ancak analitik yaklaşımlar, içerdikleri çok fazla kısıtlama nedeniyle çoğunlukla istenenlere yanıt verememektedir.

O.1.2.7.2 Evrik Sonlu Elemanlar Modeli

Evrik sonlu elemanlar modelinde, deney yapılan bölge ve yakın çevresinin sonlu elemanlar modeli hazırlanır. Gerekli sınır koşulları, deney sırasında uygulanan yükler, dokunun uyması beklenen bünye denklemi modele girilir. Ancak bünye denklemi ile ilgili katsayılar bilinmediği için başlangıç değerleri seçilir. Rastgele seçilen bu değerlerle sonlu elemanlar andırımı çalıştırılır, malzeme sabitleri rastgele seçilmiş dokunun tepkisi elde edilir. Üzerinde deney yapılmış gerçek dokunun malzeme sabitleri, rastgele seçilen malzeme sabitlerinden farklı olacağı için, bilgisayar anırımından elde edilen tepki de gerçek dokudan elde edilenden farklı olacaktır. Aradaki farkı kapatmak üzere bilgisayar andırımındaki malzeme sabitleri değiştirilerek andırım yeniden çalıştırılır. Andırımdan elde edilen tepki, gerçek dokudan deneysel olarak elde edilen tepkiye istenen ölçüde yaklaştığında, andırımda kullanılan malzeme sabitlerinin de gerçek yumuşak dokunun malzeme sabitlerine istenen ölçüde yaklaştığı varsayılır ve böylece yumuşak doku mekanik malzeme sabitleri istenen hassasiyetle kestirilebilir.

Evrik sonlu elemanlar yönteminin kullanımı sırasında dikkat edilmesi gereken noktalar şunlardır:

- Yumuşak dokunun uyması beklenen bünye denkleminin önceden bilindiği varsayılır. Eğer kullanılacak bünye denklemi üzerinde deney yapılan dokunun mekanik davranışını modellemede yetersiz kalırsa evrik sonlu elemanlar yönteminden bünye denkleminin değiştirilmesine yönelik bir bilgi edinilmez.

- Genellikle deney koşullarında yumuşak dokuda büyük gerinmeler, büyük yer değiştirmeler, başka bir cisme dokunma ve doğrusal olmayan bünye denklemleri gibi problemin yüksek derecede doğrusallıktan sapmasına neden olan kaynaklar vardır. Bu durumda, elde edilecek malzeme sabitleri kestiriminin tek (kapalı, dışbükey bir komşuluk içerisinde) olduğuna dikkat edilmelidir.

Evrik yöntemlerle yumuşak doku mekanik özelliklerinin belirlenmesine ilişkin daha ayrıntılı bilgiler için Flynn [62] ve Tönük'ün [9] çalışmalarına başvurulabilir.

Kaynaklar

1. Zhang, M., Lord, M., Turner-Smith, A. R., Roberts, V. C., 1995, "Development of a Nonlinear Finite Element Modeling of the Below-Knee Prosthetic Socket Interface", Med. Eng. Phys, v. 17, pp. 559-566.
2. Zhang, M., Mak, A. F. T., 1996, "Finite Element Analysis of the Load Transfer betwen an Above-knee residual limb and its prosthetic socket-Roles of Interface Friction and Distal-end Boundary Conditions", IEEE Trans. Rehab. Eng. V. 4, pp. 337-346.
3. Zhang, M, Mak, A. F. T., Roberrts, V. C., 1998, Finite Element Modeling of a Residual Lower Limb in a Prosthetic Socket": A Survey of Development in the First Decade", Med. Eng Phy, v. 20, pp. 360-373.
4. Zachariah, S. G., Sanders, J. E., 1996, "Interface Mechanics in Lower-Limb External Prosthetics: A Review of Finite Element Methods", IEEE, Trans. Rehab. Eng, v. 4, pp 288-302.
5. Vannah, W. M., Childress, D. S., 1996, "Indentor Tests and Finite Element Modeling of Bulk Muscular Tissue in vivo", J. Rehabil. Res. Dev., v. 33, pp. 239-252.
6. Commean, P. K., Smith, K. E., Vannier, M. W., Szabo, B. A., Actis, R. L. 1997, "Finite Element Modeling and Experimental Verification of Lower Extremity Shape Change Under Load", J. Biomech, v. 30, pp. 531-536.
7. Tönük, E., Silver-Thorn, M. B., 2003, Nonlinear Elastic Material Property Estimation of Lower Extremity Residual Limb Tissues, IEEE Transactions on Neural Systems and Rehabilitation Engineering, vol. 11, pp. 43-53.
8. Tönük, E., Silver-Thorn, M. B., 2003, "Nonlinear Elastic Material Property Estimation of Lower Extremity Residual Limb Tissues". IEEE, Transactions on Rehabilitation Engineering Vol 11, No 1, pp. 43-53.
9. Tönük, E., 2004b, Evrik Sonlu Elemanlar Yöntemi ile Malzeme Özelliklerinin Kestirilmesi ve Biyomekanik Uygulamaları, MSC.Software Kullanıcılar Konferansı, sf. 25-32, 3-4 Haziran 2004, İstanbul.
10. Yang W., Fung, T. C., Chian, K. S., Chong, C. K., 2006, Investigations of the viscoelasticity of esophageal tissue using incremental stress-relaxation test

and cyclic extension test, Journal of Mechnaics In Medicine and Biology, v. 6 pp. 261-272.
11. Lu, X. L., Mow V. C., 2008, Biomechanics of articular cartilage and determination of material properties, Medicine and Science in Sports and Exercise, v. 40, pp 193-199.
12. Hurschler, C., Loitz-Ramage, B., Vanderby, R. Jr, 1997, A structurally based stress-stretch relationship for tendon and ligament, Journal of Biomechanical Engineering, v. 119, pp. 392-399.
13. Suh J.K., DiSilvestro M.R., 1999, "Biphasic poroviscoelastic behavior of hydrated biological soft tissue", Journal of Applied Mechanics, ASME, v. 66, pp. 528-535.
14. Lu X.L., Miller C., Chen F.H., Guo X.E., Mow V.C., 2007, "The generalized triphasic correspondence principle for simultaneous determination of the mechanical properties and proteoglycan content of articular cartilage by indentation", Journal of Biomechanics, v. 40, pp. 2434-2441.
15. Fung, Y. C., 1993, Biomechanics, mechanical Properties of Living Tissues, Second Ed. Springer-Verlag.
16. Humphrey, J. D., 2002, Cardiovascular Solid Mechanics, Cells, Tissues, Organs, Springer.
17. Bönniger, M., 1905, "Die elastische Spannung der Haut und deren Beziehung zum Oedem," Ztschr. F. Exper. Path. U. Therapie, Vol. 1, pp. 163-183.
18. Kirk, E., Kvorning, S. A., 1949, "Quantitative Measurements of the Elastic Properties of the Skin and Subcutaneous Tissue in Young and Old Individuals," J. Gerontol., Vol. 4, pp. 273-284.
19. Sokolof, L., 1966, "Elasticity of aging cartilage," Fed. Proc., Vol.25, N.3, pp. 1089-1095.
20. Zheng Y. P., Mak A. F. T., Lue B. K., 1999, "Objective assessment of limb tissue elasticity: development of a manual indentation procedure," J Rehabil Res Dev, Vol.36, N.2, pp. 71-85
21. Lawrence, A.J., Rossman, P.J., Mahowald, J.L., Manduca, A., Hartmann, L.C., Ehman, R.L., 1999, "Palpating Breast Cancer by Magnetic Resonance Elastography," Proceedings of the 7th Annual Meeting of ISMRM, Philadelphia, pp. 215.
22. Manduca, A., Oliphant, T.E., Dresner, M.A., Mahowald, J.L., Kruse, S.A., Amromin, E., Felmlee, J.P., Greenleaf, J.F., Ehman, R.L., 2001, "Magnetic resonance elastography: Non-invasive mapping of tissue elasticity," Medical Image Analysis, Vol.5, pp. 237–254.
23. Gefen, A., Megido-Ravid, M., Azariah, M., Itzchak, Y., Arcan, M., 2001, "Integration of Plantar Soft Tissue Stiffness Meausurements in Routine MRI of the Diabetic Foot," Clinical Biomechanics, Vol.16, pp.921-925
24. Geyer, M. J., Brienz, D. M., Chib, V., Wang, J., 2004, "Quantifying Fibrosis in Venous Disease: Mechanical Properties of Lipodermatosclerotic and Healthy Tissue", Adv Skin Wound Care, Vol.17, pp. 131-142
25. Brown, J.D., Rosen, J., Kim, Y. S., Chang, L. C., Sinanan, M. N., Hannaford, B., 2003, "In-Vivo and In-Situ Compressive Properties of Porcine Abdominal Soft Tissues," in Proc. Medicine Meets Virtual Reality, v.94, pp.26-32.

26. Gefen, A., Margulies, S. S., 2003, "Are in vivo and in situ brain tissues mechanically similar?," J. Biomechanics, Vol.37, pp. 1339-1352
27. Ottensmeyer, M. P., Kerdok, A. E., Howe, R. D., Dawson, S. L., 2004, "The Effects of Testing Environment on the Viscoelastic Properties of Soft Tissues," International Symposium on Medical Simulation, pp. 9-18.
28. Fung, Y. C., 1984, "Structure and Stress-Strain Relationship of Soft Tissues," Amer. Zool., Vol.24, pp.13-22.
29. Klaesner J. W, Hastings M. K., Zou D., Lewis C., Mueller M. J.,2002, Plantar tissue stiffness in patients with diabetes mellitus and peripheral neuropathy. Archives of Physical Medicine and Rehabilitation, Vol. 83(12), pp.1796-1801.
30. Ottensmeyer, M. P., 2002, In Vivo Measurement of Solid Organ Tissue Mechanical Properties, Studies in Health Technology and Informatics, Vol.85, pp.328-333.
31. Tanaka, E., Tanaka, M., Aoyamaa, J., Watanabe, M., Hattori, Y., Asai, D., Iwabea, T., Sasaki, A., Sugiyama, M., Tane, K., 2002, "Viscoelastic properties and residual strain in a tensile creep test on bovine temporomandibular articular discs," Archives of Oral Biology, Vol.47, pp.139–146.
32. Prete, Z. D., Antoniucci, S., Hoffman, A. H. ,Grigg, P., 2004, "Viscoelastic properties of skin in Mov-13 and Tsk mice," J. Biomechanics, Vol.37, pp. 1491-1497.
33. Planar-Biaxial Soft Tissue Test System, Instron, 2004, http://www.instron.com.tr/wa/library/streamfile.aspx?doc=527 27. Mart. 2008 tarihinde alınmıştır.
34. Alexander, H., Cook, T. H., 1977, Accounting for natural tension in the mechanical resting of human skin, The Journal of Investigative Dermotology, Vol.69, pp.310-314.
35. Miller, K., Chinzei, K., 2002, "Mechanical properties of brain tissue in tension," ," J. Biomechanics, Vol.35, pp. 483-490.
36. Payne, P. A., 1991, "Measurement of Properties and Function of Skin", Clinical Physics and Physiological Measurement, Vol:12(2), pp.105-129.
37. DiSilvestro, M. R., Suh, J. F., 2001, A cross-validation of the biphasic poroviscoelastic model of articular cartilage in unconfined compression, indentation, and confined compression, J. Biomechanics, Vol.34, pp. 519-525.
38. Bischoff, J. E., 2006, Reduced parameter formulation for incorporating fiber level viscoelasticity into tissue level biomechanical models, Annals of Biomedical Engineering, v. 34, pp. 1164-1172.
39. Tong, P. and Fung, Y. C.,1976, The Stress-Strain Relationship for the Skin, J. Biomechanics, vol. 9, pp. 649-657.
40. Fung, Y. C., 1980, On Pseudo-elasticity of Living Tissues, Mechanics Today J., vol. 5, pp. 487-504.
41. Vaishnav, R. N., Young, J. T., Janicki, J. S. and Patel, D. J., 1972, Nonlinear Anisotropic Elastic Poperties of the Canine Aorta, Biophysical J., vol. 12, pp. 1008-1027.

42. Fung, Y. C., 1973, Biorheology of Soft Tissues, Biorheology J., vol. 10, pp. 139-155.
43. Hoppin, F. G., Lee, G. C., Dawson, S. V., 1975, Properties of Lung Parenchyma in Distortion, J. Applied Physiology, vol. 39, pp. 742-751.
44. Fung, Y. C., 1967, Elasticity of Soft Tissues in Simple Elongation, Am. J. Physiology, vol. 213, pp. 1532-1544.
45. Mooney, M., 1940, A Theory of Large Elastic Deformation, Journal of Applied Physics, vol. 11, pp. 582-592.
46. Bland, D. R., 1960, The Theory of Linear Viscoelasticity, Pergamon Press.
47. Bergen, J. T. (ed), 1960, Viscoelasticity, Phenomenological Aspects, Academic Press.
48. Flügge, W, 1967, Viscoelasticity, Blaisdell Publishing Company.
49. Ferry, J. D., 1970 Viscoelastic Properties of Polymers, John Wiley & Sons.
50. Lockett, F. J., 1972, Nonlinear Viscoelastic Solids, Academic Press.
51. Christensen, R. M., 1982, Theory of Viscoelasticity, An Itroduction, Second Edition, Academic Press.
52. Lakes, R. S., 1998, Viscoelastic Solids, CRC Press.
53. Schwartz, J. M., Denninger, M., Rancourt, D., Moisan, C., Laurendeau, D., 2005, Modeling Liver Tissue Properties Using a NonLinear Viscoelastic Model for Surgery Simulation, Medical Image Analysis, vol. 9, pp. 103-112.
54. Sanjeevi, R., 1982, A Viscoelastic Model for the Mechanical Properties of Biological Materials, J. Biomechanics, vol. 15, pp. 107-109.
55. Dehoff, P. H., 1978, On the Nonlinear Viscoelastic Behavior of Soft Biological Tissues, J. Biomechanics, vol. 11, pp. 35-40.
56. Cowin, S. C., 2004, Anisotropic Poroelasticity: Fabric Tensor Formulation, Mechanics of Materials, vol. 36, pp. 665-677.
57. Zhu, C. ,J., http://www.orl.columbia.edu/nyohrl_new/hmpage/tutorial, 21. Haziran. 2001 tarihinde alınmıştır.
58. Ün K., Spilker R. L. , 2006a, A penetration-based finite element method for hyperelastic 3D biphasic tissues in contact: Part 1 - Derivation of contact boundary conditions, Journal of Biomechanical Engineering, v. 124, pp. 124-130.
59. Ün K., Spilker R. L. , 2006b, A penetration-based finite element method for hyperelastic 3D biphasic tissues in contact. Part II: Finite element simulations, Journal of Biomechanical Engineering, v. 124, pp. 934-942.
60. Hayes, W. C., Keer, L. M., Herrmann, G., Mockros, L. F., 1970, A Mathematical Analysis for Indentation Tests of Articular Cartilage, Journal of Biomechanics, v. 5, pp. 541-551.
61. Argobast, K.B., Thibault, K. L., Pinheiro, B. S., Winey, K. I., Margulies, S. S., 1997, A high-frequency shear device for testing soft biological tissues, Journal of Biomechanics, v. 30, pp. 757-759.
62. Flynn, D. M., Peura, G. D., Grigg, P., Hoffman, A. H., 1998, A finite element based method to determine the properties of planar soft tissue, J. Biomed.i Eng., v. 120, pp. 202-210.

APPENDIX P

PAPER I PREPARED FOR BIOMUT 08

YUMUŞAK DOKU BÜNYE DENKLEMLERİ I: SANKİ-DOĞRUSAL VİSKOELASTİK MODEL

Constitutive Equations for Soft Tissues I: Quasi-linear Viscoelastic Model

Kerem Üsü[1], Ergin Tönük[1,2]
keremusu@gmail.com, tonuk@metu.edu.tr

[1] Orta Doğu Teknik Üniversitesi, Makina Mühendisliği Bölümü, Ankara, Türkiye
[2] Orta Doğu Teknik Üniversitesi, Biyomedikal Mühendisliği Lisansüstü Programı, Ankara, Türkiye

Özetçe: **Yumuşak dokuların mekanik davranışı mühendislik malzemeleri ile karşılaştırıldığına, karmaşıktır. Alışma (Mullin etkisi) sünme, gevşeme, ve histeris gibi elastik malzemelerde gözlenmeyen davranışlar sergilerler. Bu davranışların modellenebilmesi için çeşitli bünye denklemleri önerilmiştir. Bunlardan birisi olan sanki-doğrusal viskoelastik model, yumuşak dokuların zamana bağlı ve doğrusal olmayan davranışını modellemede sıklıkla kullanılmıştır [1]. Bu çalışmada sanki-doğrusal viskoelastik model kullanılıp indentör deneyleri sonucu elde edilen verilerden faydalanılarak model katsayılarının bulunması amaçlanmıştır. Elde edilen katsayıların sonlu elemanlar analizi programında kullanılmasıyla oluşturulan modelin yumuşak doku mekanik davranışını kestirebileceği umulmaktadır. Ayrıca elde edilen katsayı setinin, başka laboratuarlarda başka sistemlerle ve farklı dokular üzerinde yapılan deneyler sonucu elde edilen katsayılarla kıyaslanabilecek bir kaynak olabileceği düşünülmektedir.**

Anahtar Sözcükler: yumuşak doku, sanki-doğrusal viskoelastik model, gevşeme.

Abstract: **Mechanical behavior of soft tissues complicated compared to engineering materials. They exhibit preconditioning (Mullin's effect), relaxation, creep, and hysteresis which are not encountered in elastic materials. Many constitutive equations have been proposed to simulate soft tissue mechanical response. One of these, the quasi-linear viscoelastic model, has been frequently used to model the time-dependent and non-linear behavior of soft**

tissues [1]. In this study, it is aimed to estimate the model parameters by utilizing the experimental data and by using the quasi-linear viscoelastic model. By integrating the model into a finite element code it is hoped that the soft tissue mechanical response could be modeled. Besides, the parameter set obtained is will be a reference to be compared with the different studies done in other laboratories by different experimental systems used on different soft tissues.

Keywords: soft tissue, quasi-linear viscoelastic model, relaxation.

I. GİRİŞ

Biyolojik yumuşak dokular çok karmaşık davranış biçimlerine sahip malzemeler olarak bilinirler ve davranışını tam olarak kestirebilmek çok güçtür. Çevreleriyle mekanik etkileşimleri sonucu alışılageldik mühendislik malzemelerinden çok farklı tepkiler verirler. Yumuşak dokuların modellemesinin hassas olarak yapılabilmesi, onların bu davranışlarının en iyi biçimde bilinmesiyle mümkün olabilir. Yumuşak dokular;

- gerilim-gerinim bağıntısı doğrusal değildir,
- anizotropiktir,
- elastik malzeme davranışına uymaz,
- homojen değildir,
- her döngüde (özellikle ilk döngülerde) aynı deplasman değerine karşı farklı tepki kuvveti değerleri gösterirler, fakat zamanla direngenlik azalarak tekrar edilebilir sonuçlar alınmaya başlanır (alışma, Mullin etkisi), (Şekil 1) [19],
- her döngüde gerinimin artması ve azalması sırasında verdikleri gerilim – gerinim değerleri farklıdır, bu fark mekanik enerji kaybı olarak kendini gösterir (histeris), (Şekil 2) [19],
- sabit gerinim altında sabit gerilim zamanla azalır (gevşeme), (Şekil 3) [19],
- sabit gerilim altında gerinim zamanla artar (sünme), (Şekil 4) [19].

Yukarıda bahsedilen ve elastik malzemelerden çok farklı olan özellikleri kestirebilmek için çeşitli modeller oluşturulmuştur. Bunlarda bazıları derinin modellenmesi [2, 16, 18], üst ve alt bacağın modellenmesi [3, 4], atardamarların modellenmesi [5, 17, 18], kalp kapakçığının modellenmesi [6], akciğer dokusunun modellenmesi [7, 18], ayak tabanının modellenmesi [8], eklem kıkırdağının modellenmesi [9], bağların modellenmesi [10, 11, 15], göğüs dokusunun modellenmesi [12, 13] ve karaciğer dokusunun modellenmesi [14] verilebilir.

Bu modellerin oluşturulmasında çeşitli yöntemler kullanılmıştır. Örneğin bazı bilim adamları dokunun yükleme ve boşaltma sırasında farklı tepkiler vermesi üzerine dokuyu yükleme sırasında bir elastik malzeme yük boşaltma sırasında başka bir elastik malzeme olarak modellemişlerdir. Böylelikle malzemeyi iki elastik malzemenin birleşimi olarak kabul etmiş ve görece daha yalın olan elastisite teorisinin kullanılmasını olanaklı kılmışlardır. Doku elastik olmamasına rağmen onu elastik malzeme kabul eden yönteme bu yüzden *sanki-elastik modelleme* denilmiştir

[5, 18]. Ancak, sanki-elastik malzeme modelleri zamana bağımlı davranışı (gevşeme ve sünme gibi) gözardı ettiği için kullanım alanı sınırlıdır.

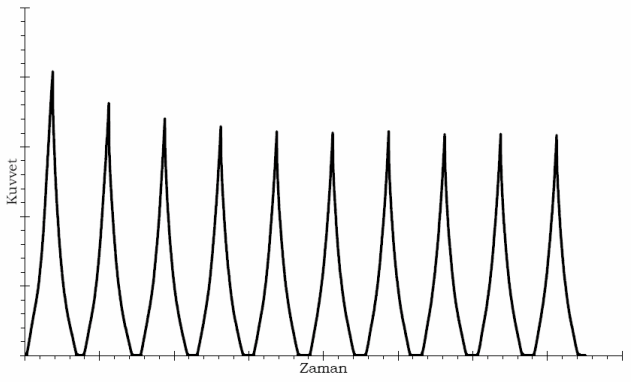

Şekil 1 – Yumuşak Dokunun Ard Arda Yapılan Yüklemelerde Gösterdiği Alışma Etkisi

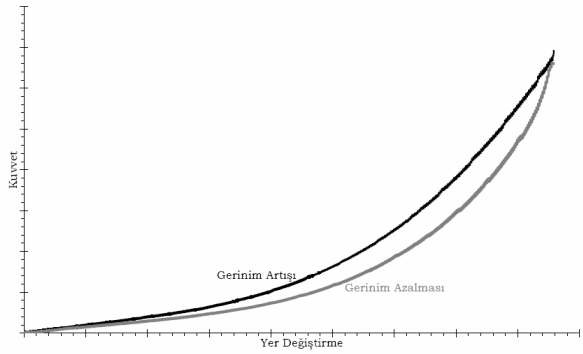

Şekil 2 – Yumuşak Dokunun Yükleme ve Yük Boşaltma Sırasındaki Davranışı

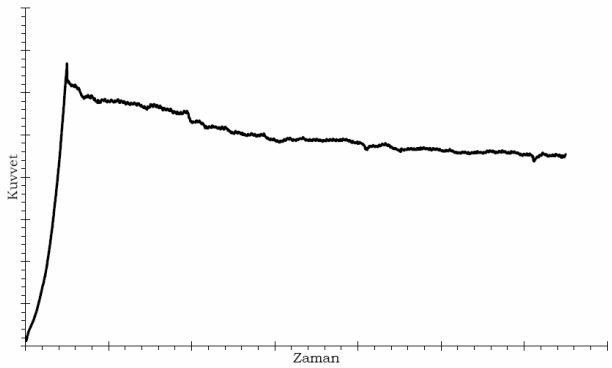

Şekil 3 - Yumuşak Dokunun Sabit Gerinimde Gevşeme Davranışı

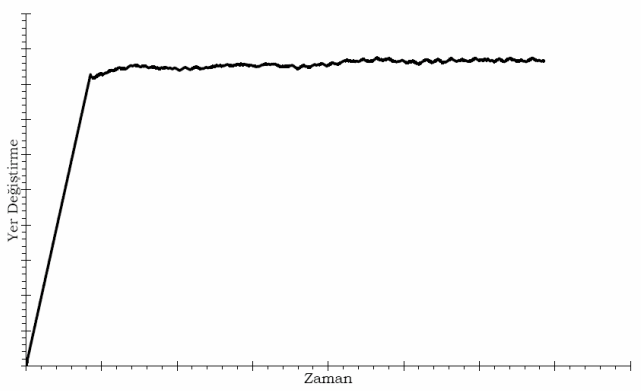

Şekil 4 - Yumuşak dokunun sabit gerilimde sünme davranışı

Başka bir grup bilim insanı ise viskoelastik malzeme modelleri kullanarak yumuşak dokularda görülen histeris yani gerinim-gerilim tepkisinin gerilimin artışı ve azalışı yönlerinde farklı olması (Şekil 2), gevşeme (Şekil 3) ve sünme (Şekil 4) davranışlarını modellemeye çalışmışlardır [11, 14, 15].

Günümüzde en yaygın olarak kullanılan yumuşak doku bünye denklemleri viskoelastik olanlardır. Bu modeller geliştirilerek sanki-doğrusal viskoelastik modeller geliştirilmiştir. Bu modelin temeli indirgenmiş gevşeme fonksiyonunun elastik gerilim fonksiyonunun zamana göre türeviyle çarpımının deney zamanında integralinin alınmasına dayanır.

Yumuşak dokuların bu özellikleri deneyler sonucu ortaya çıkarılmıştır. Yumuşak doku mekanik yanıtının belirlenebilmesi için değişik deney yöntemleri kullanılmıştır. Her yöntemin kendine özgü avantaj ve dezavantajları vardır. Kullanım amacına göre bu deney tiplerinden en uygunu seçilmelidir. Deneylerle, yumuşak dokunun modellenmek istenen davranışı tespit edilir, bu davranışa en uygun bünye denklemi seçilir, deney sonuçları kullanılarak model içindeki parametreler hesaplanır ve son olarak modelin gerçek davranışı ne ölçüde ve hangi sınırlar içerisinde andırabildiği kontrol edilir.

II. MATERYALLER ve YÖNTEMLER

Sanki-Doğrusal Visko-elastik Model

Gelişen bilgisayarlar ve hesaplama yöntemleri ile andırım programları sayesinde son yıllarda en sık ve başarılı biçimde kullanılan yöntem, yumuşak dokuların viskoelastik olarak modellenmesidir. Çünkü yumuşak dokular, neredeyse tüm viskoelastik malzeme davranışlarını sergilemektedirler. Dolayısıyla bu çalışmada da viskoelastik

malzeme modellerinin bir alt kolu olan sanki-doğrusal viskoelastik bünye denklemleri kullanılmıştır.

Sanki-doğrusal viskoelastik modelin temeli indirgenmiş gevşeme fonksiyonunun elastik gerilim fonksiyonunun zamana göre türeviyle çarpımının deney zaman süresince integralinin alınmasına dayanır ve şu şekilde ifade edilir:

$$\sigma(t) = \int_{\tau=0}^{t} G(t-\tau) \frac{\partial \sigma^{(e)}(\varepsilon)}{\partial \varepsilon} \frac{\partial \varepsilon}{\partial \tau} d\tau \tag{1}$$

Burada; *t* zamanı; $\sigma(t)$ gerilimin zamana göre değişimini; $G(–)$ indirgenmiş gevşeme fonksiyonunu (Şekil 5); ε gerinimi ve $\sigma^{(e)}(\varepsilon)$ gerinime bağlı anlık elastik gerilim fonksiyonunu temsil eder.

Bu çalışmada kullanılan ve literatürde bulunanlar arasında en az malzeme sabitine sahip olan indirgenmiş gevşeme fonksiyonu şu şekildedir:

$$G(t) = \frac{1 + C\left[E_1(t/\tau_2) - E_1(t/\tau_1)\right]}{1 + C \ln(\tau_2/\tau_1)} \tag{2}$$

Burada; *C* gevşemenin genliğini, τ_1 ve τ_2 sırasıyla kısa ve uzun dönem gevşeme davranışlarını kontrol eder. İfade içerisindeki $E_1(–)$ birinci üstel integral fonksiyonu olarak adlandırılır ve şu şekilde ifade edilir:

$$E_1(y) = \int_y^{\infty} e^{-z}/z \; dz \tag{3}$$

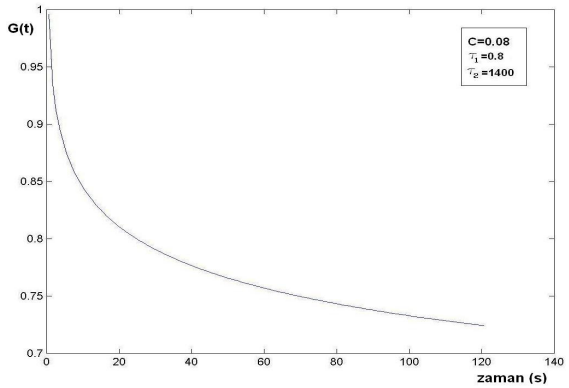

Şekil 5 – İndirgenmiş gevşeme fonksiyonu

Şekil 5'de modelin ana elemanı olan indirgenmiş gevşeme fonksiyonunun C = 0.08, τ_1 = 0.8 s ve τ_2 = 1400 s parametreleri baz alınarak çizilmiş eğrisi sunulmuştur. Buradaki C katsayısı gevşemenin genliğini belirlediğinden büyültülmesi toplam

gevşeme miktarının artmasına, küçültülmesi de azalmasına neden olur. τ_1 katsayısı kısa dönem gevşeme davranışını kontrol eder ve büyültülmesi ani gevşeme süresini uzatır. τ_2 katsayısı uzun dönem gevşeme davranışını kontrol eder ve büyültülmesi uzun dönem gevşeme süresini uzatır.

Gerilime bağlı anlık elastik gerilim fonksiyonu olarak aşağıdaki doğrusal olmayan üstel ifade kullanılmıştır:

$$\sigma^{(e)}(\varepsilon) = A\left(e^{B\varepsilon} - 1\right) \tag{4}$$

Buradaki A ve B, diğer iki malzeme katsayısıdır.

Gerekli ifadeler (1) numaralı denklemde yerine konularak modelin son şekli elde edilir. Modelin beş parametre (C, τ_1, τ_2, A, B) ile yumuşak doku mekanik yanıtını büyük ölçüde modelleyebileceği tahmin edilmektedir.

III. SONUÇLAR

Modelleme sırasında gerinim hızı sabit ve 0.03125 s^{-1} alınmıştır (bu değer, indentör deneyi sırasında ilk kalınlığı yaklaşık 32 mm olan dokuya indentörün 1 mm/s sabit hız ile basması sırasında oluşan gerinim hızıdır [19]). Kullanılan malzeme katsayı değerleri Tablo 1'de sunulmuştur.

Tablo 1 – Modelde kullanılan katsayılar

A	B	C	τ_1	τ_2
50	42	0.08	0.8	1400

IV. TARTIŞMA

İfadeler (1) numaralı denklemde yerine konulup zamana bağlı gerilim tepkisinin son hali oluşturulmuştur. Matlab 6.5 yazılımı kullanılarak sabit gerinim altında gerilim tepkisi Şekil 6'daki gibi elde edilmiştir.

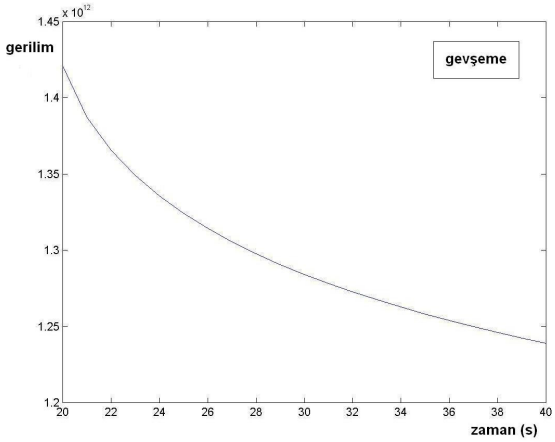

Şekil 6 - Gevşeme davranışının modellenmesi

Şekil 6'da, gevşeme davranışının, hızlı gevşemenin gerçekleştiği ilk 20 saniyelik periyodu sunulmuştur. Sanal deney sırasında, ilk 20 saniyede 1 mm/s ile yükleme yapılıp sonra 120 saniye beklenmiştir.

Yapılan bu ilk denemeler, önerilen modelin, yumuşak dokulardan elde edilen deneysel verileri [19] modelleyebildiğini göstermiştir. Önerilen malzeme modelinin MSC.Marc 2003 sonlu elemanlar programına kullanıcı altprogramı aracılığıyla tanıtılması ile yumuşak doku deneysel verilerinden evrik sonlu elemanlar yöntemiyle [22] malzeme katsayılarının elde edilmesi ve bu katsayılar kullanılarak değişik durumların andırımlarının gerçekçi olarak yapılması olanaklı hale gelecektir.

Oluşturulan bu model, az sayıda katsayıya sahip olması ve bu katsayıların karmaşık olmayan deneylerle elde edilebilmesi nedeniyle kolaylıkla kullanılabilmektedir. Literatürde önceden kullanılan benzer model ve parametre setlerine katkıda bulunacağı düşünülmektedir.

KAYNAKLAR

[1] **Fung, Y. C., Perrone, N., Anliker, M.,** *Stress-Strain History Relations of Soft Tissues in Simple Elongation,* Biomechanics: Its Foundations and Objectives, chapter 7, pp. 181-208, Prentice-Hall, 1970.

[2] **Bischoff, J. E, Arruda, E. M., Grosh, K.,** *Finite Element Modeling of Human Skin Using an Isotropic, Nonlinear Elastic Constitutive Model,* Journal of Biomechanics, vol. 33, pp. 645-652, 2000.

[3] **Commean, P. K., Smith, K. E., Vannier, M. W., Szabo, B. A., Actis, R. L.,** *Finite Element Modeling and Experimental Verification of Lower Extremity Shape Change Under Load,* J. Biomechanics, vol. 30, pp. 531-536, 1997.

[4] **Deng, B., Hubbard, R.,** *Measuring and Modeling Force-Deflection Responses of Human Thighs in Seated Posture,* Advances in Biomechanics, vol. 28, pp. 101-102, 1994.

[5] **Fung, Y. C., Fronek, K. and Paticucci, P.,** *On Pseudo-elasticity of Arteries and the Choice of its Mathematical Expression,* Amer. J. of Physiology, vol. 237, pp. 620-631, 1979.

[6] **Grashow, J. S., Sacks, M. S., Liao, J., Yoganathan, A. P.,** *Planar Biaxial Creep and Stress Relaxation of the Mitral Valve Anterior Leaflet,* Annals of Biomedical Engineering, vol. 34, pp. 1509-1518, 2006.

[7] **Hoppin, F. G., Lee, G. C. and Dawson, S. V.,** *Properties of Lung Parenchyma in Distortion,* J. Applied Physiology, vol. 39, pp. 742-751, 1975.

[8] **Ledoux, W. R., Blevins, J. J.,** *The Compressive Material Properties of the Plantar Soft Tissue,* Journal of Biomechanics, vol. 40, pp. 2975-2981, 2007.

[9] **Mow, V. C.,** *Biphasic Creep and Stress Relaxation of Articular Cartilage in Compression,* Journal of Biomechanical Engineering, vol. 10, pp.73-84, 1980.

[10] **Oza, A., Vanderby Jr., R., Lakes, R. S.,** *Generalized Solution for Predicting Relaxation from Creep in Soft Tissue: Application to Ligament,* International Journal of Mechanical Sciences, vol. 48, pp. 662-673, 2006.

[11] **Provenzano, P. P., Lakes, R. S., Corr, D. T., Vanderby, R.,** *Application of Nonlinear Viscoelastic Models to Describe Ligament Behavior,* Biomechan Model Mechanobiol, vol. 1, pp. 45-57, 2002.

[12] **Samani, A., Plewes, D.,** *A Method to Measure the Hyperelastic Parameters of ex vivo Breast Tissue Samples,* Physics in Medicine and Biology, vol. 49, pp. 4395-4405, 2004.

[13] **Samani, A., Plewes, D.,** *An Inverse Problem Solution for Measuring the Elastic Modulus of Intact ex vivo Breast Tissue Tumours,* Physics in Medicine and Biology, vol. 52, pp. 1247-1260, 2007.

[14] **Schwartz, J. M., Denninger, M., Rancourt, D., Moisan, C., Laurendeau, D.,** *Modeling Liver Tissue Properties Using a NonLinear Viscoelastic Model for Surgery Simulation,* Medical Image Analysis, vol. 9, pp. 103-112, 2005.

[15] **Toms, S. R., Dakin, G. J., Lemons, J. E., Eberhardt, A. W.,** *Quasi-Linear Viscoelastic Behavior of the Human Periodontal Ligament,* Journal of Biomechanics, vol. 35, pp. 1411-1415, 2002.

[16] **Tong, P. and Fung, Y. C.,** *The Stress-Strain Relationship for the Skin,* J. Biomechanics, vol. 9, pp. 649-657, 1976.

[17] **Vaishnav, R. N., Young, J. T., Janicki, J. S. and Patel, D. J.,** *Nonlinear Anisotropic Elastic Poperties of the Canine Aorta,* Biophysical J., vol. 12, pp. 1008-1027, 1972.

[18] **Fung, Y. C.,** *On Pseudo-elasticity of Living Tissues*, Mechanics Today J., vol. 5, pp. 487-504, 1980.

[19] **Petekkaya, A. T., Tönük, E. T.,** *İndentör Deneyleri ile Yumuşak Biyolojik Dokuların Anizotropik Mekanik Davranışının Yerinde Belirlenmesi*, Biyomut 2008, 13. Biyomedikal Mühendisliği Ulusal Toplantısı, Ankara, 29-31 Mayıs 2008.

[20] **Abramowitch, S. D., Woo, S. L.-Y.,** *An Improved Method to Analyze the Stress Relaxation of Ligaments Following a Finite Ramp Time Based on the*

Quasi-Linear Viscoelastic Theory, J. Biomechanical Engineering, vol. 126, pp. 92-97, 2004.

[21] **Fung, Y. C.,** *Biomechanics: Mechanical Properties of Living Tissues,* Springer-Verlag, Second Edition, pp. 23-65, 1993.

[22] **Tönük, E.**, *Evrik Sonlu Elemanlar Yöntemi ile Malzeme Özelliklerinin Kestirilmesi ve Biyomekanik Uygulamaları*, MSC.Software Kullanıcılar Konferansı, sf. 25-32, İstanbul, 3-4 Haziran 2004.

APPENDIX Q

PAPER II PREPARED FOR BIOMUT 08

YUMUŞAK DOKU BÜNYE DENKLEMLERİ II: GELİŞTİRİLMİŞ SANKİ-DOĞRUSAL VİSKOELASTİK MODEL

Constitutive Equations for Soft Tissues II: Enhanced Quasi-linear Viscoelastic Model

Kerem Üsü[1], Ergin Tönük[1,2]
keremusu@gmail.com, tonuk@metu.edu.tr

[1] Orta Doğu Teknik Üniversitesi, Makina Mühendisliği Bölümü, Ankara, Türkiye
[2] Orta Doğu Teknik Üniversitesi, Biyomedikal Mühendisliği Lisansüstü Programı, Ankara, Türkiye

Özetçe: **Literatürde bulunan neredeyse tüm yumuşak doku malzeme modellerinin gerçek davranışı modellemede yetersiz kaldığı yönler vardır. Bazıları sadece belirli bir davranış üzerine yoğunlaşır. Bazıları ise birden fazla davranışı tek bir modelle kestirebilmek için çok sayıda model katsayısı kullanır ve bu katsayıların deneylerle elde edilmesi zahmetli olur. Bu çalışmanın amacı mümkün olan en az model parametresi kullanarak mümkün olabildiği kadar fazla davranışı gerçeğe yakın modelleyebilmektir. Bu doğrultuda sanki-doğrusal viskoelastik malzeme modeli geliştirilmiştir. Deneysel verilerden elde edilen sonuçlar ile model parametrelerinin belirlenmesi planlanmaktadır. Parametrelerin elde edilmesiyle oluşturulan modelin devirli yükleme, gevşeme, sünme ve alışma davranışlarını kestirebileceği umulmaktadır.**

Anahtar Sözcükler: yumuşak doku, geliştirilmiş sanki-doğrusal visko-elastik model, devirli yükleme, gevşeme, alışma.

Abstract: **Almost all of the soft tissue models in the literature have some deficiencies in modeling real soft tissue mechanical response. Some of them only focus in a specific behavior. Some others use many model parameters to be able to simulate more than one behavior in a single model however it is rather hard to determine these parameters experimentally. The aim of this study is, to model as many behavior of soft tissue as possible by using possible minimum number of model parameters. To achieve this, the quasi-linear viscoelastic model was**

enhanced. The parameters of the model will be determined with the help of experimental data. The final form of the model, which will be obtained by substituting the model parameters into the model, is expected to simulate cyclic loading and unloading, relaxation, creep and preconditioning.

Keywords: soft tissue, enhanced quasi-linear visco-elastic model, cyclic loading and unloading, relaxation, preconditioning.

I. GİRİŞ

İnsan vücudunun dış yüzeyi tamamen yumuşak dokularla örtülüdür ve çevreyle mekanik etkileşimin tümü bu yumuşak dokular aracılığıyla gerçekleştirilir. Bu fiziksel (başka bir deyişle mekanik) etkileşimlerin sonuçlarının doğru olarak kestirilebilmesi için öncelikle bu etkileşimleri gerçekleştiren yumuşak dokuların mekanik davranışı hakkında ayrıntılı bilgi sahibi olunmalıdır. Bunların, çeşitli kuvvet tip ve büyüklüklerine nasıl tepki vereceği mümkün olduğu kadar ayrıntılı ve doğru bilinmelidir. Bu bilgiler ışığında yumuşak doku mekanik davranışının bilgisayarda andırımı (simülasyonu) yapılabilir, etkileşimin istenen biçimde olması için gerekli değişiklikler üzerinde çalışılabilir.

Derinin modellenmesi [1, 15, 17], üst ve alt bacağın modellenmesi [2, 3], atardamarların modellenmesi [4, 16, 17], kalp kapakçığının modellenmesi [5], akciğer dokusunun modellenmesi [6, 17], ayak tabanının modellenmesi [7], eklem kıkırdağının modellenmesi [8], bağların modellenmesi [9, 10, 14], göğüs dokusunun modellenmesi [11, 12], karaciğer dokusunun modellenmesi [13] yumuşak doku mekanik davranışının bilinmesinin gerekliliğini gösteren bazı örneklerdir.

Yukarıda bahsedilen modeller yumuşak dokuların bazı tipik mekanik yanıtlarını ortaya çıkarmak için oluşturulmuştur. Bunlar;

- Dokunun ilk birkaç yüklemede daha direngen davranması, sonraki yüklemelerde direngenliğinin azalarak tekrar edilebilir bir gerilim-gerinim özelliğine kavuşması (alışma, Mullin etkisi), (Şekil 1).
- Yükleme ve yük boşaltma yönlerinde görülen iki farklı direngenlik ve bir yükleme - boşaltma çeviriminde ihmal edilemeyecek düzeyde mekanik enerji kaybı (histeris), (Şekil 2).
- Sabit yer değiştirme (veya gerinim) altında tepki kuvvetinin (gerilimin) azalması yani gevşeme, (Şekil 3).
- Sabit kuvvet (veya gerilim) altında yer değiştirmenin (veya gerinimin) artması yani sünme, (Şekil 4).

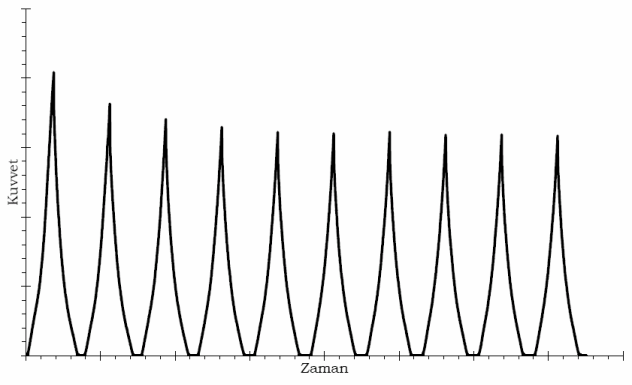

Şekil 1 – Yumuşak Dokunun Ard Arda Yapılan Yüklemelerde Gösterdiği Alışma Etkisi

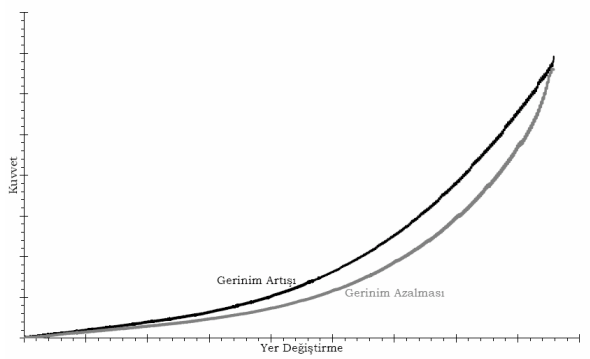

Şekil 2 – Yumuşak Dokunun Yükleme ve Yük Boşaltma Sırasındaki Davranışı

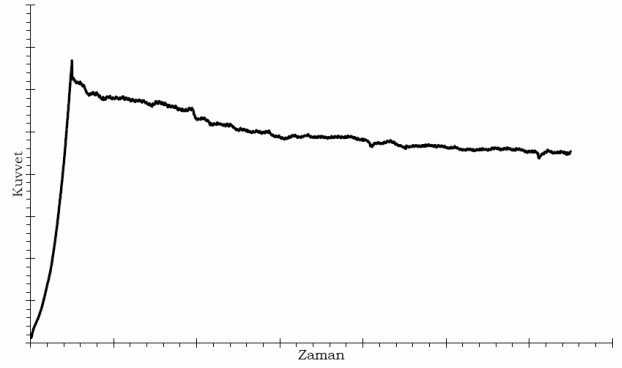

Şekil 3 - Yumuşak Dokunun Sabit Gerinimde Gevşeme Davranışı

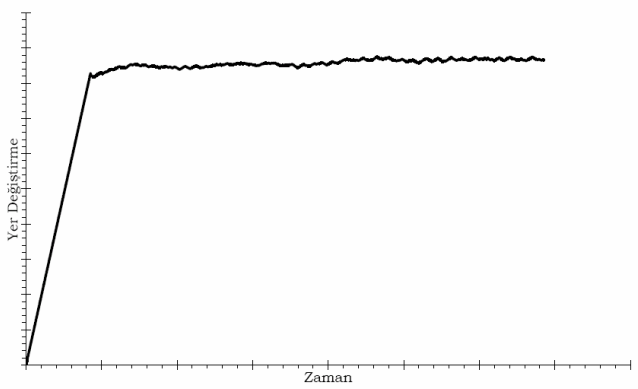

Şekil 4 - Yumuşak dokunun sabit gerilimde sünme davranışı

Yumuşak dokuların bu özellikleri deneyler sonucu ortaya çıkarılmıştır. Yumuşak doku mekanik yanıtının belirlenebilmesi için değişik deney yöntemleri kullanılır. Her yöntemin kendine özgü avantaj ve dezavantajları vardır. Kullanım amacına göre bu deney tiplerinden en uygunu seçilmelidir.

Yumuşak doku mekanik davranışını modellemek için kullanılan bünye denklemlerinden en yaygın kabul görenleri sanki-elastik malzeme modelleri [4, 15, 17], ve bu çalışmada da kullanılan viskoelastik malzeme modelleridir [10, 13, 14].

Sanki-elastik malzeme modellerinde yumuşak doku, yükleme yönünde bir elastik malzeme, boşaltma yönünde başka bir elastik malzeme olarak modellenmiştir. Çünkü, Şekil 2'de de görüldüğü gibi doğrusal olmayan yumuşak dokunun davranışı yükleme sırasında farklı boşaltma sırasında farklı tepki kuvveti–yer değiştirme eğrileri ile temsil edilmektedir. Bu nedenle oldukça basit bir yaklaşımla, gerinmenin artması yönünde bir elastik malzeme katsayısı seti, azalması yönünde başka bir elastik malzeme katsayısı seti kullanılmaktadır. Dokunun gerçek davranışı elastik olarak modellenemeyeceği için bu modele sanki-elastik denmiştir. Ancak sanki-elastik malzeme modelleri zamana bağımlı davranışı (gevşeme ve sünme gibi) gözardı ettiği için kullanım alanı sınırlıdır.

Viskoelastik malzeme modelleri ise viskoelastik malzeme özellikleri olarak kabul edilen histeris (Şekil 2), gevşeme (Şekil 3) ve sünme (Şekil 4) davranışlarını modellemek için geliştirilmiştir. Son yıllarda en sık ve başarılı bir şekilde kullanılan model ise sanki-doğrusal viskoelastik modeldir. Bu modelin temeli indirgenmiş gevşeme fonksiyonunun elastik gerilim fonksiyonunun zamana göre türeviyle çarpımının deney zamanısüresince integralinin alınmasına dayanır.

II. MATERYALLER ve YÖNTEMLER

Sanki-Doğrusal Visko-elastik Model

Gelişen bilgisayarlar ve hesaplama yöntemleri ile andırım programları sayesinde son yıllarda en sık ve başarılı biçimde kullanılan yöntem, yumuşak dokuların visko-elastik modellenmesidir. Çünkü yumuşak dokular, neredeyse tüm visko-elastik malzeme davranışlarını sergilemektedirler [23]. Dolayısıyla bu çalışmada da viskoelastik modellemenin bir alt kolu olan sanki-doğrusal viskoelastik modellemenin geliştirilmiş bir modelini kullanılmıştır.

Sanki-doğrusal visko-elastik modelin temeli indirgenmiş gevşeme fonksiyonunun elastik gerilim fonksiyonunun zamana göre türeviyle çarpımının deney zamanında integrallenmesine dayanır ve şu şekilde ifade edilir:

$$\sigma(t) = \int_{\tau=0}^{t} G(t-\tau)\frac{\partial \sigma^{(e)}(\varepsilon)}{\partial \varepsilon}\frac{\partial \varepsilon}{\partial \tau} d\tau \tag{1}$$

Burada; t zamanı; $\sigma(t)$ gerilimin zamana göre değişimini; $G(–)$ indirgenmiş gevşeme fonksiyonunu; ε gerinimi ve $\sigma^{(e)}(\varepsilon)$ gerinime bağlı anlık elastik gerilim fonksiyonunu temsil eder.

Bu çalışmada kullanılan ve literatürde kullanılanlar arasında en az malzeme sabitine sahip olan indirgenmiş gevşeme fonksiyonu şu şekildedir:

$$G(t) = \frac{1 + C\left[E_1(t/\tau_2) - E_1(t/\tau_1)\right]}{1 + C\ln(\tau_2/\tau_1)} \tag{2}$$

Burada; C gevşemenin genliğini, τ_1 ve τ_2 sırasıyla kısa ve uzun dönem gevşeme davranışlarını kontrol eder. İfade içerisindeki $E_1(–)$ birinci üstel integral fonksiyonu olarak adlandırılır ve şu şekilde ifade edilir:

$$E_1(y) = \int_y^{\infty} e^{-z}/z \; dz \tag{3}$$

Gerilime bağlı anlık elastik gerilim fonksiyonu olarak aşağıdaki doğrusal olmayan üstel ifade tercih edilmiştir:

$$\sigma^{(e)}(\varepsilon) = A\left(e^{B\varepsilon} - 1\right) \tag{4}$$

Buradaki A ve B, diğer iki malzeme parametresidir [23].

Bu aşamaya kadar temel durumdaki sanki-doğrusal viskoelastik model oluşturulmuştur. Gerekli ifadeler (1) numaralı denklemde yerine konularak modelin son şekli elde edilir. Model beş parametre (C, τ_1, τ_2, A, B) ile gevşeme davranışını modelleyebilmektedir.

Bu model temel alınarak geliştirilen model ise hem dokuda bulunan anizotropiyi göz önüne alır hem de zaman ile beraber gerinime de bağlıdır. Bu model;

$$T_{11}(\varepsilon,t)=\frac{a^2\varepsilon_1^2}{8\Lambda}\sigma(t) \tag{5}$$

$$T_{22}(\varepsilon,t)=\frac{b^2\varepsilon_2^2}{8\Lambda}\sigma(t) \tag{6}$$

$$T_{33}(\varepsilon,t)=\frac{c^2\varepsilon_3^2}{8\Lambda}\sigma(t) \tag{7}$$

denklemleri ile ifade edilir. Bu denklemlerde T_{11}, T_{22} ve T_{33} üç malzeme eksenindeki gerilimler; ε_1, ε_2 ve ε_3 üç malzeme eksenindeki asal gerinimler; *a, b* ve *c* anizotropiye izin veren birim hücre ölçüleridir. $\sigma(t)$ ifadesi (1) numaralı denklem ile hesaplanan baz durumdaki sanki-doğrusal viskoelastik gerilimdir. Λ aşağıdaki biçimde ifade edilir:

$$\Lambda=\frac{a^2+b^2+c^2}{8} \tag{8}$$

Anizotropinin modellenebilmesi için modele üç yeni parametre (*a, b, c*) eklenmiştir. Geliştirilen model sekiz parametrelidir. Gerekli ifadeler yerlerine koyulup integrasyon işlemi tamamlandıktan sonra *A* parametresi *a, b* ve *c* parametrelerinin içine alınarak model yedi parametreye indirgenebilir.

III. SONUÇLAR

Modellemeler sırasında gerinim hızı sabit ve 0.03125 s^{-1} alınmıştır (bu değer, indentör deneyi sırasında ilk kalınlığı yaklaşık 32 mm olan dokuya indentörün 1 mm/s sabit hız ile basması sırasında oluşan gerinim hızıdır [22]). Kullanılan parametre değerleri Tablo 1'de sunulmuştur.

Tablo 1 – Modelde kullanılan katsayılar

C	τ_1	τ_2	B	a	b	c
0.08	0.8	1400	42	3.1E-9	2.8E-9	2.6E-9

IV. TARTIŞMA

Yukarıda bahsedilen ve türetilen denklemlerden (5) numaralı olan kullanılarak modelin son hali oluşturulmuş ve Matlab 6.5 yazılımı kullanılarak Şekil 5-7'deki sonuçlar elde edilmiştir.

Şekil 5'te 20 saniyelik periyotlarla yapılan gerinim artışı ve azaltması işlemlerinin eğrileri görülmektedir. Alışma etkisi, yani ilk birkaç döngüden sonra tekrarlanabilir gerilim tepkisi şekilden görülebilir.

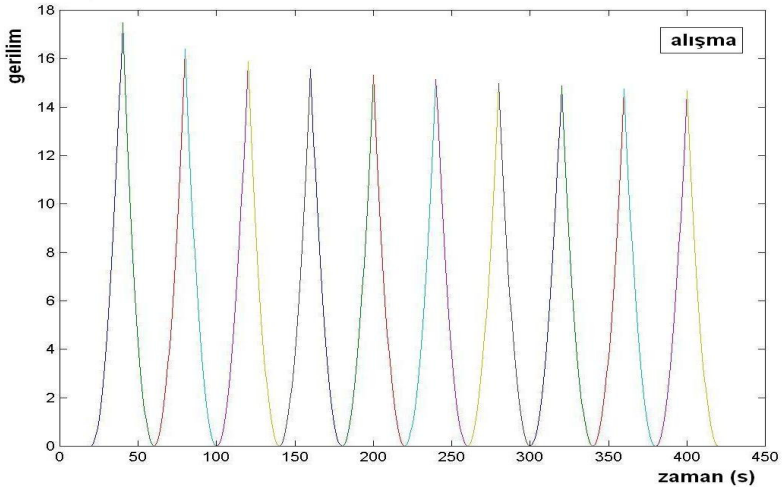

Şekil 5 – Alışma Davranışının Modellenmesi

Şekil 6'da yine gerinimin bu kez bir devirde artması ve azalması işlemleri görülüyor. Bu kez tekrar edilebilir sonuç alındıktan sonraki tek bir döngünün gerilim–gerinim eğrisi sunulmuştur. Bu grafikte bir devir sırasında kaybedilen mekanik enerji (histeris) iki eğrinin arasındaki alan olarak görülmektedir.

Şekil 7'de, gevşeme davranışının, hızlı gevşemenin gerçekleştiği ilk 20 saniyelik periyodu sunulmuştur. Sanal deney sırasında, ilk 20 saniyede gerinim arttırılıp sonra 120 saniye beklenmiştir.

Yapılan bu ilk denemeler, önerilen modelin, yumuşak dokulardan elde edilen deneysel verileri [22] modelleyebildiğini göstermiştir. Önerilen malzeme modelinin MSC.Marc 2003 sonlu elemanlar programına kullanıcı altprogramı aracılığıyla tanıtılması ile yumuşak doku deneysel verilerinden evrik sonlu elemanlar yöntemiyle malzeme katsayılarının elde edilmesi ve bu katsayılar kullanılarak değişik durumların andırımlarının gerçekçi olarak yapılması olanaklı hale gelecektir.

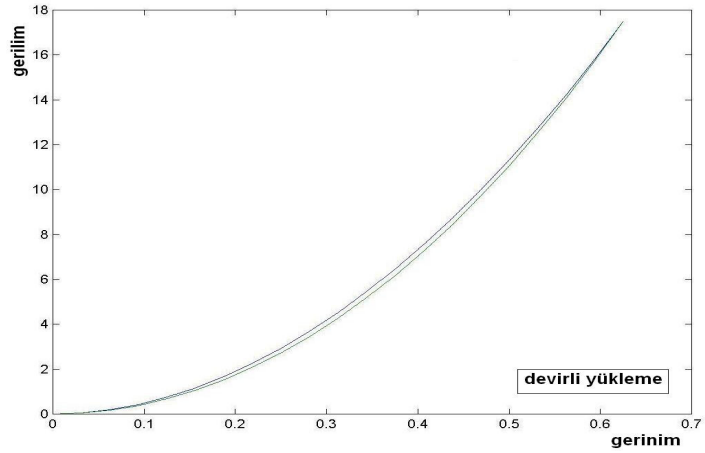

Şekil 6 – Devirli yükleme davranışının modellenmesi

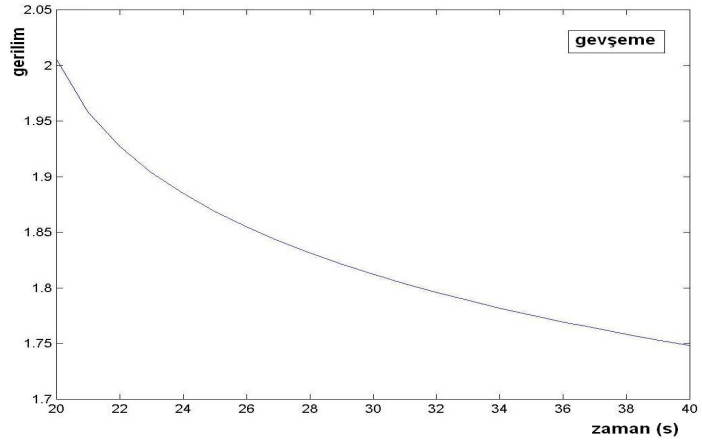

Şekil 7 – Gevşeme davranışının modellenmesi

Oluşturulan bu model, tek bir ifade ile yumuşak doku mekanik yanıtını ayrıntılı biçimde modelleyebilmesi ve az sayıda malzeme katsayısına bağlı olması nedeniyle literatürdeki yumuşak doku modellerine önemli bir katkıda bulunmaktadır.

KAYNAKLAR

[1] **Bischoff, J. E, Arruda, E. M., Grosh, K.,** *Finite Element Modeling of Human Skin Using an Isotropic, Nonlinear Elastic Constitutive Model,* Journal of Biomechanics, vol. 33, pp. 645-652, 2000.

[2] **Commean, P. K., Smith, K. E., Vannier, M. W., Szabo, B. A., Actis, R. L.,** *Finite Element Modeling and Experimental Verification of Lower Extremity Shape Change Under Load,* J. Biomechanics, vol. 30, pp. 531-536, 1997.

[3] **Deng, B., Hubbard, R.,** *Measuring and Modeling Force-Deflection Responses of Human Thighs in Seated Posture,* Advances in Biomechanics, vol. 28, pp. 101-102, 1994.

[4] **Fung, Y. C., Fronek, K. and Paticucci, P.,** *On Pseudo-elasticity of Arteries and the Choice of its Mathematical Expression,* Amer. J. of Physiology, vol. 237, pp. 620-631, 1979.

[5] **Grashow, J. S., Sacks, M. S., Liao, J., Yoganathan, A. P.,** *Planar Biaxial Creep and Stress Relaxation of the Mitral Valve Anterior Leaflet,* Annals of Biomedical Engineering, vol. 34, pp. 1509-1518, 2006.

[6] **Hoppin, F. G., Lee, G. C. and Dawson, S. V.,** *Properties of Lung Parenchyma in Distortion,* J. Applied Physiology, vol. 39, pp. 742-751, 1975.

[7] **Ledoux, W. R., Blevins, J. J.,** *The Compressive Material Properties of the Plantar Soft Tissue,* Journal of Biomechanics, vol. 40, pp. 2975-2981, 2007.

[8] **Mow, V. C.,** *Biphasic Creep and Stress Relaxation of Articular Cartilage in Compression,* Journal of Biomechanical Engineering, vol. 10, pp.73-84, 1980.

[9] **Oza, A., Vanderby Jr., R., Lakes, R. S.,** *Generalized Solution for Predicting Relaxation from Creep in Soft Tissue: Application to Ligament,* International Journal of Mechanical Sciences, vol. 48, pp. 662-673, 2006.

[10] **Provenzano, P. P., Lakes, R. S., Corr, D. T., Vanderby, R.,** *Application of Nonlinear Viscoelastic Models to Describe Ligament Behavior,* Biomechan Model Mechanobiol, vol. 1, pp. 45-57, 2002.

[11] **Samani, A., Plewes, D.,** *A Method to Measure the Hyperelastic Parameters of ex vivo Breast Tissue Samples,* Physics in Medicine and Biology, vol. 49, pp. 4395-4405, 2004.

[12] **Samani, A., Plewes, D.,** *An Inverse Problem Solution for Measuring the Elastic Modulus of Intact ex vivo Breast Tissue Tumours,* Physics in Medicine and Biology, vol. 52, pp. 1247-1260, 2007.

[13] **Schwartz, J. M., Denninger, M., Rancourt, D., Moisan, C., Laurendeau, D.,** *Modeling Liver Tissue Properties Using a Non-Linear Viscoelastic Model for Surgery Simulation,* Medical Image Analysis, vol. 9, pp. 103-112, 2005.

[14] **Toms, S. R., Dakin, G. J., Lemons, J. E., Eberhardt, A. W.,** *Quasi-Linear Viscoelastic Behavior of the Human Periodontal Ligament,* Journal of Biomechanics, vol. 35, pp. 1411-1415, 2002.

[15] **Tong, P. and Fung, Y. C.,** *The Stress-Strain Relationship for the Skin,* J. Biomechanics, vol. 9, pp. 649-657, 1976.

[16] **Vaishnav, R. N., Young, J. T., Janicki, J. S. and Patel, D. J.,** *Nonlinear Anisotropic Elastic Poperties of the Canine Aorta,* Biophysical J., vol. 12, pp. 1008-1027, 1972.

[17] **Fung, Y. C.,** *On Pseudo-elasticity of Living Tissues*, Mechanics Today J., vol. 5, pp. 487-504, 1980.

[18] **Fung, Y. C**., *Structure and Stress-Strain Relationship of Soft Tissues,* Am. Zool., vol. 24, pp. 13-22, 1984.

[19] **Abramowitch, S. D., Woo, S. L.-Y.,** *An Improved Method to Analyze the Stress Relaxation of Ligaments Following a Finite Ramp Time Based on the Quasi-Linear Viscoelastic Theory,* J. Biomechanical Engineering, vol. 126, pp. 92-97, 2004.

[20] **Bischoff, J. E**., *Reduced Parameter Formulation for Incorporating Fiber Level Viscoelasticity into Tissue Level Biomechanical Models,* Annals of Biomedical Engineering, vol. 34, pp. 1164-1172, 2006.

[21] **Bischoff, J. E**., *Static Indentation of Anisotropic Biomaterials Using Axially Asymmetric Indenters - a Computational Study,* Journal of Biomechanical Engineering, vol. 126, pp. 498-505, 2004.

[22] **Petekkaya, A. T., Tönük, E. T.,** *İndentör Deneyleri ile Yumuşak Biyolojik Dokuların Anizotropik Mekanik Davranışının Yerinde Belirlenmesi*, Biyomut 2008, 13. Biyomedikal Mühendisliği Ulusal Toplantısı, Ankara, 29-31 Mayıs 2008.

[23] **Üsü, K., Tönük, E. T.,** *Yumuşak Doku Bünye Denklemlei I: Sanki-doğrusal Viskoleastik Model,* Biyomut 2008, 13. Biyomedikal Mühendisliği Ulusal Toplantısı, Ankara, 29-31 Mayıs 2008.

APPENDIX R

PAPER SUBMITTED FOR PUBLICATION FOR MATİM

İn Vivo İndentör Deneylerinden Elde Edilen Yumuşak Doku Mekanik Davranışını Modellemek için Sanki-Doğrusal Viskoelastik Malzeme Modelleri

Kerem Üsü[1], Ergin Tönük[1,2]

[1] Orta Doğu Teknik Üniversitesi, Makina Mühendisliği Bölümü, Ankara, Türkiye
[2] Orta Doğu Teknik Üniversitesi, Biyomedikal Mühendisliği Lisansüstü Programı, Ankara, Türkiye

Bu çalışmanın amacı yumuşak biyolojik dokuların farklı deney protokollerindeki mekanik davranışlarını sanki-doğrusal viskoelastik malzeme modeli kullanarak mümkün olan en az malzeme sabiti değişimi ile andırmaktır. Yumuşak dokular yüklemeye doğrusal olmayan gerilim-gerinim davranışı, gevşeme, sünme, histeris ve alışma (Mullin etkisi) gibi alışılageldik mühendislik malzemelerinden farklı tepkiler verirler. Yumuşak dokular modelleme amaçlı olarak genelde sanki-elastik veya viskoelastik kabul edilirler. Bu çalışmada, indentör deneyleri sonucunda elde edilen yumuşak doku yer değiştirme-tepki kuvveti-zaman verileri kullanılarak deney bölgesi ve yakın çevresinin, sonlu elemanlar modeli oluşturulmuştur. Yumuşak doku malzeme modeli olarak viskoelastik malzeme modeli, rastgele başlangıç katsayıları ile kullanılmış, evrik sonlu elemanlar yöntemi aracılığıyla sonlu elemanlar andırımındaki yumuşak doku yer değiştirmesi-tepki kuvveti-zaman sonuçları deneysel sonuçlarla arzu edilen yakınlığa ulaşıncaya kadar malzeme katsayıları değiştirilmiştir. Andırım sonuçları, deneysel gevşeme ve sünme davranışlarını sırasıyla % 0.74 ve % 0.31 normalize edilmiş hata kareleri toplamı değerleriyle modellemiştir. Bu değerler, kullanılan malzeme modelinin yumuşak biyolojik doku davranışının kestirimine uygun olduğunu ve elde edilen malzeme katsayılarının yumuşak dokuyu istenen hassasiyette temsil ettiğini göstermektedir. İndentör deney sonuçları ve burada sunulan yöntem kullanılarak insan bedeninin çevre ile mekanik etkileşimi kişiye ve dokuya özel olacak biçimde ve hassas olarak modellenebilir.

Anahtar Kelimeler: Yumuşak Doku, Viskoelastik, Evrik Sonlu Elemanlar

GİRİŞ

İnsanoğlu yaşamını devam ettirdiği sürece sürekli çevresi ile etkileşim içindedir. Bazen algılayabilmek için koklar ya da dinler; bazen de dokunur. Hiç farkında olmadan gün içerisinde defalarca cisimlerle fiziksel temasta bulunur. Örneğin bir koltuğa oturur ve saatlerce kalkmaz veya bütün gece aynı kolunun üzerinde uyur.

İnsan vücudunun dışı büyük ölçüde yumuşak dokulardan oluşmuştur ve dolayısıyla fiziksel temasların çoğu bu yumuşak dokular aracılığıyla gerçekleştirilir. Örneğin, kalça üzerine oturulur ve zamanla kalça oturulan zeminin şeklini alır, en ufak bir kıpırdanma sonucu tekrar şekil değiştirir ve yeni pozisyonuna adapte olmaya çalışır; uzun yürüyüşler sonucunda vücut ağırlığından dolayı ayak tabanlarına uygulanan periyodik değişen kuvvet sonucu çeşitli yumuşak doku zedelenmeleri meydana gelebilir ve ağrı hissedilebilir. Felçli hastaların uzun süre hareketsiz yatmaları sonucu vücutlarıyla yatağın temas ettiği yerlerde yatak yaraları meydana gelir. Protez veya ortez kullanan kişiler bunların vücutlarıyla uyumsuzluklarından dolayı oluşan yaralardan şikayet ederler.

İnsan vücudunda olan bu fiziksel etkileşimlerin mekanik sonuçlarının doğru olarak kestirilebilmesi için öncelikle bu etkileşimleri gerçekleştiren yumuşak dokuların mekanik davranışları hakkında bilgi sahibi olunmalıdır. Bunların, çeşitli kuvvet tip ve büyüklüklerine nasıl tepki vereceği mümkün olduğu kadar ayrıntılı ve doğru bilinmelidir.

Yumuşak dokuların hangi kuvvete ne şekilde tepki vereceği deneylerle belirlenir. Bu deneyler *ex vivo*, *in vitro* ve *in vivo* olmak üzere üç şekilde yapılır [25].

Ex vivo deneylerde, yumuşak doku yerine benzer karakteristik gösteren polimer benzeri malzemeler kullanılır. Dolayısıyla doğru sonuca en uzak deney tipidir. Bunun yanında bilindik geometrilere sahip numuneler kullanılarak deneyin yapılışı kolaylaştırılabilir. In vitro deneylerde ise kadavradan kesilip alınmış gerçek ama ölü yumuşak dokular kullanılır. Dokunun gerçek ortamında (vücudun bir parçası olarak) bulunmaması ve canlı olmaması mekanik özelliklerinin değişmesine sebep olur. Sonuçları ex vivo deneylere göre daha gerçekçi olsa da tatmin edici değildir. Son olarak bu çalışmada faydalanılan in vivo deneyler yumuşak doku kendi ortamında ve canlı haldeyken yapılır. Dolayısıyla, canlı dokunun kendi biyolojik çevresindeki mekanik davranışı hakkında en doğru bilgiler in vivo deneyler sonucu elde edilir. Bu deneylerin en büyük sakıncası ise dokuların karmaşık geometrisinden dolayı uygulanmalarının zor olması ve malzeme yasasını elde etmek için gerilim-gerinim-zaman bağıntılarının elde edilmesi için ek işlemlere gereksinim duymasıdır.

Yapılan deneyler sonucu elde edilen veriler, yumuşak doku mekanik özelliklerini modelleyen ve genellikle doğrusal olmayan karmaşık matematiksel denklemlerin katsayılarının bulunmasında kullanılmaktadır.

YUMUŞAK DOKU MEKANİK MALZEME MODELLERİ

Yumuşak dokular üzerinde yapılan deneysel çalışmalar sonucu, onların genel olarak şu mekanik özellikleri gösterdiği gözlenmiştir:

1. Mekanik davranışları büyük yer değiştirme ve büyük gerinmeler altında doğrusal elastik malzeme davranışından önemli oranda sapmaktadır (Şekil 1).
2. Belirgin bir alışma davranışı (Mullin etkisi) sergilerler (ilk birkaç yüklemenin, daha sonra gelen ve tekrarlanabilen yüklemelerden sapması) (Şekil 2).
3. Sabit deformasyon altında tutulduğunda yumuşak dokunun gösterdiği tepki kuvveti zamanla azalmaktadır (gevşeme) (Şekil 3).
4. Sabit yükleme altında tutulduğunda yumuşak dokuda meydana gelen deformasyon zamanla artmaktadır (sünme) (Şekil 4).

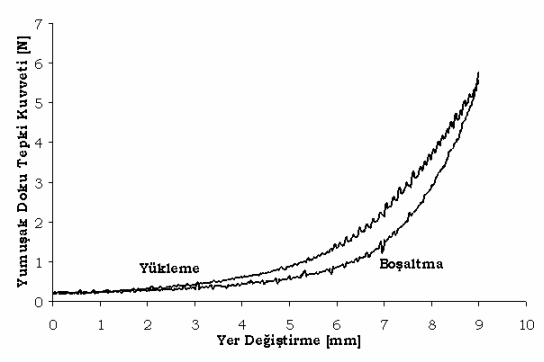

Şekil 1. Yumuşak Doku Devirli Yükleme Deneyi

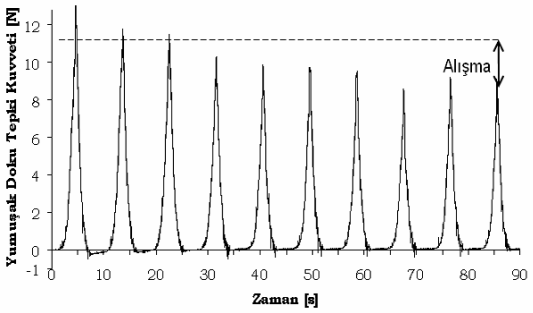

Şekil 2. Yumuşak Doku Alışma Deneyi

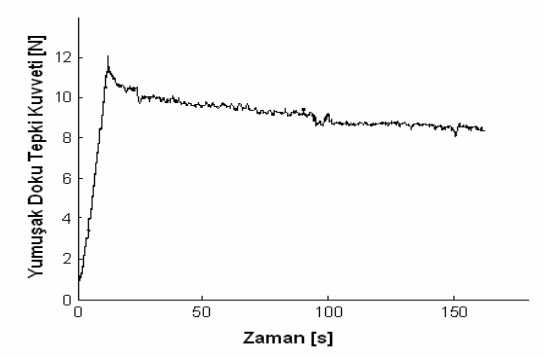

Şekil 3. Yumuşak Doku Gevşeme Deneyi

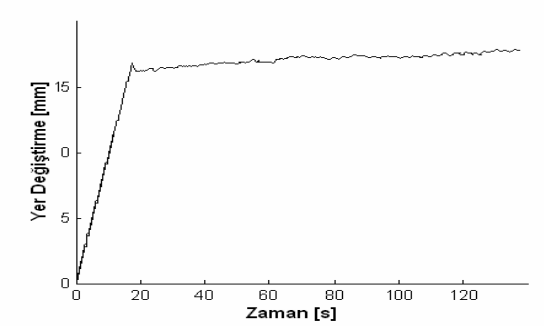

Şekil 4. Yumuşak Doku Sünme Deneyi

Yumuşak dokuların bu özelliklerini mümkün olabildiğince az katsayılı ve fazla karmaşık olmayan matematiksel denklemlerle modelleyebilmek yıllardır süregelen çalışmaların amacıdır. Bunun için çeşitli yöntemler denenmiştir. Bunlardan bazıları; derinin modellenmesi [2, 16, 18], üst ve alt bacağın modellenmesi [3, 4], atardamarların modellenmesi [5, 17, 18], kalp kapakçığının modellenmesi [6], akciğer dokusunun modellenmesi [7, 18], ayak tabanının modellenmesi [8], eklem kıkırdağının modellenmesi [9], bağların modellenmesi [10, 11, 15], göğüs dokusunun modellenmesi [12, 13] ve karaciğer dokusunun modellenmesi [14] olarak gösterilebilir.

Bu modellemeler sırasında, aşağıda değinilen başlıca iki yaklaşım kullanılmıştır.

1. Psödoelastik Model

Şekil 1'de görüldüğü gibi yumuşak dokular yükleme ve boşaltma hareketlerinde farklı eğrilerle temsil edilirler. Tek bir döngü esnasında bu iki eğri arasında oluşan alan *histeris* olarak tanımlanır ve dokuların elastik olmadığının kanıtıdır (elastik malzemelerde yükleme ve boşaltma hareketleri tek eğri ile ifade edilir ve yükleme boşaltma döngüsünde mekanik enerji kaybı yoktur).

Psödoelastik modellemenin temeli, bu iki eğriyi ayrı ayrı ele almaya dayanır. Böylece iki farklı elastik malzeme varmış gibi düşünülüp elastisite teorileri kullanılarak mekanik davranış modellenebilir.

Psödoelastik modellemenin en büyük avantajı, denklemlerin gerinme hızından bağımsız olmasıdır. Fakat her doku için ayrı bir sanki-elastik gerinme enerjisi fonksiyonunun oluşturulmasının gerekliliği, basit ve az katsayılı denklem oluşturma çalışmalarına tamamen ters düşmektedir. Literatürde bulunan, farklı yumuşak dokular için önerilmiş sanki-elastik gerinme enerjisi fonksiyonlarından birkaçı sunulmaktadır.

Vaishnav [17] tarafından kullanılan gerinme enerjisi fonksiyonu damarlar gibi silindirik yapılar içindir, silindirik koordinat sisteminde ifade edilmiştir ve bir polinom biçimindedir:

$$\rho_0 W = AE_{\theta\theta}{}^2 + BE_{\theta\theta}E_{zz} + CE_{zz}{}^2 + DE_{\theta\theta}{}^3 + EE_{\theta\theta}{}^2E_{zz} + FE_{\theta\theta}E_{zz}{}^2 + GE_{zz}{}^3 \tag{1}$$

Burada *A, B, C, D, E, F* ve *G* malzeme sabitleri olup deneysel verinin fonksiyon tarafından kestirilen davranışa uyumunu sağlayacak biçimde belirlenir.

Akciğer özekdokusu için Hoppin [7] tarafından önerilen fonksiyon ise aşağıda sunulmuştur:

$$\begin{aligned}\rho_0 W = &\sum_{i=1}^{4} a_i\left(\lambda_1^{2i} + \lambda_2^{2i} + \lambda_3^{2i}\right) + \sum_{i=1}^{2} b_i\left(\lambda_1^{2i}\lambda_2^{2i} + \lambda_2^{2i}\lambda_3^{2i} + \lambda_1^{2i}\lambda_3^{2i}\right) \\ &+ c_1\lambda_1^2\lambda_2^2\lambda_3^2 + \sum_{i=2}^{3} c_i\left(\lambda_1^{2i}\lambda_2^2 + \lambda_2^{2i}\lambda_3^2 + \lambda_3^{2i}\lambda_1^2 + \lambda_1^2\lambda_2^{2i} + \lambda_2^2\lambda_3^{2i} + \lambda_3^2\lambda_1^{2i}\right)\end{aligned} \tag{2}$$

Burada a_i, b_i ve c_i malzeme sabitleridir ve fonksiyon genel bir üç boyutlu gerilme durumu için geçerlidir.

Mezenter ve kaslar için önerilen gerinme enerjisi fonksiyonu [26, 27] şöyledir:

$$\rho_0 W = \frac{dT}{dE}\alpha T + \beta \tag{3}$$

Burada T birim alandaki çekme kuvveti, E gerinme, α ve β ise malzeme sabitleridir. Bu denklem gerilmesiz duruma çok yakın durumlar için iyi sonuç vermese de diğer tüm gerilmelerde istenen hassasiyette kestirim yapabilmektedir.

Alt ekstremite yumuşak dokularının modellenebilmesi için Tönük [28] tarafından kullanılmış olan James-Green-Simpson modelinin eksenel simetrik ve sıkıştırılamaz malzemelere uygulanmış tipi şu şekildedir:

$$W = C_1(I-3) + C_J(I-3)^2 + C_K(I-3)^3 \quad (4)$$

Burada *I* sıkıştırılamaz malzeme için eksenel simetrik Green-Lagrange gerinme tensörünün tek bağımsız değişmezi, C_i ise malzeme sabitleridir.

Her doku vce her yükleme tipi ve hızı için ayrı bir psödo-elastik gerinme enerjisi fonksiyonunun oluşturulmasının gerekliliği, basit ve az katsayılı denklem oluşturma çalışmalarına ters düşmektedir. Bu sebeple, daha genel denklemler aracılığıyla yumuşak doku modellenmesine imkan veren viskoelastik malzeme modelleri geliştirilmiştir.

2. Viskoelastik Model

Viskoelastik malzemeler katılarla ağdalı sıvıların özelliklerini bir arada gösteren malzemelerdir. Bu malzemeler, katı veya sıvı özelliklerinin baskınlığına göre katıya daha yakın veya sıvıya daha yakın davranabilirler [25]. Viskoelastik malzeme mekanik davranışı yumuşak doku mekanik davranışına çok benzemektedir. Yumuşak dokular gibi histeris (Şekil 1), gevşeme (Şekil 3) ve sünme (Şekil 4) gibi tipik davranışları sergilerler.

En temel iki tip viskoelastik malzeme modeli Maxwell ve Voigt modelleri olup tek boyutlu mekanik model olarak Şekil 5'deki gibi gösterilebilir. Burada yay, elastik davranışı; amortisör ise ağdalı davranışı temsil etmektedir. Maxwell modeli viskoelastik akışkanları modellemekte uygundur. Voigt modelinin tepkisi gerçek viskoelastik katılarla uyuşmadığı için en basit viskoelastik katı modeli için üç elemanlı (bazen Kelvin modeli olarak anılır) model (Şekil 6) önerilmiştir [25].

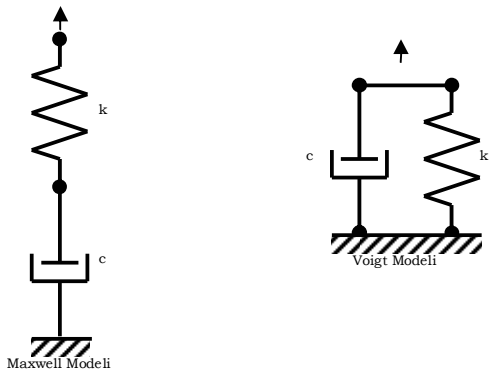

Şekil 5. Temel Viskoelastik Malzeme Modellerinin Tek Boyutlu Mekanik Modelleri

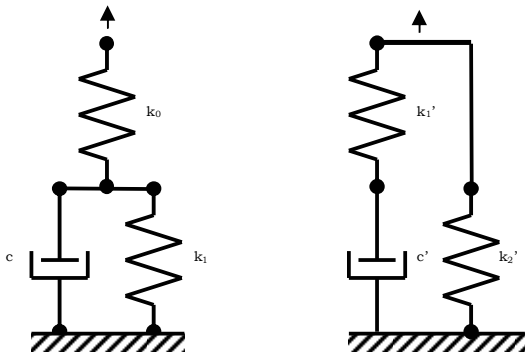

Şekil 6. Üç Elemanlı (Kelvin) Viskoelastik Malzeme Modelinin İki Farklı Gösterimi

Üç elemanlı modelde gerçek viskoelastik katılarda görülen anlık elastik yanıt görülebilmektedir. Bu modellerde gevşeme ve sünme davranışı tek bir üstel ifade ile temsil edilmektedir ve çoğu gerçek viskoelastik katının davranışı bu temsile uymamaktadır. Bu tür modellerdeki en büyük kısıt, elde edilen bünye denklemlerinin cebirsel değil diferansiyel olmasıdır. Bunun sonucunda, elastik malzemeye göre daha karmaşık bir bünye denkleminin çözülmesi gereği, sistem denklemlerini daha da karmaşık hale getirecektir.

Fung [21] tarafından önerilen ve yumuşak doku modellemesi konusunda çok bilinen bir standart model olan sanki-doğrusal viskoelastik kuram (*quasi-linear viscoelastic theory*) doğrusal olmayan, zaman ve yükleme geçmişine bağlı yumuşak doku mekanik davranışını modellemek üzere pek çok araştırmacı tarafından başarı ile kullanılmıştır. Bu kurama göre gerilme ile gerinme arasındaki ilişki şu şekilde genel bir formül ile gösterilebilir:

$$\sigma(t) = G(t) * \sigma^{e}(\varepsilon) \tag{5}$$

Burada $\sigma(t)$ gerilimin zamana bağlı değişimini, $G(t)$ indirgenmiş gevşeme fonksiyonunu ve $\sigma^{e}(\varepsilon)$ anlık elastik gerilim tepkisi fonksiyonunu ifade eder. Farklı $G(t)$ ve $\sigma^{e}(\varepsilon)$ fonksiyonları kullanılarak farklı modellerin elde edilebilmesiyle birlikte literatürde en fazla kullanılanları şu şekildedir;

$$G(t) = \frac{1 + C\left[E_1(t/\tau_2) - E_1(t/\tau_1)\right]}{1 + C\ln(\tau_2/\tau_1)} \tag{6}$$

$$\sigma^{(e)}(\varepsilon) = A\left(e^{B\varepsilon} - 1\right) \tag{7}$$

Buradaki indirgenmiş gevşeme fonksiyonu içerisinde üç parametre bulunmaktadır. Bunlardan τ_1 ile τ_2 sırasıyla kısa ve uzun dönem gevşeme davranışlarını kontrol

ederken, *C* parametresi de gevşemenin genliğini belirlemektedir. İfade içerisindeki E_1 birinci üstel integral fonksiyonudur ve şu şekilde tanımlanır:

$$\mathrm{E}_1(\mathrm{y}) = \int_{\mathrm{y}}^{\infty} \frac{\mathrm{e}^{-\mathrm{z}}}{\mathrm{z}} \mathrm{dz} \tag{8}$$

Anlık elastik gerilme tepkisi fonksiyonunu içerisindeki iki parametre *(A, B)* ile birlikte toplam beş parametreli bir model oluşmaktadır.

Bu denklemler kullanılarak elde edilen model ise şu şekildedir;

$$\sigma(t) = \int_{\tau=0}^{t} G(t-\tau) \frac{\partial \sigma^{(e)}(\varepsilon)}{\partial \varepsilon} \frac{\partial \varepsilon}{\partial \tau} d\tau \tag{9}$$

EVRİK SONLU ELEMANLAR ANALİZİ

In-vivo deneylerle elde edilen yer değiştirme-kuvvet-zaman ilişkileri malzeme kanununun belirlenmesi için gerinme-gerilme-zaman verisine kolaylıkla çevrilemez. Bu amaçla evrik sonlu elemanlar analizi kullanılmaktadır.

Evrik sonlu elemanlar analizinde, deney yapılan bölge ve yakın çevresinin sonlu elemanlar modeli hazırlanır. Gerekli sınır koşulları, deney sırasında uygulanan yükler, dokunun uyması beklenen bünye denklemi modele girilir. Ancak bünye denklemi ile ilgili katsayılar bilinmediği için başlangıç değerleri rastgele seçilir. Rastgele seçilen bu değerlerle sonlu elemanlar andırımı çalıştırılır, malzeme sabitleri rastgele seçilmiş dokunun tepkisi elde edilir. Üzerinde deney yapılmış gerçek dokunun malzeme sabitleri, rastgele seçilen malzeme sabitlerinden farklı olacağı için, bilgisayar andırımından elde edilen tepki de gerçek dokudan elde edilenden farklı olacaktır. Aradaki farkı kapatmak üzere bilgisayar andırımındaki malzeme sabitleri değiştirilerek andırım yeniden çalıştırılır. Andırımdan elde edilen tepki, gerçek dokudan deneysel olarak elde edilen tepkiye istenen ölçüde yaklaştığında, andırımda kullanılan malzeme sabitlerinin de gerçek yumuşak dokunun malzeme sabitlerine istenen ölçüde yaklaştığı varsayılır ve böylece yumuşak doku mekanik malzeme sabitleri istenen hassasiyetle kestirilebilir [25].

Evrik sonlu elemanlar yönteminin kullanımı sırasında yumuşak dokunun uyması beklenen bünye denkleminin önceden bilindiği varsayılır. Eğer kullanılacak bünye denklemi deney yapılan dokunun mekanik davranışını modellemede yetersiz kalırsa evrik sonlu elemanlar yönteminden bünye denkleminin değiştirilmesine yönelik bir bilgi edinilemez.

İNDENTÖR DENEYLERİNDEN MALZEME KATSAYILARININ BELİRLENMESİ

Bu çalışmada evrik sonlu elemanlar yöntemi ile sabitleri bulunan bünye denklemleri, viskoelastik malzeme modeli temel alınarak geliştirilmiştir. Buna göre (9) numaralı denklem geliştirilerek gerilmenin gerinme ve zamana bağlı tepkisini veren anizotropik denklemler oluşturulmuştur. Bu denklemler şu şekildedir:

$$T_{11}(\varepsilon,t)=\frac{a^2\varepsilon_1^2}{8\Lambda}\sigma(t) \tag{10}$$

$$T_{22}(\varepsilon,t)=\frac{b^2\varepsilon_2^2}{8\Lambda}\sigma(t) \tag{11}$$

$$T_{33}(\varepsilon,t)=\frac{c^2\varepsilon_3^2}{8\Lambda}\sigma(t) \tag{12}$$

Bu denklemlerde T_{11}, T_{22} ve T_{33} üç asal eksenindeki gerilmeler; ε_1, ε_2 ve ε_3 üç asal eksendeki gerinmeler; *a, b* ve *c* anizotropiye izin veren birim hücre ölçüleridir. $\sigma(t)$ ifadesi (9) numaralı denklem ile hesaplanan baz durumdaki sanki-doğrusal viskoelastik gerilimdir. Λ aşağıdaki biçimde ifade edilir:

$$\Lambda=\frac{a^2+b^2+c^2}{8} \tag{13}$$

Yukarıda verilen bünye denklemleri kullanılarak yumuşak dokuların karakteristik özellikleri modellenmeye, yani deneysel veriler andırılmaya çalışılmıştır. Sonlu elemanlar andırımları sırasında model Patran 2005 ile oluşturulmuş ve gerekli sınır koşulları ile diğer tanımlamalar Marc/Mentat 2005r2 ile yapılmıştır. Modelin Marc/Mentat ile çalıştırılması sırasında ise malzeme modeli Digital Fortran 6.0 ile derlenerek kullanılmıştır. Her denemede malzeme modelinin kodu içerisindeki katsayı değerleri değiştirilmiştir.

Andırma çalışmaları, gevşeme davranışı ile başlamıştır. Gevşeme davranışına ait deneysel veri (Şekil 7) eliptik indentör ucunun dokuya 1 mm/s sabit hızla 20 saniyede 20 mm basılıp oluşan deplasmanın 120 saniye boyunca sabit tutulmasıyla elde edilmiştir. Aynı prosedür, oluşturulan sonlu elemanlar modeli ile de gerçekleştirilmiş ve altı sonlu elemanlar denemesi sonucunda deneysel veri yeterli doğrulukla andırılmıştır. Her deneme için zamana karşı oluşan tepki kuvveti eğrileri Şekil 7'de [29] görülmektedir. Ayrıca her sonlu elemanlar çözümünde kullanılan malzeme sabitleri Tablo 1'de [29] verilmiştir.

İlk denemedeki (SE1) gevşeme periyodunun başında (t=20s) elde edilen tepki kuvveti değerini doğru olarak kestirebilmek için ikinci denemede (SE2) kısa dönem gevşeme katsayısı (τ_1) küçültülmüş ve gevşemenin başında oluşan tepki kuvveti andırılabilmiştir.

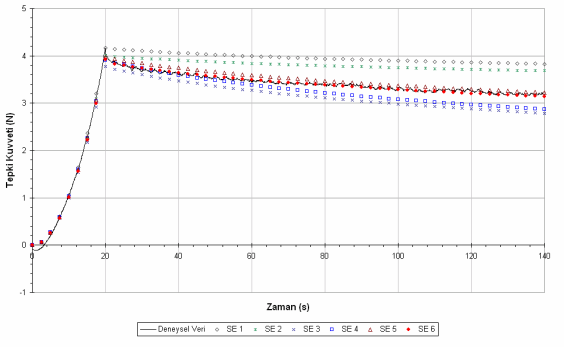

Şekil 7. Gevşeme Davranışının Modellenmesi

Üçüncü adımda (SE3), gevşeme genlik sabiti (C) büyültülerek toplam gevşeme miktarı arttırılmıştır. Şekil 7'de görüldüğü gibi bu değişiklikten sonra hem kısa dönem hem de uzun dönem gevşeme miktarlarında artış olmuştur. Fakat, uzun dönem gevşeme miktarındaki artışın kısa dönemdekinden daha fazla olması, toplam gevşeme genliğinin artmasını sağlamıştır. Dördüncü denemede (SE4), kısa dönem gevşeme katsayısı bir miktar büyültülerek eğrinin solu sağından biraz daha fazla yukarıya kaldırılmış ve gevşemenin başlangıcındaki tepki kuvveti yeniden yakalanmıştır.

Daha sonra uzun dönem gevşeme miktarını azaltmak, yani eğrinin sağ tarafını yukarıya kaldırmak için beşinci denemede (SE5) uzun dönem gevşeme katsayısı (τ_2) büyültülmüştür. Son olarak altıncı denemede (SE6) kısa dönem gevşeme katsayısı yeniden küçültülerek deneysel veri yeterli doğrulukla andırılabilmiştir ve % 0.74'lük hata kareleri toplamı (NSSE) elde edilmiştir [29].

Tablo 1- Gevşeme Davranışının Andırımında Kullanılan Malzeme Sabitleri

	A	B	C	τ_1	τ_2	a	b	c
SE1	7.6E-37	42	0.08	8.0	1400	0.7	0.8	0.9
SE2	7.6E-37	42	0.08	4.0	1400	0.7	0.8	0.9
SE3	7.6E-37	42	8.0	4.0	1400	0.7	0.8	0.9
SE4	7.6E-37	42	8.0	5.0	1400	0.7	0.8	0.9
SE5	7.6E-37	42	8.0	5.0	14000	0.7	0.8	0.9
SE6	7.6E-37	42	8.0	4.0	14000	0.7	0.8	0.9

Gevşeme davranışı başarılı bir şekilde modellenebildikten sonra, aynı bünye denklemi ve malzeme katsayıları kullanılarak sünme davranışının andırımı yapılmıştır. Sünme davranışına ait deneysel veri (Şekil 8) eliptik indentör ucunun dokuya 1 mm/s sabit hızla 20 saniyede 20 mm basılıp, basma sonunda oluşan tepki kuvvetinin 120 saniye boyunca sabit tutulmasıyla elde edilmiştir. Aynı yöntem, oluşturulan sonlu elemanlar modeli ile de gerçekleştirilmiş ve üç sonlu elemanlar denemesi sonucunda deneysel veri yeterli doğrulukla andırılmıştır. Her deneme için zamana karşı oluşan tepki kuvveti eğrileri Şekil 8'de [29] görülmektedir. Ayrıca her sonlu elemanlar çözümünde kullanılan malzeme sabitleri Tablo 2'de [29] verilmiştir.

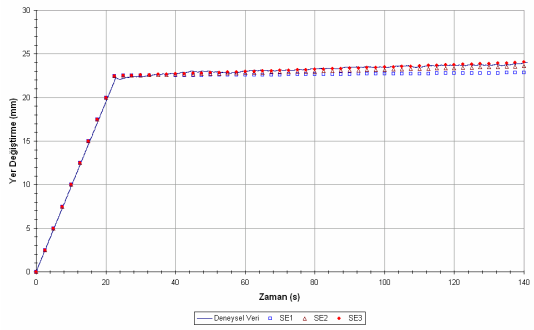

Şekil 8. Sünme Davranışının Modellenmesi

İlk denemede (SE1), gevşeme davranışını andıran son katsayı seti kullanılmıştır. Bu denemede Şekil 8'de de görüldüğü gibi yeterli miktarda sünme tepkisi elde edilememiştir. Dolayısıyla ikinci ve üçüncü denemelerde elastik malzeme katsayısı (A) azaltılarak deneydeki gibi sünme elde edilmeye çalışılmıştır. Son denemenin (SE3) ardından % 0.31 hata kareleri toplamı değeri ile bu andırım da başarıyla gerçekleştirilmiştir.

Tablo 2- Sünme Davranışının Andırımında Kullanılan Malzeme Sabitleri

	A	B	C	τ_1	τ_2	a	b	c
SE1	7.6E-37	42	8.0	4.0	14000	0.7	0.8	0.9
SE2	3.4E-37	42	8.0	4.0	14000	0.7	0.8	0.9
SE3	2.6E-37	42	8.0	4.0	14000	0.7	0.8	0.9

SONUÇ

Önerilen bu yeni malzeme modeli sayesinde gevşeme ve sünme davranışlarının her ikisi de tek bir bünye denklem kullanılarak ve sadece bir sabitin değeri değiştirilerek andırılabilmiştir. Bu değişim, malzeme modelinin her iki davranışı modellemede

yetersiz kalması nedeniyle olabileceği gibi deneysel hatalar ve canlı yumuşak doku üzerinde deney yapılırken dokunun özelliklerindeki değişimler ve adaptasyon nedeniyle de olabilir. Gevşemenin modellenmesi % 0.74 ve sünmenin modellenmesi % 0.31 gibi çok küçük hata payları ile gerçekleştirilebilmiştir. Aynı şekilde yine bu malzeme modeli kullanılarak histeris ve alışma davranışlarının modellenebileceği düşünülmektedir.

Yumuşak doku modellemesi ile ilgili literatür incelendiğinde, yazarların bilgisi dahilinde, sünme ve gevşeme davranışların her ikisini tek bir bünye denklemi ve çok az katsayı değişikliği ile andırabilen modele rastlamak mümkün değildir. Bugüne kadar bazı bilim adamları sadece gevşeme davranışını modelleyebilmiş, bazıları da gevşeme andırımının sonuçlarından faydalanarak sünmeyi modelleyebilmiştir. Yumuşak doku mekanik davranışları matematiksel serilere uydurulmaya ve model içerisindeki sabitler azaltılmaya çalışılmıştır. Bu çalışma, tüm yumuşak doku davranışlarını tek bir model ve çok az sayıda sabit değişimi ile andırabilmesi bakımından önemlidir.

Bu model kullanılarak; amputasyon güdüğü ile protez soketi arasında etkileşim modellenerek protez soketi tasarımında iyileştirme sağlanabilir; ayakkabı ile ayak arasındaki etkileşim modellenerek özellikle yaraları geç iyileşen diyabetli hastalar için ayakkabı tasarımında iyileştirme sağlanabilir; yatan hasta ile yatak arasındaki etkileşim modellenerek özellikle felçli hastalarda oluşan yatak yaralarını en az seviyeye indirmek için yatak tasarımına yenilikler getirilebilir.

Gelişen teknolojinin de yardımıyla, çok daha ayrıntılı sonlu elemanlar modelleri oluşturularak, ve çok daha hassas deneyler sonucu daha doğru veriler elde edilerek, yumuşak doku davranışları daha da küçük hatalarla hassas olarak yapılabilir.

TEŞEKKÜR

Bu çalışmada kullanılan deney birimi ilk olarak TÜBİTAK MİSAG-183 kapsamında üretilmiş, Yüksek Lisans öğrencisi Ali Tolga Petekkaya tarafından geliştirilmiştir. Yazarlar, indentör için eliptik uçları özenle üreten Birant Makina'dan Makina Mühendisi Sayın Emir Birant'a ve yumuşak doku deneylerini yapan ODTÜ Makina Mühendisliği Bölümü yüksek lisans öğrencisi Ali Tolga Petekkaya'ya teşekkür eder.

QUASI-LINEAR VISCOELASTIC MATERIAL MODELS TO MODEL THE MECHANICAL BEHAVIOR OF SOFT BIOLOGICAL TISSUES OBTAINED VIA IN VIVO INDENTOR EXPERIMENTS

The purpose of this thesis is to simulate the mechanical behavior of soft biological tissues by using quasi-linear viscoelastic model with the minimum possible change in the coefficients. Different sections of human body exhibit different responses like stress relaxation, creep, hysteresis and preconditioning to external loading conditions. These body sections are generally assumed as pseudoelastic or

viscoelastic. After making the choice of the material model from one of these for the current study, the finite element model and the material model to be used with this model have been created. Then, the constants in the code which simulates the in vivo experimental data that was obtained by indenting the elliptic indenter tip into the forearm, medial part as close as possible, have been derived by inverse finite element method. Consequently, the characteristic behaviors of the soft tissue could be simulated. Despite the big size of the finite element model and very long submission times, relaxation and creep behaviors could be simulated with the maximum normalized sum of square errors of 0.74 % and 0.31 %, respectively. These values prove that this material model is well suited for the simulation of the behavior of soft biological tissues. By using different experimental data obtained from another sections of human body, simulation of the behavior of different soft tissues can be achieved by using this material model.

Keywords: Soft Tissue, Viscoelastic, Inverse Finite Elements.

KAYNAKÇA

[1] **Fung, Y. C., Perrone, N., Anliker, M.,** *Stress-Strain History Relations of Soft Tissues in Simple Elongation,* Biomechanics: Its Foundations and Objectives, chapter 7, pp. 181-208, Prentice-Hall, 1970.

[2] **Bischoff, J. E, Arruda, E. M., Grosh, K.,** *Finite Element Modeling of Human Skin Using an Isotropic, Nonlinear Elastic Constitutive Model,* Journal of Biomechanics, vol. 33, pp. 645-652, 2000.

[3] **Commean, P. K., Smith, K. E., Vannier, M. W., Szabo, B. A., Actis, R. L.,** *Finite Element Modeling and Experimental Verification of Lower Extremity Shape Change Under Load,* J. Biomechanics, vol. 30, pp. 531-536, 1997.

[4] **Deng, B., Hubbard, R.,** *Measuring and Modeling Force-Deflection Responses of Human Thighs in Seated Posture,* Advances in Biomechanics, vol. 28, pp. 101-102, 1994.

[5] **Fung, Y. C., Fronek, K. and Paticucci, P.,** *On Pseudo-elasticity of Arteries and the Choice of its Mathematical Expression,* Amer. J. of Physiology, vol. 237, pp. 620-631, 1979.

[6] **Grashow, J. S., Sacks, M. S., Liao, J., Yoganathan, A. P.,** *Planar Biaxial Creep and Stress Relaxation of the Mitral Valve Anterior Leaflet,* Annals of Biomedical Engineering, vol. 34, pp. 1509-1518, 2006.

[7] **Hoppin, F. G., Lee, G. C. and Dawson, S. V.,** *Properties of Lung Parenchyma in Distortion,* J. Applied Physiology, vol. 39, pp. 742-751, 1975.

[8] **Ledoux, W. R., Blevins, J. J.,** *The Compressive Material Properties of the Plantar Soft Tissue,* Journal of Biomechanics, vol. 40, pp. 2975-2981, 2007.

[9] **Mow, V. C.,** *Biphasic Creep and Stress Relaxation of Articular Cartilage in Compression,* Journal of Biomechanical Engineering, vol. 10, pp.73-84, 1980.

[10] **Oza, A., Vanderby Jr., R., Lakes, R. S.,** *Generalized Solution for Predicting Relaxation from Creep in Soft Tissue: Application to Ligament,* International Journal of Mechanical Sciences, vol. 48, pp. 662-673, 2006.

[11] **Provenzano, P. P., Lakes, R. S., Corr, D. T., Vanderby, R.,** *Application of Nonlinear Viscoelastic Models to Describe Ligament Behavior,* Biomechan Model Mechanobiol, vol. 1, pp. 45-57, 2002.

[12] **Samani, A., Plewes, D.,** *A Method to Measure the Hyperelastic Parameters of ex vivo Breast Tissue Samples,* Physics in Medicine and Biology, vol. 49, pp. 4395-4405, 2004.

[13] **Samani, A., Plewes, D.,** *An Inverse Problem Solution for Measuring the Elastic Modulus of Intact ex vivo Breast Tissue Tumours,* Physics in Medicine and Biology, vol. 52, pp. 1247-1260, 2007.

[14] **Schwartz, J. M., Denninger, M., Rancourt, D., Moisan, C., Laurendeau, D.,** *Modeling Liver Tissue Properties Using a NonLinear Viscoelastic Model for Surgery Simulation,* Medical Image Analysis, vol. 9, pp. 103-112, 2005.

[15] **Toms, S. R., Dakin, G. J., Lemons, J. E., Eberhardt, A. W.,** *Quasi-Linear Viscoelastic Behavior of the Human Periodontal Ligament,* Journal of Biomechanics, vol. 35, pp. 1411-1415, 2002.

[16] **Tong, P. and Fung, Y. C.,** *The Stress-Strain Relationship for the Skin,* J. Biomechanics, vol. 9, pp. 649-657, 1976.

[17] **Vaishnav, R. N., Young, J. T., Janicki, J. S. and Patel, D. J.,** *Nonlinear Anisotropic Elastic Poperties of the Canine Aorta,* Biophysical J., vol. 12, pp. 1008-1027, 1972.

[18] **Fung, Y. C.,** *On Pseudo-elasticity of Living Tissues*, Mechanics Today J., vol. 5, pp. 487-504, 1980.

[19] **Petekkaya, A. T., Tönük, E. T.,** *İndentör Deneyleri ile Yumuşak Biyolojik Dokuların Anizotropik Mekanik Davranışının Yerinde Belirlenmesi*, Biyomut 2008, 13. Biyomedikal Mühendisliği Ulusal Toplantısı, Ankara, 29-31 Mayıs 2008.

[20] **Abramowitch, S. D., Woo, S. L.-Y.,** *An Improved Method to Analyze the Stress Relaxation of Ligaments Following a Finite Ramp Time Based on the Quasi-Linear Viscoelastic Theory,* J. Biomechanical Engineering, vol. 126, pp. 92-97, 2004.

[21] **Fung, Y. C.,** *Biomechanics: Mechanical Properties of Living Tissues,* Springer-Verlag, Second Edition, pp. 23-65, 1993.

[22] **Tönük, E.**, *Evrik Sonlu Elemanlar Yöntemi ile Malzeme Özelliklerinin Kestirilmesi ve Biyomekanik Uygulamaları*, MSC.Software Kullanıcılar Konferansı, sf. 25-32, İstanbul, 3-4 Haziran 2004.

[23] **Üsü, K., Tönük, E.,** *Yumuşak Doku Bünye Denklemleri I: Sanki-Doğrusal Viskoelastik Model*, 13. Biyomedikal Mühendisliği Ulusal Toplantısı, Ankara, 29-31 Mayıs 2008.

[24] **Üsü, K., Tönük, E.,** *Yumuşak Doku Bünye Denklemleri II: Geliştirilmiş Sanki-Doğrusal Viskoelastik Model*, 13. Biyomedikal Mühendisliği Ulusal Toplantısı, Ankara, 29-31 Mayıs 2008.

[25] **Petekkaya, A. T., Üsü K., Tönük, E.,** *Yumuşak Doku Mekanik Modelleri*, Ortopedi Biyomekaniği Kitabı, 2009.

[26] **Fung, Y. C**., *Biorheology of Soft Tissues, Biorheology* J., vol. 10, pp. 139-155, 1973.

[27] **Fung, Y. C**., *Elasticity of Soft Tissues in Simple Elongation*, Am. J. Physiology, vol. 213, pp. 1532-1544, 1967.

[28] **Tönük, E., Silver-Thorn, M. B.,** *Nonlinear Elastic Material Property Estimation of Lower Extremity Residual Limb Tissues*, IEEE Transactions on Neural Systems and Rehabilitation Engineering, vol. 11, pp. 43-53, 2030.

[29] **Üsü, K.,** *Identification Of Soft Tissue Mechanical Material Model And Corresponding Parameters From In Vivo Experimental Data By Using Inverse Finite Element Method*, M.S. Thesis, Middle East Technical University, 2008.

APPENDIX S

POSSIBILITY OF SIMULATING THE EXPERIMENTAL DATA BY DIFFERENT SETS OF CONSTANTS WITHIN THE MATERIAL MODEL

In Chapter 9, all the characteristic behaviors of the soft biological tissue were simulated by three material models. The constants in the material models were determined for the best fit between the models and experiments. However, these constants are not unique, i.e. the experimental data can be simulated by using different constant values. In this chapter, this will be proved with the simulation of the relaxation behavior with the third material model by using different constants than the ones used in the Chapter 9.3.1.

Relaxation experiment data is the same as the original one used in Chapter 9.3.1. (continuous line in Figure S1). For the alternative simulation of the experimental data, six finite element (FE) trials were performed which can be seen in Figure S1. The normalized sums of square errors (NSSE) for each trial were presented in Figure S2.

In the first FE trial, the base material model (subroutine) which was presented in Appendix M was used. This trial was not able to simulate the magnitude of the reaction force at the beginning of the relaxation period. The reaction force for this simulation was starting from about 4.2 N, whereas the reaction force of the experimental data was starting from somewhere close to 4 N. The great majority of the NSSE of 86.86 % for this simulation was arising from this force difference. So, in the second FE trial, the elastic constant (B), which had never been changed during the previous simulation processes, was decreased from 42 MPa to 41.974 MPa. As

seen in Figure S1, by decreasing the value of this elastic constant, the reaction force at the beginning of the relaxation period could be simulated. This can also be seen from the value of NSSE which decreased to 30.74 % in one step. The majority of this error was due to the deficiency in the amount of total relaxation magnitude which causes the long term relaxation magnitude to deviate from the experimental data more and more as time passes.

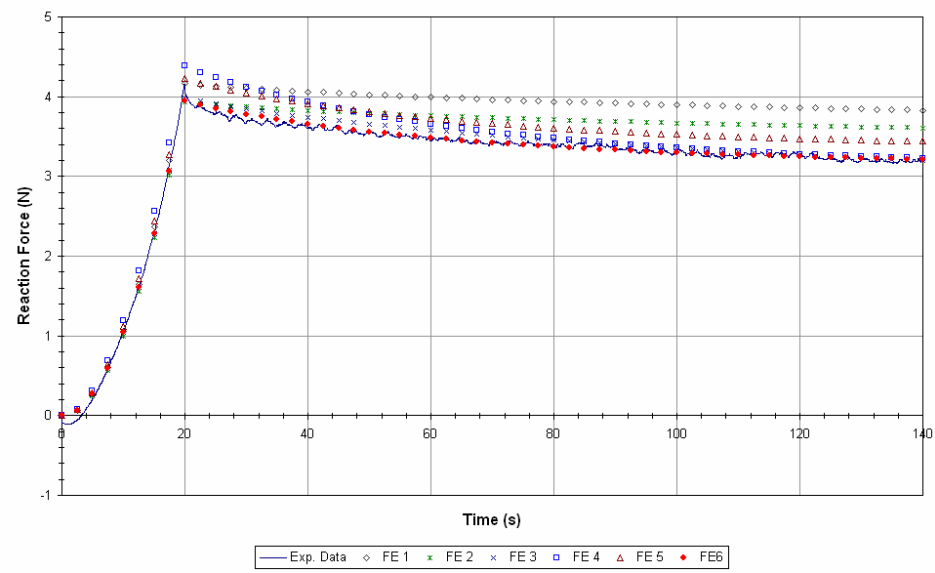

Figure S1 – Relaxation Curves for the Alternative Simulation of the Third Model with Different Constants

To increase the amount of total relaxation magnitude, the relaxation amplitude constant (C) in the material model was increased from 0.08 to 0.53 in the third FE trial. This procedure increased the magnitude of relaxation amount as seen in Figure S1. In the fourth FE trial, the long term relaxation constant (τ_2) was decreased from 1400 seconds to 200 seconds and curvature of the relaxation curve was changed. Then, in the fifth FE trial, the relaxation amplitude constant was decreased to catch the real amount of relaxation amplitude again.

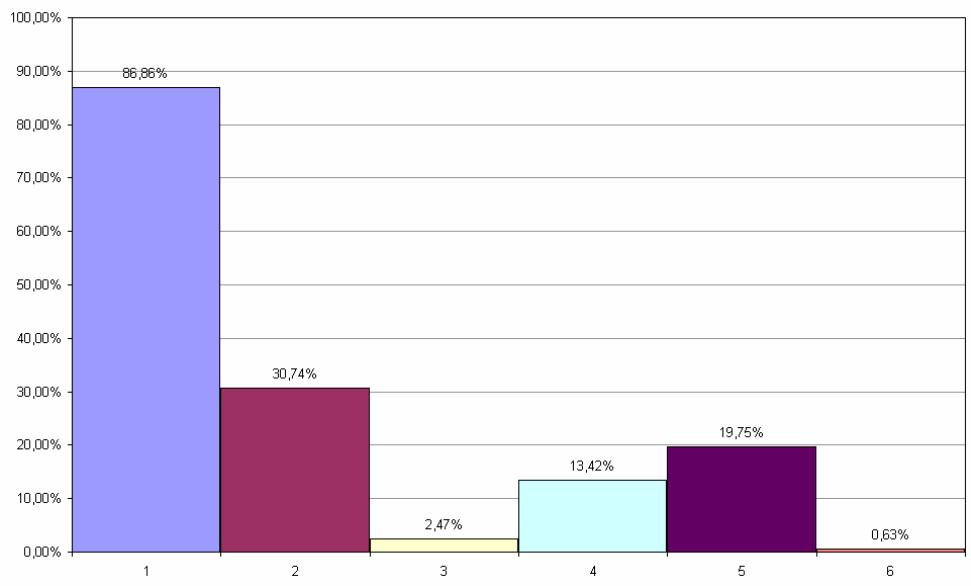

Figure S2 - Normalized Sums of Square Errors for the Alternative Relaxation Simulation of the Third Model with Different Constants

The last finite element trial was performed to decrease the magnitude of reaction force for all the simulation points by decreasing the value of the other elastic constant (*A*). After that step, there occurred a great fit between the experimental data and simulation response which was proved by the NSSE value of 0.63 % given in Figure S2. The constants used in the original simulation (Chapter 9.3.1) and alternative simulation are summarized in Table S1.

Table S1 – Constants of the Third Material Model Used in the Original and the Alternative Simulations of Relaxation Behavior

Trial	A	B	C	τ_1	τ_2	a	b	c
FE-original	7.6E-37	42	8.0	4.0	14000	0.7	0.8	0.9
FE-alternative	7.1E-37	41.974	0.53	4.0	200	0.7	0.8	0.9

Consequently, what can be seen is the fact that the simulation of the mechanical behaviors of soft biological tissues can be performed by using different sets of constants within the material models. In this chapter, that was proved by simulating the relaxation behavior with the third material model by using another set of constants than the one used in the original simulation. This can also be applied to creep and cyclic loading simulations and the experimental data can be simulated by many different sets of constants with different NSSE values.